UNIVERSIDADE FEDERAL DE SANTA CATARINA
CAMPUS FLORIANÓPOLIS
PROGRAMA DE PÓS-GRADUAÇÃO ENGENHARIA DE ALIMENTOS

Jéssica de Matos Fonseca

Hydroxypropyl methylcellulose-TiO_2 and gelatin-TiO_2 photocatalytic nanocomposites applied in fruit postharvest for ethylene scavenging

Florianópolis
2021

Jéssica de Matos Fonseca

Hydroxypropyl methylcellulose-TiO_2 and gelatin-TiO_2 photocatalytic nanocomposites applied in fruit postharvest for ethylene scavenging

Tese submetida ao Programa de Pós-graduação em Engenharia de Alimentos da Universidade Federal de Santa Catarina para obtenção do título de doutora em engenharia de alimentos.
Orientadora: Profª. Alcilene Rodrigues M. Fritz, Drª.
Coorientadores: Prof. Germán Ayala Valencia, Dr; Profª. Regina de Fátima P. M. Moreira, Drª.

Florianópolis
2021

Ficha de identificação da obra elaborada pelo autor,
através do Programa de Geração Automática da Biblioteca Universitária da UFSC.

Fonseca, Jéssica de Matos
Hydroxypropyl methylcellulose-TiO2 and gelatin-TiO2 photocatalytic nanocomposites applied in fruit postharvest for ethylene scavenging / Jéssica de Matos Fonseca ; orientadora, Alcilene Rodrigues Monteiro Fritz, coorientador, Germán Ayala Valencia, coorientador, Regina de Fátima Peralta Muniz Moreira, 2021.
188 p.

Tese (doutorado) - Universidade Federal de Santa Catarina, Centro Tecnológico, Programa de Pós-Graduação em Engenharia de Alimentos, Florianópolis, 2021.

Inclui referências.

1. Engenharia de Alimentos. 2. Embalagem de alimentos. 3. Nanocompósito. 4. Fotocatálise. 5. Tecnologia pós colheita. I. Rodrigues Monteiro Fritz, Alcilene . II. Ayala Valencia, Germán. III. de Fátima Peralta Muniz Moreira, Regina IV. Universidade Federal de Santa Catarina. Programa de Pós-Graduação em Engenharia de Alimentos. V. Título.

Jéssica de Matos Fonseca

HYDROXYPROPYL METHYLCELLULOSE-TiO_2 AND GELATIN-TiO_2 PHOTOCATALYTIC NANOCOMPOSITES APPLIED IN FRUIT POSTHARVEST FOR ETHYLENE SCAVENGING

O presente trabalho em nível de doutorado foi avaliado e aprovado por banca examinadora composta pelos seguintes membros:

Prof(a). Dr(a) Alcilene R Monteiro Fritz - Presidente - UFSC
Prof(a). Dr(a) Cristiane Fagundes - Membro externo - IFC-EA
Prof(a). Dr(a) Jurandir Gonçalves Oliveira - Membro externo - UENF
Prof(a). Dr(a) Dachamir Hotza - Membro externo - UFSC
Prof(a). Dr(a) Marco Di Luccio - Membro interno -UFSC

Certificamos que esta é a **versão original e final** do trabalho de conclusão que foi julgado adequado para obtenção do título de doutora em Engenharia de Alimentos.

Documento assinado digitalmente
Sandra Regina Salvador Ferreira
Data: 06/08/2021 08:07:14-0300
CPF: 564.352.079-68
Verifique as assinaturas em https://v.ufsc.br

Profa. Dra. Sandra Regina Salvador Ferreira
Coordenadora do Programa

Documento assinado digitalmente
Alcilene Rodrigues Monteiro Fritz
Data: 06/08/2021 10:07:14-0300
CPF: 291.697.122-04
Verifique as assinaturas em https://v.ufsc.br

Profa. Dra. Alcilene R Monteiro Fritz
Orientador(a)

Florianópolis, 2021.

Este trabalho é dedicado aos meus pais Ângela e Carlos, que tanto lutaram pela minha educação.

AGRADECIMENTOS

Primeiramente agradeço a Deus pela saúde, maturidade e resiliência concedidos para a execução deste trabalho, uma vez que a pesquisa exige um grande comprometimento do seu investigador. Em seguida, agradeço aos meus pais, Ângela e Carlos, pelo amor, educação, formação e completa doação para que eu pudesse ser quem sou hoje.

Agradeço à Profª Alcilene pela orientação e amizade. Sempre tão solícita, humana, participativa e preocupada com a pesquisa e com o bem-estar dos seus alunos.

Agradeço ao meu coorientador Germán por seu exemplo como profissional, pela paciência e disponibilidade em ensinar, sugerir novas ideias e discutir resultados.

Agradeço à Profa. Regina, também minha coorientadora, por todos os ensinamentos na parte de fotocatálise, a qual se constituiu o meu grande desafio neste trabalho, e por indicar-me ao *Laboratory of Separation and Reaction Engineering - Laboratory of Catalysis and Materials* (LSRE-LCM) da Universidade do Porto (PT) para a realização do meu doutorado sanduíche.

Agradeço a todos os outros professores parceiros neste trabalho, principalmente à Profa. Marta Elisa Rosso Dotto e ao Prof. Carlos Eduardo Campos Maduro, que disponibilizaram seus laboratórios para que eu pudesse fazer várias análises e que participaram ativamente na discussão dos resultados e redação de artigos científicos do nosso grupo de pesquisa.

Agradeço ao Leandro, técnico responsável pela central de análises do EQA, pela confiança, amizade, comprometimento e pelo suporte técnico-científico.

Agradeço ao Nelson por todo apoio emocional, motivacional e por todos os dias em que me acompanhou nos experimentos noturnos e aos fins de semana. Agradeço também pelo seu suporte técnico ao longo de toda construção desta tese.

Agradeço aos meus amigos de SC, MG e SP, especialmente as minhas amigas Amanda e Adriana, e aos colegas de laboratório pela amizade, companheirismo, torcida, ajuda técnico-científica e por compartilharem momentos tanto bons quanto ruins comigo, os quais serviram para meu crescimento pessoal e profissional.

"O homem não teria alcançado o possível se, repetidas vezes, não tivesse tentado o impossível."

MAX WEBER

"A persistência é o caminho do êxito."

CHARLES CHAPLIN

RESUMO

Prolongar a vida útil de alimentos frescos como os frutos climatéricos é um desafio para a indústria de alimentos. Esse grupo de frutos exibe um aumento de respiração e produção do fitormônio etileno, que gerencia a síntese de enzimas de degradação, no início do estágio de maturação. Ambos os processos aceleram a atividade metabólica do fruto e o seu amadurecimento. Embora existam várias tecnologias aplicadas à preservação de frutos, eles podem requerer alto investimento, produzir compostos tóxicos ou favorecer desordens fisiológicas indesejáveis que comprometem a qualidade sensorial e microbiológica dos frutos. Essas limitações motivaram a elaboração desta tese, a qual objetivou desenvolver de um material inovador, de baixo custo, sustentável e capaz de sequestrar etileno sem causar danos físicos ao fruto. A tecnologia pós-colheita proposta trata-se de redes de espuma de polietileno expandido (EPE) revestidas com nanocompósito fotocatalítico à base de gelatina e dióxido de titânio (TiO_2) capaz de degradar etileno sob luz UV-A (λ = 315-400 nm). Assim, esta tese foi dividida em três etapas experimentais. Na primeira etapa, foi estudado o efeito de diferentes concentrações de TiO_2 (0 – 2 % m/m) nas propriedades físico-químicas e estruturais de nanocompósitos à base de matrizes biopoliméricas com diferentes hidrofilicidades (hidroxipropilmetilcelulose- HPMC e gelatina) na forma de filmes preparados por *casting*. Os filmes de gelatina-TiO_2 mostraram ser mais resistentes à água e ao aumento de opacidade com a incorporação de TiO_2, sugerindo melhor dispersão do fotocatalisador. Na segunda etapa, a atividade fotocatalítica dos filmes sobre o etileno foi testada. Os filmes de gelatina-TiO_2 contendo 1 % m/m TiO_2 (Gel-1%TiO_2) apresentaram a maior constante de taxa de reação (k_{app}= 0.186 ± 0.021 min^{-1}). Portanto, essa formulação foi utilizada no recobrimento das espumas de EPE, o qual foi realizado por imersão. Dentre os números de camadas de cobertura avaliados (0 – 4), a bicamada de Gel-1%TiO_2 sobre o EPE (EPE-2x-Gel-1%TiO_2) foi mais eficiente na degradação de etileno (18.212 ± 1.157 ppmv m^2 $g_{TiO_2}{}^{-1}$) do que na sua forma de filme (13.297 ± 0.178 ppmv m^2 $g_{TiO_2}{}^{-1}$). A geometria 3D do EPE aumentou a área superficial fotocatalítica melhorando o desempenho do nanocompósito. Na última etapa, as redes EPE-2x-Gel-1%TiO_2 foram testadas *in vivo*. Mamões (*Carica papaya* L. cv. 'Golden') foram utilizados como modelo de fruto climatérico e armazenados sob luz UV-A à 30 ± 1°C e UR = 85 % por 4 dias. Os frutos embrulhados em EPE-2x-Gel-1%TiO_2 apresentaram acúmulo de etileno 60% menor do que frutos embrulhados em EPE puro, redução das taxas de produção de etileno e respiração no pico climatérico, ausência de crescimento visual de fungos e maior preservação da cor verde da casca, cor amarela da polpa e firmeza. Esses resultados mostraram que o material EPE-2x-Gel-1%TiO_2 reduziu a produção autocatalítica de etileno sem causar desordens fisiológicas nos mamões. Além disso, a remoção do etileno do ambiente provavelmente diminuiu a atividade metabólica dos frutos, retardando a degradação enzimática de pigmentos (clorofila) e macromoléculas estruturais (pectinas). Assim, a tecnologia inovadora desenvolvida eficientemente retardou o amadurecimento dos mamões, exibindo elevado potencial para aplicação agroindustrial.

Palavras-chave: Embalagem ativa. Nanotecnologia. Alimentos.

RESUMO EXPADIDO

Introdução

O transporte e o armazenamento de frutos frescos, especialmente os climatéricos, constituem um grande desafio para o setor agroindustrial devido ao seu rápido amadurecimento desencadeado pelo aumento da produção autocatalítica do fitormônio etileno e da respiração no início da sua maturação. Várias tecnologias como refrigeração, atmosfera controlada e modificada, aplicação de cera na casca, aplicação de gases inibidores de etileno e utilização de materiais adsorventes e oxidantes de etileno já tem sido empregadas para reduzir a atividade metabólicas de frutos e aumentar sua vida pós-colheita. No entanto, algumas dessas tecnologias podem requerer elevados custos de implementação, produzir compostos tóxicos, causar desordens fisiológicas como amadurecimento manchado ou desuniforme, formação de escaldaduras e de odores desagradáveis ou até mesmo contaminação fúngica. Essas limitações tem motivado a busca por outras tecnologias de baixo custo e sustentáveis que possam ser aplicadas com a mesma finalidade em frutos. Uma dessas tecnologias, a qual consistiu no objetivo de aplicação desta tese é a fotocatálise à base de dióxido de titânio (TiO_2). O TiO_2 é um óxido semicondutor que quando exposto a comprimentos de onda (λ) $\leq$ 387,5 nm gera espécies de oxigênio reativas (ROS) como íons superóxido($O_2^{\bullet -}$), hidróxido ($HO^{\bullet}$) e hidroperoxila, ($HOO^{\bullet}$), as quais são capazes de degradar uma variedade de moléculas orgânicas. Assim, fotocatálise à base de TiO_2 pode ser aplicada à pós-colheita de frutos tanto para degradar etileno quanto micro-organismos em sua superfície, e atualmente, uma das formas de aplicação mais investigada para esse propósito é a utilização de filmes e/ou coberturas nanocompósitos fotocatalíticos à base de biopolímeros de grau alimentar (*e.g.* gelatina e hidroxipropilmetilcelulose- HPMC) e TiO_2, visando a sua aplicação final em embalagens ativas. Os biopolímeros gelatina e HPMC destacam-se pela sua capacidade de formação de filmes inodoros, o que não altera caraterísticas organolépticas do alimento, e translúcidos, o que facilita a absorção de luz por pelos cristais deTiO_2. Dentre as principais vantagens dos nanocompósitos de bipolímeros-TiO_2 podem ser destacadas suas propriedades antimicrobiana e sequestradora de etileno, versatilidade quanto à forma de aplicação, sustentabilidade, biodegradabilidade e baixo custo. Assim como outros materiais que apresentam TiO_2 em sua constituição, a principal desvantagem dos nanocompósitos de bipolímeros-TiO_2 está relacionada à tendência à aglomeração do TiO_2, o que causa espalhamento da luz incidida e diminui sua eficiência fotocatalítica. A fim de melhorar a eficiência fotocatalítica do TiO_2, pode-se melhorar a sua homogeneização na dispersão nanocompósita e aumentar a área superficial fotocatalítica. Objetivando-se o aumento da área superficial fotocatalítica, os nanocompósitos de biopolímeros-TiO_2 podem ser aplicados como coberturas sobre redes de espuma de polietileno expandido (EPE), os quais são materiais com geometria tridimensional utilizados na proteção de frutos contra danos físicos durante seu transporte e armazenamento. O aumento da área reacional melhora a absorção de luz e adsorção de etileno na superfície catalisadora. Além da proteção física, as redes de EPE não interagem quimicamente com os frutos, não interferem na permeabilidade gasosa e podem auxiliar na imobilização do TiO_2, dificultando a migração de nanopartículas metálicas do nanocompósito para o fruto. Assim, redes de espuma de EPE cobertas com nanocompósitos de HPMC-TiO_2 e/ou gelatina-TiO_2 podem ser materiais eficientes e inovadores para retardar o amadurecimento de frutos.

Objetivos

Esta tese teve como objetivo principal desenvolver uma tecnologia pós-colheita barata, sustentável, inovadora e capaz de sequestrar etileno visando retardar o amadurecimento de frutos. O material desenvolvido é composto de redes de espuma de polietileno expandido (EPE) revestidas com nanocompósitos fotocatalíticos de biopolímero-TiO_2. Especificamente , os objetivos da tese foram: preparar filmes nanocompósitos de HPMC-TiO_2 e gelatina-TiO_2 via *casting* e estudar a influência da concentração de TiO_2 em suas propriedades estruturais, físico-químicas e fotocatalíticas; estudar a capacidade dos filmes nanocompósitos de HPMC-TiO_2 e gelatina-TiO_2 de degradar o etileno, aplicar a formulação de nanocompósito mais eficiente como revestimento em redes de espuma de EPE e avaliar a influência de seu carregamento na degradação fotocatalítica de etileno e realizar a aplicação *in vivo* de redes de espuma de EPE revestidas com nanocompósito fotocatalítico utilizando mamão (*Carica papaya* L. cv. 'Golden') como modelo de fruto climatérico e estudar as suas alterações fisiológicas e físico-químicas.

Metodologia

Esta tese foi dividida em três etapas experimentais. Na primeira etapa, os filmes de HPMC-TiO_2 e gelatina-TiO_2 foram preparados por *casting* e caraterizados estruturalmente. Biopolímeros (4 g) foram solubilizados separadamente em solução acética (70 g, pH 3.2) sob agitação vigorosa, adicionados de plastificante glicerol (25 % m/m, polímero) e gradualmente aquecidos (85 °C). Após o resfriamento natural das dispersões a 50°C, 30 g suspensão de TiO_2 (0, 0,5, 1 e 2 % m/m, polímero) em ácido acético foram gotejados gradualmente nas dispersões poliméricas. As dispersões finais foram homogeneizadas em ultraturrax, sonicadas em ultrassom de banho para a remoção de bolhas, vertidas em placas de acrílico e secas em incubadora BOD à 25ºC por 48 h. Após destacados das placas, os filmes foram armazenados à 25ºC e UR = 58 %. Os filmes foram caraterizados juntamente com as dispersões nanocompósitas quanto ao tamanho de partícula (DLS), carga superficial (potencial zeta), morfologia de superfície (SEM), conteúdo de umidade, solubilidade em água, permeabilidade ao vapor de água (WVP), propriedades ópticas (cor, opacidade, absorção UV, índices de brancura e amarelecimento), composição e interações químicas (FTIR, Raman), cristalinidade (XRD), propriedades mecânicas (elasticidade, tensão de ruptura, fragilidade) e propriedades térmicas (T_g e T_m, DSC). Na segunda etapa, os filmes foram avaliados quanto as suas propriedades fotocatalíticas para a degradação de etileno. Inicialmente os filmes foram pré-selecionados quanto à ativação da sua superfície fotocatalítica. Para isso, avaliou-se o aumento de hidrofilicidade de sua superfície pela diminuição do ângulo de contato com a água ao serem expostos à luz UV-A (λ_{pico} = 365 nm). Os filmes que apresentaram ativação do catalisador na superfície foram selecionados para a aplicação dos testes fotocatalíticos de degradação de etileno, os quais foram realizados em um sistema em batelada carregado com 5 ppmv de etileno a 30ºC ± 1ºC e UR = 85 % e intensidade luminosa UV-A (λ_{pico} = 365 nm) de 9.8 mW cm^{-2}. A quantificação de etileno foi realizada por cromatografia gasosa. Os filmes foram também caraterizados antes e depois dos testes fotocatalíticos quanto à rugosidade de superfície (AFM) e composição química (FTIR) para investigar possível fotodegradação do biopolímero. A formulação nanocompósita que apresentou a melhor atividade fotocatalítica para a degradação de etileno foi utilizada para a cobertura das redes de espuma de EPE, a qual foi realizada por consecutivas imersões do suporte EPE em dispersão nanocompósita intercaladas com secagens em BOD para a obtenção de diferentes números de camadas de cobertura nanocompósita (0, 1, 2 e 4). As redes de espuma de EPE foram avaliadas quanto à composição química, morfologia de superfície, carregamento de dispersão nanocompósita e

catalisador na superfície e quanto à atividade fotocatalítica para a degradação de etileno utilizando o mesmo sistema e parâmetros de processo utilizados para os filmes nanocompósitos. As redes de espuma de EPE cobertas com nanocompósito que apresentaram maior eficiência para a degradação de etileno sintético foram aplicadas *in vivo*. Para a realização dos testes *in vivo*, mamões *Carica papaya* L. cv. 'Golden' em estágio de maturação 1 (90 – 100% da casca verde) foram escolhidos como modelo de fruto climatérico. Os mamões sanitizados foram embrulhados em redes de espuma de EPE revestidas ou não com dispersão nanocompósita e armazenados em uma câmara equipada com luz UV-A (λ_{pico} = 365 nm, $I_{topo\ do\ fruto}$ = 4.40 mW cm^{-2}, $I_{base\ do\ fruto}$ = 1.44 mW cm^{-2}) a 30ºC ± 1ºC e UR = 85 % durante 4 dias para o monitoramento da evolução de etileno e respiração ([O_2], [CO_2]), simulando condições drásticas de armazenamento para os frutos. Os frutos foram caracterizados quanto a cor, peso, firmeza, pH, sólidos solúveis e crescimento visual fúngico antes e depois do período de armazenamento do reator. Todos os experimentos foram realizados ao menos em triplicata.

Resultados e discussão

Os filmes nanocompósitos de gelatina-TiO_2 mostraram ser mais resistentes à água e apresentou menor opacidade relativa do que os filmes de HPMC-TiO_2, sugerindo melhor dispersão do TiO_2 na matriz de gelatina devido ao seu caráter hidrofóbico quando não exposto à luz UV-A. As micrografias obtidas por SEM corroboraram os resultados de opacidade, evidenciando a crescente aglomeração do fotocatalisador na matriz de HPMC com o aumento de sua concentração. Os filmes de HPMC-TiO_2 apresentaram redução gradual de elasticidade e de resistência à tração e mais elásticos e menos resistentes à tração do que os filmes de gelatina-TiO_2, os quais não apresentaram alterações de propriedades mecânicas com a variação da concentração de TiO_2. Os resultados indicaram que a incorporação de TiO_2 nas matrizes biopoliméricas causou uma reorganização microestrutural dos filmes, induzindo a separação de fases. Essas fases são caracterizadas por regiões bifásicas ricas em polímero, glicerol e água, podendo ou não conter aglomerados de TiO_2. Esses microdomínios são maiores para os filmes que contém 2 % m/m TiO_2 e menores para os filmes que contém 1% m/m TiO_2, caracterizando menor aglomeração do fotocatalisador em ambas as matrizes biopoliméricas nessa concentração. Quanto à fotoatividade da superfície fotocatalítica, apenas a superfície dos filmes de HPMC e gelatina contendo 1% m/m TiO_2 (HPMC-1%TiO_2 e gel-1%TiO_2) apresentaram aumento de hidrofilicidade (redução do ângulo de contato com a água) ao serem expostos a luz UV-A. Assim, essas formulações juntamente com formulações de filmes sem catalisador (HPMC-0%TiO_2 e gel-0%TiO_2) foram testadas quanto a sua atividade fotocatalítica para a degradação de etileno em sistema em batelada. Ambos os filmes, HPMC-1%TiO_2 e gel-1%TiO_2, degradaram aproximadamente 40% do etileno carregado no reator, sendo que o filme gel-1%TiO_2 apresentou uma cinética de degradação mais rápida caraterizada por uma maior constante de taxa de reação (k_{app} = 0.186 ± 0.021 min^{-1}). Ambos os filmes também apresentaram estagnação da reação caracterizando uma possível desativação do fotocatalisador. Micrografias de AFM e espectros de FTIR apontaram que essa possível desativação pode estar associada à fotodegradação do biopolímero e deposição de fragmentos carbonáceos (*fouling*) na superfície do filme que diminui a absorção de luz e adsorção do etileno nos sítios ativos do fotocatalisador. A maior erosão (diminuição da rugosidade) detectada na superfície dos filmes de gelatina-TiO_2 justifica sua capacidade de degradação mais rápida do etileno. Antes da suposta deposição carbonácea desativar o fotocatalisador, a fotodegradação do biopolímero intensifica a exposição do TiO_2 à luz UV-A, o que aumenta sua atividade fotocatalítica durante o início da reação. Algumas características dos filmes gel-1%TiO_2 como degradação mais rápida de etileno e menor solubilidade em água foram consideradas mais importantes para a sua aplicação em frutos climatéricos. Assim, essa

formulação foi utilizada para revestir as redes de espuma de EPE por imersão. As micrografias de SEM juntamente com a estimativa de massas de TiO_2 carregado sobre as redes de EPE evidenciaram que uma monocamada nanocompósita de gel-1%TiO_2 (EPE-1x-gel-1%TiO_2) seria insuficiente para condução de testes fotocatalíticos. Portanto, apenas as redes de espuma de EPE revestidas com bicamada (EPE-2x-gel-1%TiO_2) ou tetracamada (EPE-4x-gel-1%TiO_2) nanocompósita foram testadas quanto à sua capacidade de degradar etileno. Ambas as redes de espuma EPE-2x-gel-1%TiO_2 e EPE-4x-gel-1%TiO_2 degradaram 23% do etileno carregado no reator. No entanto, normalizando-se os dados cinéticos de filmes e redes, ou seja, dividindo-se a concentração de etileno degradado por área superficial fotocatalítica iluminada e massa de TiO_2 carregado nessa superfície, a rede de espuma EPE-2x-gel-1%TiO_2 apresentou uma degradação de etileno retardada e estendida, caracterizada pela diminuição da constante cinética de reação (k_{app} = 0.023 ± 0.005 min^{-1}) e não estagnação (maior eficiência), enquanto as redes de espuma EPE-4x-gel-1%TiO_2 apresentaram estagnação da reação assim como os filmes nanocompósitos. A maior eficiência fotocatalítica das redes de espuma EPE-2x-gel-1%TiO_2 (18.212 ± 1.157 ppmv m^2 $g_{TiO_2}{}^{-1}$) foi atribuída a possível diminuição da espessura de nanocompósito sobre a espuma e ao aumento da área superficial fotocatalítica, os quais podem ter reduzido a deposição carbonácea e melhorado a iluminação e a dispersão do fotocatalisador e a adsorção de etileno. A menor eficiência fotocatalítica das redes EPE-4x-gel-1%TiO_2 pode ser justificada pelo excesso de nanocompósito carregado na sua superfície, o que pode causar uma aglomeração do TiO_2 e possível reticulação física da gelatina, dificultando a absorção de luz e adsorção do etileno, além do aumento de deposição carbonácea. Considerando os resultados obtidos, a rede de espuma EPE-2x-gel-1%TiO_2 foi a formulação selecionada para a aplicação *in vivo*, para a qual foi utilizado o mamão *Carica papaya* L. cv. 'Golden' em estágio de maturação 1 como modelo de fruto climatérico. Após 4 dias de armazenamento à 30ºC ± 1ºC, UR = 85 % e sob luz UV-A, os frutos embrulhados em redes de espuma EPE-2x-Gel-1%TiO_2 apresentaram acúmulo de etileno 60% menor do que frutos embrulhados em redes de espuma de EPE puro, redução do pico de respiração climatérica, preservação dos perfis de evolução de etileno e do padrão respiratório, ausência de crescimento visual de fungos na sua superfície e maior preservação da cor verde da casca, cor amarela da polpa e da firmeza tanto da casca quanto da polpa. Esses resultados sugerem que o material EPE-2x-Gel-1%TiO_2 reduziu a produção autocatalítica de etileno sem causar desordens fisiológicas nos mamões. Além disso, a remoção do etileno do ambiente provavelmente diminuiu a atividade metabólica dos frutos, retardando a expressão de enzimas responsáveis pela degradação de pigmentos como clorofila e de macromoléculas estruturais as pectinas. As redes de espuma EPE-2x-Gel-1%TiO_2 eficientemente retardou processos típicos do amadurecimento dos mamões, principalmente alteração de cor e redução de firmeza. exibindo elevado potencial para aplicação agroindustrial.

Considerações finais

Esta tese propôs uma nova tecnologia pós-colheita para aplicação em frutos baseada na degradação fotocatalítica de etileno. Os nanocompósitos de hidroxipropilmetilcelulose-TiO_2 e gelatina-TiO_2 exibiram atividade fotocatalítica sobre o etileno. No entanto, nanopartículas de TiO_2 mostraram ser mais dispersas em gelatina do que filme à base de hidroxipropilmetilcelulose, o que contribuiu para a degradação mais rápida do etileno pelo filme de gelatina-TiO_2 contendo 1% m/m de TiO_2 (Gel-1% TiO_2). O uso de redes de espuma de polietileno expandido (EPE) como suporte para o revestimento do nanocompósito Gel-1%TiO_2 melhorou sua atividade fotocatalítica devido ao aumento da área superficial reativa. As redes de espuma EPE revestidas com uma bicamada de Gel-1%TiO_2 exibiram a maior

concentração de etileno degradada por unidade de massa de TiO_2 carregado por unidade de área de superfície EPE iluminada.

O mamão foi um modelo adequado de fruto climatérico para avaliar o desempenho da aplicação *in vivo* de redes de espuma EPE revestidas com gelatina-TiO_2. O amadurecimento dos frutos tratados com fotocatálise foi retardado, sendo a cor e a firmeza os parâmetros fisiológicos mais preservados, o que possivelmente contribuiu para a preservação de compostos antioxidantes e da estrutura da parede celular do fruto. A degradação fotocatalítica do etileno pelas redes de espuma EPE revestidas com gelatina-TiO_2 no estágio inicial de maturação foi essencial para preservar a cor verde e a firmeza da casca do fruto. Indiretamente, a preservação da firmeza do fruto provavelmente retardou o desenvolvimento fúngico observado na superfície do fruto controle.

Com base no papel crítico desempenhado pela rede de espuma EPE revestida com nanocompósito à base de gelatina de TiO_2 no amadurecimento do mamão, espera-se que este novo material também possa ser aplicado para estender a vida útil de outros frutos e possa ser amplamente utilizado como uma tecnologia de pós-colheita de frutos no futuro.

ABSTRACT

Extending fresh food shelf life, such as climacteric fruit, is a challenge for the food industry. This fruit group exhibits an increase in respiration and production of ethylene phytohormone at the beginning of the maturation stage. Both processes accelerate the fruit metabolic activity and its ripening. Although several technologies are applied to fruit preservation, they can require high investment, produce toxic compounds or facilitate undesirable physiological disorders that compromise the fruit sensory and microbiological qualities. These limitations motivated the elaboration of this thesis, which aimed to develop an innovative, low-cost, and sustainable material able to scavenger ethylene without causing physical damages in fruit. The postharvest technology proposed is composed of expanded polyethylene (EPE) foam nets coated with photocatalytic nanocomposite based on gelatin and titanium dioxide (TiO_2) capable of degrading ethylene under UV-A light (λ = 315 - 400 nm). Thus, this thesis was divided into three steps. On the first step, it was studied the different TiO_2 concentration effects (0 -2 wt%) on nanocomposite physicochemical and structural properties based on biopolymer matrices with different hydrophilicity (hydroxypropyl methylcellulose- HPMC and gelatin) in the film form, prepared by casting. The gelatin-TiO_2 films showed more resistance to water, and opacity increase as the TiO_2 incorporated, suggesting better photocatalyst dispersion. On the second step, the HPMC-TiO_2 and gelatin-TiO_2 film photocatalytic activities were tested on ethylene. Gelatin-TiO_2 films containing 1 wt% TiO_2 (Gel-1%TiO_2) showed the highest constant reaction rate (k_{app} = 0.186 ± 0.021 min^{-1}). Therefore, this formulation was used in the EPE foam net coating, which was carried out by immersion. Among the numbers of coatings evaluated (0 – 4), the Gel-1%TiO_2 bilayer on EPE (EPE-2x-Gel-1%TiO_2) was more efficient to degrade ethylene (18.212 ± 1.157 ppmv m^2 $g_{TiO_2}{}^{-1}$) than its film form (13.297 ± 0.178 ppmv m^2 $g_{TiO_2}{}^{-1}$). The 3D geometry of the EPE increased the photocatalytic surface area, improving the nanocomposite performance. On the last step, EPE foam nets coated with gelatin-TiO_2 were tested *in vivo*. Papayas (*Carica papaya* L. cv. 'Golden') were used as a climacteric fruit model and stored under UV-A light at 30 ± 1°C and RH = 85 % for four days. The fruit wrapped in EPE-2x-Gel-1%TiO_2 showed ethylene accumulation 60% less than fruit wrapped in blank EPE, reduction of ethylene production and respiration rates in climacteric peak, fungi visual growth absence, and higher peel green color, pulp yellow color, and firmness preservation. These results show that the material EPE-2x-Gel-1%TiO_2 reduced the autocatalytic ethylene production without causing physiological disorders in papayas. In addition, the environmental ethylene scavenging probably decreased the fruit metabolic activity, delaying enzymatic degradation of pigments (chlorophyll) and structural macromolecules (pectin). Thus, the developed innovative technology efficiently delayed the papaya ripening, displaying high potential for agro-industrial application.

Key-words: Active package. Nanotechnology. Food.

LIST OF FIGURES

LIST OF CHARTS

LIST OF TABLES

LISTA DE ABREVIATURAS E SIGLAS

1-MCP- 1-Methylcyclopropen

AFM- atomic force microscopy

ATR- Attenuated Total Reflectance

C_2H_4- ethylene

$C_{C_2H_4,\max(N)}$- maximum normalized concentration of ethylene degraded

DLS- dynamic light scattering

EB- elongation at break

EPE- expanded polyethylene

EPE-1x-Gel-1%TiO_2- expanded polyethylene foam net coated with a monolayer of nanocomposite based on gelatin and 1 wt%TiO_2

EPE-2x-Gel-1%TiO_2- expanded polyethylene foam net coated with a bilayer of nanocomposite based on gelatin and 1 wt%TiO_2

EPE-4x-Gel-1%TiO_2-expanded polyethylene foam net coated with a tetra-layer of nanocomposite based on gelatin and 1 wt%TiO_2

FTIR- Fourier transform infrared

Gelatin-TiO_2- nanocomposite based on gelatin and titanium dioxide (0 – 2wt%: Gel-0%TiO_2, Gel-0.5%TiO_2; Gel-1.0%TiO_2 and Gel-2.0%TiO_2)

HPMC- hydroxypropyl methylcellulose

HPMC-TiO_2- nanocomposite based on hydroxypropyl methylcellulose and titanium dioxide (0 – 2wt%: HPMC-0%TiO_2, HPMC-0.5%TiO_2, HPMC-1%TiO_2 and HPMC-2%TiO_2)

k_{app}- apparent rate constant

OA- oleic acid

RH- relative humidity

ROS- reactive oxygen species

R_{RMS}- Surface root-mean-squared roughness

SEM- Scanning electronic microscopy

T_g- glass transition temperature

TiO_2- Titanium dioxide

T_m- melting temperature

TS- tensile strength

TSS- total soluble solids

TTA- titratable acidity

UV- ultraviolet irradiation (types: UV-A, UV-B, UV-C)

UV-vis- ultraviolet-visible

WVP- water vapor permeability

$X_{C_2H_4}$- ethylene conversion value

$X_{C_2H_4,max}$- ethylene maximum conversion value

XRD- X-ray diffraction

YM- Young's modulus

θ_{OA}- oleic acid contact angle

SUMÁRIO

CONCEPTUAL DIAGRAM

HYDROXYPROPYL METHYLCELLULOSE-TiO_2 AND GELATIN-TiO_2 PHOTOCATALYTIC NANOCOMPOSITES APPLIED IN FRUIT POSTHARVEST FOR ETHYLENE SCAVENGING

Why?

- Fruit is commodities that contribute to a large part of global food losses due to high perishability.
- TiO_2 photocatalysis is a sustainable technology capable of degrading ethylene, a phytohormone that stimulates fruit ripening.
- Postharvest technologies already applied for fruit preservation can require high investment cost, produce toxic products, and facilitate undesirable physiological disorders that compromise the fruit sensory and microbiological quality.
- Hydroxypropyl methylcellulose (HPMC) and gelatin are non-toxic and sustainable materials (biopolymers) for immobilizing TiO_2 nanoparticles.
- Expanded polyethylene (EPE) foam nets are widely used to protect the fruit against physical damages without influencing their metabolism.
- The three-dimensional EPE foam nets geometry can improve the ethylene photocatalytic degradation, providing a high surface area for the biopolymers-TiO_2 coating deposition.

What has been researched?

- There are no reports in the literature about EPE foam nets coated with biopolymers-TiO_2 nanocomposites for degrading fruit ethylene.
- Until now, there are four reports about biopolymers-TiO_2 nanocomposites applied as ethylene scavengers and only one about their *in vivo* application.
- Most studies about biopolymers-TiO_2 nanocomposites are focused on their antimicrobial potential for food applications.
- Most papers about ethylene photocatalytic degradation report the TiO_2 immobilization into inorganic supports such as borosilicate glass.

Hypothesis:

It is possible to delay the fruit ripening by using EPE foam nets coated with HPMC-TiO_2 and (or) gelatin-TiO_2 nanocomposites as ethylene scavengers.

Scientific methodology:

- HPMC-TiO_2 and gelatin-TiO_2 nanocomposite films containing different TiO_2 concentrations were prepared by casting and physicochemically and structurally characterized.
- Photocatalytic degradation of synthetic ethylene by HPMC-TiO_2 and gelatin-TiO_2 films were studied in a batch system. The most efficient nanocomposite formulation was applied as a coating on EPE foam nets by the dip-coating technique. The ethylene photocatalytic degradation was evaluated according to the number of coating layers.
- EPE foam nets containing the most efficient biopolymer-TiO_2 coating were used for *in vivo* applications. Papayas (*Carica papaya* L. cv. 'Golden') were used as climacteric fruit models and wrapped in EPE foam nets coated with biopolymer-TiO_2. Fruit physiological and physicochemical alterations were studied before and after photocatalysis treatment. The ethylene degradation influence on fruit ripening was evaluated.

Questions answered:

- How did the TiO_2 agglomeration into nanocomposite films influence their physicochemical, structural and photocatalytic properties?
- What was the most efficient loading of HPMC-TiO_2 or gelatin-TiO_2 nanocomposites on the surface of EPE foam nets for degrading ethylene according to the tested conditions?
- Did the biopolymer-TiO_2 coating on the EPE foam nets exhibit better ethylene degradation efficiency than in its film form?
- How did the biopolymer-TiO_2-coated EPE foam nets change the physiological and papaya physicochemical characteristics?

1.INTRODUCTION

The food losses from production to consumption is a global-scale problem. It is estimated that nearly 45% of the total food loss worldwide is directly associated with horticulture (FAO, 2013; SANTOS et al., 2020). Fresh fruit and vegetables are highly perishable, especially climacteric fruit. It exhibits a rapid increase in its respiration rate and autocatalytic ethylene production at the beginning of maturation (CHITARRA; CHITARRA, 2005). Ethylene (C_2H_4) is a gas phytohormone managing expression of genes and enzymes that trigger fruit and vegetable ripening (FABI; DO PRADO, 2019). Thus, the maintenance of their freshness and quality during transportation and storage is one of the biggest challenges for the agribusiness sector.

The most commonly postharvest technologies applied to preserve fruit and vegetables are refrigeration, ethylene inhibition by 1-methyl cyclopropane, modified atmosphere, waxy coating and ethylene oxidation by potassium permanganate ($KMnO_4$) immobilized into absorbent materials. Most of them can require high investment cost, release toxic products and (or) facilitate the development of undesirable physiological disorders in the plant tissue. These disorders involve heterogeneous ripening, unpleasant flavor generation and microbial contamination (ACOSTA LEZCANO FOSCACHES et al., 2012; AN; PAULL, 1990; MANENOI et al., 2007; OLIVEIRA-JR et al., 2006; PATHAK et al., 2017; PAULL et al., 1997). Thus, these technological limitations have motivated the search for alternative, low cost and sustainable preservation methods.

Over the last few years, nanocomposites with photocatalytic properties based on sustainable materials such as biopolymers and titanium dioxide (TiO_2) were developed and tested as active films for degrading ethylene (scavenging materials) and deteriorating microorganisms (antimicrobial materials) on the fruit surface (BALASUBRAMANIAN et al., 2019; BISWAS; CHAKRABORTY; JANA, 2018; HE et al., 2016; KAEWKLIN et al., 2018; MUKHERJEE et al., 2020; SIRIPATRAWAN; KAEWKLIN, 2018; WANG et al., 2019; XIE; HUNG, 2018; XING et al., 2020; ZHANG et al., 2019, 2017). However, studies about *in vivo* application of these materials as fruit ethylene scavengers are scarce and were more focused on antimicrobial activity.

The photocatalytic properties of TiO_2 have already been explored for the degradation of a large variety of organic pollutants (ANI et al., 2018; CHATERJI; KWON; PARK, 2007; KHALID et al., 2017; SINGH et al., 2010; ZENG et al., 2010). The TiO_2 photocatalytic mechanism is based on the chemical attack to a target organic compound from reactive

oxygen species (ROS, $O_2^{\bullet -}$, $HO^{\bullet}$ and $HOO^{\bullet}$). The ROS are produced from electron/hole (e^- /h^+) pairs photogenerated as the TiO_2 is exposed to ultraviolet light (UV, λ = 290 – 400 nm) (FUJISHIMA; ZHANG; TRYK, 2008).

Due to their biodegradability and non-toxicity, food-grade biopolymers are the most used materials as the nanocomposite continuous phase applied in food packages. Especially for fruit application, biopolymers provide exciting characteristics such as gas exchange control (CO_2, O_2 and C_2H_4) and protective barrier against cross-contamination (DEHGHANI; HOSSEINI; REGENSTEIN, 2018; FARRIS et al., 2011). Hydroxypropyl methylcellulose (HPMC) and gelatin are examples of saccharide and protein biopolymers widely used as barrier materials (SHIT; SHAH, 2014). They can form transparent and odorless films and coatings, contributing to preserving food flavors and visual aspect (VALENCIA et al., 2016; WENG; ZHENG, 2015). Thus, their composite association with TiO_2 nanoparticles could provide some advantages. The high transparency of HPMC and gelatin-based films and coatings constitute a promising optical property to ensure the TiO_2 light-harvesting. Furthermore, these biopolymers can play an essential role as TiO_2 immobilizing matrix, hindering its migration from material to food and minimizing its aggregation. The TiO_2 agglomeration causes UV-light scattering, decreasing its photocatalytic performance. (BASSO; DE FÁTIMA PERALTA MUNIZ MOREIRA; JOSÉ, 2018; NAWI et al., 2011; RAMESH et al., 2016a).

In this context, materials providing high surface area could also support the deposition of coatings based on HPMC-TiO_2 or gelatin-TiO_2 to increase the illuminated photocatalytic surface area. One of these materials is the expanded polyethylene (EPE) foam net, which is extensively used as a wrapper to protect the fruit against physical damages (ZANON BARÃO, 2011). Its three-dimensional net geometry does not change fruit gas exchanges and transpiration. It can provide a high surface area to the light irradiation and hinder the TiO_2 nanoparticle migration to the fruit surface. Thus, EPE foam nets coated with HPMC-TiO_2 and (or) gelatin-TiO_2 can be an efficient and innovative nanocomposite design to delay the fruit ripening. This technology design has not been reported in the literature and it is expected that it encourages new advances for the agro-industrial sector and researches directed to the scale-up of this system and this use as an efficient postharvest technology.

1.1 OBJECTIVES

1.1.1 Main objective

This thesis aimed to develop a new ethylene scavenging material design based on expanded polyethylene (EPE) foam nets coated with biopolymer-TiO_2 nanocomposite to delay the fruit ripening.

1.1.2 Specific objectives

a) Preparing the HPMC-TiO_2 and gelatin-TiO_2 nanocomposite films and studying the influence of the TiO_2 concentration on their structural, physicochemical and photocatalytic properties.

b) Studying the ability of HPMC-TiO_2 and gelatin-TiO_2 nanocomposite films to degrade ethylene.

c) Applying the most efficient nanocomposite formulation as a coating on EPE foam nets and evaluating the influence of their loading on ethylene photocatalytic degradation.

d) Performing an *in vivo* application of EPE foam nets coated with photocatalytic nanocomposite using papayas as a climacteric fruit model and studying their physiological and physicochemical changes.

1.2 THESIS OUTLINE

This thesis is structured into one introduction section and six chapters:

Section 1. Introduction

This section presents an overview of problematic issues involving the freshly harvested fruit perishability. Also, it is discussed why biopolymers-TiO_2 nanocomposite films and coatings are a promising postharvest technology.

Chapter 1. Literature Review

In this chapter, physiological aspects managing climacteric fruit ripening, including papayas, are presented, and the limitations of conventional postharvest technologies are highlighted. The TiO_2 photocatalytic properties and their limitations are discussed. Also, a review about TiO_2 application as a fruit ethylene scavenger and an antimicrobial agent is presented.

Chapter 2. Summary of experimental steps

This chapter contains a brief presentation about experimental steps, materials used to synthesize nanocomposites and preparation and characterization methodologies of developed materials. All assays are described in detail in their respective experimental steps (chapters 3, 4 and 5).

Chapter 3. Physicochemical and structural properties of hydroxypropyl methylcellulose - TiO_2 and gelatin-TiO_2 nanocomposite films

In this chapter, the preparation, structural and physicochemical characterization of HPMC-TiO_2 and gelatin-TiO_2 nanocomposite films are presented. It was carried out an investigative study about the dispersion of different TiO_2 concentrations into biopolymer matrices and its implications in their structural and physicochemical properties.

Chapter 4. Photocatalytic properties of hydroxypropyl methycellulose-TiO_2 and gelatin-TiO_2 films and expanded polyethylene foam nets coated with gelatin- TiO_2

This chapter reports the evaluation of photocatalytic properties of HPMC- and gelatin-TiO_2 films and EPE foam nets coated with gelatin-TiO_2 using different methods. Film photocatalytic properties were studied by water contact angle and oleic acid and ethylene degradations. In contrast, photocatalytic properties of EPE foam nets coated with different layers of gelatin-TiO_2 were studied by ethylene degradation.

Chapter 5. Application of gelatin-TiO_2-coated expanded polyethylene on papaya

This chapter reports the application of EPE foam nets coated with gelatin-TiO_2 nanocomposite on papayas (*in vivo*) and the evaluation of physiological alterations and visual fungi growth over their ripening.

Chapter 6. Final conclusions and future researches

This chapter is dedicated to the final remarks, main conclusions and suggestions for future researches.

Chapter 1. LITERATURE REVIEW

This chapter was based on the review article titled "*A review on TiO_2-based photocatalytic systems applied in postharvest of fruits: set-ups and perspectives*", published in the journal *Food Research International* (impact factor (2020): 4.972; https://doi.org/10.1016/j.foodres.2021.110378). According to Elsevier subscription rules, the authors retain the right to include the article in a thesis, provided it is not published commercially.

1.1 PHYSIOLOGICAL ASPECTS INVOLVING THE FRUIT LIFE CYCLE

The fruit life cycle comprises five physiological stages: fertilization, formation, pre-maturation, maturation and senescence (**Figure 1**). After pollination and germination of flowers, seeds and fruit are generated from ovule fertilization and ovary, respectively. The fruit development involves the formation stage and pre-maturation phase (growth and beginning of maturation). The pre-maturation phase is characterized by the flower wilting and intense cell division in the ovary, resulting in a fruit volume extensive increase (CHITARRA; CHITARRA, 2005).

Figure 1 – Physiological stages of fruit not harvested or harvested at the beginning of maturation

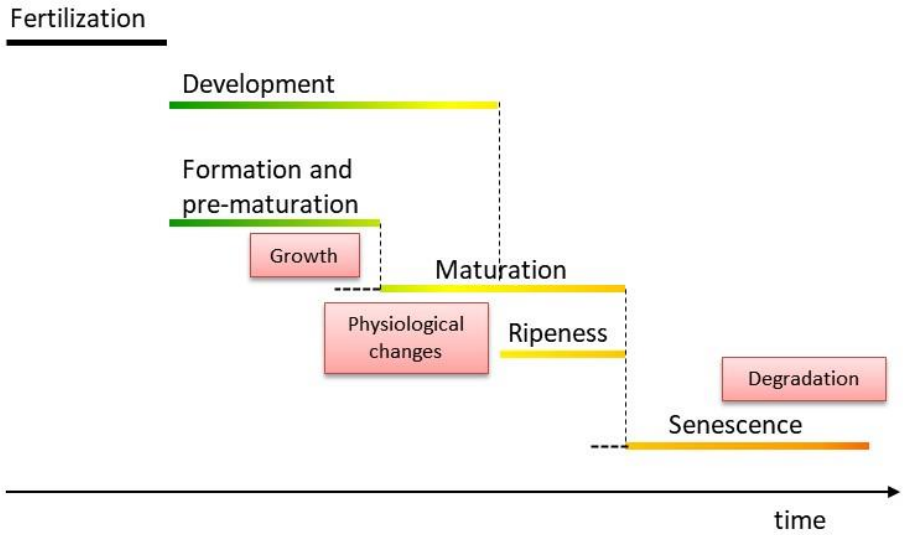

Source: Based on Chitarra & Chitarra (2005).

During the ripeness stage, fruit exhibit several physiological and biochemical alterations highlighting: color change, firmness loss, increase of histological permeability and respiration

rate, ethylene production, macromolecule degradation (carbohydrate and proteins), synthesis and degradation of pigments and organic acids, including phenolic compounds, seed development and wax formation on the fruit surface (RYALL; LIPTON; PENTZER, 1979). At the final of the maturation stage, the fruit reaches its complete ripeness, and chemical degradation reactions are predominant. Compared to the non-matured fruit, the fully ripe fruit shows high sweetness, softness and flavors concentrations. Concentrations of pigments such as anthocyanin and carotenoids also increase, while chlorophyll decrease due to chloroplast degradation (BIALE, 1964).

Then, the fruit reaches the last stage of its life cycle: senescence. In this stage, biochemical ageing reactions replace those from ripening, and the synthesis of compounds in the plant tissue is limited, which can cause dehydration and microbial contamination. These fast biochemical reactions cause plant tissue death (CHITARRA; CHITARRA, 2005).

In the plant tissue, two biochemical events can be highlighted as the fruit ripening primary triggers: the rise of respiration and ethylene production rates (RHODES, 1970). Thus, the fruit respiration patterns and ethylene production are discussed in a special section of this thesis.

1.1.1 Implications of respiration pattern and ethylene production in fruit ripening

During the postharvest life, the plat tissue keeps its metabolic activity. Because of this, the fruit uses its nutrients accumulated during the growth to supply its energy demand. Thus, respiration became the most important fruit physiological process after being harvested. The energy released in this process is used to synthesize molecules and enzymes during its maturation. Fruit respiratory activity affects the balance of carbohydrates, protein, lipids, organic acids, vitamins, minerals, water, and some specific cell wall components such as hemicellulose and pectin. When these alterations are not controlled, the fruit ripeness and senescence are accelerated because of its susceptibility to microbial contamination and dehydration (CHITARRA; CHITARRA, 2005).

During the respiration process, compounds synthesized over photosynthesis are oxidized. This process is used to generate energy (adenosine triphosphate – ATP), CO_2 and H_2O. These products are used to synthesize other vital compounds to maintain the cell metabolism, controlled by the active transport of substances across the plasmatic membrane, ionic exchanges and cell division, growth and development (NELSON; COX, 2014). The

global reaction and aerobic respiration inside the plant cell are summarized and schematized by **equation 1** and in **Figure 2**.

$$C_6H_{12}O_6 + 6O_2 \rightarrow 6CO_2 + 6H_2O + 38ATP \quad (1)$$

Figure 2 - Schematic representation of the plant cell respiration process.

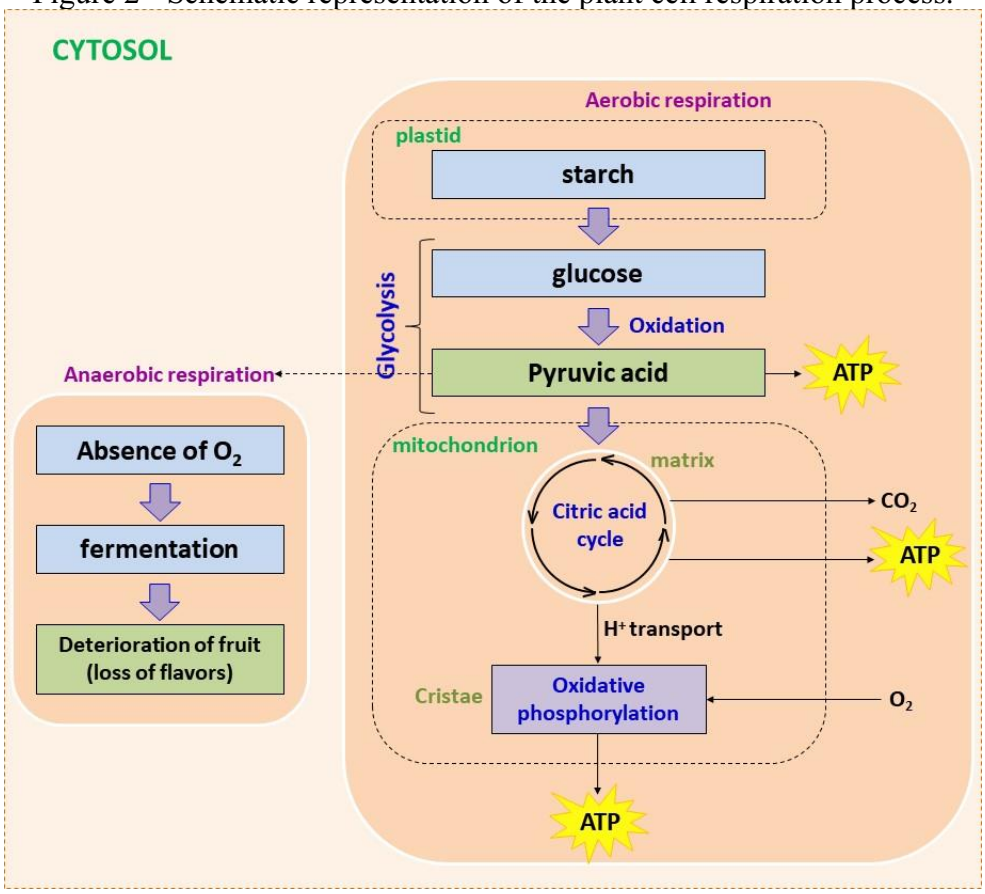

Source: Author.

The respiration process can also occur under oxygen absence (anaerobic conditions) (**Figure 2**), causing the fermentation. In this process, products such as lactic acid and ethanol are generated and can accelerate the deterioration and cause undesirable organoleptic alterations in fruit (NELSON; COX, 2014).

Fruit exhibits different respiratory activity patterns and can be classified into two groups: non-climacteric and climacteric. Non-climacteric fruit displays a decrease in respiration activity over its development and maturation. On the other hand, climacteric fruit shows an accentuated increase in respiration rate at the beginning of ripeness, characterized by the accelerated rise of CO_2 production and reduction of O_2 consumption. The respiration rate increase can be accompanied by an ethylene production increase (CHITARRA; CHITARRA, 2005). Some examples of climacteric fruit are papaya, avocado, peach, melon,

nectarine, plum, apple, banana, mango, pear, tomato and passion fruit (URBANO; PEDRO, 2007).

Therefore, climacteric respiration can be defined as the transition phase between fruit growth and senescence, highlighted by intense O_2 consumption and CO_2 production and fast biochemical changes in plant tissue. These changes are triggered by autocatalytic ethylene production (RHODES, 1970). Different from non-climacteric fruit, climacteric fruit is not ready for consumption when it achieves its physiological maturity. Because of this, climacteric fruit is harvested and starts its ripening process detached from the plant (CHITARRA; CHITARRA, 2005).

The ethylene is the phytohormone responsible for trigging physiological events such as fruit abscission, ripening and senescence (CHITARRA; CHITARRA, 2005). Its biosynthesis starts with the enzymatic conversion of *L*-methionine amino acid in *S*-adenosyl methionine (SAM). A part of SAM is used to synthesize new *L*-methionine molecules, and another part is used to synthesize 1-aminocyclopropanecarboxylic acid (ACC; ethylene precursor). The complete conversion SAM → ACC → ethylene occurs in aerobic conditions, and it is catalyzed by ACC synthase and ACC oxidase enzymes (ZHOU et al., 2020). In climacteric fruit, the intracellular ethylene concentration is low until the initial maturation stage. The increase of intracellular ethylene production stimulates ethylene diffusion from the plant tissue to the external environment until it reaches enough concentration for inducing its autocatalytic production (LELIEVRÈ et al., 1997).

The external environment ethylene molecules bind to membrane proteins (cell receivers) and manage specific genes coordinating the DNA transcription and messenger RNA translation. The synthesis of enzymes that catalyze the fruit ripening biochemical reactions essentially depends on this process (LELIEVRÈ et al., 1997).

1.1.2 Papaya physiology and ripeness

Papaya (*Carica papaya* L.) is one of the most consumed climacteric fleshy fruit worldwide, and it is considered a commodity (ADAMI et al., 2017; FABI; DO PRADO, 2019). In 2019, the global papaya production reached approximately 1.4 million tons, and the tropical countries are the biggest producers. Asian countries lead the production, accounting for 56.6 %, followed by American countries that account for 32.4 %. South America accounts for 13 %. From this, approximately 8.5 % of papayas were produced by Brazil (FAOSTAT, 2019).

One of the most consumed papaya genotypes worldwide is the cv ‘Golden’ (**Figure 3**). Female and hermaphrodite fruit exhibit oval and pyriform shapes, respectively. Both present slightly pinkish pulp at the beginning of their maturation, star-shaped internal cavity, smooth peel, uniform size and an average weight of 450 g (FARIA et al., 2009).

Figure 3 - Morphology of *Carica papaya* L. cv. 'Golden'.

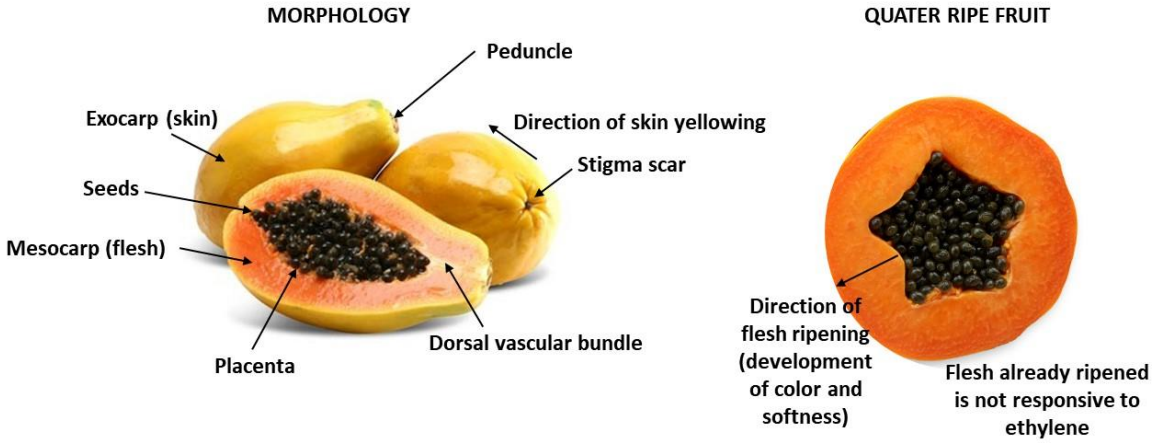

Source: Adapted from Jardim de minas (2019) and Paull et al. (1997).

Papaya is considered a nutritious fruit, rich in fibres, vitamins A and C, flavonoids, carotenoids, lycopene, water and minerals such as calcium and potassium (NEPA - UNICAMP, 2011). Due to papaya to be a climacteric fruit, it exhibits fast physiological changes caused by increased respiration and ethylene production rates at the beginning of the maturation stage (FABI; DO PRADO, 2019). Experimental data of ethylene and CO_2 productions from freshly harvested papaya fruit cv. ‘Golden’ stored at a relative humidity (RH) of 80% and 25°C are presented in **Figure 4** (SOUZA et al., 2014). These data illustrate a typical climacteric pattern characterized by the pre-climacteric, climacteric and post-climacteric periods. These periods correspond to the rising, maximum (climacteric peak) and falling respiration rates (CO_2 production), respectively. In general, the climacteric peak and the highest ethylene production in papaya cv. ‘Golden’ occur synchronously, but it is not a rule.

The ripeness biochemical reactions and the metabolic activity increase for climacteric fruit start early in the pre-climacteric phase. Delaying these reactions is a challenge for the fruit postharvest sector. The main physiological changes observed in papayas during their development and ripeness are summarized in **Table 1**.

Figure 4 - Ethylene (a) and CO_2 (b) production rates of *Carica papaya* L. cv. 'Golden' after being harvested and stored at 80% RH and 25°C.

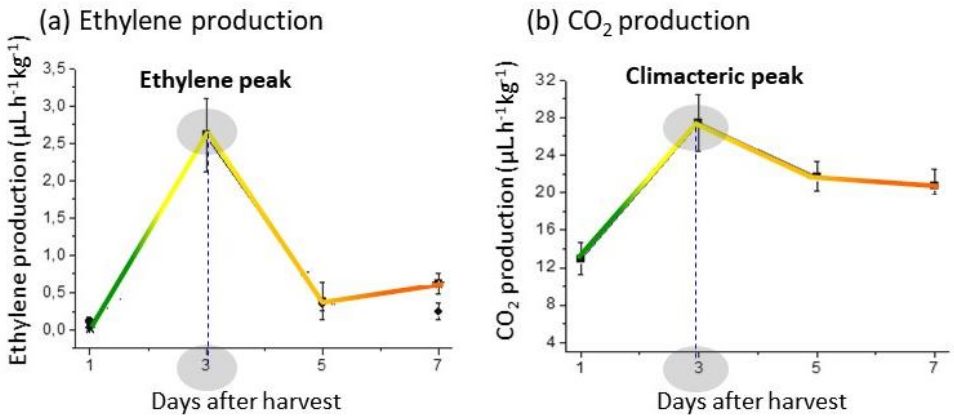

Source: Adapted from Souza et al. (2014).

Table 1 - Main physiological changes of papayas observed during their maturation stage.

Parameters	Physiological changes	Causes
Volume	• Increase of fruit volume (accentuated cellular expansion). • Storage of water during the growth, achieving from 87% to 94% of total fruit weight. • Maximum volume is reached after complete development.	• Formation and growth of pulp (flesh) and seeds. • Lower turgor pressure.
Color	• Color variation of peel from green to orange. • Color variation of pulp from white to orange. • Rising of yellow strips on the peel.	• Enzymatic degradation of chlorophyll. • Synthesis of carotenoids. • Climacteric period (increased respiration and ethylene production rates).
Total Soluble solids (TSS)	• Increase of TSS and sweetness. • TSS content increases until the papaya peel is 80% yellow in covering.	• Papaya does not have enough starch supply to increase its sweetness after being harvested. • Glucose, fructose and saccharose are the main carbohydrates that compose papaya TSS, and they are stored in the fruit before being harvested. • Increase of saccharose and decrease of glucose and fructose contents over the maturation stage. • Enzymatic hydrolysis of saccharose to the glucose and fructose at the final of the maturation stage.
Acidity	• Decrease of the pulp acidity (malic and citric acids). • Slight decrease of acidity near papaya peel.	• Malic and citric acids are the acids present in papaya in equivalent proportion. • Decrease of malic and citric acid concentrations in the pulp due to their dilution caused by water storage and tissue expansion during the growth. • Enzymatic hydrolysis of pectin to the galacturonic acid.
Firmness	• Slow firmness loss at the beginning of the maturation stage (40 – 50% of yellow peel) and fast firmness loss until complete fruit ripening.	• Enzymatic degradation of pectin from peel and expression of genes related to the consistency loss.

Source: Based on Martins; Costa (2003).

The firmness loss and color change are the most perceptible physiological changes during the papaya maturation stage (SOUZA et al., 2014). Peel color change can indicate the maturation stage and adequate papaya harvest time (**Chart 1**).

Chart 1 - Classification of papaya maturation stage as to its peel and pulp colors.

Maturation stages		Variation of peel and pulp colors
0		**Peel:** 100% green, from dark-green to light-green (at the beginning of the physiological maturity). **Pulp:** from white to light-yellow with or not some slightly pinkish regions.
1		**Peel:** 1% - 15% yellow, 1 almost imperceptible yellow strip. **Pulp:** from white to light-yellow (near peel) and moderate-yellow (near placenta).
2		**Peel:** 15% - 25% yellow, 2 highlighted yellow strips. **Pulp:** moderate-yellow near peel and red-orange near the placenta.
3		**Peel:** 25% - 50% yellow, 3 or 4 highlighted yellow strips from stigma scar to the peduncle. **Pulp:** almost imperceptible white-yellow layers near the peel and red-orange near the placenta.
4		**Peel:** 50% - 75% yellow. **Pulp:** completely red-orange flesh.
5	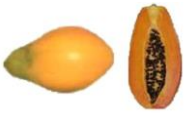	**Peel:** 75% - 100% yellow. **Pulp:** completely red-orange flesh.

Source: Based on CEAGESP (2003), Martins; Costa (2003) and Basulto et al.(2009).

When papayas achieve their maximum ripeness degree, characterized by the climacteric peak, they begin the senescence (post-climacteric phase). In this stage, papayas exhibit a drastic firmness loss, production of undesirable flavors, nutritional loss and high susceptibility to microbial cross-contamination and physical damage (MARTINS; COSTA, 2003). Among the most undesirable papaya postharvest diseases, it can be highlighted Anthracnose. This disease consists of rotting both peduncle and peel and internal infections caused by the fungus *Colletotrichum gloesporioides*. This fungus can attack papayas during any stage of their life cycle by remaining in a latent state. They develop preferably during the papaya maturation stage (TRINDADE et al., 2000).

1.2 POSTHARVEST TECHNOLOGIES COMMONLY APPLIED FOR FRUIT PRESERVATION

The most used technologies for preserving fruit are refrigeration (GARCIA-BENITEZ; MELGAREJO; DE CAL, 2017), ethylene inhibitors (PATHAK et al., 2017), controlled and modified atmosphere (WILSON et al., 2019), waxy coatings (LI et al., 2018) and ethylene absorbent materials (OLIVEIRA-JR et al., 2006). These technologies decrease the fruit metabolic activities (respiration; ethylene production) and (or) provide an additional barrier against cross-contamination. However, the implementation cost for some of these technologies is expensive, and they can cause undesirable sensorial alterations in some fruit species, including papayas (ACOSTA LEZCANO FOSCACHES et al., 2012; AN; PAULL, 1990; MANENOI et al., 2007; OLIVEIRA-JR et al., 2006; PAULL et al., 1997).

1.2.1 Refrigeration

The adequate refrigeration temperature of fruit and vegetables will vary according to the fruit species (5 – 20 °C), being the respiration rate increased by the temperature increase. Temperature and RH are controlled at values near minimum condition tolerated by the fruit aiming to decrease its respiration rate and suppress its climacteric peak (BIALE, 1964).

In general, plant tissues present normal metabolism at the temperature and RH ranges of 25 °C – 35 °C and 80 % - 95 %. The application of temperatures lower than lower critical temperature or higher than upper critical temperature tolerated by a determined fruit can cause chilling or accelerating its metabolism. Simultaneously, the RH values lower than the minimum and higher than the maximum RH values tolerated by fruit can cause excessive transpiration (water loss) and fungi development, respectively (CHITARRA; CHITARRA, 2005).

Papaya is a tropical fruit and sensitive to cold. Its lower critical refrigeration temperature varies from 9 °C to 12 °C, and its adequate RH differs from 85 % to 95 % depending on its maturation stage, genotype and environmental conditions of production (ALMEIDA et al., 2006; FARIA et al., 2009). Papaya is susceptible to cold injuries when stored at very low temperatures and heterogeneous ripening (blotchy ripening), accompanied by increased ethylene sensitivity after the refrigeration. RH lower than 85 % can cause wrinkling and brightness loss of papaya peel, whereas RH higher than 95 % favors the fungal growth (AN; PAULL, 1990; NAZEEB; BROUGHTON, 1978; PAULL et al., 1997).

The biggest challenge of fruit refrigeration is storing different species in the same chamber under the same conditions. Sometimes, using a single postharvest technology can be unfeasible, which requires a combination of different technologies. In addition, refrigerated transportation requires a high implementation cost (ACOSTA LEZCANO FOSCACHES et al., 2012).

1.2.2 Controlled and modified atmosphere and waxy coating

The controlled atmosphere extends the fruit postharvest life controlling the O_2 and CO_2 concentrations in the storage chamber. Its basic principle consists of increasing the CO_2 concentration and reducing the O_2 concentration. On the other hand, the modified atmosphere does not control the O_2 and CO_2 concentrations in the environment. The fruit is packaged in plastic film, whose headspace is filled with certain O_2 and CO_2 concentrations that vary over fruit storage. This variation is caused by fruit respiration rate and gas diffusions that depend on storage time, temperature, film permeability, and gas concentration in the headspace (CHITARRA; CHITARRA, 2005). The atmosphere modification inside the package is determined by the interaction between three processes: fruit respiration, gas diffusion through the fruit and gas film permeability. Both postharvest technologies can be combined with refrigeration, and N_2 is used as inert gas to remove O_2 from the environment. Waxy coatings such as carnauba wax are also used to decrease gas exchanges between fruit and the environment. Also, they provide additional protection to the fruit against cross-contamination and water loss (HAGENMAIER; SHAW, 1992).

The atmospheric air is composed of 21 v/v % O_2 and 0.03 v/v % CO_2. Both O_2 reduction and CO_2 increase in an environment decrease the respiration rate and inhibit enzymes that catalyze the ethylene biosynthesis. However, a lower O_2 critical concentration, O_2 absence (anaerobiosis) and high CO_2 concentrations favor plant tissue fermentation. This process is featured by producing ethyl alcohol and acetaldehyde, generating undesirable flavors (CALBO; MORETTI; HENZ, 2007; MARTINS; COSTA, 2003).

Studies using controlled atmosphere for papayas showed that the fruit stored at 10 °C and 90 – 95 % RH, O_2 and CO_2 concentrations lower than 2 v/v % and higher than 10 v/v %, respectively, exhibit physiological disorder, heterogeneous ripeness and flavor alteration (KADER, 1997; MARTINS; DE RESENDE, 2013). Faria et al. (2009) also affirm that the modified atmosphere implementation can also require high costs.

1.2.3 Inhibitors and absorbent materials of ethylene

The most widely used fruit ethylene inhibitor is the gas 1-Methylcyclopropene (1-MCP). When applied in fruit, 1-MCP binds irreversibly to the ethylene receptors located on the cell membrane. Thus, ethylene molecules are not able to manage the gene expression and enzymatic syntheses. However, cells can reorganize and form new ethylene receptor sites (BRACKMANN et al., 2013). Besides, 1-MCP is unstable in solutions, which can cause undesirable alterations in the fruit such as heterogeneous and very slow ripeness, internal reddening in nectarines and peaches, chilling in citric fruit and increase of susceptibility to the diseases in avocado, mango and papaya (PATHAK et al., 2017). The 1-MCP application can also require the use of supplementary postharvest technologies (WATKINS, 2006).

Some studies about the 1-MCP application in papayas (cv. 'Golden') revealed that 1-MCP controlled the ripeness of the fruit containing up to 10 % of yellow peel. Fruit containing 10% - 25% of yellow peel exhibited a rubbery aspect after ripening, and that containing more than 25% of yellow peel did not have its ripeness affected by the 1-MCP (MANENOI et al., 2007; SOUZA et al., 2009).

Concerning the ethylene absorbent materials, the potassium permanganate ($KMnO_4$) is incorporated into porous materials as an ethylene oxidizing agent, including packages for papayas (OLIVEIRA-JR et al., 2006). However, some $KMnO_4$ characteristics make unfeasible the long-term storage of the fruit that produces high ethylene concentration (PATHAK et al., 2017). The fast saturation of $KMnO_4$ and its conversion to manganese oxide (MnO_2) and potassium hydroxide (KOH) during ethylene oxidation to CO_2 and H_2O highlight its need for constant replacement and its potential toxicity when it is in contact with fruit (KELLER et al., 2013).

The limitations of these postharvest technologies have motivated the search for alternative, low cost and sustainable technologies to delay the fruit shelf life. One of these technologies is heterogeneous photocatalysis.

1.3 HETEROGENEOUS PHOTOCATALYSIS AS POSTHARVEST TECHNOLOGY

Heterogeneous photocatalysis is an advanced oxidative photochemical process in which chemical reactions are accelerated by photoactivated semiconductor catalysts (solid phase).

When photoactivated, catalysts generate reactive oxygen species (ROS) capable of oxidizing other molecules (liquid or gas phase) (PELAEZ et al., 2012).

One of the most widely used catalysts in food preservation is titanium dioxide (TiO_2). The possibility of degrading volatile organic compounds (VOCs) such as ethylene and microorganisms at environmental temperature and under atmospheric pressure have motivated studies about its application to delay the fruit ripening (HE et al., 2016; PATHAK et al., 2017; ZHANG et al., 2019).

1.3.1 Titanium dioxide (TiO_2)

1.3.1.1 Characteristics and applications

The amphoteric oxide TiO_2 is a suitable semiconductor for food industry applications due to low toxicity, eco-friendly, low cost, abundance, biological and chemical inertness (CHAWENGKIJWANICH; HAYATA, 2008; ETACHERI et al., 2015; GOUDARZI; SHAHABI-GHAHFARROKHI; BABAEI-GHAZVINI, 2017a; MANEERAT; HAYATA, 2006). It has a high redox potential and good thermal and chemical stability compared with other photocatalysts (ETACHERI et al., 2015; NAWI et al., 2011).

TiO_2 has three polymorphic crystalline structures: anatase, rutile and brookite, which exhibit tetragonal, tetragonal and orthorhombic geometries. Regarding activity and stability, anatase is the most photocatalytically active phase, and it is thermally metastable. Rutile is the most thermally stable phase, and it has an intermediary photocatalytic activity. Finally, brookite is the least photocatalytically active phase, and it exhibits the highest thermal stability(CHEN et al., 2008; ETACHERI et al., 2015; JOSÉ et al., 2012). Generally, pure anatase nanoparticles or anatase/rutile nanoparticles mixtures are used as photocatalysts (OHNO et al., 2001).

Figure 5 - Polymorphic structures of titanium dioxide.

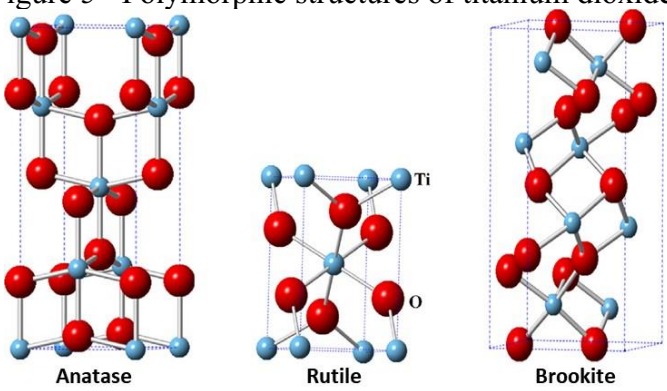

Source: ETACHERI et al. (2015), with permission.

TiO_2 has been used to degrade several types of pollutants as organic dyes (AHMED, 2016; BERGER et al., 2010; NAWI et al., 2011), improve the sunscreen protection against solar radiation (VAN DER MOLEN et al., 1998), increase the paper whiteness (MANDA; BLOK; PATEL, 2012), provide self-cleaning and anti-fogging properties to other materials (BERGER et al., 2010), disinfect water (NAN et al., 2010), inactive microorganisms (OTHMAN et al., 2014; ZHANG et al., 2017; ZHU; CAI; SUN, 2018a) and degrade fruit ethylene (HUSSAIN et al., 2011; KAEWKLIN et al., 2018; LOURENÇO et al., 2017a; ZHANG et al., 2019).

1.3.1.2 Photocatalytic oxidation mechanism

1.3.1.2.1 TiO_2 photocatalysis general mechanism

Semiconductor materials exhibit valence and conduction bands filled with electrons and holes, respectively. These bands are separated by an energy gradient called band gap (MILLS; LE HUNTE, 1997). The TiO_2 energy gap depends on its polymorphic phase structure being 3.2, 3.0 and 3.4 eV its values for the anatase, rutile, and brookite phases, respectively (ETACHERI et al., 2015).

The adsorbate global degradation mechanism by TiO_2 photocatalysis and its steps are schematically shown in **Figure 6**. When TiO_2 is exposed to the UV-light wavelengths ≤ 387.5 nm, the energy ($h\nu$) from photons irradiated under its surface is absorbed and causes the migration of electron from the valence band to the conduction band (e^-_{CB}). Thus, a positive hole is generated in the valence band (h^+_{VB}) (I) (FUJISHIMA; ZHANG; TRYK, 2008). Electron-hole pairs (e^-_{CB}/ h^+_{VB}) can be trapped as lattice defect sites (Ti^{3+} e O^-), and dissipate

energy by recombination (II), or start redox reactions with chemical species (H_2O, HO^-, O_2) (III, IV, V) adsorbed on the photocatalyst surface. In the redox reactions, the electron (e_{CB}^-) reduces the oxygen molecule to the superoxide radical ($O_2^{\bullet-}$) (IV), which can react with H^+ generating hydroperoxyl radical ($HOO^\bullet$) (VI). $HOO^\bullet$ that can be reduced to H_2O_2 (VII) (FUJISHIMA; ZHANG; TRYK, 2008; PELAEZ et al., 2012). The hole (h_{VB}^+) can react with hydroxide ion (HO^-) or water molecules (H_2O) generating hydroxyl radical ($HO^\bullet$) (III).

Finally, these reactive oxygen species (ROS), $O_2^{\bullet-}$ (VIII), $HO^\bullet$ (V) e $HOO^\bullet$ (IX), can attack and degrade several types of organic molecules, microorganisms and virus adsorbed on the TiO_2 surface both in the aqueous phase and gas phase (AHMED, 2016; DALRYMPLE et al., 2010a; KARTHIKEYAN; NITHYA; JOTHIVENKATACHALAM, 2017; PELAEZ et al., 2012; SINGH et al., 2010; XIE; HUNG, 2018; XING et al., 2020).

Figure 6 - Schematic representation of a general mechanism for TiO_2 photocatalysis.

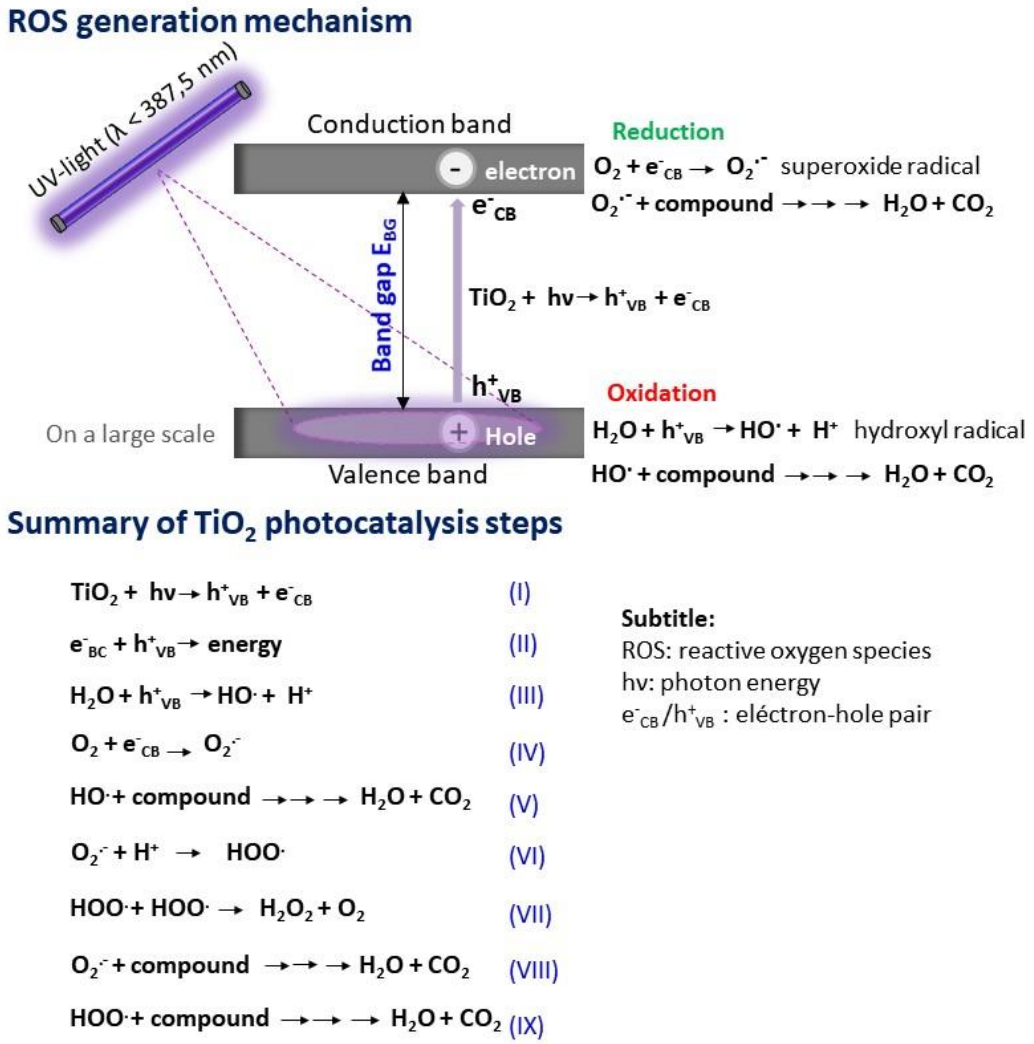

Source: Fonseca et al. (2021b), with permission.

1.3.1.2.2 Ethylene photocatalytic oxidation mechanism

Several studies have been reported the entire ethylene mineralization to CO_2 and H_2O by TiO_2 photocatalysis. However, there is no consensus about the molecular mechanism and reaction pathways that form several intermediate compounds from ethylene degradation (KELLER et al., 2013; TANAKA et al., 2006; YAMAZAKI; TANAKA; TSUKAMOTO, 1999). The global reaction of ethylene molecule degradation is presented in **equation 2**.

$$C_2H_4 + 3O_2 \rightarrow 2CO_2 + 2H_2O \quad (2)$$

Several authors proposed detailed mechanisms for this process using TiO_2 as a photocatalyst. Yamazaki et al. (1999) suggested that ethylene molecule reacts with a hydroxyl radical ($HO^{\bullet}$) before its reaction with oxygen (O_2), forming a carbon centered radical (C_2H_4OH). This radical would be a precursor of peroxyl radical ($RO^{\bullet}$), which will conduce to the production of carbonic dioxide (CO_2). Park et al. (2001) proposed that ethylene is firstly degraded to the carbonic monoxide (CO) and after CO is converted to CO_2 in the presence of excess O_2. Tanaka et al. (2006) performed ethylene photocatalytic oxidation tests using porous films based on polyvinylpyrrolidone (PVP) and TiO_2 incorporated into adsorbents (silica and zeolite) as catalysts. Authors pointed formic acid (CH_2O_2), formaldehyde (CH_2O) and carbonate ions (CO_3^{2-}) as intermediates from the ethylene oxidation mechanism. Lastly, Hauchecorne et al. (2011) observed alterations in the dipole momentum of ethylene molecules in contact with TiO_2. They proposed a new hypothesis for the ethylene double bond (C=C) cleavage (**Figure 7**). Ethylene is mainly oxidized by HO● radicals, forming coordinately bonded formaldehyde, bidentate formaldehyde, formic acid and CO_2 and H_2O. Equations of the mechanism proposed by Hauchecorne et al. (2011) were available in **Appendix A**.

Figure 7 - Reactional mechanism proposed for the ethylene photocatalytic oxidation by TiO_2.

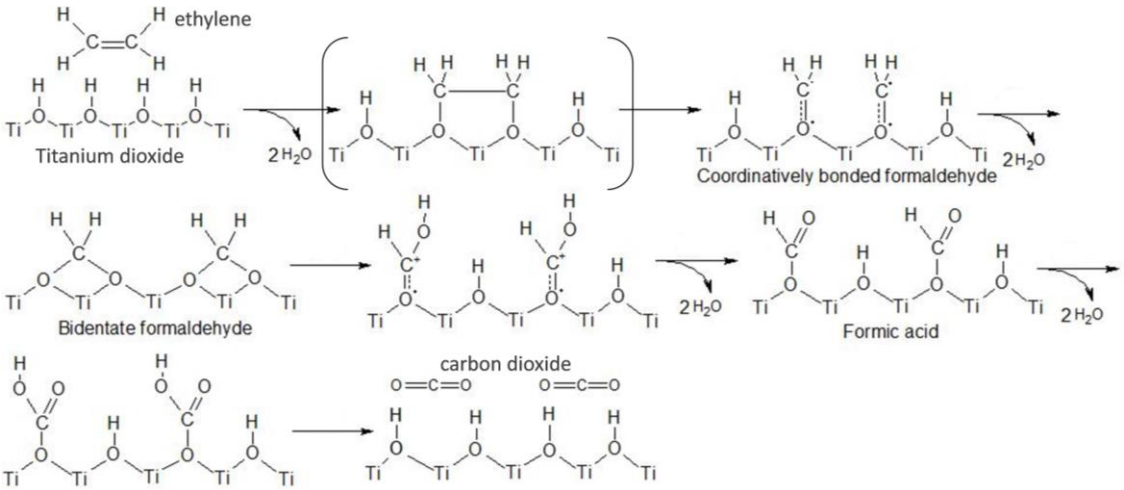

Source: Fonseca et al. (2021b), with permission.

1.3.1.2.3 Factors affecting the ethylene degradation by TiO_2 photocatalysis

Photocatalysis efficiency depends on the photogeneration of e_{CB}^{-}/h_{VB}^{+} pairs for enough time to ensure the ROS formation. Thus, several factors related to the TiO_2 preparation, application and physicochemical properties affect its photocatalytic activity. It depends on: reactor design, initial degraded adsorbate concentration, reaction temperature, relative humidity, radiation wavelength, incident radiation intensity, gas flow and residence time and TiO_2 loading, particle size and aggregation, doping, lattice defects, synthesis method and polymorphism (phase purity, composition, crystallinity). (PATHAK et al., 2017). The TiO_2 crystalline forms are more photoactive than amorphous TiO_2 due to the lower recombination probability (ETACHERI et al., 2015). The following topics present a discussion about the factors affecting the ethylene photocatalytic degradation assisted by TiO_2.

Initial concentration and flow rate of ethylene

Lin et al. (2014) and Lin, Weng, & Chen (2014) considered that the ethylene degradation rate by TiO_2 photocatalysis depends strongly on its initial concentration process. According to the authors, the ethylene photocatalytic oxidation rate increases linearly for initial ethylene concentration values between 0 and 200 ppmv. On the other hand, initial ethylene concentrations between 500 ppmv and 900 ppmv tend to constant photocatalytic oxidation rate. It occurs because the amount of ethylene adsorbed on the photocatalyst surface

increases as its concentration increases. Thus, all available active sites are occupied, and no further increase in the reaction rate would be measured.

The contact period between ethylene molecules and the photocatalytic surface should also be sufficient to ensure gas adsorption. In the gas recycling or continuous flow photocatalytic systems, a good gas flow choice is based on optimizing the shortest gas residence time for the highest gas-solid adsorption rate. (BASSO; DE FÁTIMA PERALTA MUNIZ MOREIRA; JOSÉ, 2018; EINAGA et al., 2015; LIN et al., 2014; PATHAK et al., 2017). The control of ethylene concentration and flow for fruit applications is a challenge due to the changes in the gas volume produced by the fruit. Thus, it is essential to know the physiological changes of the fruit over its ripening.

Temperature, relative humidity and O_2 supply

The increase of temperature, relative humidity (RH) and O_2 supply can also improve the TiO_2 photocatalytic activity (MANEERAT et al., 2003; PARK et al., 2001). The temperature rise accelerates water desorption on the TiO_2 surface due to the breaking of water-TiO_2 hydrogen bonds (MANEERAT et al., 2003; OBEE; HAY, 1997). Thus, more active sites on the TiO_2 surface are available to interact with the gas adsorbate. Ethylene molecules are nonpolar and interact with TiO_2 by induced dipole-induced dipole forces, which are weaker than hydrogen bonds. Therefore, ethylene molecules are more poorly adsorbed on the TiO_2 surface than water molecules (OBEE; HAY, 1997). This phenomenon was reported by Fu et al. (1996), Yamazaki; Tanaka; Tsukamoto (1999), Hussain et al. (2011), Westrich et al. (2011) and Pathak et al. (2019).

The increase in RH and O_2 supply favors ROS generation (hydroxyl and superoxide) (PARK et al., 2001). Water molecules can also fill vacancy defects, avoiding their filling by electrons (LIN; WENG; CHEN, 2014; LIN et al., 2014). However, high RH values (> 90 %) cause competition between H_2O and C_2H_4 molecules for adsorption. In this case, water molecules are preferentially adsorbed on the photocatalyst (LIN; WENG; CHEN, 2014; LIN et al., 2014). Considering the application of TiO_2 photocatalysis in fruit postharvest, two issues about RH values should be highlighted. Although the TiO_2 photocatalytic efficiency decreases at RH > 90 %, lower RH values are not recommended for fruit applications because of its excessive transpiration. RH values higher than 95 % can cause fungal growth in fruit (NAZEEB; BROUGHTON, 1978). Thus, the fruit should be stored at RH levels between 90 % and 95 %. The second issue is related to the excessive O_2 concentration in the reactor,

which increases and decreases the CO_2 and CO concentrations, respectively (LEE et al., 2015). A sealed reactor containing high CO_2 concentration or low O_2 concentration can cause fruit fermentation and ethyl alcohol and acetaldehyde accumulation (SANCHIS et al., 2007).

Some studies reported that the low water vapor content favors the ethylene photocatalytic oxidation by TiO_2 (HUSSAIN; RUSSO; SARACCO, 2011; WESTRICH et al., 2011). Other authors have also already reported a synergistic effect between high O_2 concentrations and low RH values on the ethylene degradation increase (LIN et al., 2014; PATHAK et al., 2019). In this case, the high O_2 concentration can supply the low ROS generation caused by the RH decrease.

Source and intensity of light

The volatile organic compound photocatalytic oxidation can be accelerated by increasing the irradiated light intensity to generate more ROS (EINAGA et al., 2015; NIELSEN et al., 2015). However, highly powerful lamps can overheat the reactor, which can cause physical damages to fruit such as scalds (KELLER et al., 2013). Thus, the photocatalytic system design should ensure that the radiation distribution covers the largest reactive surface area uniformly (DA COSTA FILHO et al., 2019).

The UV-radiation wavelength (λ) used to photoactive the TiO_2 is limited to values less than 387.5 nm because of the widest TiO_2 anatase band gap (3.2 eV). Anatase is the most TiO_2 crystalline phase (DALRYMPLE et al., 2010a; MANEERAT; HAYATA, 2008). The UV-radiation is classified in three wavelength ranges: UV-A (λ = 315-400 nm), UV-B (λ = 280-315 nm) and UV-C (λ = 200-280 nm) (PAULINO-LIMA et al., 2016). UV-A radiation is the most exciting source used to perform photoreactions catalyzed by TiO_2 that exhibits the highest light harvest under λ = 387.5 nm (LI et al., 2011). Studies reported by Chang et al. (2013) showed that ethylene is mostly photolyzed and photo-oxidized under UV-C radiation at two conjugated wavelengths: λ = 254 nm and 185 nm. The wavelengths λ = 254 nm and 365 nm, individually applied, exhibited an unexpressive ethylene degradation.

TiO_2 particle size

The TiO_2 photocatalytic performance also is affected by the size and tendency to aggregation of its particles loaded on the reactor walls or supports (PATHAK et al., 2017). TiO_2 particle aggregation causes scattering of the light, decreasing its absorption and

photocatalytic reaction efficiency (BASSO; DE FÁTIMA PERALTA MUNIZ MOREIRA; JOSÉ, 2018). Thus, the light scattering limits applications of both TiO_2 suspensions impregnated on the inorganic supports, *e.g.* borosilicate, and TiO_2 powder incorporated into organic supports, *e.g.* biopolymers (FONSECA et al., 2020; NAWI et al., 2011). The use of nanosized TiO_2 as a photocatalyst improves its photocatalysis efficiency. The reduction of TiO_2 particle size increases the ratio between particle surface area exposed to the radiation and its volume (LIAN; ZHANG; ZHAO, 2016; SIRIPATRAWAN; KAEWKLIN, 2018).

TiO_2 doping

Doping is the combination of TiO_2 with compounds or elements to increase the electrical charge separation and (or) extend its light absorption ability to visible light (λ = 400 – 700 nm). Metallic and non-metallic elements are used as dopants for TiO_2 to generate new energy levels in its band gap from electrons photogenerated and transferred from the valence band. This amplification of TiO_2 light absorption to the visible light spectrum improves the electrons trapping and inhibits the e_{CB}^{-}/ h_{VB}^{+} pair recombination (ZALESKA, 2008). Some examples of metallic and non-metallic elements commonly used for doping TiO_2 are Pt, Ag, Fe, Cu, Ni and N, C, S, B, F, respectively (SHAYEGAN; LEE; HAGHIGHAT, 2018). Specifically, for degrading ethylene, TiO_2 doped with N, C and Bi_2WO_6 have already been used to increase its degradation rate (LIN; WENG; CHEN, 2014; LIN et al., 2014; WANG et al., 2019).

1.3.1.2.4 Inactivation mechanism of microorganisms by TiO_2 photocatalysis

TiO_2 photocatalysis can also be used to inactive and destroy microorganisms such as bacteria, fungi, algae, and viruses. However, the photocatalytic mechanism causing cell death has not been fully clarified (RAMESH et al., 2016b). One considered hypothesis (**Figure 8**) is that the ROS oxidize organic compounds from the microorganism cell membrane, mainly phospholipids. This reaction disrupts the cell membrane, provoking protein amino acids and DNA oxidations, chemical modifications and cell membrane permeability disorganization, including the K^+ ion leakage (DALRYMPLE et al., 2010b; ZHU; CAI; SUN, 2018b). Therefore, TiO_2 photocatalysis has been used as a nonthermal technology to inactivate food microorganisms (ZHU; CAI; SUN, 2018b).

Figure 8 - Schematic representation of the microbial cell destruction mechanism by TiO_2 photocatalysis.

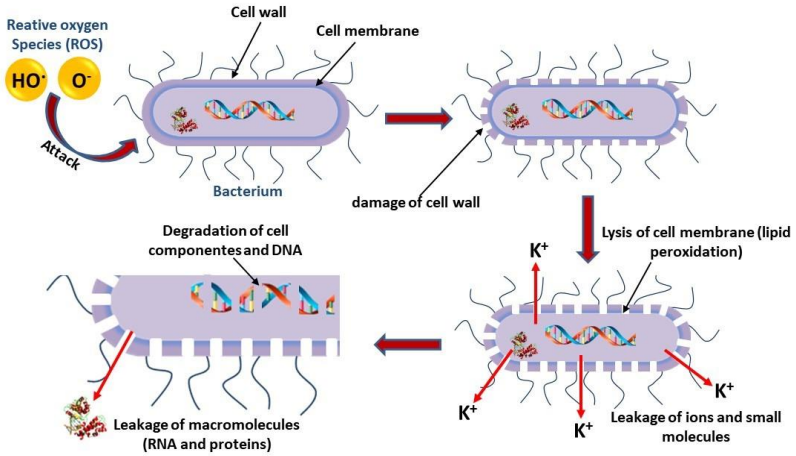

Source: Fonseca et al. (2021b), with permission.

1.3.2 Systems based on TiO_2 photocatalysis used to preserve fruit

Two reaction systems based on TiO_2 are most used to degrade ethylene from fruit. The first system is the TiO_2 nanoparticle impregnation on inorganic supports such as borosilicate and quartz. The inorganic supports can be the reactor walls or separated supports fixed on the reactor (**Figure 9**) (BASSO; DE FÁTIMA PERALTA MUNIZ MOREIRA; JOSÉ, 2018). The photocatalytic reactors can exhibit different designs and operation modes such as batch, batch with gas recycling and continuous flow (BASSO; DE FÁTIMA PERALTA MUNIZ MOREIRA; JOSÉ, 2018; HUSSAIN et al., 2011; PATHAK et al., 2019). The second system is the nanocomposites based on polymers and TiO_2 as the continuous and dispersant phases. These materials are mainly used as films and coatings, and the photocatalytic reactions to degrade ethylene are generally conducted in batch systems (**Figure 10**) (KAEWKLIN et al., 2018; MANEERAT; HAYATA, 2008; MUKHERJEE et al., 2020; XING et al., 2020; ZHANG et al., 2019). Due to their versatility, polymers-TiO_2 nanocomposites are also used to degrade contaminant microorganisms on the fruit surface (ZHANG et al., 2017).

Figure 9 - Schematic representation of ethylene degradation by TiO_2 immobilized into inorganic support using a continuous flow photocatalytic system.

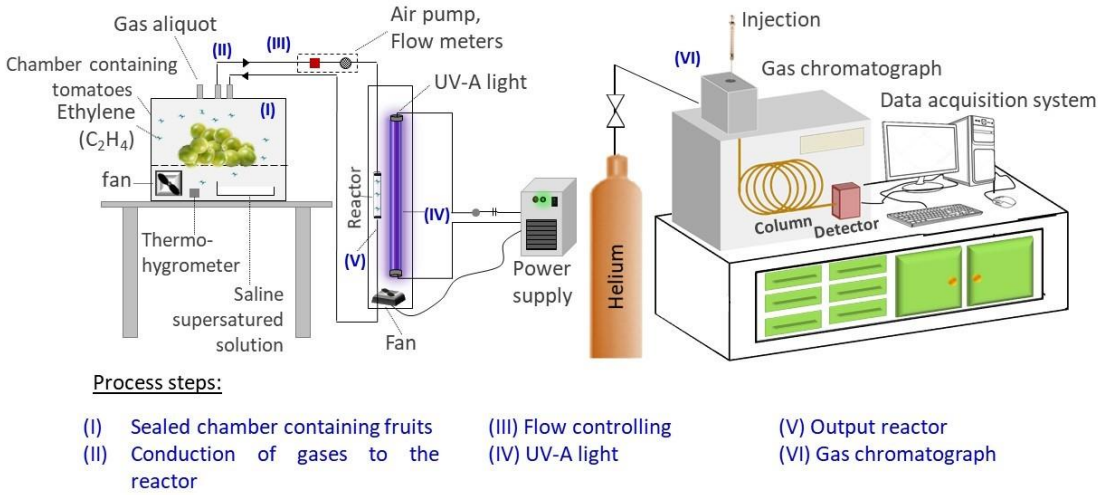

Source: Fonseca et al. (2021b), with permission.

Figure 10 - Schematic representation of ethylene degradation by polymers-TiO_2 nanocomposites films using a photocatalytic batch system.

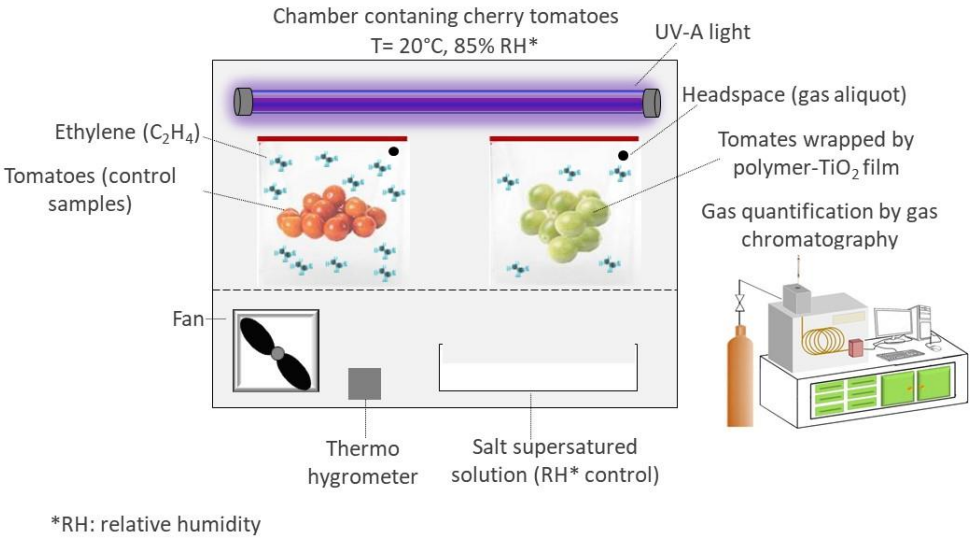

Source: Fonseca et al. (2021b), with permission.

In the photocatalytic system shown in **Figure 9**, ethylene from fruit stored in a sealed chamber (I) is pumped toward the reactor containing support or walls impregnated with dried TiO_2 suspension (II). The photocatalyst surface is under UV-light (IV). The gas flow and residence time are controlled for maximizing the ethylene adsorption on the photocatalyst active sites. The remaining ethylene and products from its degradation (V) can be recycled and quantified by gas chromatography (VI). The most significant limitation of this system is the light scattering caused by the TiO_2 agglomeration. The TiO_2 film thickness rise intensifies the photocatalytic surface opacity, harming the light harvest and generating excessive TiO_2

consumption (BASSO; DE FÁTIMA PERALTA MUNIZ MOREIRA; JOSÉ, 2018). Besides, the complete inorganic support cleaning and photocatalyst recovering after its impregnation become infeasible.

In contrast, polymers-TiO_2 nanocomposite films (**Figure 10**) neither support a large amount of TiO_2 nor require expensive immobilizing materials. Polymers are cheap in comparison with other materials and versatile, allowing the application of polymers-TiO_2 nanocomposites to delay the fruit ripening not only as films and coatings (KAEWKLIN et al., 2018; SIRIPATRAWAN; KAEWKLIN, 2018; XING et al., 2020) but also nanofibers (LI et al., 2012; ZHU et al., 2019a) and pellets (YANES et al., 2015). These nanocomposites can act as antimicrobial, ethylene scavenging material or both. Synthetic polymers as polyethylene (ALTAN; YILDIRIM, 2012; KAMRANNEJAD et al., 2014; YANES et al., 2015) and polypropylene (MANEERAT; HAYATA, 2008), and biopolymers as chitosan (KAEWKLIN et al., 2018; SIRIPATRAWAN; KAEWKLIN, 2018; XING et al., 2020; ZHANG et al., 2017, 2019) and starch (FEI et al., 2013; GOUDARZI; SHAHABI-GHAHFARROKHI; BABAEI-GHAZVINI, 2017b; LIU et al., 2015; OLEYAEI et al., 2016; WANG et al., 2019) are among the most used materials for this purpose.

1.3.2.1 Nanocomposites based on biopolymers and TiO_2 to postpone fruit ripening

The preference for biopolymers as TiO_2 supports increased over the last twelve years, according to papers presented in **Table 2**.

Table 2 – Main researches in polymer-TiO_2 nanocomposites with potential application in fruit postharvest published between 2008 and 2021.

Polymers, blends and composites	TiO_2 composition (size)	Nanocomposite form (method)	Target (SC[1], ED[2], AA[3])	Fruit application	References
PP[4]	100% anatase (7 nm) and 100% anatase (5µm)	Coating on oriented PP[4] film (bar coating)	ED[2]	Tomato	(MANEERAT; HAYATA, 2008)
WPI[6]	100% anatase (< 20 nm)	Film (casting)	SC[1]	-	(ZHOU; WANG; GUNASEKARAN, 2009)
WPI[6]	98.5% Anatase	Film (casting)	SC[1]	-	(LI et al., 2011)
PVP[10]	Anatase/rutile mixture (7 – 12.6 nm; pore size) and 80% anatase/20% rutile (21 nm)	Nanofiber (electrospinning)	ED[2]	-	(LI et al., 2012)
PP[4]	SEBS-*g*-MA[11]/ Silane-coated TiO_2 [100% anatase (20 nm)]	Granule (injection molding)	AA[3]	-	(ALTAN; YILDIRIM, 2012)
PCL[12]/starch	100% anatase (60 nm)	Film (compression molding)	SC[3]	-	(FEI et al., 2013)
PE[13], LLDPE[14]	TiO_2 nanotubes with organic modification	Powder (polymerization by precipitation)	AA[3]	-	(YANES et al., 2015)
SSPS[15]	100% anatase (< 20 nm)	Film (casting)	AA[3]	-	(TEYMOURPOUR; ABDORREZA; NAHIDI, 2015)
High-amylose starch/PVA[16]	99.8% anatase (60 nm)	Film (casting)	AA[3]	-	(LIU et al., 2015)
PVA[16]/xylan	100% anatase (1.27 µm) and 100% rutile (1.27 µm)	Film (casting)	SC[1]	-	(REN et al., 2015)
Potato starch	80% anatase/20% rutile (21 nm)	Film (casting)	SC[1]	-	(OLEYAEI et al., 2016)
Gelatin (shark skin)	Anatase/ -	Film (casting)	SC[1], AA[3]	-	(HE et al., 2016)
Chitosan	TiO_2 nanoparticles (50 - 80 nm)	Film (casting)	AA[3], cellular substance linkage, visual food preservation	Grape	(ZHANG et al., 2017)
Wheat starch	Anatase (20 nm)	Film (casting)	SC[1]	-	(GOUDARZI; SHAHABI-GHAHFARROKHI; BABAEI-GHAZVINI, 2017b)
PLA[17], PCL[12], Cellulose acetate	80% anatase/20% rutile (21 nm)	Film (casting)	AA[3]		(XIE; HUNG, 2018)
Chitosan	80% anatase/20% rutile (21 nm)	Film (casting)	ED[2], AA[3]	Cherry tomato	(KAEWKLIN et al., 2018; SIRIPATRAWAN; KAEWKLIN, 2018)
CMC[18]/Na-MTT[19]	100% anatase (< 20 nm)	Film (casting)	SC[1]	-	(FATHI ACHACHLOUEI; ZAHEDI, 2018)

Table 2- Main researches in polymer-TiO_2 nanocomposites with potential application in fruit postharvest published between 2008 and 2021 (continuation).

Polymers, blends and composites	TiO_2 composition (size)	Nanocomposite form (method)	Target (SC[1], ED[2], AA[3])	Fruit application	References
Sage seed gum	80% anatase/20% rutile (21 nm)	Hydrogel (Magnetic stirring, sonication)	Rheo-mechanical characterization	-	(AMIR et al., 2018)
Chitosan/anthocyanin	Anatase/rutile mixture (60 nm)	Film (casting)	ED[2], AA[3], pH-sensitiveness	-	(ZHANG et al., 2019)
Starch	TiO_2 [80% anatase/20% rutile (21 nm)] doped with Bi_6WO_6	Film (casting)	ED[2]	-	(WANG et al., 2019)
PAN[20]	100% anatase; titanium (IV) oxide	Nanofiber (electrospinning)	ED[2]	Bananas	(ZHU et al., 2019a)
κ-carrageenan/ xanthan/gellan gum	Anatase/rutile mixture (21 nm)	Film (casting)	AA[3]	-	(BALASUBRAMANIAN et al., 2019)
Chitosan	TiO_2 modified by sodium laurate (30 nm)	Coating for fruit (dip-coating)	AA[3], enzymatic activity, fruit physicochemical properties	Mango	(XING et al., 2020)
Sodium caseinate/ guar gum/ Cumin essential oil	99% anatase/ -	Film (casting)	AA[3]	-	(MAHMOOD et al., 2020)
Polyacrylate/ PEG[22]	TiO_2 nanorod (30 – 100 nm) co-doped with N and F (nanoparticles)	Polymer-coated doped nanoparticle (Core-shell; *in situ* polymerization in a reverse micelle) (dip coating)	AA[3]	Tomato	(BISWAS; CHAKRABORTY; JANA, 2018; MUKHERJEE et al., 2020)
PLA[17]/ lycopene	TiO_2 nanoparticles, 99% of purity	Film (casting)	AA[3]	-	(ASADI; PIRSA, 2020)

[1] Structural characterization. [2] ED: ethylene degradation. [3] AA: antimicrobial activity. [4] Polypropylene. [5] Ultraviolet. [6] Whey protein isolate. [7] Ultraviolet type A. [8] Ultraviolet type B. [9] Ultraviolet type C. [10] Polyvinylpyrrolidone. [11] Maleic anhydride grafted styrene-ethylene-butylene- styrene. [12] Poly(ε-caprolactam). [13] Polyethylene. [14] Polyethylene-1-octadecene. [15] Soluble soybean polysaccharide. [16] Polyvinyl alcohol. [17] Polylactic acid. [18] Carboxymethylcellulose. [19] Sodium montmorillonite. [20] Polyacrylonitrile. [21] Hydroxypropyl methylcellulose. [22] Poly (ethylene glycol).

Source: Adapted from Fonseca et al. (2021b).

This preference is due to characteristics of several biopolymers such as high biodegradability, non-toxicity, inexpensiveness, food-grade and good properties for forming films, coatings and fibers (DEHGHANI; HOSSEINI; REGENSTEIN, 2018; YOUSSEF; EL-SAYED, 2018). Biopolymers can be derived from carbohydrates, proteins and lipids (GOSWAMI et al., 2018). Hydroxypropyl methylcellulose (HPMC) and gelatin (**Figure 11**) are food-grade and inexpensive saccharide and protein biopolymers widely used to form films and coatings (SHIT; SHAH, 2014) and could be used to immobilize TiO_2.

Figure 11 - Chemical structure of hydroxypropyl methylcellulose and gelatin.

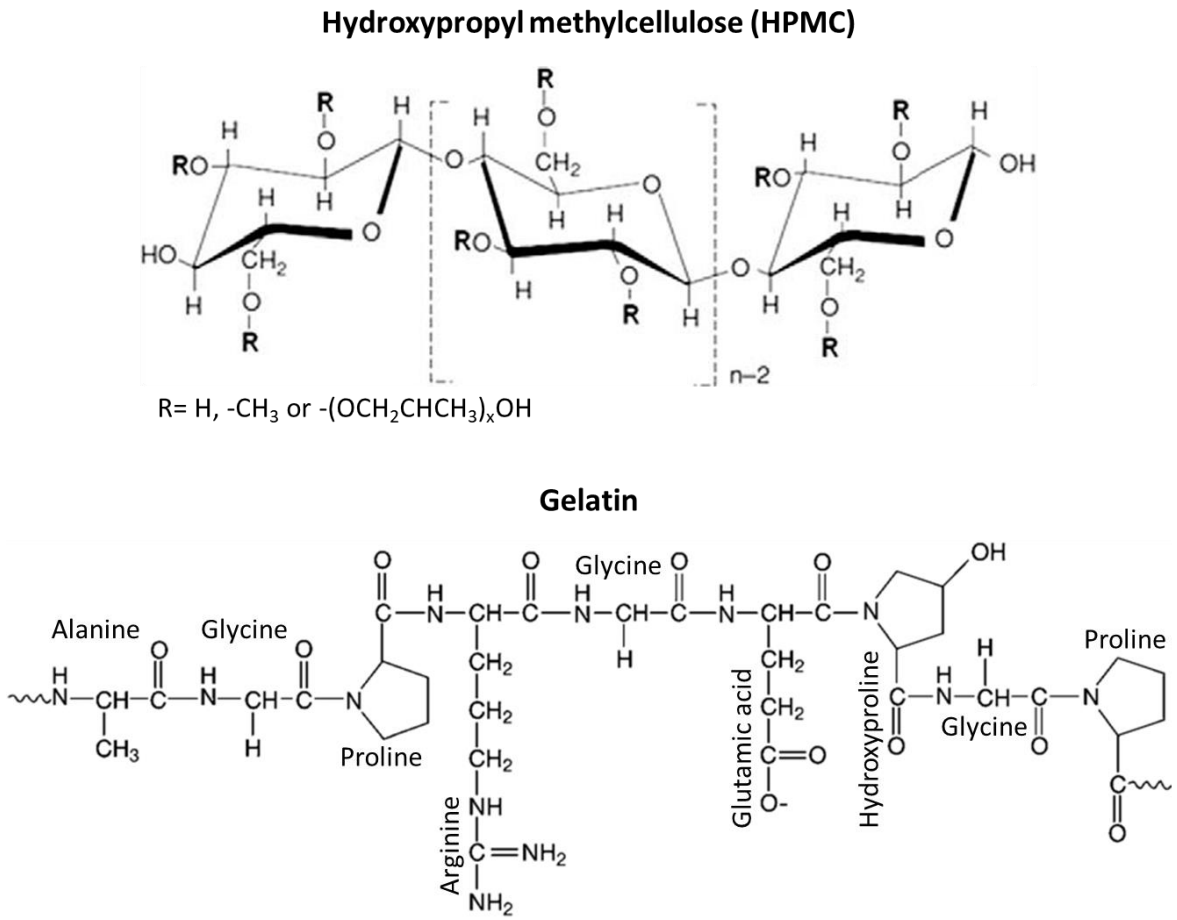

Source: Adapted from Fahs et al. (2010) and Sahoo et al. (2015).

HPMC is a cellulose derivative and exhibits a non-ionic structure, high water solubility and moderate solubility in organic solvents (DOW, 2012; SAKATA; SHIRAISHI; OTSUKA, 2006). Also, HPMC has good stability in solution (pH 2 - 13) and forms films with good elasticity and resistance to the oleic compounds compared with other biopolymers (DOW, 2012; FAHS et al., 2010). In contrast, gelatin is a denatured fibrous protein produced

from controlled thermal hydrolysis of collagen, a protein extracted from animal bones, tissues and skin (MIHALY COZMUTA et al., 2015; NUR HAZIRAHA; ISAB; SARBONA, 2016). The gelatin side chains are composed of hydrophobic amino acids, and their stability depends on the pre-treatment received. Gelatin type A displays an isoelectric point between pH 8 and 9, and it is obtained under acid conditions. In contrast, gelatin type B shows an isoelectric point between pH 4 and 5, and it is produced in an alkaline medium (GOMEZ-GUILLEN et al., 2011). As well as HPMC, gelatin forms transparent and odorless films and coatings, which are exciting characteristics for food applications (VALENCIA et al., 2016; WENG; ZHENG, 2015).

Among papers presented in **Table 2**, the recent researches from Kaewklin et al. (2018) and Xing et al. (2020) illustrate the biopolymers-TiO_2 nanocomposite functionalities for fruit. Kaewklin et al. (2018) used chitosan-TiO_2 films containing 1 wt % TiO_2 to delay the cherry tomato ripening. The fruit was wrapped in nanocomposite films, packaged in low-density polyethylene pouches and stored at 20°C and 85 % RH for 14 days. Tomatoes wrapped in nanocomposite films showed a lower ethylene production rate, and their ripeness was delayed. Over the whole storage period, their firmness loss was lower than control fruit, and there was a decrease in their respiration rate during the climacteric period. Moreover, their soluble solid content, lycopene and ascorbic acid concentrations were lower than control fruit and the green color was predominant.

Xing et al. (2020) also prepared chitosan-based nanocomposites for fruit application. However, the TiO_2 nanoparticles were modified using sodium laurate as disperse phase, and two modified TiO_2 concentrations were used to delay mango ripening (1 wt % and 3 wt % TiO_2, polymer). Mangoes were coated with chitosan-TiO_2 dispersions, and physiological changes and antimicrobial effects were studied. Nanocomposite coatings containing 1 wt % TiO_2 were more effective for reducing the fungal and bacterial growth on the mango surface than those containing 3 wt % TiO_2. It occurred probably due to better dispersion of 1 wt % TiO_2 into chitosan-based films than 3 wt % TiO_2. Both nanocomposites delayed the fruit climacteric peak for the fifteenth day of storage. They also decreased the weight loss and total soluble solids of mangoes compared to control. It can be attributed to the reduction of gas exchanges promoted by the nanocomposite coating. Lastly, nanocomposite coatings containing 3 wt % TiO_2 exhibited higher efficiency for preserving the fruit firmness and flavonoids. Probably, the highest TiO_2 concentration minimized the photo-oxidation of fruit pigments and enzymatic degradation.

Finally, other papers focused on the TiO_2 support development from blends and composites using a wide variety of materials such as poly(ε-caprolactam) (PCL), starch, polyvinyl alcohol (PVA), xylan, carboxymethylcellulose (CMC), montmorillonite, κ-carrageenan, xanthan, sodium caseinate, gellan and guar gums, polyacrylate, and poly (ethylene glycol) (FATHI ACHACHLOUEI; ZAHEDI, 2018; FEI et al., 2013; LIU et al., 2015; MAHMOOD et al., 2020; MUKHERJEE et al., 2020; REN et al., 2015).

Finally, active compounds such as anthocyanin (ZHANG et al., 2019) and cumin essential oil (BALASUBRAMANIAN et al., 2019) have been incorporated into the biopolymer-TiO_2 nanocomposites to provide them multifunctional properties. In addition, the TiO_2 structure has also been modified by adding dopants to potentialize the photocatalytic ability of these nanocomposites (ALTAN; YILDIRIM, 2012; MUKHERJEE et al., 2020; WANG et al., 2019; XING et al., 2020; YANES et al., 2015).

1.3.2.2 Limitations of photocatalytic and structural properties of biopolymers-TiO_2 nanocomposites and improvement strategies

Studies about biopolymers-TiO_2 photocatalytic properties have shown that the persistent TiO_2 agglomeration decreases their ethylene degradation efficiency (SIRIPATRAWAN; KAEWKLIN, 2018; WANG et al., 2019). Siripatrawan & Kaewklin (2018) reported the development of chitosan-TiO_2 nanocomposite films with different TiO_2 concentrations (0, 0.25, 0.5, 1 and 2 wt% related to the polymer mass) to degrade synthetic ethylene (25°C at 85% RH) and microorganisms as *S. aureus*, *E. coli*, *S. Typhimurium*, *P. aeruginosa*, *Aspergillus* e *Penicillium*. The authors observed a significant increase in ethylene degradation as the TiO_2 content increased from 0 to 1 wt%. The ethylene degradation rate stagnation for the films containing 2 wt % TiO_2 was attributed to the low photocatalyst dispersion in the chitosan matrix. The nanocomposite films containing 1 wt% TiO_2 also showed higher antimicrobial activity against *S. aureus* and *E. Coli* than chitosan blank films.

In a previous paper, Li et al. (2011) investigated possible limitations in the electron-hole pairs (e^-_{CB}/ h^+_{VB}) and ROS generation from TiO_2 nanoparticles incorporated into films based on whey protein isolate (WPI) by fluorescence spectroscopy. Authors supposed that electron transported from excited amino acids, tyrosine (Y) and tryptophan (W), present in the WPI matrix filled positive holes (h^+_{VB}) of TiO_2 excited structure (**Figure 12**). Associated with TiO_2 nanoparticles agglomerates, this electron transport problably caused the fluorescence quenching in the films as the TiO_2 concentration increased from 0.25 to 2 wt% related to the

polymer. An opposite effect was reported by Zhang et al. (2019) for chitosan-anthocyanin-TiO_2 nanocomposites. Incorporating anthocyanin extract into chitosan-TiO_2 nanocomposites resulted in a synergistic effect with TiO_2 to degrade ethylene and microorganisms. The antioxidant character of the anthocyanin facilitated interfacial electron transfer and ROS generation.

Figure 12 - Schematic representation of photocatalytic activity and fluorescence quenching of low concentrations (≤ 0.25 wt%) (a) and high concentrations (> 0.25 wt%) (b) of TiO_2 nanoparticles incorporated into whey protein isolate-based films. W: tryptophan, Y: tyrosine.

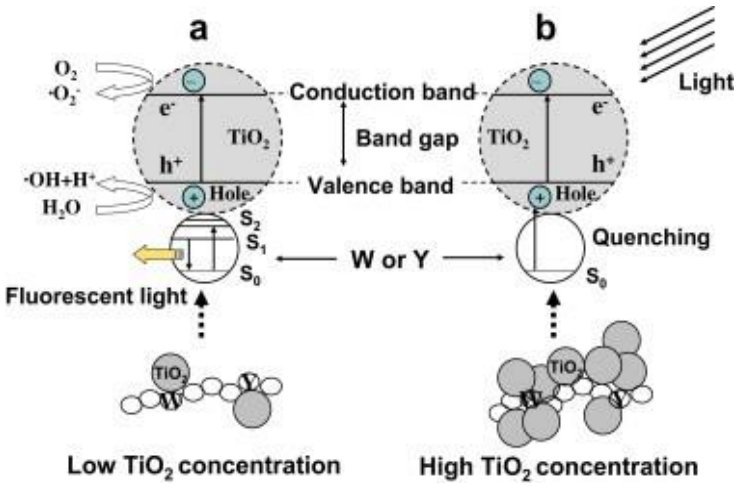

Source: Li et al. (2011), with permission.

Wang et al. (2019) proposed to improve the nanocomposite activity by synergistic action between two photocatalysts. One of them is characterized by a wide band gap (TiO_2), and the other by a narrow band gap (Bi_2WO_6, bismuth tungstate). In association, these materials can be an efficient way to minimize the recombination probability and extend the TiO_2 absorption to visible light. Bi_2WO_6-TiO_2 nanoparticles were synthesized by the solvothermal method, immobilized into starch-based films and used to degrade ethylene at 25 °C and 75 – 90 % RH. Results showed that the association between these photocatalysts overcame their limitations when individually immobilized in the starch matrix. This synergic action potentialized ethylene photocatalytic degradation. It was also noticed that there was an increase both in the ethylene degradation rate constant and ethylene degradation efficiency as the Bi_2WO_6-TiO_2 concentration increased from 0 to 4 wt % related to the polymer. Nanocomposites containing 5 wt % Bi_2WO_6-TiO_2 showed a decrease in their photocatalytic activity. It was attributed to the light scattering caused by the excess photocatalyst in the matrix.

Additionally, the biopolymers-TiO_2 mechanical properties have also shown to be negatively affected by TiO_2 agglomeration, as reported by Goudarzi et al. (2017), Li et al. (2011), Siripatrawan and Kaewklin (2018) and Zhou et al. (2009). TiO_2 heterogeneous dispersion into the biopolymer damages the film network microstructure and its mechanical weakening (LI et al., 2011). In this context, reinforce additives can be used to improve mechanical properties of these nanocomposites since biopolymer-based films and coatings have a natural mechanical fragility even when added of plasticizers (AZEREDO; ROSA; MATTOSO, 2017; BERGO; SOBRAL, 2007; GOSWAMI et al., 2018; NOORBAKHSH-SOLTANI; ZERAFAT; SABBAGHI, 2018). Fathi Achachlouei and Zahedi (2018) used sodium montmorillonite nanoclay (Na-MTT) to minimize the carboxymethylcellulose (CMC)-TiO_2 film mechanical weakness caused by TiO_2 incorporation. Results showed that the films added of 1 wt% TiO_2 and 5 wt% Na-MTT exhibited the highest resistance to tensile strength.

From these researches, it is observed that TiO_2 also tends to agglomerate into biopolymer-based films affecting their photocatalytic and mechanical properties. This characteristic is not a rule, but it is an important issue that should be considered to amplify the fruit application of these systems to a pilot scale. One possible alternative to improve the photocatalytic activity of biopolymers-TiO_2 nanocomposites would be to use them as a coating on high surface area materials. It can provide a better nanocomposite adhesion, TiO_2 light harvest and ethylene adsorption. The expanded polyethylene (EPE) foam nets are examples of these materials for fruit applications. EPE foam nets are commercial materials widely used to protect the fruit against physical damages (ZANON BARÃO, 2011). Beyond the high surface area, EPE foam nets do not alter the fruit gas exchanges due to their mesh design. They are mechanically resistant, inexpensive, and they do not interact with fruit surface.

EPE foam nets can also improve the immobilization of TiO_2 nanoparticles avoiding or hindering their migration to the fruit. The possible toxicity of metal nanoparticles due to their small size and interactions with cells is still intensively discussed (FRIEHS et al., 2016).

1.3.2.3 Differences between food-grade TiO_2 and photocatalyst TiO_2: possible toxicity

The use of TiO_2 by the food, pharmaceutics and cosmetics sectors is regulated. The possible harmfulness of its micro and nanoscale particles to human health has stimulated studies about its toxicity when inhaled, ingested, spontaneously released from coating or

freely discarded in the environment. Although TiO_2 is considered a low-toxicity material, there is still no concise study about harmful health effects caused by the inhalation, ingestion or contact with TiO_2 particles (DUDEFOI et al., 2017; FRIEHS et al., 2016).

Food-grade TiO_2 (E171 or CI 77891) is used as a white pigment (color additive) without nutritional contribution. In 1966, its use was approved in the United States by the Food and Drug Administration (FDA), and in 1969 it was approved in Europe by the European Union based on Codex Alimentarius of Food and Agriculture Organization (FAO, 2018; ROPERS et al., 2017).

TiO_2 E171 comprises micro and nanoparticles of both anatase and rutile crystalline phases with a heterogeneous size distribution (300 – 400 nm) and an average size of 110 nm. These particles absorb wavelengths (λ) higher than 395 nm, and less than 36 % of them contain at least one of their dimensions lower than 100 nm (WEIR et al., 2012). These characteristics limit the TiO_2 E171 application as a photocatalyst because of the light scattering on its particle surface. This same irradiation scattering causes the whiteness effect on the food surface (WEIR et al., 2012).

Photocatalytic applications require smaller crystalline TiO_2 nanoparticles due to their high surface area. It ensures adequate light absorption and adsorbate adsorption (FRIEHS et al., 2016). TiO_2 P25 Evonik Degussa Corporation (80/20 of anatase/rutile, 21 nm) and TiO_2 Hombikat UV100 (pure anatase, 10 nm) are examples of efficient commercial photocatalysts (EVONIK INDUSTRIES, 2015; SACHTLEBEN CHEMIE GMBH, [s.d.]).

Dudefoi et al. (2017) studied the toxic effect of two types of food grade TiO_2 (E171-1 and E171-6a) and one non-food-grade photocatalyst TiO_2 (P25 Evonik Degussa Corporation) on bacterial strains from the human intestine. E171-1 and E171-6a particles were identified as pure anatase containing a maximum of 17 % and 21 % of particles smaller than 100 nm. In contrast, TiO_2 P25 was identified as a mixture of anatase/rutile (85/15) phases containing nanoparticles with an average size of 25 nm. Results showed no significant decrease of intestinal microbiota exposed to the TiO_2 concentrations from 100 to 250 ppm, equivalent to the ingestion of 12 candies containing different types of TiO_2 in their composition. However, accumulative effects from TiO_2 P25 chronic ingestion still need to be evaluated.

Proquin et al. (2017) obtained contrary results for the TiO_2 toxicological tests using human intestine cells. Micro and nanoparticles of TiO_2 E171 were able to generate radical species that caused oxidative stress to the cells and DNA potential damages. Weir et al. (2012) and Bachler; Von Goetz & Hungerbuhler (2015) reported a TiO_2 E171 daily ingestion limits of 0.2 – 0.7 $mg_{TiO_2} kg_{body\ weight}$ for the American adult population and 1

$mg_{TiO_2} kg_{body\ weight}$ for the both British and Germanic adult populations. According to Occupational Safety and Health Administration (OSHA), the occupational exposition to the TiO_2 was considered out of risk for the inhalation levels of powder lower than 15 $mg_{TiO_2} m^{-3}_{dust}$ (STEFANIAK; HOOVER; NANOTECHNOLOGY, 2011).

1.4 CONSIDERATIONS ABOUT ART STATE

Several papers about biopolymers-TiO_2 nanocomposites that aim the fruit application were presented in **Table 2** (section 1.3.2.1). Most of them focused on the antimicrobial properties of biopolymers-TiO_2 nanocomposites. However, few papers have performed direct application (*in vivo*) of these materials on fruit (KAEWKLIN et al., 2018; MANEERAT; HAYATA, 2008; MUKHERJEE et al., 2020; XING et al., 2020; ZHANG et al., 2017; ZHU et al., 2019a) and few biopolymers in composite association with TiO_2 were evaluated as ethylene scavengers. Hydroxypropyl methylcellulose and gelatin have not been evaluated for this purpose by other authors. Most importantly, the fruit physiological changes caused by biopolymers-TiO_2 nanocomposite application as ethylene scavenger and antimicrobial material were not completely understood. Several gaps should be filled, especially to demonstrate the biopolymers-TiO_2 application during the fruit transportation and storage. Besides, EPE foam nets coated with biopolymers-TiO_2 nanocomposites has not been reported, and they could be used to preserve fruit against physical damages and postpone its ripening. These considerations stand out the biopolymers-TiO_2 nanocomposites as a rising technology for the fruit postharvest that deserves to be more explored.

Chapter 2.SUMMARY OF EXPERIMENTAL STEPS

Experimental steps of this thesis are summarized in this chapter. This thesis comprises:

1- (Chapter 3) The preparation and structural characterization of HPMC-TiO_2 and gelatin-TiO_2 nanocomposite films containing different TiO_2 concentrations and the study about the influence of TiO_2 nanoparticle dispersion on film properties.

2- (Chapter 4) The evaluation of synthetic ethylene degradation ability from HPMC-TiO_2 and gelatin-TiO_2 films and EPE foam nets coated with the nanocomposite formulation exhibiting the highest efficiency to degrade ethylene.

3- (Chapter 5) The application of EPE foam nets coated with HPMC-TiO_2 or gelatin-TiO_2 application on papayas as ethylene scavengers and the study about their physiological and physicochemical changes.

Chart 2 – Thesis experimental steps.

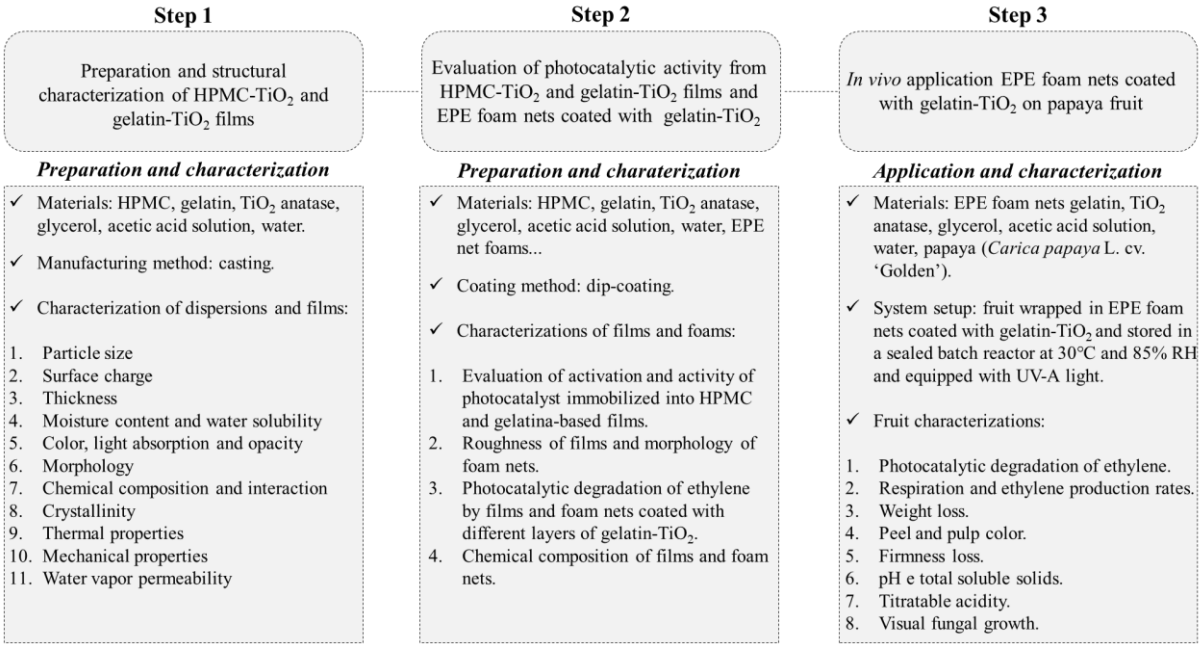

Subtitle:
HPMC: hydroxypropyl methylcellulose; EPE: expanded polyethylene.

Source: Author.

Chapter 3.PHYSICOCHEMICAL AND STRUCTURAL PROPERTIES OF HYDROXYPROPYL METHYLCELLULOSE- TiO_2 AND GELATIN-TiO_2 NANOCOMPOSITE FILMS

This chapter reports the first thesis experimental phase of this thesis: the preparation and physicochemical and structural characterizations of hydroxypropyl methylcellulose-TiO_2 (HPMC-TiO_2) and gelatin-TiO_2 nanocomposite films.

From this step, it was written the first research paper, titled "*Hydroxypropyl methylcellulose-TiO_2 and gelatin-TiO_2 nanocomposite films: preparation and structural properties*", published in the *International Journal of Biological Macromolecules* (impact factor (2020): 5.162; https://doi.org/10.1016/j.ijbiomac.2019.11.082). According to Elsevier subscription rules, the authors retain the right to include the article in a thesis, provided it is not published commercially.

3.1 INTRODUCTION

Several papers reported that the efficient photocatalytic activity of nanocomposites based on titanium dioxide (TiO_2) and biopolymers, such as chitosan (KAEWKLIN et al., 2018; SIRIPATRAWAN; KAEWKLIN, 2018; XING et al., 2020; ZHANG et al., 2017, 2019), gelatin (HE et al., 2016), starch (OLEYAEI et al., 2016; WANG et al., 2019) and whey protein (LI et al., 2011), exhibit potential application for fruit preservation.

The TiO_2 homogeneous dispersion into immobilizing supports is essential for its performance (BASSO; DE FÁTIMA PERALTA MUNIZ MOREIRA; JOSÉ, 2018; SIRIPATRAWAN; KAEWKLIN, 2018), and the biopolymer-TiO_2 nanocomposite structural organization has been poorly discussed in the literature.

Thus, this chapter presents a complete study of physicochemical, thermal, mechanical, and barrier properties of HPMC-TiO_2 and gelatin-TiO_2 films. In addition, it was evaluated how different concentrations of TiO_2 nanoparticles and the biopolymer hydrophilicity influence their dispersion.

3.2 MATERIALS AND METHODS

3.2.1 Materials

Commercial HPMC (Methocel E19, Dow Chemical Company, USA) and bovine gelatin type B, bloom 250 (Gelnex, Brazil) were used as biopolymer matrices. Glycerol (99 %, Neon, Brazil) was used as the plasticizer. Commercial titanium dioxide nanopowder (TiO_2 anatase, Hombikat UV 100), with an average crystallite diameter smaller than 10 nm, was used as a photocatalyst. Distilled water and acetic acid (99 %, Navelab, Brazil) were used as solvents.

3.2.2 Methods

3.2.2.1 HPMC-TiO_2 and gelatin-TiO_2 nanocomposite film preparation

HPMC-TiO_2 and gelatin-TiO_2 nanocomposite films were prepared by the casting method adapted from Oleyaei et al. (2016) and Valencia et al. (2016), respectively (**Figure 13**). HPMC (4 g) was dissolved in acetic acid solution (70 g, 0.087M) under magnetic stirring (1,000 rpm) for 30 min for each formulation. Separately, TiO_2 nanopowder (0, 0.5, 1 and 2 wt %, related to HPMC) was suspended in acetic acid solutions (30 g, 0.087M), homogenized in ultrasonic bath (Ultrasonic Maxi Clean 1400 A Unique,40 kHz) for 15 min and stirred (1,500 rpm) for 20 min. Each HPMC dispersion (pH 3.2) was heated to 70°C and added plasticizer glycerol (25 wt %, related to HPMC). The polymer dispersions were gradually heated to 85°C and cooled to 50°C. TiO_2 suspensions (pH 3.2) were dripped (1.5 $mL.min^{-1}$) into HPMC dispersions (HPMC-0%TiO_2, HPMC-0.5%TiO_2, HPMC-1%TiO_2 and HPMC-2%TiO_2, respectively). After, HPMC-TiO_2 film-forming dispersions were homogenized in an Ultraturrax T25, IKA (16,000 rpm,10 min) and degassed in ultrasonic bath. Film-forming dispersions (10 g) were casted on acrylic Petri-dishes (9 cm, internal diameter).

For the preparation of gelatin-TiO_2 nanocomposite films, 4 g of gelatin was dissolved in acetic acid solution (60 g, 0.087M) for each formulation, maintained under magnetic stirring (1,000 rpm) for 20 min and added glycerol (25 wt %, related to gelatin) and acetic acid solution (10 g, 1 M). After 10 minutes, gelatin dispersions (pH 3.2) were put in a water bath, moderately stirred and heated at 85°C for 10 minutes, cooled to 50°C, and TiO_2 suspensions were added (Gel-0%TiO_2, Gel-0.5%TiO_2; Gel-1.0%TiO_2 and Gel-2.0%TiO_2). Gelatin-TiO_2

film-forming dispersions were homogenized (16,000 rpm, 3 min, Ultraturrax), degassed and cast on Petri-dishes.

The acetic acid solution was used to enhance the TiO_2 dispersion, stabilizing its positive charge (PACIA; WARSZYŃSKI; MACYK, 2014).

HPMC-TiO_2 film-forming dispersions were dried at 25°C for 48 h in a BOD refrigerated incubator. In comparison, gelatin-TiO_2 film-forming dispersions were firstly stored at 15°C for 15 min to avoid TiO_2 nanoparticle aggregation and dried at 25°C for 48 h. All films were stored in a chamber (at 25ºC and 58 % RH) for at least 48 h before characterizations. For the scanning electronic and atomic force microscopy, Fourier-transform infrared and Raman spectroscopy, X-ray diffraction and solubility analyses, the film samples were stored in desiccators containing silica gel (0 % RH) at 25°C for at least 7 days. All experiments and characterizations related to the preparation of the film-forming dispersions and nanocomposite films were carried out at least in triplicate.

Figure 13 - Flowchart of the process used to prepare HPMC-TiO_2 and gelatin-TiO_2 nanocomposite films.

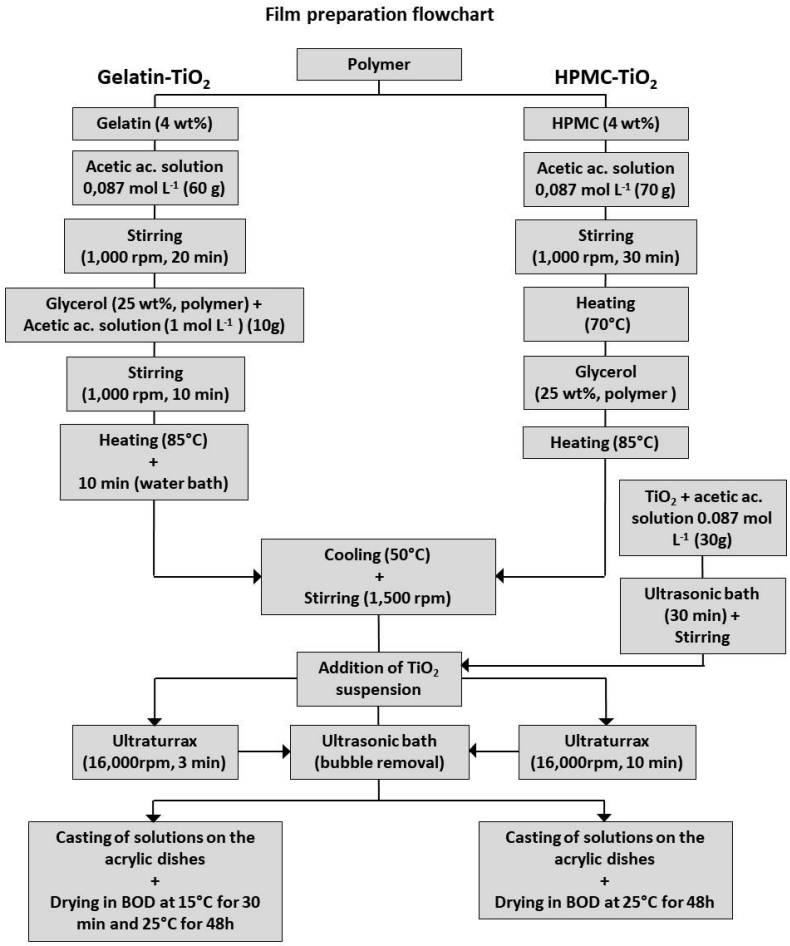

Source: Author.

3.2.2.2 Characterizations of HPMC-TiO_2 and gelatin-TiO_2 film-forming dispersions

3.2.2.2.1 Particle size and surface charge

Particle sizes (hydrodynamic diameter) of TiO_2 agglomerates suspended/dispersed into water, acetic acid solution and HPMC and gelatin dispersions were measured by the dynamic light scattering (DLS) (Zetasizer Nano ZS, Malvern Instruments, UK). Three measurements were taken for each sample after diluting a drop of the original solution in 4 ml of acetic acid solution (0.087 M) or water. Pure water, acetic acid solution and biopolymers dispersions were used as blank. The TiO_2 nanoparticle surface charge was evaluated by electrophoretic mobility measurements (zeta potential) using the same equipment and conditions set to the DLS analysis.

3.2.2.3 Characterizations of HPMC-TiO_2 and gelatin-TiO_2 nanocomposite films

3.2.2.3.1 Thickness

The average thickness was determined using a digital micrometer (0.001 mm, Mitutoyo). and calculated from the measurement of twelve different points in each film (VALENCIA et al., 2016).

3.2.2.3.2 Moisture content and water solubility

The moisture content of the HPMC-TiO_2 and gelatin-TiO_2 nanocomposite films was determined according to Jiang et al.(JIANG, Y., LI, Y., CHAI, Z., & LENG, 2010). One piece of each film (approximately 0.54 g) was dried in an oven at 105°C for 24 h, cooled in a desiccator containing silica gel to room temperature (25°C) and immediately weighted. The moisture content values of the samples were expressed in percentage (**equation 3**):

$$Moisture\ content\ (\%) = \frac{w_i - w_f}{w_i}\ x\ 100\% \qquad (3)$$

Where w_i and w_f are the sample weight before and after being dried at 105°C for 24 h, respectively.

The film water solubility was obtained from the film sample weight gradient (2 cm in diameter) after being stored in a desiccator containing silica gel for 48 h and immersed into water (50 ml) under slight stirring for 24 h at 25°C and dried in an oven at 105°C for 24 h (GONTARD; GUILBERT; CUQ, 1992). The nanocomposite film water solubility (%) was determined by **equation 4**:

$$Water\ solubility\ (\%) = \frac{w_i - w_f}{w_i}\ x\ 100\% \quad (4)$$

Where w_i and w_f are the sample weight after being stored in a desiccator containing silica gel for 24 h and an oven at 105°C for 24 h, respectively.

3.2.2.3.3 Color, light absorption and opacity

The film color was determined by a computational vision system composed of one high-resolution camera (AF-S DX NIKKOR 18-55mm f/3.5-5.6G VR, Nikon) containing a fluorescent lamp connected to an illumination diffuser. The captured film images were evaluated in the Color Space Converter version 4.0-ImageJ software. The parameters L^*, a^* and b^* obtained from the software were used to calculate the total color difference (ΔE^*, **equation 5**) and whiteness (WI, **equation 6**) and yellowness (YI, **equation 7**) indexes (CAIVANO, DEL PILAR BUERA, 2012). The camera was configured in the manual mode, D65 illuminant, exposure level 0.0, according to Arzate-Vázquez et al. (ARZATE-VÁZQUEZ et al., 2011). Due to their tendency to the white color, the films were fixed on a black standard plate.

$$\Delta E^* = \sqrt{(\Delta L^*)^2 + (\Delta a^*)^2 + (\Delta b^*)^2} \quad (5)$$

$$WI = 100 - \sqrt{(100 - L^*_{sample})^2 + a^2_{sample} + b^2_{sample}} \quad (6)$$

$$YI = \frac{142.86\ b}{L} \quad (7)$$

Where $\Delta L^* = L^*_{sample} - L^*_{standard}$, $\Delta a^* = a^*_{sample} - a^*_{standard}$ and $\Delta b^* = b^*_{sample} - b^*_{standard}$.

A spectrophotometer UV-VIS USB4000 Ocean Optics, equipped with a deuterium light source, was used to evaluate the film light absorbance properties. Rectangular film pieces (1.5 cm x 2 cm) were directly placed in a spectrophotometer test cell. Films without TiO_2 were used as standard. Film UV-vis absorbance spectra were recorded at the wavelength range from 200 to 650 nm.

Film relative opacity was defined as the area below the recorded absorbance curve at the absorbance spectrum from 400 to 650 nm, which was calculated from the integration curve using the OriginPro software version 2018 according to López, García and Zaritzky (2008) and Gontard, Guilbert and Cuq (1992). The relative opacity was expressed in absorbance units per wavelength in nanometers (AU.nm).

3.2.2.3.4 Morphology

The film surface morphology (0.5 cm x 0.5 cm) was evaluated by scanning electronic microscopy (SEM) using a scanning electronic microscope model JSM 6390 LV-JEOL, Japan, with an accelerating voltage of 15 kV (ZHANG et al., 2017). All samples were sputtered with a thin gold layer before microscopic observations.

3.2.2.3.5 Chemical composition

Film chemical composition and possible interactions between biopolymers and TiO_2 were evaluated by Fourier transform infrared (FTIR) and Raman spectroscopy. Nanocomposite film FTIR spectra were recorded at a wavenumber range from 600 to 4000 cm^{-1}, a spectral resolution of 4.0 cm^{-1} and 32 scans by using a spectrometer model Tensor 27 Bruker equipped with Universal Attenuated Total Reflectance (ATR). TiO_2 powder FTIR spectrum was recorded from KBr pellets. Films and TiO_2 Raman spectra were obtained at 23°C ± 2°C. It was used a Raman spectrometer PeakSeeker PRO-785™, Agiltron/Raman Systems, equipped with a red solid-state laser (excitation source, λ=785 nm) and L20 x objective lens from a conventional optical microscope. The laser power was maintained at 100 mW for all measurements.

3.2.2.3.6 Crystallinity

Film crystallinity was evaluated by X-ray diffraction (XRD) using an X'PERT-PRO Multipropose Powder diffractometer equipped with Position-Sensitive Detector Xcelerator (Cu*Kα* radiation, $\lambda_{K\alpha 1}$ =1.5406Å and $\lambda_{K\alpha 2}$ =1.5440 Å). The film XRD patterns were recorded at 25°C and 2θ from 5° to 90° at 0.3°.s^{-1}.

The TiO_2 crystallite average diameter was calculated using the Scherrer equation (**equation 8**) from X-ray pattern data (JOSÉ et al., 2012).

$$d = \frac{0.89\,\lambda}{\beta\,(cos\ \theta)} \tag{8}$$

Where d, λ, β and θ correspond to the TiO_2 crystallite average diameter, the Cuκα radiation wavelength, peak width at half peak height (0.01499 rad) and the Bragg angle for the typical anatase peak (25.3°), respectively.

3.2.2.3.7 Thermal properties

Glass temperature (T_g), melting temperature (T_m), and enthalpy melting (ΔH) of films were determined by differential scanning calorimetry (DSC). It was used a differential scanning calorimeter Perkin Elmer Jade, USA, equipped with a cryogenic quench cooling accessory and adapted the method used by Nascimento et al. (2019). Approximately 10.00 ± 0.01 mg of each film were hermetically sealed into an aluminum pan and scanned twice at a scan rate of 10°C.min^{-1}. The film samples were heated from -40°C to 200°C, and from -40°C to 150°C, respectively. Data were treated in the Pyris Data Analysis software.

3.2.2.3.8 Mechanical properties

Film mechanical properties were evaluated by carrying tensile tests (Young's modulus, *YM*, elongation at break, *EB* and tensile strength, *TS*) in a texture analyzer TA.HD.plus Stable Micro Systems at 23°C ± 2°C according to the ASTM Standard Test Method D 882 (ASTM, 2010). The films were cut in strips (2.5 cm x 7.5 cm), fixed on the tension grip system at an initial grip separation distance of 50 mm and a grip separation rate of 1 mm.s^{-1}. Eight repetitions were performed for each film. *TS*, *EB* and *YM* (at elastic deformation) were

calculated according to Siripatrawan & Kaewklin (2018) and Valencia et al. (2016) (**equations 9 - 11**)

$$TS\ (\mathrm{MPa}) = \frac{Maximum\ strength\ (N)}{cross\ section\ initial\ area\ (m^2)} \tag{9}$$

$$EB(\%) = \frac{deformation\ to\ break\ (m)}{initial\ length\ (m)} * 100 \tag{10}$$

$$YM(\mathrm{GPa}) = \frac{Strength\ \ (GPa) * cinitial\ length\ (m)}{deformation\ (m)} \tag{11}$$

3.2.2.3.9 Water vapor permeability

Film water vapor permeability (WVP, [g.mm.m^{-2}.h^{-1}.kPa^{-1}]) was gravimetrically determined according to the ASTM Standard Test Method E96 (ASTM, 2010). Film circular pieces were sealed in aluminum cells (internal diameter 6.3 cm) containing silica gel (0% RH) and stored in a chamber with a distilled water container (100% RH) at 25°C. The cells were periodically weighed for at least 7 days to ensure steady-state permeation. The WVP values were calculated using **equation 12**:

$$WVP = \frac{\Delta W}{\Delta t}\ (\frac{X}{A * \Delta P}) \tag{12}$$

Where $\Delta w/\Delta t$ [g/h] is the cell weight variation during a determined interval of time or the mass transfer rate of water vapor through the film (area A = 0.0031 m^2). The parameters x and ΔP are the film thickness [mm] and the partial water vapor pressure gradient (3.171 kPa at 25°C) generated by the RH difference (0 and 100%) inside and outside the sealed capsules.

3.2.2.3.10 Statistical analysis

The significant differences between experimental data were assessed by one-way analysis of variance (ANOVA) and Tukey test of multiple comparisons ($p \leq 0.05$) using Statistica software (version 13.0).

Laboratories, in which experiments and analyses were carried out, are presented in **Table 3**.

Table 3 - Laboratories located at UFSC used to carry out the first step of this thesis.

Experiments/Characterizations	Laboratories
Manufacture, thickness, color, moisture content, water solubility and WVP of films.	Laboratório de propriedades físicas dos alimentos (PROFI/EQA).
Particle size and surface charge of film-forming dispersions.	Laboratório interdisciplinar para o desenvolvimento de nanoestruturas (LINDEN/EQA).
FTIR of powder samples and tensile tests of films	Central de Análises do Departamento de Engenharia Química e de Alimentos da UFSC (CA/EQA)
FTIR-ATR of films	Laboratório de Pesquisa em Polímeros e Compósitos (POLICOM/EMC)
SEM of films	Laboratório Central de Microscopia Eletrônica (LCME).
Light absorption of films	Laboratório de Optoeletrônica Orgânica e Sistemas Anisotrópicos (LOOSA/CFM)
XRD and Raman of films	Laboratório de Síntese e Caracterização de nanoMateriais (LSCnM/CFM).

Source: Author.

3.3 RESULTS AND DISCUSSIONS

3.3.1 Evaluation of particle size and surface charge of film-forming dispersions

TiO_2 nanoparticles suspended or dispersed in different media showed differences ($p \leq 0.05$) in their colloidal stability **(Table 4)**. It was observed that the particle size of TiO_2 agglomerates suspended in acetic acid solution was smaller than in water, and their zeta potential value, when suspended in acetic acid solution (27.8 ± 0.93 mV), was significantly higher than in water (10.17 ± 0.28 mV) ($p \leq 0.05$).

The HPMC addition in acetic acid solution decreased the TiO_2 particle size as the TiO_2 concentration increased from 0.5 to 1 wt %. However, the TiO_2 particle size remained constant at 2 wt % TiO_2. Unlike HPMC, the gelatin addition in acetic acid solution caused an increase in the TiO_2 particle size, and there was no TiO_2 particle size difference between gelatin-TiO_2 formulations.

About the colloidal dispersity, HPMC-0.5%TiO_2 dispersion showed the highest dispersity value. In comparison, the TiO_2 dispersity in gelatin-TiO_2 formulations was not significantly influenced by the TiO_2 content.

Table 4 - Particle size of TiO_2 suspended in water, acetic acid solution and dispersed in biopolymer film-forming dispersions.

Group 1: Water-, acetic acid solution-, HPMC-TiO_2 [3]		
Suspension/Dispersion[2]	**Particle size (nm) [2]**	**Dispersity [2]**
TiO_2 + Water	859.53 ± 49.37^{a}	0.31 ± 0.03^{b}
TiO_2 + Ac. Sol[1]	537.27 ± 26.90^{b}	0.37 ± 0.03^{b}
HPMC-0.5%TiO_2	397.13 ± 27.40^{c}	0.88 ± 0.12^{a}
HPMC-1%TiO_2	293.57 ± 22.40^{d}	0.62 ± 0.09^{ab}
HPMC-2%TiO_2	256.80 ± 31.16^{d}	0.33 ± 0.05^{b}
Group 2: Water-, acetic acid solution-, gelatin-TiO_2 [3]		
Suspension/Dispersion[2]	**Particle size (nm) [2]**	**Dispersity [2]**
TiO_2 + Water	859.53 ± 49.37^{a}	0.31 ± 0.03^{a}
TiO_2 + Ac. Sol[1]	537.27 ± 26.90^{b}	0.37 ± 0.03^{a}
Gel-0.5%TiO_2	773.10 ± 10.40^{a}	0.23 ± 0.05^{a}
Gel-1%TiO_2	761.33 ± 54.59^{a}	0.31 ± 0.03^{a}
Gel-2%TiO_2	817.30 ± 11.85^{a}	0.22 ± 0.04^{a}

[1]Ac. Sol: acetic acid solution (0.087M).
[2]All values were expressed as mean ± standard error (n = 3). Means within the same column and the same group with different superscripts are different at the level of $\alpha = 0.05$.
[3]HPMC: hydroxypropyl methylcellulose; Gel: gelatin; TiO_2: titanium dioxide.

Source: Fonseca et al. (2020), with permission.

According to Derjaguin-Landau-Verwey-Overbeek (DLVO) theory or surface steric force theory, a multi-phase system can be considered stable when its components have a zeta potential value near or higher than ± 30 mV (AMIR et al., 2018). TiO_2 nanoparticles presented higher colloidal stability in acetic acid solution (near ± 30 mV, pH = 3.2) than in water, probably due to their ionization (Ti^{4+}) and repulsion from each other. This charge repulsion hindered their agglomeration, generating smaller aggregates in acetic acid solution than in water (PACIA; WARSZYŃSKI; MACYK, 2014). The HPMC and gelatin played the role of TiO_2 nanoparticle stabilizers. The stabilizers provide a steric hindrance due to their migration to nanoparticle-solvent interface and adsorption on the hydrophobic nanoparticle surface, preventing crystal growth (SADEGHI et al., 2016). Concentrations of 1 wt % and 2 wt % TiO_2 were better stabilized in HPMC dispersion than 0.5 wt % TiO_2 due to their smaller particle size.

The gelatin complex structure composed of a triple helix probably increased the particle size of TiO_2 agglomerates. It has already been well-documented that the disulfide and intermolecular hydrogen bonds, Van der Waals attractive forces and electrostatic interactions cause the protein flocculation, increasing the gelatin particle size (JIANG, Y., LI, Y., CHAI, Z., & LENG, 2010). Similar results were obtained by He et al. (2016) and Ding, Zhang & Li (2015) for the gelatin-TiO_2 (pH 4.0) and whey protein-TiO_2 film-forming dispersions,

respectively. He et al. (2016) supposed that interactions between gelatin (initial particle size of 648 nm) and TiO_2 increased its particle size (622 – 785 nm) as the TiO_2 content increased. Yadav; Kumar (2014) also reported HPMC and gelatin as efficient stabilizers to prevent curcumin nanocrystal growth in polymer dispersions.

3.3.2 Characterization of HPMC-TiO_2 and gelatin-TiO_2 nanocomposite films

3.3.2.1 Thickness, moisture content and water solubility

The film thickness did not change by incorporating TiO_2 into biopolymer matrices, remaining around 0.077 ± 0.001 mm and 0.072 ± 0.003 mm, respectively ($p > 0.05$). The thickness preservation suggests that the TiO_2 concentrations tested did not alter the film density. Ding, Zhang & Li (2015) and Valencia et al. (2016) reported similar thickness values for HPMC-based films and gelatin-laponite nanocomposite films prepared from 1.5 wt % and 4 wt % of polymer dispersions, respectively. Valencia et al. (2016) still reported that the laponite also did not change the film thickness.

The HPMC-TiO_2 film moisture content remained around 24.97 ± 0.39 % ($p > 0.05$), while gelatin-TiO_2 films showed differences ($p \leq 0.05$) (**Table 5**). Thus, the total void volume occupied by water molecules inside the gelatin-TiO_2 film microstructure decreased when TiO_2 content increased from 0 to 1 wt % (LI et al., 2011). For the Gel-2%TiO_2, the moisture content increased due to bigger TiO_2 agglomerates, which suggest a large number of gelatin sites not filled by TiO_2 nanoparticles. It is expected that the gelatin-based film water vapor permeability is also affected by the TiO_2 incorporation.

Table 5 - Moisture content and water solubility of the gelatin-TiO_2 nanocomposite films.

Film[1, 2]	Moisture content (%)	Water solubility (%)
Gel-0%TiO_2	14.63 ± 0.07^{ab}	69.13 ± 4.75^{a}
Gel-0.5%TiO_2	13.87 ± 0.56^{ab}	50.38 ± 3.07^{ab}
Gel-1%TiO_2	13.01 ± 0.28^{b}	45.83 ± 0.94^{b}
Gel-2%TiO_2	15.96 ± 0.88^{a}	48.43 ± 3.12^{b}

[1]All values were expressed as mean ± standard error (n = 3). Means within the same column with different superscripts are different at the level $\alpha = 0.05$.
[2]Gel: gelatin; TiO_2: titanium dioxide.

Source: Fonseca et al. (2020), with permission.

The gelatin-TiO_2 film water solubility (**Table 5**) decreased as the TiO_2 content decreased ($p \leq 0.05$), while HPMC-TiO_2 films were entirely solubilized in a few minutes ($p > 0.05$). It indicates that TiO_2 nanoparticles interacted with gelatin amino and hydroxyl groups at pH 3.2 by hydrogen bonds, decreasing polymer-water interactions. TiO_2 Hombikat UV 100 is hydrophobic and becomes hydrophilic when exposed to UV-light (MANOLE et al., 2010; REDDY; DAVYDOV; SMIRNIOTIS, 2003). Similarly, the incorporation of TiO_2 98.5 % anatase (Jiang Hu Industry, China) in whey protein (LI et al., 2011) and anatase/rutile phase mixture (80/20, TiO_2 Evonik Degussa P25 GmbH, Germany) in potato starch (OLEYAEI et al., 2016) decreased the nanocomposite film water solubility. Nevertheless, TiO_2 was not sufficient to decrease the HPMC hydrophilicity ($p > 0.05$).

3.3.2.2 Color, light absorption and opacity

Images of the HPMC-TiO_2 and gelatin-TiO_2 films are presented in **Figure 14**.

Figure 14 - Images of the HPMC-TiO_2 e gelatin-TiO_2 nanocomposite films.

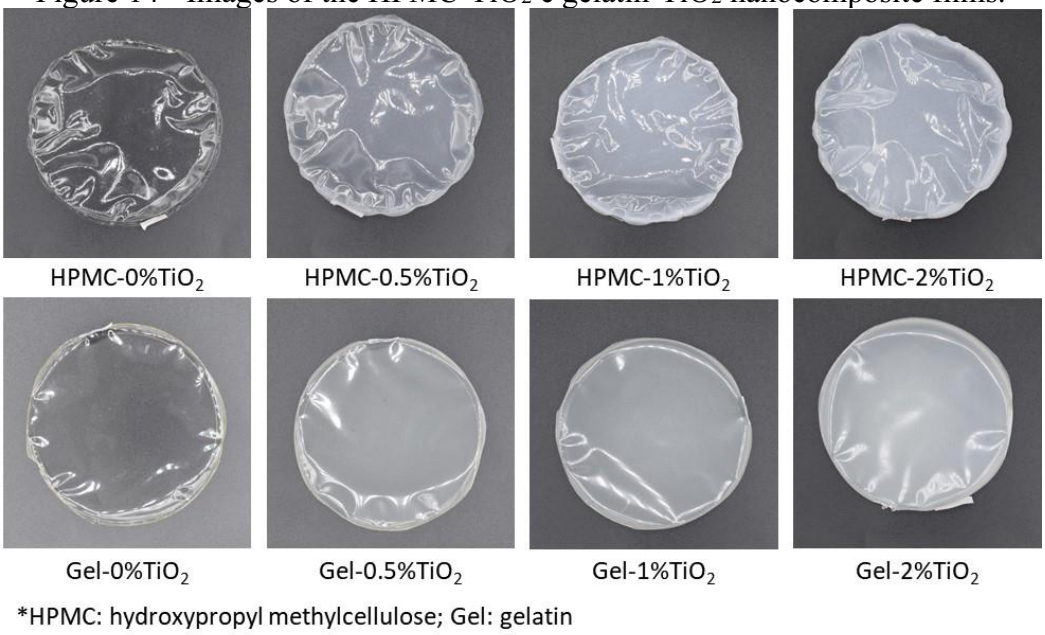

Source: Author.

The TiO_2 incorporation into biopolymers affected the film color parameters ($p \leq 0.05$) (**Table 6**). Color changes were more evident in gelatin-TiO_2 films than HPMC-TiO_2 films. The gelatin-TiO_2 film lightness (L^*) and total color difference (ΔE) gradually increased as the TiO_2 content increased, while the parameters a* and b* decreased. Although HPMC-TiO_2 films have also exhibited a gradual ΔE increase, the parameters L^* and b* did not present

differences ($p > 0.05$) for the films containing TiO_2. Finally, the parameter a* was different only for the film containing 2 wt % TiO_2.

The yellowness index (*YI*) decreased for both HPMC and gelatin-based films containing TiO_2 compared to blank films. However, there was no difference between films containing TiO_2 ($p > 0.05$). The opposite behavior was observed for the whiteness index (*WI*) as expected. The TiO_2 incorporation into HPMC increased the film *WI* ($p \leq 0.05$) but not enough to cause significant changes between films containing different TiO_2 concentrations. In contrast, the gelatin-based films containing TiO_2 exhibited a gradual *WI* increase as the TiO_2 content increased.

These results showed that the TiO_2 inherent whiteness increased the film whiteness (OLEYAEI et al., 2016). However, gelatin-TiO_2 films showed lower color change than HPMC-TiO_2 films. Similar characteristics were observed in whey protein-TiO_2 (LI et al., 2011) and starch-TiO_2 (OLEYAEI et al., 2016) nanocomposite films.

Table 6 - Color parameters, yellowness and whiteness indexes and opacity of the HPMC-TiO_2 and gelatin-TiO_2 nanocomposite films.

Group 1: HPMC-TiO_2							
Film[1,2]	**$L^{*,3}$**	**$a^{*,3}$**	**$b^{*,3}$**	**$\Delta E^{*,3}$**	**YI (%)[3]**	**WI (%)[3]**	**Relative opacity (AU.nm)[3]**
HPMC-0%TiO_2	42.47± 2.28^{b}	0.84 ± 0.04^{a}	-1.78 ± 0.15^{a}	5.71± 0.92^{c}	-6.02 ± 0.63^{a}	42.44 ± 2.28^{a}	0^{d}
HPMC-0.5%TiO_2	64.65± 2.77^{a}	0.78 ± 0.04^{a}	-6.84 ± 0.40^{b}	25.34± 4.10^{b}	-15.11 ± 0.45^{b}	63.96 ± 2.65^{b}	61.36 ± 1.34^{c}
HPMC-1%TiO_2	68.14± 2.38^{a}	0.75 ± 0.08^{a}	-6.90 ± 0.49^{b}	27.20± 2.51^{b}	-14.46 ± 0.30^{b}	67.37 ± 2.25^{b}	83.82 ± 1.86^{b}
HPMC-2%TiO_2	70.89± 1.52^{a}	0.33 ± 0.06^{b}	-6.82 ± 0.08^{b}	42.92± 0.50^{a}	-13.75 ± 0.16^{b}	70.10 ± 1.45^{b}	240.26 ± 2.06^{a}
Group 2: gelatin-TiO_2							
Film[1,2]	**$L^{*,3}$**	**$a^{*,3}$**	**$b^{*,3}$**	**ΔE^{3}**	**YI (%)[3]**	**WI (%)[3]**	**Relative opacity (AU.nm)[3]**
Gel-0%TiO_2	50.26 ± 0.91^{c}	< 10^{-3a}	-0.71 ± 0.02^{a}	9.06 ± 1.40^{c}	-2.01 ± 0.03^{a}	50.25 ± 0.91^{c}	0^{d}
Gel-0.5%TiO_2	62.99± 3.05^{b}	0.09 ± 0.04^{a}	-1.97 ± 0.02^{b}	12.23 ± 0.29^{c}	-4.50 ± 0.20^{b}	62.93 ± 3.05^{b}	45.88 ± 2.23^{c}
Gel-1%TiO_2	66.89± 2.86^{ab}	-0.21 ± (0.01)^{b}	-2.69 ± 2.35^{c}	27.95 ± 2.34^{b}	-5.76 ± 0.43^{b}	66.78 ± 2.85^{ab}	81.44 ± 1.43^{b}
Gel-2%TiO_2	73.87± 0.48^{a}	-0.52 ± 0.04^{c}	-2.43 ± 0.23^{bc}	38.86 ± 0.50^{a}	-4.69 ± 0.40^{b}	73.75 ± 0.46^{a}	164.44 ± 2.82^{a}

[1]All values were expressed as mean ± standard error (n=3). Means within the same column and the same group with different superscripts are different at the level of $\alpha = 0.05$.
[2]HPMC: hydroxypropyl methylcellulose; Gel: gelatin; TiO_2: titanium dioxide.
[3] L*: luminosity (black-white; 0-100); a* (green/red; -a*/a*); b* (blue/yellow; -b*/b*); ΔE: total color difference; YI: yellowness index; WI: whiteness index; AU.nm: absorbance units per wavelength in nanometers

Source: Fonseca et al. (2020), with permission.

.

Light absorption results (**Figure 15**) showed that HPMC-TiO_2 (**Figure 15.a**) and gelatin-TiO_2 (**Figure 15.b**) films containing 2 wt% TiO_2 exhibited higher light absorbance (λ = 222 - 380 nm) than other films ($p \leq 0.05$). The wavelength range absorbed includes the three regions of UV-radiation spectrum: UV-A (λ = 315-400 nm), UV-B (λ = 280-315 nm) and UV-C (λ = 200-280 nm) (PAULINO-LIMA et al., 2016). These results agree with the wavelength range absorbed by pure TiO_2 ($\lambda \leq 387.5$ nm) (ETACHERI et al., 2015).

Figure 15 - UV-vis spectra of the HPMC-TiO_2 (a) and gelatin-TiO_2 (b) nanocomposite films.

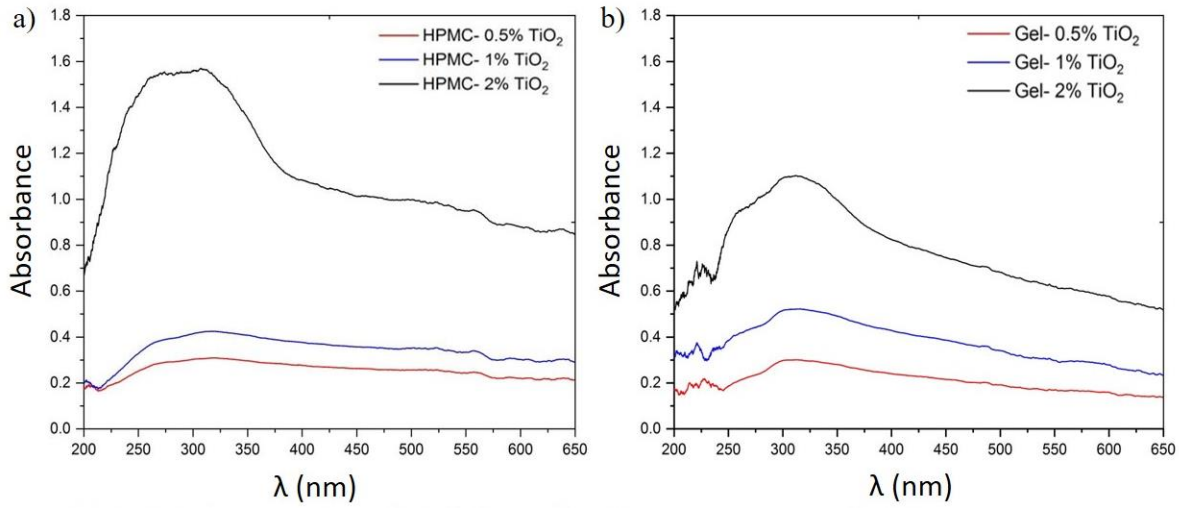

[1] HPMC: hydroxypropyl methylcellulose; Gel: gelatin; TiO_2: titanium dioxide

Source: Fonseca et al. (2020), with permission.

The film relative opacity was calculated using a visible light spectrum wavelength (λ = 400 - 650 nm). HPMC-0%TiO_2 and Gel-0%TiO_2 films were used as standards with relative opacity values of approximately zero. There was a sharp and progressive increase in film relative opacity as the TiO_2 content increased, indicating the film reflectance rising ($p \leq 0.05$). The TiO_2 agglomeration causes UV-light scattering on the film surface, which increases its reflectance, lightness (L*) and whiteness (WI) (WANG et al., 2019). So, it suggests that films containing 2 wt % TiO_2 did not show a photocatalyst homogeneous dispersion. The slighter relative opacity increase for the gelatin-TiO_2 films than HPMC-TiO_2 films also suggests that TiO_2 nanoparticles are more homogeneously dispersed in gelatin than HPMC. Similar opacity results were obtained by Siripatrawan & Kaewklin (2018) for chitosan-TiO_2 films.

3.3.2.3 Morphology

TiO_2 agglomerates were observed in film SEM micrographs (**Figure 16**). HPMC-2%TiO_2 films displayed bigger and more TiO_2 agglomerates than other film formulations, while gelatin-TiO_2 films did not exhibit perceptible TiO_2 aggregation. It was also observed an apparent surface relief increase (protuberance rising) in films containing TiO_2, especially for the HPMC-TiO_2 films. It indicates that the TiO_2 incorporation into the biopolymer matrices increased the film surface roughness. This result confirms the hypothesis that the increase of the opacity, lightness and whiteness indexes of films is related to TiO_2 agglomeration. So, the gelatin dispersed the photocatalyst better than HPMC.

Figure 16 - Cross-section (350 x of magnification) and surface (30 x of magnification) SEM micrographs of HPMC-TiO_2 and gelatin-TiO_2 nanocomposite films containing different concentrations of TiO_2 (0, 0.5, 1 and 2 wt % TiO_2).

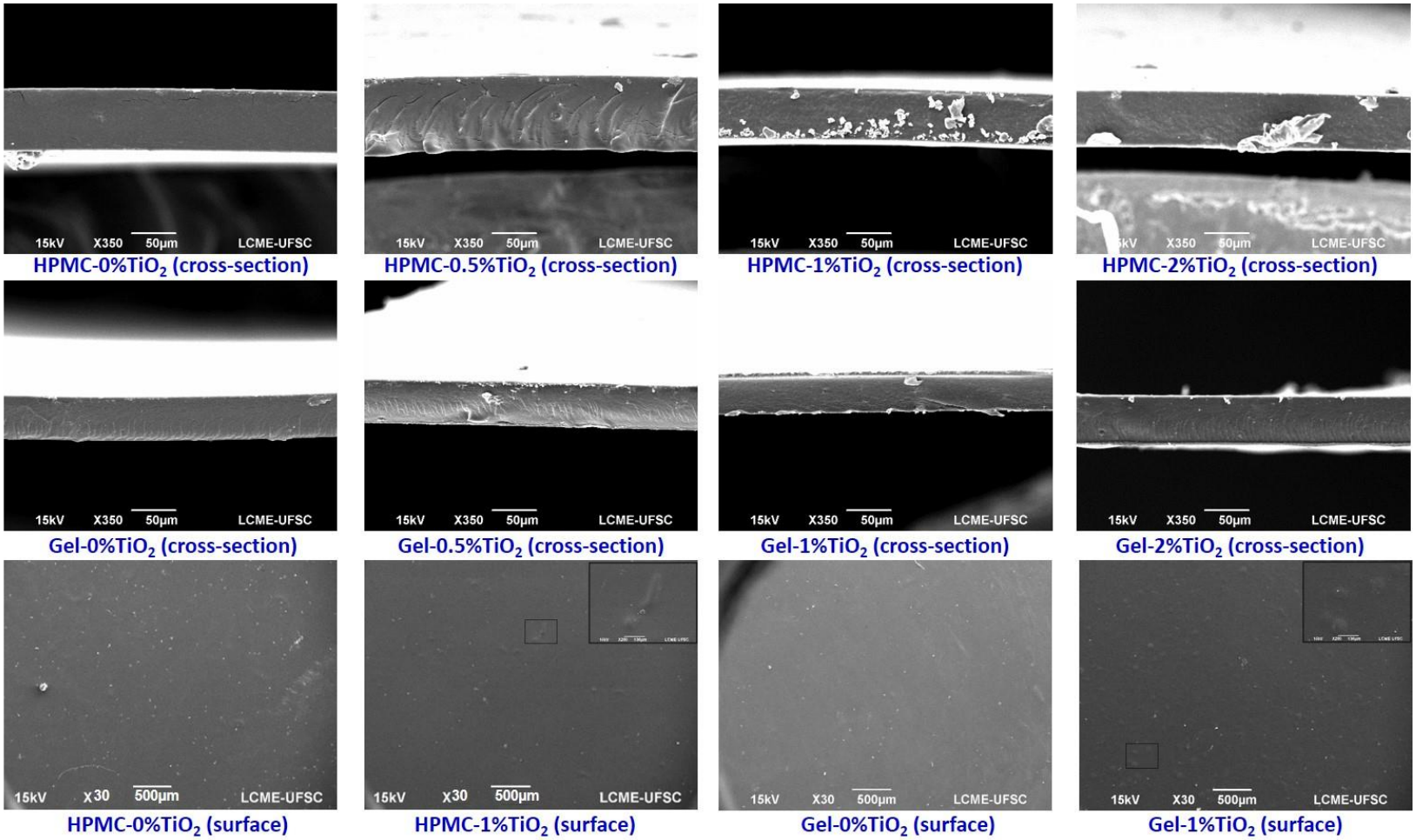

[1] HPMC: hydroxypropyl methylcellulose; Gel: gelatin; TiO_2: titanium dioxide

Source: Fonseca et al. (2020), with permission.

3.3.2.4 Chemical composition

Chemical composition and possible interactions between TiO_2 and biopolymers were evaluated by FTIR and Raman spectroscopy (**Figure 17**). TiO_2 FTIR spectrum exhibited a broad band centered at 3401 cm^{-1} associated with the stretching vibrational band of free O-H axial stretching and hydrogen bonds on the TiO_2 surface formed due to the water absorption (OLEYAEI et al., 2016). The –OH groups absorption play an essential role in photocatalysis. They stimulate the charge trapping by photoreceptors to generate ROS (OH●). These radicals trigger photocatalysis and act as absorbents, activating sites to degrade the adsorbate (HAIDER et al., 2018). The band at 1634 cm^{-1} attributed to the water adsorption disappeared in the nanocomposite spectra. It suggests that the TiO_2 incorporated into biopolymers reduced the film water adsorption when not exposed to the UV-light (HAIDER et al., 2018). Finally, the broadband at 800 - 430 cm^{-1} was attributed to the Ti-O-Ti stretching band (YUN et al., 2016).

Figure 17 - FTIR spectra of TiO_2 nanopowder (a,b), ATR-FTIR (a,b) and Raman (c,d) spectra of HPMC-TiO_2 and gelatin-TiO_2 films.

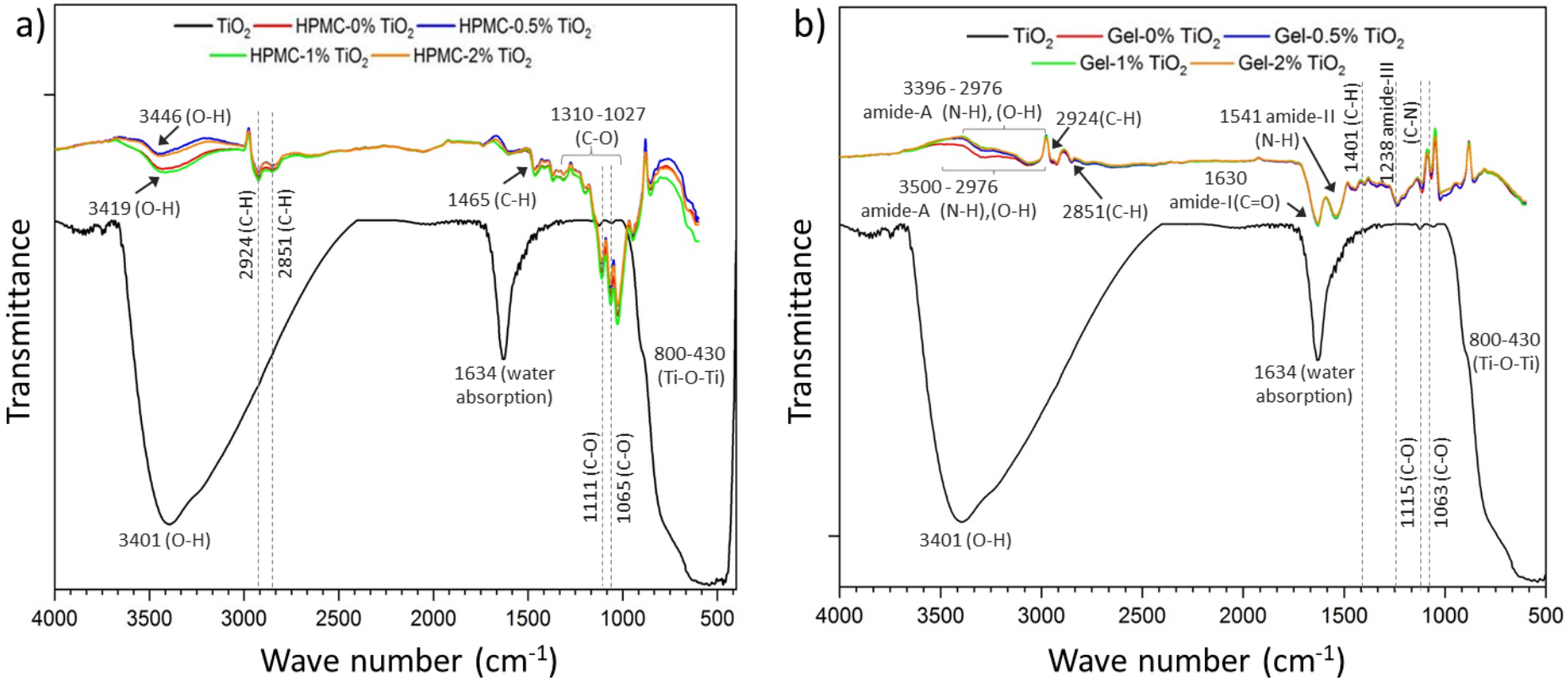

[1] HPMC: hydroxypropyl methylcellulose; Gel: gelatin; TiO_2: titanium dioxide

Source: Fonseca et al. (2020), with permission.

Figure 17 - FTIR spectra of TiO_2 nanopowder (a,b), ATR-FTIR (a,b) and Raman (c,d) spectra of HPMC-TiO_2 and gelatin-TiO_2 films. (continuation).

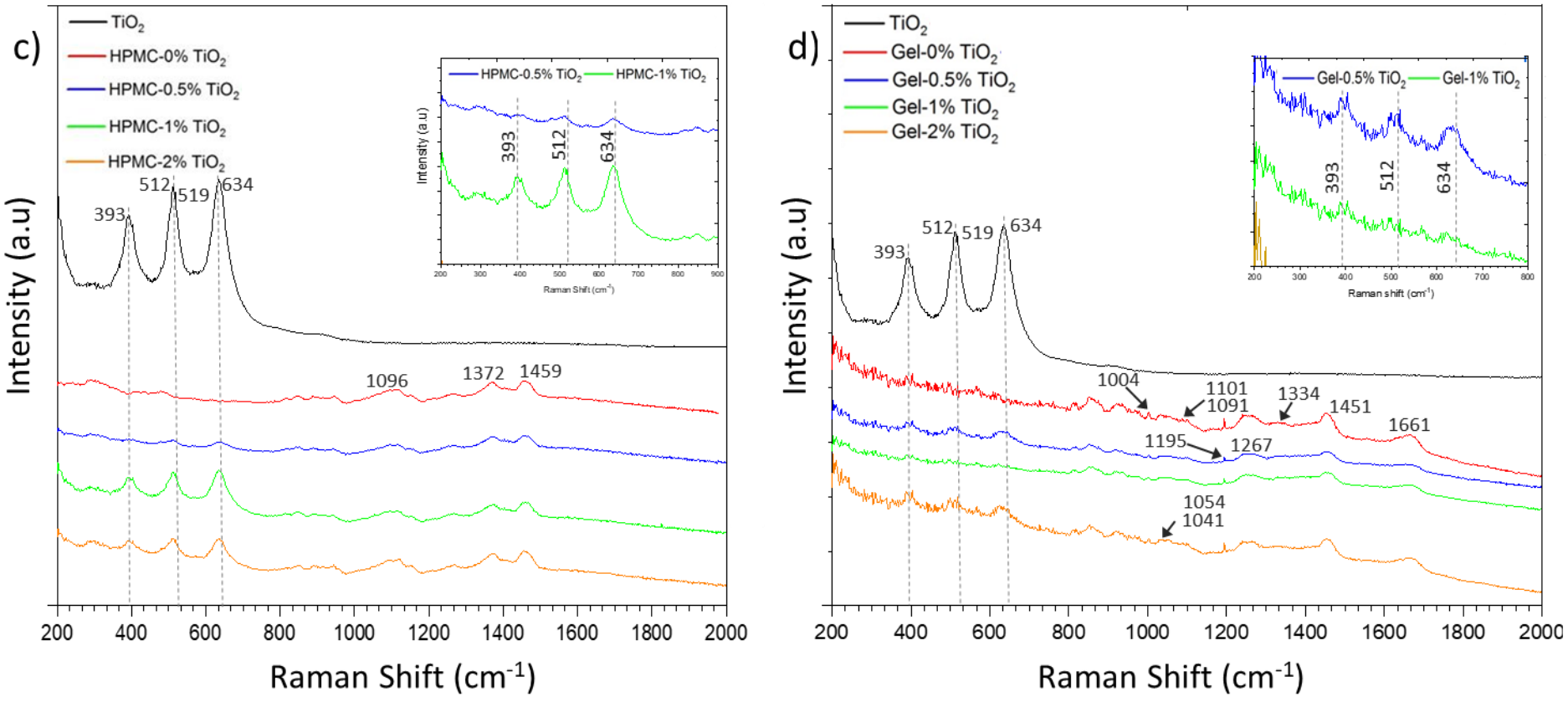

[1] HPMC: hydroxypropyl methylcellulose; Gel: gelatin; TiO_2: titanium dioxide

Source: Fonseca et al. (2020), with permission.

The HPMC-0%TiO_2 spectrum also displayed a broad band centered at 3419 cm^{-1} attributed to the O-H axial stretching from HPMC and hydrogen bonds between polymer chains and water molecules (DING; ZHANG; LI, 2015). This band was shorted, and its center was displaced to 3419 cm^{-1} in the HPMC-0.5%TiO_2 and HPMC-2%TiO_2 spectra. For the HPMC-1%TiO_2 film, this band did not change when compared to the blank film. It is suggested that 1 wt % TiO_2 nanoparticles dispersed into HPMC preserved hydrogen bonds between HPMC and water, or new hydrogen bonds between TiO_2 and water were formed (HE et al., 2016).

The bands at 2924 cm^{-1} and 2851 cm^{-1}, also presented in gelatin-TiO_2 film spectra, were attributed to the C-H stretching from -CH_3 and -CH_2 groups, respectively (MATOS FONSECA et al., 2019). HPMC-TiO_2 films also exhibited a band at 1465 cm^{-1} associated with C-H in-plane bending from -CH_2 groups (MOHAN et al., 2012). The bands from 1310 to 1027 cm^{-1}, especially bands at 1111 cm^{-1} and 1065 cm^{-1}, are associated with a combination of ether C-O stretching and secondary alcohol hydroxyl groups (O-H) from HPMC chains (JACQUOT et al., 2012). These bands can also have been superimposed by the C-H in-planes and O-H bending from glycerol molecules. Polymer-glycerol interactions have also been observed at bands below 1000 cm^{-1} for both biopolymers (HAZIMAH; OOI; SALMIAH, 2003).

As well as HPMC-0%TiO_2, the Gel-0%TiO_2 spectrum was similar to gelatin-based film spectra containing TiO_2. However, the band at 3396 – 2976 cm^{-1} exhibited a slight intensity decrease and a displacement to 3500 – 2976 cm^{-1} as the TiO_2 was incorporated into gelatin. These bands are associated with hydrogen bonds (O-H) and N-H vibrations of the gelatin amide-A groups (HE et al., 2016). The intensity decrease and displacement of the gelatin band 3396 – 2976 cm^{-1} can be attributed to the electrostatic repulsion between protonated amino groups (-NH_3^+) and Ti^{4+} ions at pH= 3.2. Siripatrawan & Kaewklin (2018) reported similar results, and He et al. (2016) obtained an intensity increase for the band 3600 - 3200 cm^{-1} as the TiO_2 content incorporated into gelatin increased. Their film-forming dispersions were prepared by dispersing gelatin in water with medium pH adjustment to 4 using NaOH solution. The counter ions (HO^-) from NaOH probably electrostatically shielded the Ti^{4+}, decreasing the repulsion between TiO_2 nanoparticles and gelatin chains (MATOS FONSECA et al., 2019). Consequently, the number of hydrogen bonds between them was increased. In this thesis, it was not used basic solution to adjust the pH of film-forming dispersions. So, the dominant electrostatic repulsion between ions -NH_3^+ and Ti^{4+} can justify the decrease in intensity of the band 3396 – 2976 cm^{-1} for the gelatin.

The TiO_2 incorporation has not changed the vibration intensity from typical gelatin chemical groups such as amide-I (C-O), amide-II or triple helix (N-H) and amide-III (C-N), and they can be observed at 1630, 1541 and 1238 cm^{-1}, respectively (ARFAT et al., 2014). The bands at 1401, 1111 and 1065 cm^{-1} were attributed to the C-H and C-O vibrations from glycerol molecules (HAZIMAH; OOI; SALMIAH, 2003). No band from the chemical group capable of indicating a possible polymeric degradation has been identified.

The TiO_2 anatase has six typical active modes determined from group theory $A_{1g} + 2B_{1g} + 3E_g$ (DUTU et al., 2017), of which four modes, 393 cm^{-1} (B_{1g}), 512 cm^{-1} (A_{1g}), 519 cm^{-1} (B_{1g}) and 634 cm^{-1} (E_g), were identified in the Raman spectral window (**Figure 18**) investigated for the single crystal TiO_2. Ohsaka (1980) identified the six typical modes from anatase ionic crystals in a wider spectral window at 144 cm^{-1} (E_g), 197 cm^{-1} (E_g), 399 cm^{-1} (B_{1g}), 513 cm^{-1} (A_{1g}), 519 cm^{-1} (B_{1g}) and 639 cm^{-1} (E_g).

Typical vibrations of the HPMC and gelatin matrices without significant alterations (**Table 7**) were identified in the Raman spectra of HPMC-TiO_2 and gelatin-TiO_2, reinforcing that biopolymers have not been degraded.

Table 7 - Typical Raman shifts for the hydroxypropyl methylcellulose (HPMC) and gelatin.

HPMC		Gelatin	
Raman shift (cm^{-1})	**Assignment**	**Raman shift (cm^{-1})**	**Assignment**
1459s	Deformation of $-CH_2$ and $-CH_3$ groups	1661s	C=O (amide I)
1372s	-COH bending	1451s	Deformation of $-CH_2$ and $-CH_3$ groups, in-plane bend of carboxyl OH
1096w	C-O stretching	1334m	CH_2 and $-CH_3$ groups
1011w	out of plane bend of carboxyl OH	1267s	Proline and hydroxyproline residues (amide III)
> 944m	Stretching C-C backbone stretch	1195w	Tyrosine
		1104w, 1091w	C-N stretching
		1054w	out of plane bend of carboxyl OH
		1041m	Proline
		1004m	Phenylalanine
		> 1000w	Stretching C-C of the amino acid residues and polypeptide chains

w: weak; m: medium; s: strong. Based on Frushour; Koenig (1975) and Remon et al. (2008).

Source: Fonseca et al. (2020), with permission.

A TiO_2 vibration intensity increase in the Raman HPMC-TiO_2 film spectra as the TiO_2 content increased from 0 to 1 wt % and a decrease at 2 wt % were observed. A slight TiO_2

band enlargement and displacement at 512 and 634 cm^{-1} in the HPMC-0.5%TiO_2 and HPMC-1%TiO_2 Raman spectra were also observed. This behavior can be attributed to the TiO_2 agglomerate size variation. As the agglomerate size increases, the TiO_2 bands are enlarged and shifted (CHOI; JUNG; KIM, 2005). This result corroborates the particle size results obtained by DLS for the HPMC-TiO_2 film-forming dispersions. The supposed HPMC matrix voids generated by its insufficient filling by 0.5 wt % TiO_2 and the excessive agglomeration of 2 wt % TiO_2 probably reduced the TiO_2 band intensity.

In the gelatin-TiO_2 Raman spectra, TiO_2 bands were overlapped by the gelatin structure typical bands. However, the slight TiO_2 band displacement at 512 and 634 cm^{-1} in the film spectra reinforce the hypothesis that the gelatin proteins flocculation masked the TiO_2 particle size values measured from DLS analysis. The differences involving TiO_2 band intensity, displacement and broadening between different gelatin-TiO_2 film formulations were less discrepant than HPMC-TiO_2 films, suggesting better dispersion of TiO_2 nanoparticles in the gelatin than HPMC.

3.3.2.5 Crystallinity

Typical peaks from the anatase phase were observed in the TiO_2 nanopowder X-ray pattern (**Figure 18)** at 2θ = 25.2°, 37.8°, 47.9°, 54.7°, 62.5°, 69.2°, 75.4° and 82.7°. They agree with *ICSD: 9852* (ICSD CODE 9852- INORGANIC CRYSTAL STRUCTURE DATABASE, [s.d.]). Peaks from the rutile phase were not observed (ICSD CODE 9161 - INORGANIC CRYSTAL STRUCTURE DATABASE, [s.d.]; SACHTLEBEN CHEMIE GMBH, [s.d.]). The calculated TiO_2 crystallite average diameter (d = (9.38 ± 0.31) nm) is in agreement with technical information provided by the supplier (d < 10 nm) (SACHTLEBEN CHEMIE GMBH, [s.d.]).

Figure 18 - X-ray patterns of TiO_2 nanopowder, HPMC-TiO_2 (a) and gelatin-TiO_2 (b) nanocomposite films.

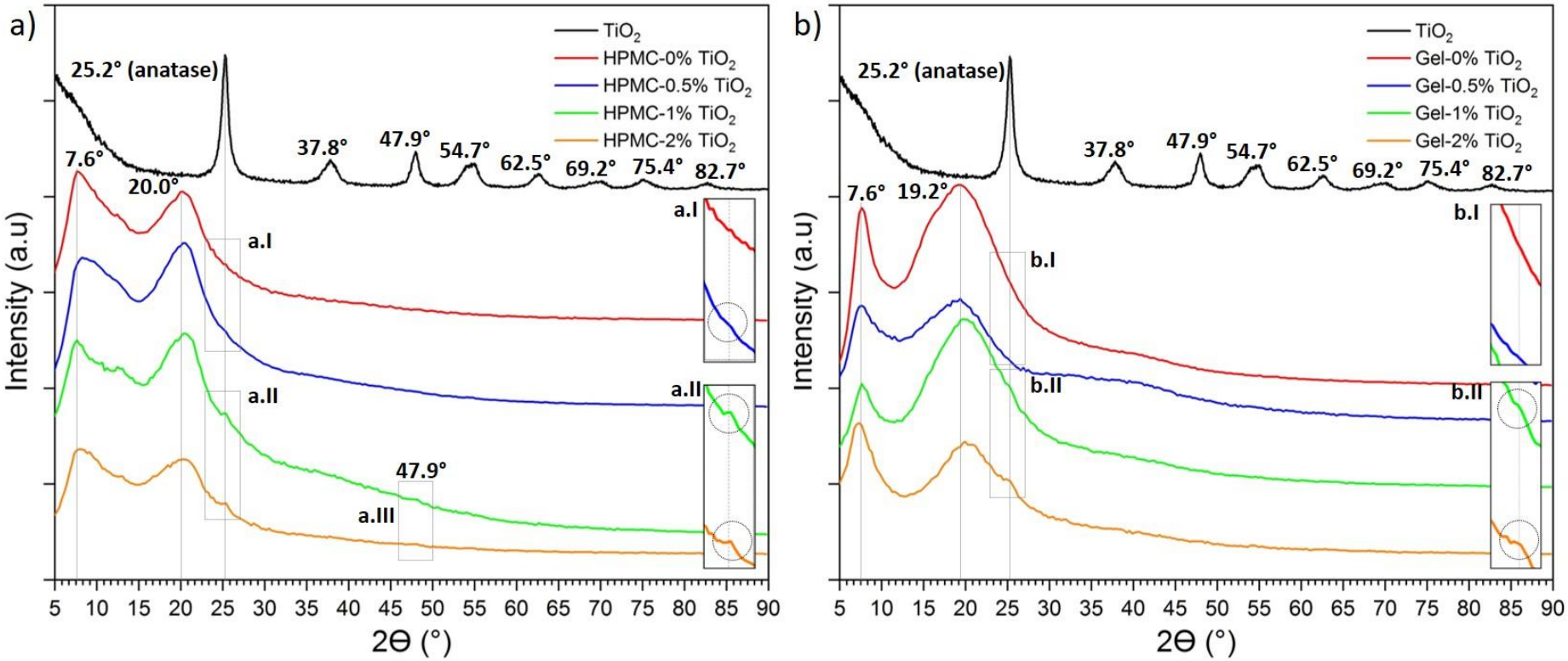

[1] HPMC: hydroxypropyl methylcellulose; Gel: gelatin; TiO_2: titanium dioxide

Source: Fonseca et al. (2020), with permission and adapted.

Except in Gel-0%TiO_2 and Gel-0.5%TiO_2 X-ray patterns, a shoulder at 2θ = 25.2° related to the TiO_2 incorporation was noticed. Similar results were observed in gelatin-TiO_2, starch-TiO_2 and chitosan-TiO_2 by He et al. (2016), Li et al. (2011), Oleyaei et al. (2016) and Siripatrawan & Kaewklin (2018). The other two intensity changes that evidence the TiO_2 incorporation were also noticed at 2θ = 47.9° in the HPMC-1%TiO_2 and HPMC-2%TiO_2 X-ray patterns.

Both biopolymers exhibited a semi-crystalline structure changed by the TiO_2 incorporation (**Figure 18)**. HPMC showed a peak at 2θ = 7.6° associated with its crystalline fraction dominated by hydrogen bonds between polymer chains. The broad peak at 2θ = 20° is related to HPMC amorphous phase, formed due to the low polymer chain packing, hindered by HPMC side polar chemical groups (ROTTA; MINATTI; BARRETO, 2011). It was observed an enlargement and gradual intensity decrease at 2θ = 7.6° for the films containing TiO_2, suggesting that the volume occupied by the TiO_2 nanoparticles in the biopolymer matrix weakened the hydrogen bonds between HPMC chains allowing their dispersion (MATOS FONSECA et al., 2019).

Supplementary, the amorphous phase intensity increase at 2θ = 20° for the HPMC-0.5%TiO_2 and HPMC-1%TiO_2 nanocomposite films can be a result of two events. First, the superimposition to the TiO_2 anatase characteristic peak centered at 2θ = 25.2°. Second, the increase of nanocomposites stability as the TiO_2 content increased, intensifying the biopolymer-TiO_2 interactions (HE et al., 2016). The decrease of HPMC-2%TiO_2 amorphous phase intensity at 2θ = 20° suggests that the TiO_2 agglomerates interacted with the HPMC matrix weakly.

Similar behavior was noticed in all gelatin-TiO_2 X-ray patterns. The non-displacement of the peak at 2θ = 7.6° indicated that the triple helix diameter from gelatin protein chains was preserved. However, the decrease of this peak as the TiO_2 was incorporated indicated that the number of triple helices was reduced (LIU et al., 2015). Finally, the gelatin amorphous phase intensity (2θ = 19.2°) depends on the distance between amino acid residues along the helix (LIU et al., 2015). The higher amorphous phase intensity for the Gel-1%TiO_2 film suggests that this film is the most physically stable.

3.3.2.6 Thermal properties

T_g and T_m of films were investigated using DSC analyses. Thermograms obtained from the first and second heating cycles for the TiO_2 nanopowder and films are presented in **Figure**

19. TiO_2 exhibited an endothermic peak in the first heat cycle at 87.3°C, attributed to the water evaporation adsorbed on its surface (MARINESCU et al., 2011). All film samples exhibited a first-order endothermic transition related to biopolymer melting (T_m). Broad melting peaks are characteristics of semi-crystalline polymers, and they are associated with biopolymer chain disorder in the amorphous phase (CALLISTER; RETHWISCH, 2011). These peaks can also be superimposed by endothermic events such as water evaporation, melting and recrystallization of polymer crystallites (MULLAH et al., 2017).

Figure 19 - DSC thermograms related to the first (a,c) and second (b,d) heat cycles of the TiO_2 nanopowder, HPMC-TiO_2 and gelatin-TiO_2 nanocomposite films.

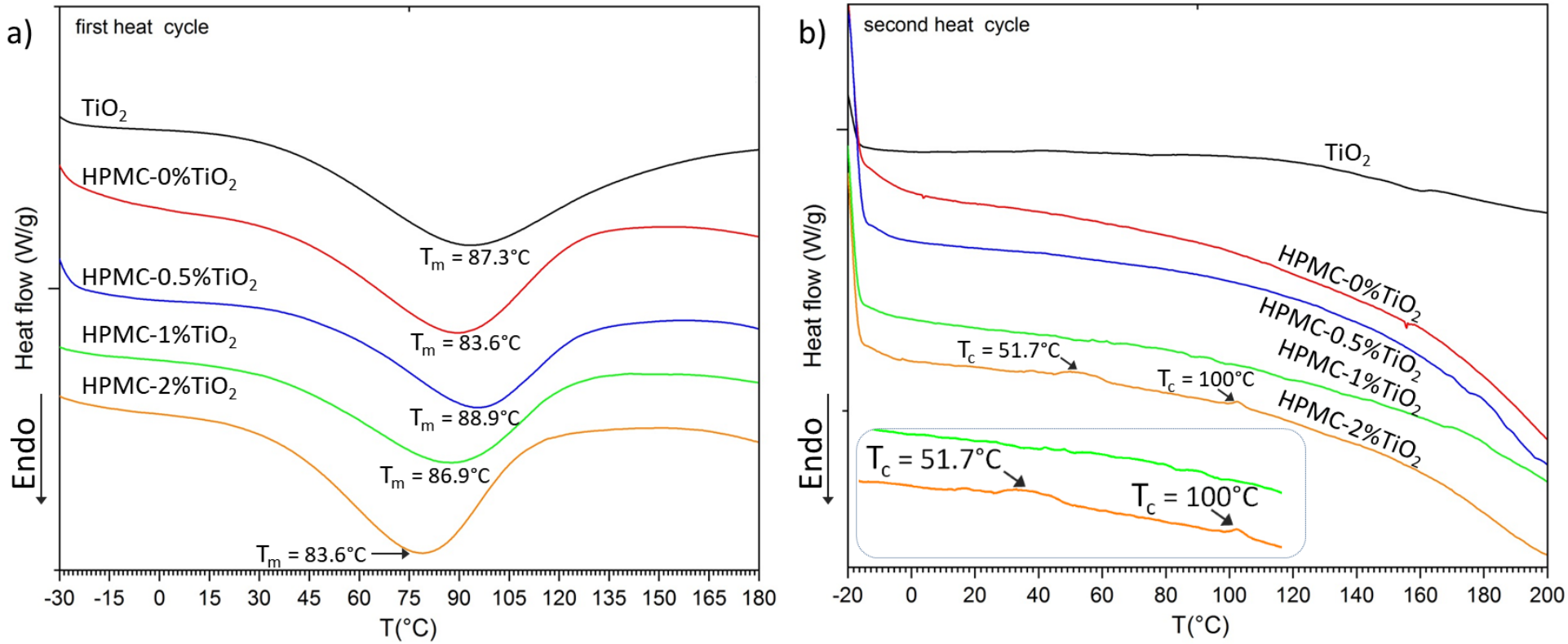

[1] HPMC: hydroxypropyl methylcellulose; Gel: gelatin; TiO_2: titanium dioxide

Source: Fonseca et al. (2020), with permission.

Figure 19 - DSC thermograms related to the first (a,c) and second (b,d) heat cycles of the TiO_2 nanopowder, HPMC- TiO_2 and gelatin- TiO_2 nanocomposite films (continuation).

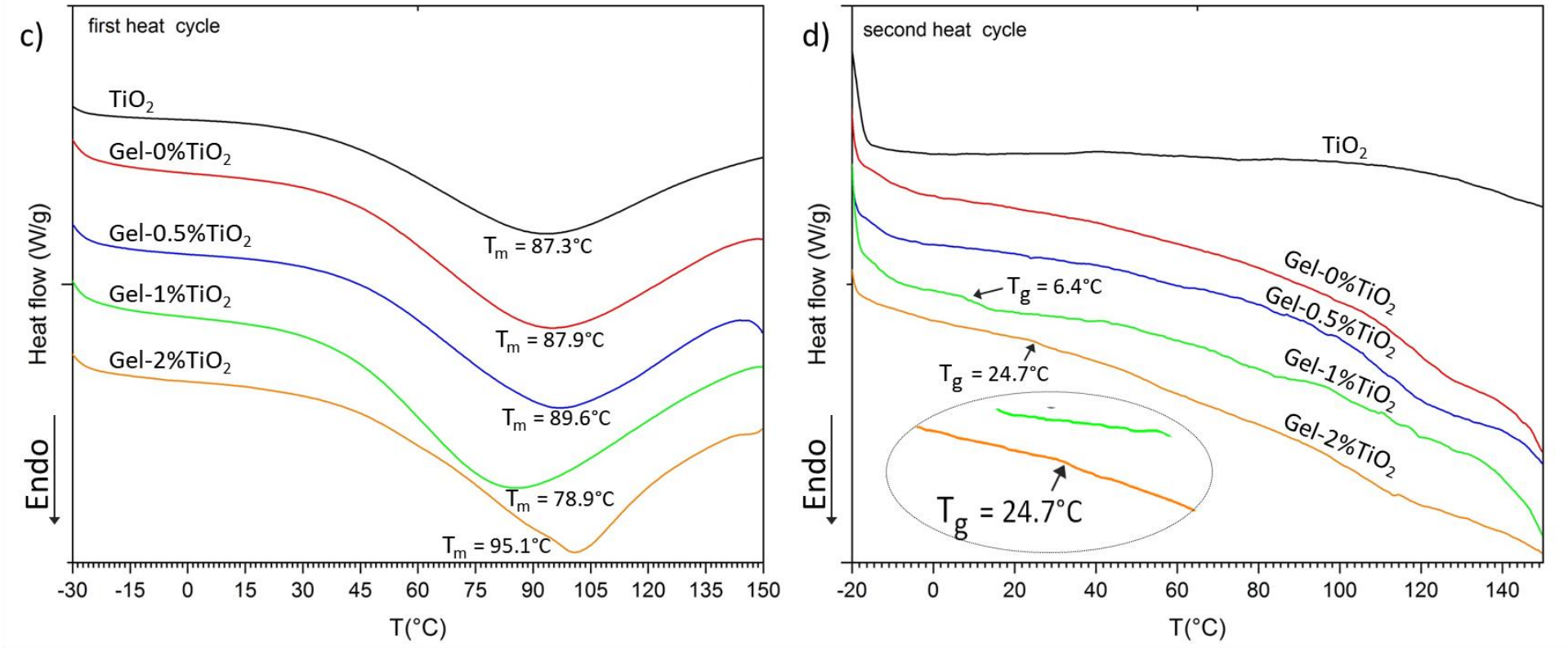

[1] HPMC: hydroxypropyl methylcellulose; Gel: gelatin; TiO_2: titanium dioxide

Source: Fonseca et al. (2020), with permission.

HPMC-0%TiO_2 exhibited T_m = 83.6°C and melting enthalpy (*ΔH*) of 147.9 $J.g^{-1}$. HPMC-0.5%TiO_2, HPMC-1%TiO_2 and HPMC-2%TiO_2 showed similar T_m values of 88.9°C, 86.9°C and 86.2°C and *ΔH* values of 118.3 $J.g^{-1}$, 130.1 $J.g^{-1}$ and 125.8 $J.g^{-1}$, respectively. The *ΔH* value decrease for the HPMC-TiO_2 films as the TiO_2 was incorporated can be caused by the lower number of hydrogen bonds between HPMC chains (MULLAH et al., 2017).

Gel-0%TiO_2 and Gel-0.5%TiO_2 showed similar T_m values, 87.9°C and 89.6°C, and melting enthalpy (*ΔH*), 175.2 $J.g^{-1}$ and 160.8 $J.g^{-1}$. It indicated that 0.5 wt % TiO_2 caused slight changes in the gelatin thermal properties. These changes were even more pronounced for the Gel-1%TiO_2, which showed a lower T_m value (78.9°C), but *ΔH* value (220.57 $J.g^{-1}$) higher than other gelatin-TiO_2 films. It characterizes a melting peak enlargement, suggesting that the hydrogen bonds between biopolymer chains decreased, and the interactions between TiO_2 nanoparticles and gelatin increased at 1 wt % TiO_2. Thus, nanocomposite amorphous phase results corroborate the XRD results. Finally, Gel-2%TiO_2 film exhibited an increase in T_m (95.1°C) and a decrease in *ΔH* (206.2 $J.g^{-1}$), accompanied by a sharpening of the melting peak. The TiO_2 agglomeration at 2 wt % probably contributed to preserving hydrogen bonds between biopolymer chains. T_m values of the HPMC-0%TiO_2 and Gel-0%TiO_2 nanocomposite films agree with results reported by Sangappa et al. (2008) and Rivero; García; Pinotti (2010), who studied structural and thermal properties of HPMC-based films modified by electron irradiation and gelatin-based films containing different plasticizer concentrations. Slight differences between results can be attributed to the different glycerol concentrations used to prepare the films (MULLAH et al., 2017).

During the second scan, it was observed a typical thermal behavior of crystalline materials in HPMC-TiO_2 films: the presence of two slight exothermic transitions at 51.7°C and 100°C, which can be associated with the HPMC chain partial recrystallization (CANEVAROLO JUNIOR, 2004). It was impossible to identify the T_g values for the Gel-0%TiO_2 and Gel-0.5%TiO_2 films, probably due to the plasticizing effect caused by water and glycerol molecules (ARFAT, 2017). However, the lower T_g value of the Gel-1%TiO_2 film (T_g = 6.4°C) in comparison with Gel-2%TiO_2 film (T_g = 24.7°C) suggests a lower number of hydrogen bonds between gelatin chains for Gel-1%TiO_2 film, and it reaffirms better TiO_2 nanoparticle distribution in it.

In general, DSC results evidenced that the poor TiO_2 dispersion has not changed the biopolymer thermal properties. It occurred both when the matrix was insufficiently filled and saturated with photocatalyst. The anatase phase presents a low dispersion due to its highly crystalline structure featured by a high T_m (1870°C) (MIAO et al., 2003) and indefinite T_g

(HOANG, 2008). Lastly, it was expected that the T_g changes in the HPMC-TiO_2 films were barely perceptible because of the insignificant moisture content difference between them. On the other hand, the lower moisture content of the gelatin-TiO_2 films probably made it possible to calculate the T_g.

3.3.2.7 Mechanical properties

HPMC-TiO_2 film mechanical properties were more affected by the TiO_2 incorporation than gelatin-TiO_2 films. Both HPMC-TiO_2 film elongation at break (*EB*) and tensile strength (*TS*) decreased as the TiO_2 concentration increased from 0 to 1 wt % ($p \leq 0.05$) (**Figure 20**). The Young's modulus (*YM*) has not been changed, exhibiting an average value of 0.34 ± 0.02 GPa ($p > 0.05$). Gelatin-TiO_2 films did not show difference for none of the evaluated parameters, so the calculated average for each parameter was *EB* = 10.5 ± 1.3 %, *TS* = 42.9 ± 2.4 MPa and *YM* = 1.01 ± 0.06 GPa.

Figure 20 - Elongation at break (*EB*) and tensile strength (*TS*) of the HPMC-TiO_2 nanocomposite films.

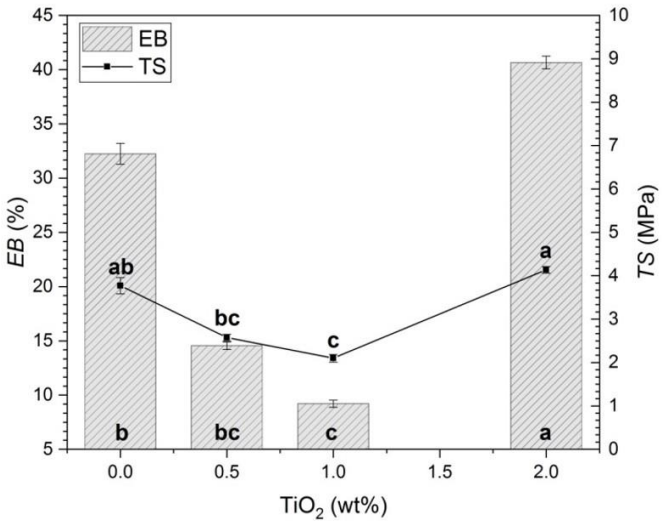

*All values were expressed as mean ± standard error (n = 3). Means within the same parameter having different letters are different at the level of α = 0.05.

Source: Fonseca et al. (2020), with permission.

In general, *YM* results evidenced that the nanocomposite films are fragile. *EB* and *TS* results revealed that the gelatin-based films are more resistant to the structural changes caused by the TiO_2 incorporation than HPMC-based films. The gelatin complex macromolecular structure, which contains side chemical groups and ionic groups (NH_3^+) (GOMEZ-GUILLEN et al., 2011; JOHLIN, 1930), hinders the polymer chain movement (OLEYAEI et al., 2016)

and becomes the gelatin-based films more resistant to the mechanical stress and less flexible. This result agrees with the SEM micrographs (**Figure 17**), in which the TiO_2 agglomeration was barely perceptible for the gelatin-TiO_2 films and evident for the HPMC-TiO_2 films. The gradual mechanical weakening of the HPMC-TiO_2 films (0 - 1 wt % TiO_2) can result from the repulsion between Ti^{4+} ions, which simultaneously hindered the TiO_2 aggregation and decreased interactions between biopolymer chains, causing the quick film mechanical failure.

HPMC-2%TiO_2 showed an unexpected increase in *EB* and *TS* values when compared to HPMC-0%TiO_2 film. However, this increase compared to HPMC-1%TiO_2 films has already been expected to preserve biopolymer matrix fractions without TiO_2.

In comparison with *EB*, *TS* and *YM* values from low-density polyethylene (LDPE; *EB* = 100 – 650 %; *TS* = 8.3 - 31.4 MPa; *YM* = 0.17 - 0.28 GPa) and high-density polyethylene (HDPE; *EB* = 10 – 1200 %; *TS* = 22.1 – 31.0 MPa; *YM* = 1.06 - 1.09 GPa) (CALLISTER; RETHWISCH, 2011), both HPMC-TiO_2 and gelatin-TiO_2 films exhibited typical *EB*, *TS* and *YM* values for polymers. HPMC-TiO_2 nanocomposite films showed lower elasticity than LPDE and stress resistance than both LDPE and HDPE and stiffness slightly higher than LDPE. Gelatin-TiO_2 nanocomposite films showed elasticity and stiffness values near HDPE and stress resistance higher than both LDPE and HDPE.

Li et al. (2011) classified the whey protein-TiO_2 film mechanical properties as catastrophic. The authors tested 0, 0.25, 0.5, 1 and 2 wt % TiO_2 related to polymer and did not report *TS* and *EB* difference between films added of 0 and 0.25 wt % TiO_2 ($p > 0.05$). However, *EB* and *TS* increased 71.9 % and 32.4 % for the films containing from 0.5 to 2 wt % TiO_2. This behavior was attributed to the polymeric matrix discontinuity and damage in its network structure caused by the TiO_2 aggregation.

3.3.2.8 Water vapor permeability

Water vapor permeability (WVP) is related to the facility or difficulty of water vapor molecules diffuse across the micro-pathways that compose the composite network microstructure (LI et al., 2011). The water diffusion can be affected by –OH groups and particles dispersed or agglomerated in the microstructure (OLEYAEI et al., 2016).

As expected, HPMC-TiO_2 nanocomposite films did not showed barrier property difference ($p > 0.05$) exhibiting an average WVP value of 0.60 ± 0.02 $g.mm.m^{-2}.h^{-1}.kPa^{-1}$. The WVP of the gelatin-TiO_2 nanocomposite films (**Table 8**) reduced as the TiO_2 content increased from 0 to 1 wt % TiO_2 and increased at 2 wt % TiO_2 ($p \leq 0.05$). These results

corroborate the moisture content and water solubility results. They also evidenced that even though TiO_2 agglomerates have probably modified the HPMC micro-pathways, the large number of –OH groups from the HPMC chains favored interactions between water molecules and polymer matrix.

On the other hand, the lower affinity between gelatin matrix and water molecules and the better TiO_2 dispersion into gelatin justify the gelatin-TiO_2 film WVP decrease. When TiO_2 nanoparticles are homogeneously dispersed into the gelatin matrix, the number of interactions between them increased and modified the film structure micro-pathways. The TiO_2 hydrophobic character, when unexposed to the UV-light, decreased the water-polymer interactions and reduced the gelatin-TiO_2 film WVP. The increased WVP for the Gel-2%TiO_2 film is associated with its larger TiO_2 agglomerates, forming sites in the gelatin matrix without TiO_2. Similar WVP values and behavior of gelatin-TiO_2 films were reported by He et al. (2016), and similar WVP values of HPMC-based films were obtained by Bilbao-Sainz et al. (2011).

Table 8 - Water vapor permeability (WVP) of gelatin-TiO_2 nanocomposite films.

Film[1,2]	**WVP** ($g.mm.m^{-2}.h^{-1}.kPa^{-1}$)
Gel- 0%TiO_2	$0.45 \pm (< 10^{-2})^{a}$
Gel- 0.5%TiO_2	$0.40 \pm (< 10^{-2})^{ab}$
Gel- 1%TiO_2	$0.36 \pm (< 10^{-3})^{b}$
Gel- 2%TiO_2	0.44 ± 0.02^{ab}

[1] All values were expressed as mean ± standard error (n=3). Means within the same column with different superscripts are different at the level of $\alpha = 0.05$.
[2] Gel: gelatin, TiO_2: titanium dioxide.

Source: Fonseca et al. (2020), with permission.

3.3.2.9 Schematic representation of HPMC-TiO_2 e gelatin-TiO_2 nanocomposite film structures

Based on all investigations carried out and the results obtained in this chapter, structures capable of representing the generation of biphasic regions in the HPMC-TiO_2 and gelatin-TiO_2 films caused by the TiO_2 aggregation (**Figure 21**) were proposed. This phase separation can be designed as micro-domains structures composed of sites containing polymer chains, glycerol and water molecules adsorbed, which can or not be filled by TiO_2 aggregates. The TiO_2 agglomeration grows up as the TiO_2 content increased, especially for HPMC-TiO_2 nanocomposite films. The formation of micro-domains induces the system microstructural

reorganization, including changes in the number of polymer-polymer, polymer-TiO_2 nanoparticles, nanocomposite-outside molecules interactions.

The best TiO_2 dispersion in gelatin does not mean that gelatin-TiO_2 films are more efficient photocatalyst materials than HPMC-TiO_2 films, but this is crucial for reaching high performance.

Figure 21 - Schematic representation of the physical structure proposed for the HPMC-TiO_2 and gelatin-TiO_2 nanocomposite films containing different TiO_2 concentrations.

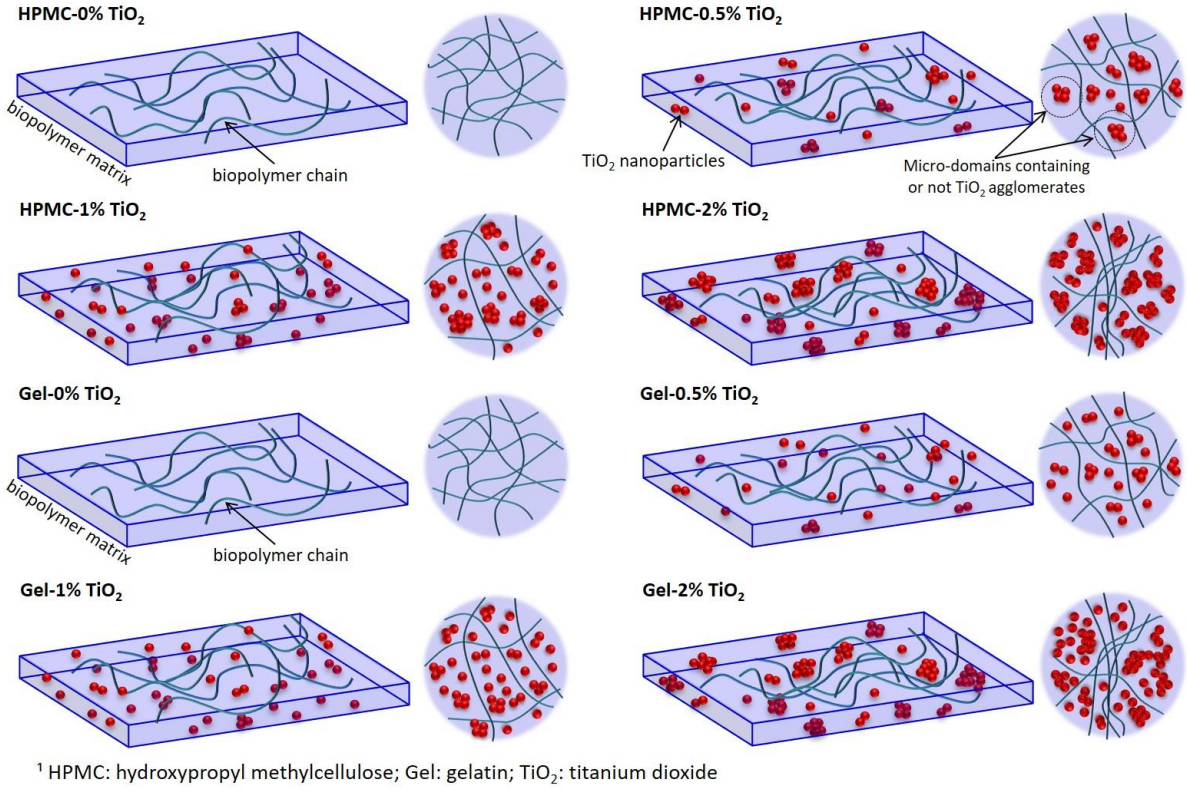

Source: Fonseca et al. (2020), with permission.

3.4 CONCLUSIONS OF CHAPTER 3

Effects of TiO_2 concentration on physicochemical, thermal, mechanical and barrier properties of the HPMC-TiO_2 and gelatin-TiO_2 dispersions and films were studied and discussed in this chapter. Results showed that all these changes are associated with photocatalyst dispersion degree into the film-forming dispersions. The biopolymer matrix hydrophilicity was a determinant characteristic for the TiO_2 dispersion. The natural hydrophobic character of TiO_2 under dark conditions improved its dispersion into the gelatin matrix, reducing its discontinuity. Thus, the gelatin-TiO_2 film solubility, moisture content and

water vapor permeability (WVP) decreased as the TiO_2 content increased. In contrast, for the HPMC-TiO_2 films, the TiO_2 concentrations tested could not change these characteristics, corroborated by the DSC results.

As well know, TiO_2 requires water and oxygen supply to generate radical species. Thus, HPMC can also be an excellent support to immobilize TiO_2 nanoparticles, supplying this requirement, while gelatin can be used to obtain better photocatalyst dispersion. Finally, the films containing 1 wt% TiO_2 (HPMC-1%TiO_2 and Gel-1%TiO_2) exhibited the most appropriate TiO_2 dispersion degree for photocatalysis application.

Chapter 4. PHOTOCATALYTIC PROPERTIES OF HYDROXYPROPYL METHYCELLULOSE-TiO_2 AND GELATIN-TiO_2 FILMS AND EXPANDED POLYETHYLENE FOAM NETS COATED WITH GELATIN-TiO_2

This chapter reports the second experimental phase of this thesis that comprises a study about the ethylene photocatalytic degradation using HPMC-TiO_2 and gelatin-TiO_2 films and gelatin-TiO_2-coated expanded polyethylene foam nets.

From this step, it was written the second experimental article titled "*Ethylene scavenging properties from hydroxypropyl methylcellulose-TiO_2 and gelatin-TiO_2 nanocomposites on polyethylene supports for fruit application*", published in the *International Journal of Biological Macromolecules* (impact factor (2020): 5.162; https://doi.org/10.1016/j.ijbiomac.2021.02.160). According to Elsevier subscription rules, the authors retain the right to include the article in a thesis, provided it is not published commercially.

4.1 INTRODUCTION

The TiO_2 aggregation tendency compromises the biopolymer-TiO_2 film structural and photocatalytic properties (FONSECA et al., 2020; LI et al., 2011; OLEYAEI et al., 2016; SIRIPATRAWAN; KAEWKLIN, 2018; ZHOU; WANG; GUNASEKARAN, 2009). So, this limitation can affect the film ethylene scavenging ability (KAEWKLIN et al., 2018; MANEERAT; HAYATA, 2008; SIRIPATRAWAN; KAEWKLIN, 2018; WANG et al., 2019; ZHANG et al., 2019).

One of the alternatives to improve the ethylene scavenging ability of HPMC-TiO_2 and gelatin-TiO_2 films is to increase their photocatalytic surface area. Thus, these materials can be applied as coatings on supports with high surface area (MATSUI et al., 2004; ZHANG; XIAO; QIAN, 2014). Some alternative supports for fruit applications are premanufactured materials commercially used for the physical protection of fruit, such as the expanded polyethylene (EPE) foam nets (ZANON BARÃO, 2011).

EPE foam nets display a tridimensional structure, providing a high surface area for light irradiation, substrate adsorption and coating adhesion. Furthermore, their mesh design allows free gas exchanges between fruit and the environment, avoiding undesirable fermentation.

In this step, the goal was to study the ethylene photocatalytic degradation by HPMC-TiO_2 and gelatin-TiO_2 films and EPE foam nets coated with different gelatin-TiO_2 loadings. Changes in the surface roughness and chemical composition of HPMC-TiO_2 and gelatin-TiO_2 films caused by the photocatalysis reaction and surface morphology of foam nets were also evaluated.

4.2 MATERIALS AND METHODS

4.2.1 Materials

EPE foam nets (13.2 x 10^{-2} m^2, W-paper Comércio de Embalagens Ltda-ME, São Paulo-Brazil) **(Figure 22)**; HPMC (Methocel E19, Dow Chemical Company, USA); bovine gelatin (bloom 250, Gelnex, Brazil); glycerol (99%, Neon, Brazil); TiO_2 (pure anatase, Hombikat UV 100, average crystallite diameter < 10 nm) and acetic acid solutions (0.087 and 1 mol L^{-1}) were used as support, polymeric matrices, plasticizer, photocatalyst and solvents, respectively. The reagents were used as purchased, and solvents are analytical-grade reagents.

Figure 22 - Expanded polyethylene (EPE) foam net.

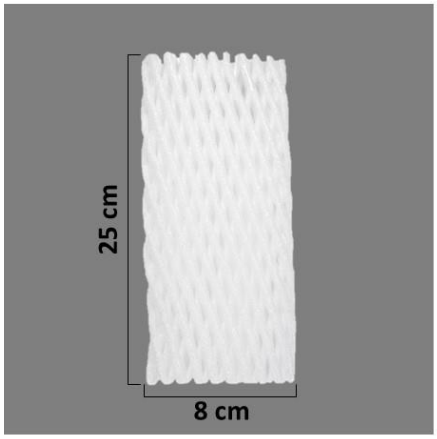

EPE[1] foam parameters	Measures (10^{-2})
Length [m]	25.0
Width [m]	8.0
Wire diameter [m]	0.4
Surface area [m^2]	13.2

[1]Expanded polyethylene

Source: Author.

4.2.2 Methods

4.2.2.1 Preparation of HPMC-TiO_2 and gelatin-TiO_2 films and gelatin-TiO_2-coated EPE foam nets

HPMC-TiO_2 and gelatin-TiO_2 coating dispersions and films were prepared according to the method described in section 3.2.2.1. Respective sample films based on HPMC and gelatin were denominated HPMC-0%TiO_2, HPMC-0.5%TiO_2, HPMC-1%TiO_2 and Gel-0%TiO_2, Gel-0.5%TiO_2, Gel-1%TiO_2 and Gel-2%TiO_2. These nanocomposites had their structural and photocatalytic properties evaluated as films.

EPE foam nets were coated with 0, 1, 2, 4 layers of gelatin-TiO_2 dispersion (EPE, EPE-1x-Gel-1%TiO_2, EPE-2x-Gel-1%TiO_2 and EPE-4x-Gel-1%TiO_2,). For the coating of EPE foam nets with a gelatin-TiO_2 monolayer (EPE-1x-Gel-1%TiO_2), blank EPE foam nets were dipped into gelatin-TiO_2 dispersion at immersion rate of 2 cm s^{-1} and kept immersed under moderated stirring at 23°C ± 1°C for 2 min. Then, foam nets were emerged (2 cm s^{-1}) and dried in a BOD refrigerated incubator at 15°C for 30 min, followed by a second drying at 25°C for 48 h. The layer-by-layer nanocomposite coatings on the EPE foam nets (EPE-2x-Gel-1%TiO_2 and EPE-4x-Gel-1%TiO_2) were prepared by performing subsequent immersion cycles (23°C ± 1°C for 2 min) alternated with drying processes (15°C for 30 min), and a final drying at 25°C for 48 h. Weight loss of gelatin-TiO_2 dispersion not adhered to the EPE foam nets was taken into account in all steps. Blank EPE and gelatin-TiO_2-coated EPE foam nets were stored in a chamber (25ºC, 58 % RH) for at least 48 h before characterizations.

4.2.2.2 Characterization of HPMC-TiO_2 and gelatin-TiO_2 films and gelatin-TiO_2-coated EPE foam nets

4.2.2.2.1 Photocatalytic activity preliminary evaluation

There are several methods to evaluate the photocatalytic properties of TiO_2 immobilized on a surface. One of them (ISO, 2009) is based on the degradation of the oleic acid (OA) layer deposited on the photocatalytic surface under UV-A light. The OA layer degradation is evaluated by the apparent water contact angle (θ,°) changes and gravimetric analysis (MILLS; HILL; ROBERTSON, 2012).

In order to determine the HPMC-TiO_2 and gelatin-TiO_2 nanocomposite formulations with the best photocatalytic activities, the tests were carried out in three steps: (1) investigation of photocatalyst activation, (2) investigation of possible interactions between OA layer and nanocomposite films and (3) evaluation of OA degradation.

On the first step, nanocomposite film samples (5.5 cm^2 in area) were fixed on the glass slides, stored in a chamber (at 25°C and 58% RH) equipped with a UV-A light (turned off, TL G5 BLB Blacklight UV Philips®, 8 W, λ_{peak} = 365 nm) and 2 µL of water were dripped on the film surfaces in different six positions. The apparent water contact angle (θ) was measured using a goniometer (Ramé-Hart Inst. Co. 250-F1 equipped with Drop-image software®). After, film samples were positioned at 2 cm far from UV-A light (2.96 mW cm^{-2}) and exposed to it for 24 h to clean their surface. Then, θ was measured again. (ISO, 2009).

On the second step, films were previously prepared under the same conditions used for the first step. Before and after exposing the films to the UV-A light for 24h, 2 µL of OA were dripped on their surfaces in six different positions, and OA contact angle (θ_{OA}) was measured.

On the third and last step, new sample films fixed on the glass slides were exposed to the UV-A light for 24 h. Then, film pieces were coated with a thin layer of OA (20 µg.cm^{-2}), corresponding to approximately 1600 nm or 800 uniform film monolayers (OLLIS, 2018). OA layer degradation was evaluated by measuring the apparent water contact angle (θ) periodically for eight days. Additional gravimetric analysis was performed to confirm the OA photocatalytic degradation. Film circular pieces (8.4 cm in diameter), previously exposed to the UV-A light (at 25°C and 58 % RH for 24 h), were coated with OA (20 µg.cm^{-2}) and periodically weighed (± 0.0001 g) in order to evaluate their weight loss during the OA degradation (WL_{OAD}, [%]). The sample weight was also monitored for eight days and calculated using **equation 13**.

$$WL_{OAD}(\%) = \frac{|W_f - W_i|}{W_i}\ x\ 100 \qquad (13)$$

Where W_i is the initial weight [g] of the cleaned film samples coated with OA layer (20 µg.cm^{-2}) at the initial time (t = day 0) and W_f is the final weight of film samples at a determined time (t, [day]).

4.2.2.2.2 Ethylene photocatalytic degradation

Ethylene photocatalytic degradation reactions were carried out in a batch system reactor (**Figure 23**). This system was composed of a glass rectangular parallelepiped reactor (40 cm x 7 cm x 7 cm) equipped with one gas homogenizer fan, one UV-A light lamp (Osram DULUX®L Blue UV-A, 24 W, λ_{peak} = 365 nm) and one stainless steel support for gripping the films (20.4 x 10^{-2} m^2) or foam nets (13.2 x 10^{-2} m^2). Two fans were installed externally to the reactor to avoid internal overheating, and the room temperature was maintained at 22°C. Reactions were carried out at 30 ± 1ºC, and supersaturated KCl solution was deposited on the bottom of the reactor for maintaining the indoor RH at 85 %, simulating a severe fruit storage condition. Films and foam nets were fixed on the support at 2 cm from the UV-A lamp (9.8 mW cm^{-2}, radiation intensity). The reactor was sealed and coated, internal fan and UV-A light were turned on for 2 h to homogenize and clear the photocatalytic surface. Then, the lamp was turned off, and the reactor (1.79 x 10^{-3} m^3; void volume) was filled with a synthetic gas mixture of ethylene/air (101 ppmv), aiming for a final ethylene concentration of 5 ppmv (SIRIPATRAWAN; KAEWKLIN, 2018). The ethylene homogenization was carried out for 2.5 h in the absence of UV-A light until the gas-solid adsorption-desorption equilibrium to be achieved. Then, the UV-A lamp was turned on again.

Figure 23 - Batch reactor design used to degrade synthetic ethylene by hydroxypropyl methylcellulose-TiO_2 and gelatin-TiO_2 films (a) and gelatin-TiO_2-coated EPE foam nets (b).

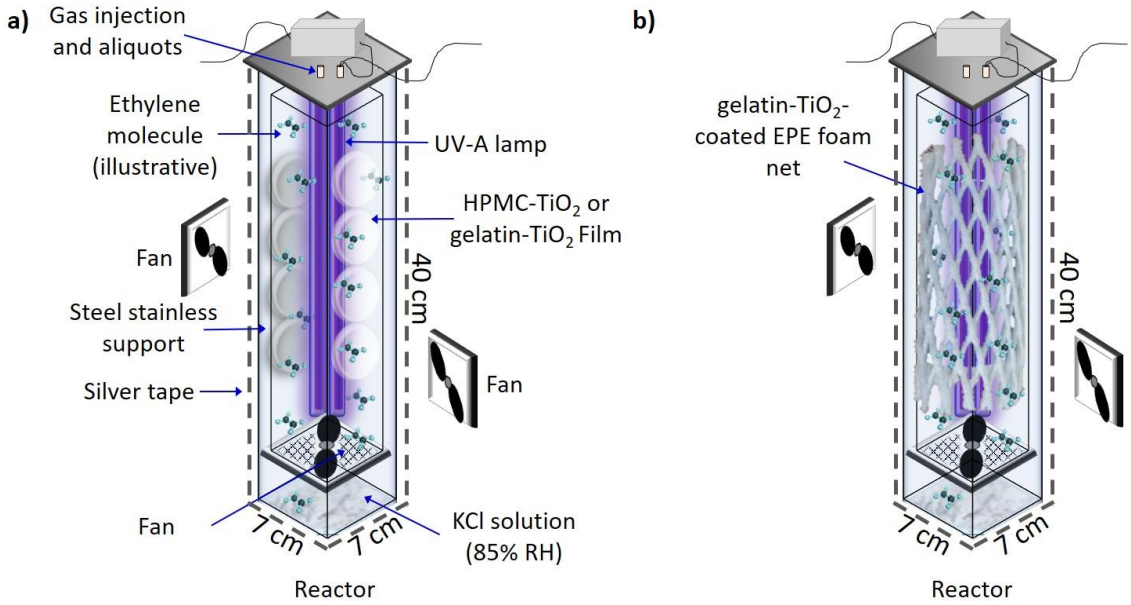

[1] HPMC: hydroxypropyl methylcellulose; [2] EPE: expanded polyethylene; [3] RH: relative humidity

Source: Fonseca et al. (2021), with permission.

Ethylene concentration was measured in a gas chromatograph coupled with mass spectrometry (GC-MS equipped with a triple-axis detector Agilent 5975C inert MSD, system Agilent 7890A GC and Supel-Q-plot, Supelco column (32 m x 0.32 mm)). The thermal program used to detect ethylene was: selected ion monitored (SIM) mode set to precisely detect the mass/charge ratio of 28 for ethylene, splitless mode and temperatures of 28°C, 120°C, 200°C and 250°C for isothermal oven, injector, detector and transfer line, respectively. Helium (5.0 White Martins) was used as carrier gas at a rate of 1.33 $mL.min^{-1}$. Gas aliquots (250 µL) were taken using a gastight syringe and measured at 0, 5, 10, 15, 30, 45, 60, 90, 120 and 150 min after beginning the reaction. After tests, all samples were stored in a chamber at 25ºC and RH = 58 % for at least 48 h before characterizations. All experiments were carried out in triplicate.

The non-converted ethylene concentration at the steady-state is given by **equation 14**:

$$C_{C_2H_4,t} = C_{C_2H_4,i} * (X_{C_2H_4,max} - X_{C_2H_4}) \quad (14)$$

Where $C_{C_2H_4,t}$ and $C_{C_2H_4,i}$ are the respective ethylene concentrations at a determined time (*t*, [min]) and initial time (*t* = 0 min) as soon as the UV-A lamp was turned on, while $X_{C_2H_4}$ and $X_{C_2H_4,max}$ are the ethylene conversions from 0 to 1 at a determined time (*t*, [min]) and final time (*t* = 150 min), respectively.

The ethylene photocatalytic degradation is frequently described according to the Langmuir-Hinshelwood model (**equation 15**).

$$-\frac{dC_{C_2H_4}}{dt} = \frac{K\,k\,C_{C_2H_4}}{1 + (K\,C_{C_2H_4})} \quad (15)$$

Where, $\frac{dC_{C_2H_4}}{dt}$ is the reaction rate, *K* is the ethylene adsorption constant, *k* is the reaction rate constant and $C_{C_2H_4}$ is the ethylene concentration.

The Langmuir-Hinshelwood model can be simplified considering the following conditions: (1) the ethylene adsorption occurs in a photocatalyst monolayer on a solid homogeneous surface, (2) active sites are uniform, (3) the equilibrium between species in fluid phase is dynamic, (4) $[C_2H_4] << [O_2]$, so $[O_2]$ is approximately constant and does not depend on the time and (5) the adsorbate (ethylene) concentration is deficient in respect to the

other gas components, so $K.C_{C_2H_4}$ << 1 and (1 + $K.C_{C_2H_4}$) ~ 1 (LODDO; RODA; PARRINO, 2019; MANEERAT; HAYATA, 2008).

After applying the previous considerations, integrating indefinitely **equation 15** and replacing the $C_{C_2H_4}$ by **equation 14**, the Langmuir-Hinshelwood model equation was rearranged as a function of ethylene conversion ($X_{C_2H_4}$) (**equation 16**):

$$X_{C_2H_4} = B - \ A\, e^{(-k_{app}\, t)} \tag{16}$$

Where, $X_{C_2H_4}$ is the ethylene conversion at a determined time (*t*, [min]), k_{app} is the apparent rate constant corresponding to the product of adsorption and reaction rate constants ($k_{app} = K\ k$), and *A* and *B* are apparent coefficients, considering the occurrence of a reaction non-competitive inhibition. In the case of first-order irreversible reactions, *A* and *B* values would be 1 and 0, respectively.

4.2.2.2.3 Topography and morphology

Possible alterations in the film surface roughness caused by the TiO_2 photocatalysis and UV-A light were investigated by topographic analysis. Topographic images of HPMC-TiO_2 and gelatin-TiO_2 films were generated by atomic force microscopy (AFM) using a microscope model Easy Scan 2 FlexAFM Nanosurf set up in semi-contact mode. Film surface root-mean-squared roughness (R_{RMS}, [nm]) was calculated by **equation 17** (LEPRINCE-WANG; YU-ZHANG, 2001) using the WSxM 5.0 Develop 9.1 software.

$$R_{RMS} \frac{\sum_{n=1}^{N}(z_n - \bar{z})^2}{(N-1)} \tag{17}$$

Where z_n is the height of the nth data, $\bar{z}$ is the medium height of z_n values, and *N* is the total pixel numbers (image resolution).

The surface and transversal section morphology of the gelatin-TiO_2-coated EPE foam nets (0.3 cm x 0.5 cm) was evaluated by scanning electronic microscopy (SEM) using a microscope model JSM 6390 LV-JEOL, Japan, with an accelerating voltage of 15 kV (ZHANG et al., 2017). All samples were sputtered with a thin gold layer before microscopic observations, and their fracture was carried out by immersion in nitrogen liquid.

4.2.2.2.4 Chemical composition

Film chemical composition changes caused by TiO_2 photocatalysis and UV-A light irradiation were investigated by Fourier-transform infrared (FTIR) spectroscopy. The FTIR spectra were recorded at a wavenumber range from 650 to 4000 cm^{-1}, the spectral resolution of 4.0 cm^{-1} and 32 scans using an FTIR spectrometer model Agilent Technology Cary 660, equipped with Universal Attenuated Total Reflectance (ATR) and a ZnSe crystal. Film pieces (1 cm x 1 cm) previously stored in silica gel (48 h) were deposited on the ATR support for taking the measurements.

FTIR spectroscopy was also used to investigate a possible photodegradation of blank EPE foam nets by UV-A light. Samples were prepared and analyzed under the same conditions used for the nanocomposite films.

4.2.2.2.5 Nanocomposite loading on the EPE surface

The gelatin-TiO_2 dispersion loading on the EPE foam surface was estimated by gravimetric analysis. Values were expressed as to the loaded wet coating (*LWC,* [g m^{-2}]), loaded TiO_2 ($TiO_{2(loaded)}$, [g m^{-2}]) and loaded dry coating (*LDC,* [g m^{-2}]) according to **equations 18 - 20**, respectively.

$$LWC = \frac{\sum_{n=1}^{N}(IWD_n - FWD_n - WNAD_n)}{A_{EPE}} \quad (18)$$

Where n is the immersion number ($0 \leq N \leq 4$), A_{EPE} is the EPE foam net surface area [m^{-2}] and IWD_n, FWD_n and $WNAD_n$ are the initial dispersion weight [g] before immersion n, the final dispersion weight [g] after immersion n and the non-adhered dispersion weight [g] at immersion n, respectively.

$$TiO_{2(loaded)} = \frac{W_{TiO_2}}{A_{EPE}} \; x \; 100 \quad (19)$$

Where W_{TiO_2} is the TiO_2 weight [g] dispersed in the wet coating fraction loaded on the EPE surface, and A_{EPE} is the EPE foam surface area [m^{-2}].

$$LDC = \frac{W_{AC} - W_{BC}}{A_{EPE}} \quad (20)$$

Where W_{AC} is the coated and dried EPE foam weight [g], W_{BC} is the non-coated EPE foam weight [g] and A_{EPE} is the EPE foam surface area [m^{-2}].

4.2.2.2.6 Statistical analysis

Significant differences between experimental data were assessed by one-way analysis of variance (ANOVA) and Tukey test of multiple comparisons ($p \leq 0.05$) using Statistica software (version 13.0).

Laboratories, in which experiments and analyses were carried out, are presented in **Table 9**.

Table 9 - Laboratories located at UFSC used to carry out the second step of this thesis.

Experiments/Characterizations	Laboratories
Manufacture of films and EPE foam nets coated with gelatin-TiO_2 nanocomposite.	Laboratório de propriedades físicas dos alimentos (PROFI/EQA).
FTIR-ATR of films and foam nets, contact angle analyses and photocatalytic degradation tests	Central de Análises do Departamento de Engenharia Química e de Alimentos da UFSC (CA/EQA)
AFM of films.	Laboratório de Optoeletrônica Orgânica e Sistemas Anisotrópicos (LOOSA/CFM)
SEM of foam nets coated with gelatin-TiO_2 nanocomposite.	Laboratório Central de Microscopia Eletrônica (LCME).

Source: Author.

4.3 RESULTS AND DISCUSSIONS

4.3.1 Photoactivation of TiO_2 immobilized into films

The good photocatalytic performance of TiO_2-based surfaces depends on relative humidity. Water molecules contribute to generating $HO^{\bullet}$ radicals triggering photocatalytic reactions. However, at the same time, they compete with adsorbate molecules by the active sites (LEE et al., 2015; LIN; WENG; CHEN, 2014; LIN et al., 2014; PARK et al., 2001). It explains the super-hydrophilic character of TiO_2-based surfaces when exposed to UV-A light (MIDTDAL; JELLE, 2013; MILLS; CROW, 2007). During the postharvest life, the fruit

continues its metabolic functions such as respiration and transpiration, so water vapor production is vital to keep enough humidity and ensure ethylene degradation efficiency.

The TiO_2 content did not cause alterations ($p > 0.05$) in the water contact angle (θ) for both HPMC-TiO_2 and gelatin-TiO_2 films in the absence of UV-A light (dirty surface) (**Table 10**). In this dark condition, HPMC-TiO_2 and gelatin-TiO_2 films presented θ averages of $\bar{\theta}$ = 47.40 ± 0.29° and $\bar{\theta}$ = 83.57 ± 1.26°, respectively. After UV-A light exposure, the HPMC-TiO_2 film clean surface presented a θ decrease as the TiO_2 concentration increased from 0 to 1 wt % and a θ increase from 1 to 2 wt % ($p \leq 0.05$), while gelatin-TiO_2 films did not present differences. When different treatments (exposition or not to the UV-A light) applied to the same film are compared, only films based on HPMC and gelatin containing 1 wt % TiO_2 presented a significant θ value reduction under the UV-A light.

Table 10 - Water contact angle (θ) for films based on hydroxypropyl methylcellulose (HPMC) and gelatin (Gel) containing titanium dioxide (TiO_2) before and after UV-A light exposure.

Biopolymer Matrix [1]	TiO_2 concentration (wt %)	θ [°]	
		Not exposure to the UV-A	**Exposure to the UV-A**
HPMC	0	$47.64 \pm 1.72^{a,A}$	$48.26 \pm 1.53^{a,A}$
	0.5	$47.91 \pm 2.26^{a,A}$	$45.61 \pm 2.47^{ab,A}$
	1	$46.12 \pm 0.99^{a,A}$	$37.75 \pm 0.66^{b,B}$
	2	$47.94 \pm 1.11^{a,A}$	$44.07 \pm 1.80^{ab,A}$
Gel	0	$80.05 \pm 5.98^{a,A}$	$75.56 \pm 3.17^{a,A}$
	0.5	$81.88 \pm 2.77^{a,A}$	$74.27 \pm 5.11^{a,A}$
	1	$88.27 \pm 0.13^{a,A}$	$74.45 \pm 1.51^{a,B}$
	2	$84.08 \pm 4.59^{a,A}$	$73.45 \pm 3.72^{a,A}$

[1] All values were expressed as mean ± standard error (n = 3). [2] Means within the same column and for the same group having different superscripts (minuscule letters) and those within the same line and for the same group having different superscripts (majuscule letters) are different at the level of α = 0.05.

Source: Fonseca et al. (2021), with permission.

The highest θ values obtained for gelatin-TiO_2 films under dark conditions confirm their higher hydrophobicity than HPMC-TiO_2 films. The θ values measured agree with Wang et al. (2018), Ding, Zhang & Li (2015), Yasuda, Okuno & Yasuda (1994) and Bialopiotrowicz & Jańczuk (2002), who reported θ = 52°, 61.8°, 90° and 95° for HPMC acetate succinate, HPMC, gelatin (15 wt %) and gelatin (4 wt %), respectively. According to Bialopiotrowicz & Jańczuk (2002), gelatin-based films can show a broad water contact angle range. It depends on raw material origin, gelatin physicochemical properties and processing, gelatin concentration in film-forming dispersion, and film preparation methods. The authors

concluded that high θ values result from functional groups on the gelatin surface (-CH_3, -CH_2-, -NH_2-, -COOH) and changes in the specific hydration of the gelatin-based film during the water drop settling.

Statistically, only HPMC-1%TiO_2 film showed a significant θ reduction from 46.12 ± 0.99° to 37.75 ± 0.66° after UV-A light exposure, indicating that HPMC-1%TiO_2 film is photoactive. The HPMC-2%TiO_2 film did not present activity, probably because of the TiO_2 agglomeration that intensified the light scattering and limited the reactive oxygen species (ROS) generation.

Similar behavior was observed in gelatin-based films. Gel-1%TiO_2 was the only film that exhibited a θ reduction, from 88.27 ± 0.13° to 74.45 ± 1.51°. So, HPMC-1%TiO_2 and Gel-1%TiO_2 films were capable of harvesting light, hydrolyzing water molecules and generating ROS.

The θ value preservation for other gelatin-TiO_2 film formulations under the UV-A light shows that the most resistance of gelatin surface to the hydrophilicity rising caused by TiO_2 incorporation.

4.3.2 Oleic acid degradation under nanocomposite films

The oleic acid film degradation was carried out using HPMC-0%TiO_2, HPMC-1%TiO_2, Gel-0%TiO_2 and Gel-1%TiO_2 films (ISO, 2009). Characteristics such as double bond, low volatility, liquidity at temperature and condensed phase stability make difficult the oleic acid removal from surfaces. Several polar intermediate products are formed from its degradation, such as nonanal, 9-oxononanoic, azelaic and nonanoic acid (RATHOUSKÝ et al., 2011). Because of this, oleic acid is a suitable standard compound to evaluate the photocatalytic activity of surfaces (RATHOUSKÝ et al., 2011). As the oleic acid film is degraded, its water contact angle decreases (OLLIS, 2018).

Before oleic acid (OA) degradation tests, the contact angle measurements between OA drop and blank or nanocomposite films (θ_{OA}) (**Table 11**) were carried out in order to investigate possible physical interactions between them**.**

Table 11 - Oleic acid (OA) contact angle (θ_{OA}) for the films based on hydroxypropyl methylcellulose (HPMC) and gelatin (Gel) containing titanium dioxide (TiO_2) before and after UV-A light exposure.

Biopolymer Matrix [1]	TiO_2 concentration (wt %)	θ_{OA} [°]	
		Not exposure to the UV-A	**Exposure to the UV-A**
HPMC	0	$19.55 \pm 0.89^{a,A}$	$19.57 \pm 1.05^{a,A}$
	1	$18.21 \pm 0.78^{a,B}$	$24.29 \pm 1.23^{b,A}$
Gel	0	$24.92 \pm 1.89^{a,A}$	$20.52 \pm 1.90^{b,A}$
	1	$15.60 \pm 0.34^{b,B}$	$29.10 \pm 2.22^{a,A}$

[1] All values were expressed as mean ± standard error (n = 3). [2] Means within of the same column and for the same group having different superscripts (minuscule letters) and those within of the same line and for the same group having different superscripts (majuscule letters) are different at the level of $\alpha = 0.05$.

Source: Fonseca et al. (2021), with permission.

The contact angle between films, previously exposed to the UV-A light, and OA drop (**Table 11**) was lower than the water drop contact angle (**Table 10**) ($\theta_{OA} < \theta$). Before UV-A light exposure, Gel-1%TiO_2 film showed θ_{OA} lower than Gel-0%TiO_2 film ($p \leq 0.05$), while HPMC-0%TiO_2 and HPMC-1%TiO_2 did not present differences (**Table 11**). In contrast, there was a θ_{OA} increase for HPMC-1%TiO_2 and Gel-1%TiO_2 films after irradiation. HPMC-0%TiO_2 and Gel-0%TiO_2 did not present θ_{OA} changes and, consequently, they did not exhibit photocatalytic properties as expected.

The result showed that HPMC and gelatin matrices have more physical interactions with OA than water ($\theta_{OA} < \theta$). These interactions are more evident for gelatin-TiO_2 than HPMC-TiO_2 films due to the θ_{OA} decrease by adding TiO_2 under dark conditions. The non-irradiated TiO_2 hydrophobic character increased the gelatin hydrophobicity and its OA affinity. On the other hand, the HPMC hydrophilicity did not decrease by adding TiO_2. The θ_{OA} increase for the irradiated HPMC-1%TiO_2 and Gel-1%TiO_2 films evidences an increased surface hydrophobicity. It resulted from film surface photoinduction (SAKAI et al., 2003; ZHANG et al., 2012).

After investigating the physical interactions between nanocomposite films and OA, new films were coated with a thin OA layer. The OA degradation was evaluated by water contact angle evolution (θ, water drop on OA layer) and gravimetric analysis **(Figure 24)**.

Figure 24 - Images of water drops (a), water contact angle (θ) evolution (b), and weight loss (c) of nanocomposite films based on hydroxypropyl methylcellulose (HPMC) and gelatin (Gel) containing 0 and 1 wt % of titanium dioxide (TiO_2) coated with oleic acid (OA) and stored under UV-A light.

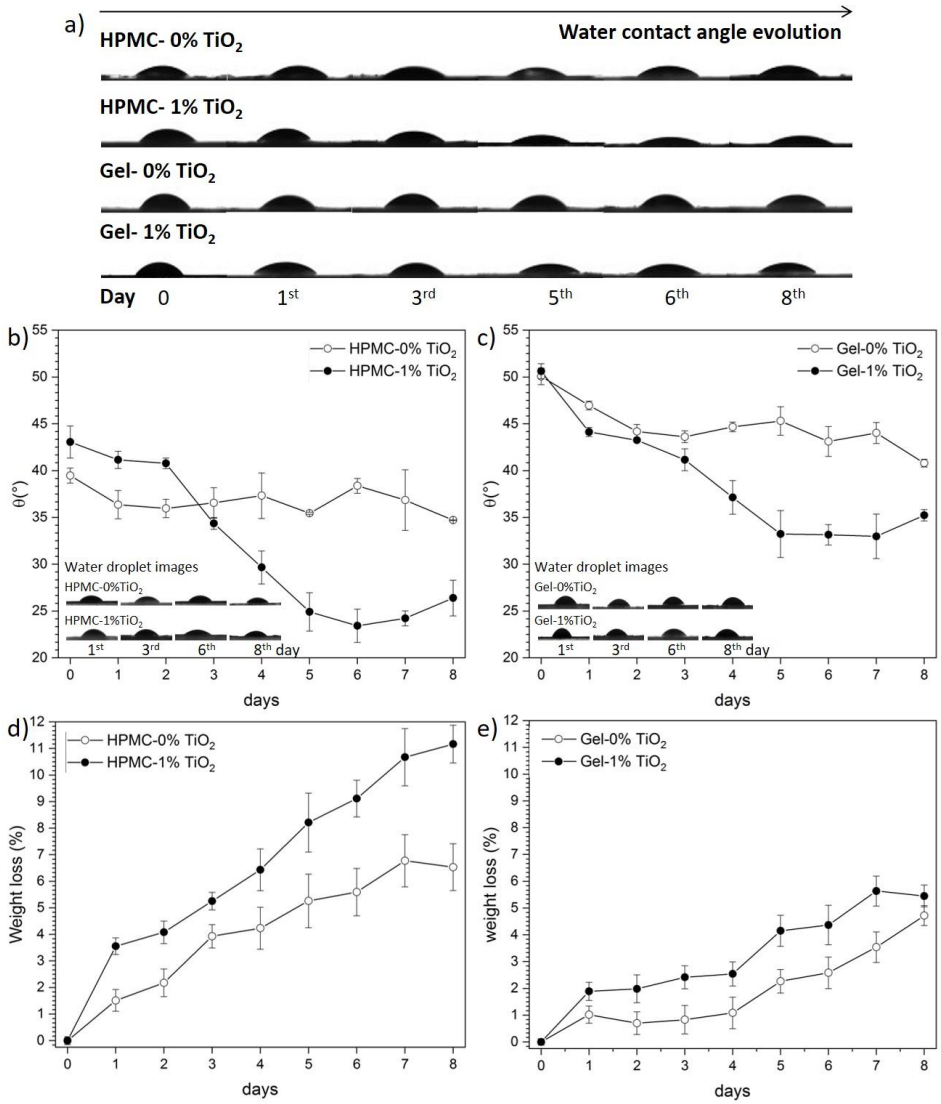

[1] HPMC: hydroxypropyl methylcellulose; Gel: gelatin; TiO_2: titanium dioxide

Source: Fonseca et al. (2021), with permission.

Over six days θ decreased 45.6 ± 0.9 % for HPMC-1%TiO_2 film. This decrease was characterized by a sharp θ reduction between the second and fifth days (**Figures 24.a, b)**. After the sixth day, θ values increased, indicating that most of the OA layer was photocatalytically degraded by TiO_2. The HPMC-0%TiO_2 film showed θ oscillations ($\bar{\theta}$ = 36.8 ± 0.5°) and a total θ decrease of 12.1 ± 0.8 % between days 0 and 8. This reduction is attributed to the possible OA and polymer photo-oxidation (MILLS; HILL; ROBERTSON, 2012; OLLIS, 2018).

Gel-1%TiO_2 nanocomposite film also showed photocatalytic activity characterized by the θ reduction (34.4 ± 4.9 %) (**Figures 24.a, c)**. However, this decrease was abrupt over the first five days of photocatalysis, followed by θ value stagnation. The Gel-0%TiO_2 film also showed OA photo-oxidation with a total θ reduction of 18.5 ± 0.9 %.

All films lost weight over the eight days under UV-A light (**Figures 24.d, e**). The weight loss was more expressive for the HPMC-1%TiO_2 (11.2 ± 0.7 %) and Gel-1%TiO_2 (6.5 ± 0.8 %) films than HPMC-0%TiO_2 (6.5 ± 0.9 %) and Gel-0%TiO_2 (5.5 ± 0.9 %) films, respectively. This result confirms that OA was degraded, but biopolymer matrices were also partially photodegraded (JACQUOT et al., 2012). Both OA and biopolymer degradations have been intensified by the water hydrolysis catalyzed by TiO_2 on the film surface, generating more ROS (HAIDER et al., 2018).

Finally, HPMC-1%TiO_2 presented higher θ reduction and weight loss than Gel-1%TiO_2 film, evidencing its better photocatalytic activity for degrading OA. Although TiO_2 nanoparticles have been better dispersed into gelatin, the highest HPMC-1%TiO_2 hydrophilicity probably enhanced the ROS generation. Water molecules can also fill vacancy defects in the TiO_2 structure, avoiding that electrons are trapped as defect sites (Ti^{3+} and O^-) (LIN; WENG; CHEN, 2014; LIN et al., 2014; PARK et al., 2001). All this contributes to the nanocomposite photocatalyst performance improvement.

4.3.3 Ethylene degradation by HPMC-TiO_2 and gelatin-TiO_2 films

HPMC-1%TiO_2 and Gel-1%TiO_2 films able to degrade OA were tested as to their abilities to degrade ethylene. Both films exhibited a maximum ethylene conversion ($X_{C_2H_4,max}$) approximately 0.4 or 40 % ($p \leq 0.05$) according to reaction kinetics data (**Figure 25**). As expected, blank films did not show photocatalytic activity. Small oscillations observed in ethylene conversion for the blank films are attributed to the gas adsorption-desorption equilibrium on the film surface. The kinetics data of HPMC-1%TiO_2 and Gel-1%TiO_2 films were well fitted to the Langmuir-Hinshelwood model. The apparent rate constant (k_{app}) and other parameters from **equation 16** are presented in **Table 12**.

Figure 25 - Photocatalytic degradation kinetics of ethylene (C_2H_4) for the films based on hydroxypropyl methylcellulose (HPMC) and gelatin (Gel) containing 0 and 1 wt% of titanium dioxide (TiO_2) and fitting to the Langmuir-Hinshelwood model.

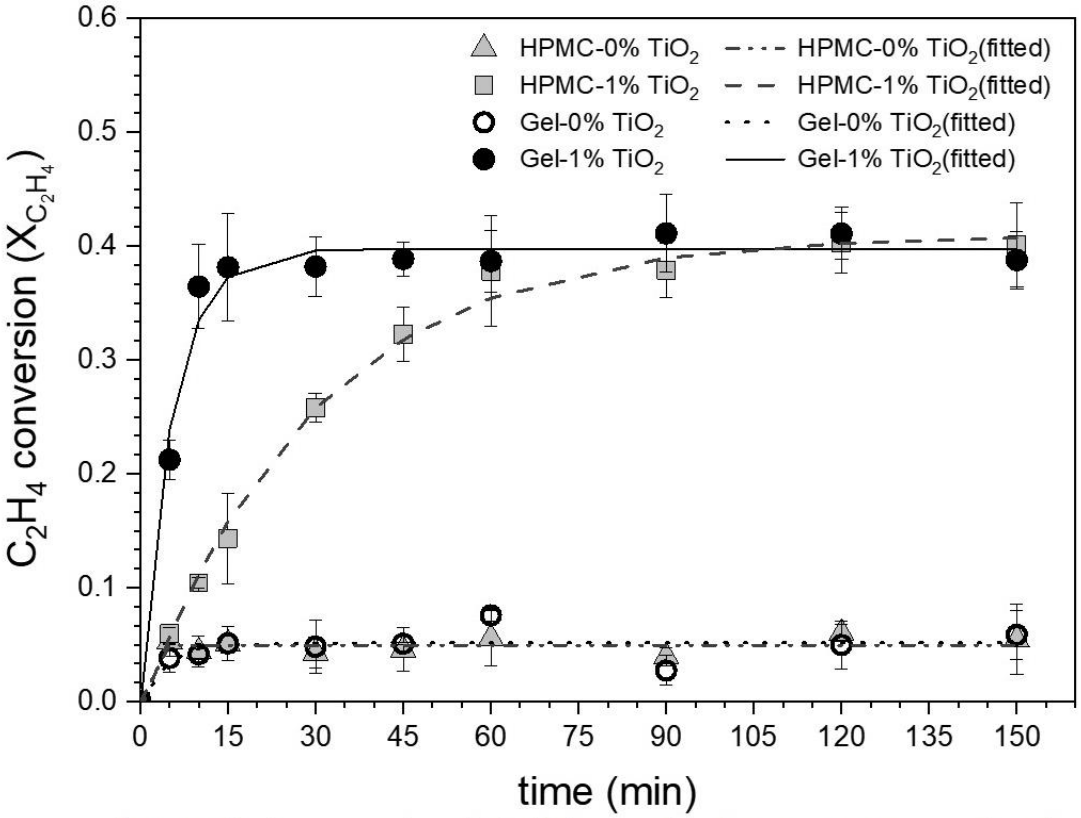

[1] HPMC: hydroxypropyl methylcellulose; Gel: gelatin; TiO_2: titanium dioxide

Source: Fonseca et al. (2021), with permission.

Table 12 - Langmuir-Hinshelwood model parameters and efficiency of ethylene (C_2H_4) degradation for the films based on hydroxypropyl methylcellulose (HPMC) and gelatin (Gel) containing 0 and 1 wt % of titanium dioxide (TiO_2).

Biopolymer matrix[1]	**TiO_2 Concentration (wt %)**	k_{app} **[min^{-1}]**	***A***	***B***	**R^2**	$X_{C_2H_4,max}$ **[%]**
HPMC	0	0.239 ± 0.146[a]	0.043 ± 0.011	0.049 ± 0.038	0.663	4.939 ± 0.229[b]
	1	0.034 ± 0.003[b]	0.418 ± 0.011	0.409 ± 0.009	0.994	39.001 ± 0.678[a]
Gel	0	0.230 ± 0.160[a]	0.051 ± 0.014	0.051 ± 0.005	0.548	4.891 ± 0.450[b]
	1	0.186 ± 0.021[a]	0.403 ± 0.020	0.398 ± 0.008	0.979	39.447 ± 0.530[a]

[1]k_{app}: apparent rate constant of reactions, A and B: coefficients of Langmuir-Hinshelwood model equation indefinitely integrated, R^2: coefficient of determination, $X_{C_2H_4,max}$: maximum ethylene conversion. All values were expressed as mean ± standard error (n = 3). Means within the same column with different superscripts are different at the level of α = 0.05.

Source: Fonseca et al. (2021), with permission.

Although HPMC-1%TiO_2 and Gel-1%TiO_2 films have shown equivalent ethylene degradation efficiencies, HPMC-1%TiO_2 film exhibited the slowest reaction kinetics (lower k_{app}), which can be a result of poorer TiO_2 dispersion into the HPMC matrix than gelatin. Two distinct regimes characterize the behavior of ethylene conversion curves. Over the first 10 and 15 min of reactions for the Gel-1%TiO_2 and HPMC-1%TiO_2 films, respectively, it was observed an approximately linear relationship between ethylene conversion ($X_{C_2H_4}$) and time, which characterizes a photocatalytic reaction controlled by the film surface reaction (LODDO; RODA; PARRINO, 2019). However, after this fast conversion, the ethylene degradation decreased and achieved its maximum conversion value ($X_{C_2H_4,max}$) around 0.4. This $X_{C_2H_4}$ reduction can be associated with a photocatalyst deactivation caused by biopolymer photodegradation.

It would be expected that a matrix erosion increases the exposure of TiO_2 to the UV-A light, accelerating the ethylene degradation. However, a high radiation intensity can also accelerate the biopolymer photodegradation and the carbonaceous fragment deposition on the film surface. This situation is analogous to the fouling deposition on the photocatalyst surface. Fouling hinders the adsorbate diffusion to the photocatalyst active sites, decreasing its performance (FOGLER, 2009). Other possible effects that could be considered due to the carbonaceous deposition are the light harvest and ROS generation limitations by the photocatalyst. From these hypotheses, it is presumed that the HPMC-TiO_2 and gelatin-TiO_2 nanocomposites would be applied in the fruit postharvest as non-reusable ethylene scavenging materials. Additional tests of ethylene degradation by nanocomposite films are required to study the complete TiO_2 deactivation.

In the kinetic curves of ethylene photocatalytic degradation by chitosan-TiO_2 films, Zhang et al. (2019) observed a limitation of the surface reaction after its first 30 min. The authors reported a maximum ethylene conversion of approximately 50 % during 180 min for nanocomposite films containing 25 wt % TiO_2 related to the polymer.

Direct comparisons between kinetic parameters of HPMC-1%TiO_2 and Gel-1%TiO_2 films and other films reported by literature are difficult due to the variability of process parameters or information missed. Examples of these parameters are light intensity, initial ethylene concentration, TiO_2 polymorphic phase, TiO_2 particle size, TiO_2 loading, dopants incorporation and photocatalytic surface area. Nevertheless, data reported by Siripatrawan & Kaewklin (2018) were used to estimate roughly kinetic parameters for comparison. The authors used chitosan-TiO_2 films containing 1 wt %TiO_2 (Chit-1%TiO_2) to degrade ethylene,

and the data were fitted to the Langmuir-Hinshelwood model. In order to compare the results, the ethylene concentration was normalized by dividing it per amount of TiO_2 [g] loaded on the photocatalytic surface area [m^2] (**Table 13**). Data obtained from Siripatrawan & Kaewklin (2018) and estimated parameters using the Langmuir-Hinshelwood equation model are available in **Appendix B**.

Table 13 – Comparison between apparent rate constant (k_{app}) and maximum normalized concentration of ethylene degraded ($C_{C_2H_4,\max(N)}$) by films based on hydroxypropyl methylcellulose (HPMC), chitosan (Chit) (SIRIPATRAWAN; KAEWKLIN, 2018) and gelatin (Gel) containing 1 wt % of titanium dioxide (TiO_2).

Films*	I [mW cm^{-2}]**	$X_{C_2H_4,max}$[%]	k_{app} [min^{-1}]**	R^{2**}	$C_{C_2H_4,max(N)}$ [[ppmv] $m^2\, g_{TiO_2}{}^{-1}$]**
HPMC-1%TiO_2	9.8	39.001 ± 0.678[a]	0.034 ± 0.003[b]	0.994	13.149 ± 0.229[a]
Gel-1%TiO_2	9.8	39.447 ± 0.530[a]	0.186 ± 0.021[a]	0.979	13.297 ± 0.178[a]
Chit-1%TiO_2	2.3	11.500 ± 0.400[b]	0.003 ± 0.001[c]	0.983	0.5448 ± 0.019[b]

[1] I: UV-A irradiation intensity, $X_{C_2H_4,max}$: maximum ethylene conversion, k_{app}: apparent rate constant of reactions, R^2: coefficient of determination, $C_{C_2H_4,\max(N)}$: maximum normalized concentration of degraded ethylene. All values were expressed as mean ± standard error (n = 3). Means within the same column having different superscripts are different at the level of α = 0.05. [2] Parameters for Chit-1%TiO_2 film were estimated using data reported by Siripatrawan & Kaewklin (2018).

Source: Fonseca et al. (2021), with permission.

The values of k_{app}, $X_{C_2H_4,max}$ and maximum normalized concentrations of degraded ethylene ($C_{C_2H_4,\max(N)}$) estimated for the Chit-1%TiO_2 film were lower than for the HPMC-1%TiO_2 and Gel-1%TiO_2 films. In all experiments, it was used the same initial ethylene concentration ($C_{C_2H_4,i}$, 5 ppmv), and reactions were monitored over the time intervals: 180 min (Chit-1%TiO_2) and 150 min (HPMC-1%TiO_2, Gel-1%TiO_2). The lowest performance of Chit-1%TiO_2 films evidenced that film efficiency highly depends on irradiation intensity (I) and indicates possible TiO_2 agglomeration into the chitosan matrix. This result highlights the importance of previous studies about TiO_2 nanoparticle dispersion into biopolymer matrices.

4.3.4 Topography of HPMC-TiO_2 and gelatin-TiO_2 films

Topographic images and surface root-mean-squared roughness (R_{RMS}) of films before and after photocatalysis were presented in **Figures 26** and **27** and **Table 14**, respectively.

Figure 26 - Topographic images of HPMC-TiO_2 films before and after photocatalysis.

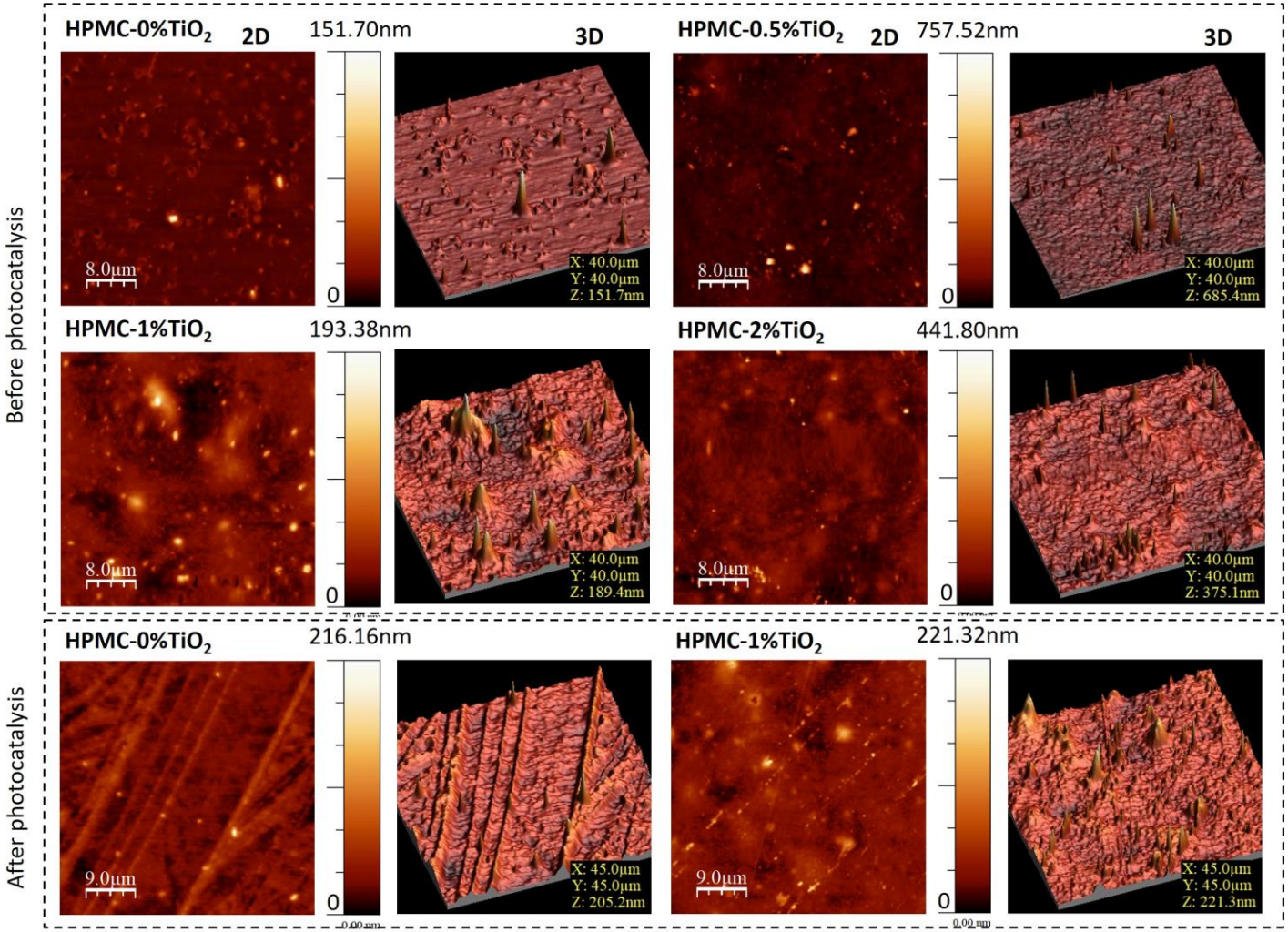

[1] HPMC: hydroxypropyl methylcellulose; TiO_2: titanium dioxide

Source: Fonseca et al. (2021), with permission.

Figure 27 - Topographic images of gelatin-TiO_2 films before and after photocatalysis.

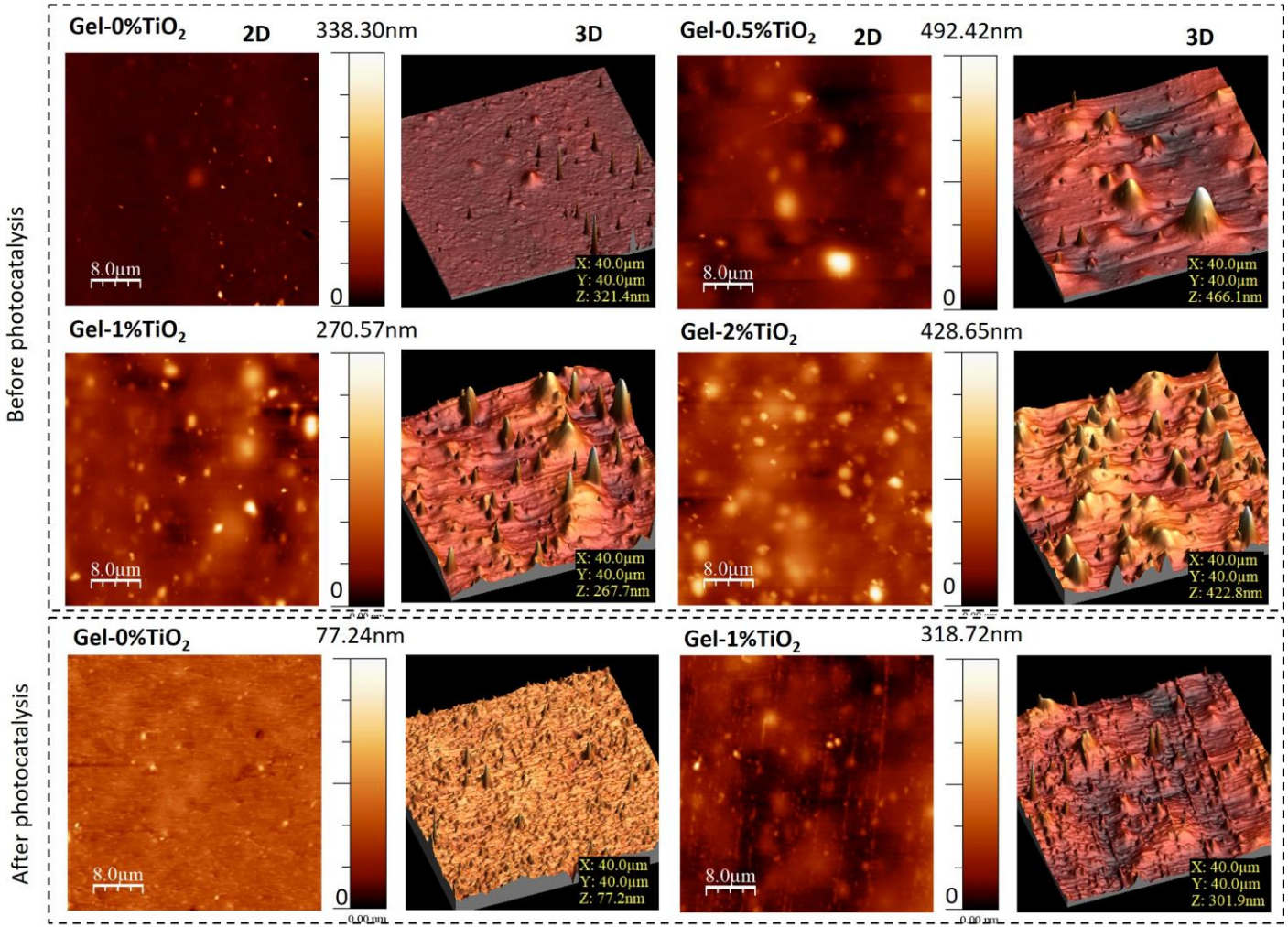

[1] Gel: gelatin; TiO_2: titanium dioxide

Source: Fonseca et al. (2021), with permission.

Table 14 - Surface root-mean-squared roughness (R_{RMS}) of films based on hydroxypropyl methylcellulose (HPMC) and gelatin (Gel) containing from 0 to 2 wt% of titanium dioxide (TiO_2) before and after photocatalysis.

Biopolymer matrix	R_{RMS}, [nm]		
	TiO_2 concentration (wt%)	**Before photocatalysis**	**After photocatalysis**
HPMC	0	$8.20 \pm 1.46^{b,A}$	$9.94 \pm 0.92^{b,A}$
	0.5	26.25 ± 1.78^{a}	-
	1	$19.80 \pm 2.84^{a,A}$	$14.13 \pm 0.92^{a,A}$
	2	$16.24 \pm 0.44^{a,b}$	-
Gel	0	$8.93 \pm 0.68^{c,A}$	$3.91 \pm 0.44^{b,B}$
	0.5	41.94 ± 2.38^{a}	-
	1	$28.80 \pm 1.90^{b,A}$	$20.30 \pm 1.30^{a,B}$
	2	48.51 ± 2.81^{a}	-

[1] All values were expressed as mean ± standard error (n = 3). [2] Means within the same column and for the same group having different superscripts (minuscule letters) and those within the same line and for the same group having different superscripts (majuscule letters) are different at the level of $\alpha = 0.05$.

Source: Fonseca et al. (2021), with permission.

Before photocatalysis, R_{RMS} (**Table 14**) increased as the TiO_2 concentration increased from 0 to 1wt % for the HPMC-TiO_2 films and reduced for the films containing 2 wt % TiO_2 ($p \leq 0.05$). Gelatin-TiO_2 films exhibited a wide R_{RMS} oscillation as the TiO_2 concentration increased, showing maximum R_{RMS} values for 1 and 2 wt % TiO_2 ($p \leq 0.05$). Also, blank films (HPMC-0%TiO_2 and Gel-0%TiO_2) presented similar R_{RMS} values. After the photocatalysis, only gelatin-TiO_2 films showed a significant R_{RMS} decrease.

The R_{RMS} increase is characterized by protuberances (light sites) rising from the film surface, rich in polymer chains (dark sites). Most of these protuberances also observed in SEM micrographs (**Figure 16**) were generated by TiO_2 aggregates distributed on the matrix, TiO_2 layer stacking, and microstructural reorganization of nanocomposite matrix (FONSECA et al., 2020; HE et al., 2016). Oleyaei et al. (2016) and Leprince-Wang; Yu-Zhang (2001) affirmed that the non-exposure to the UV-A light increases the TiO_2 agglomeration and the film surface roughness during the film drying. The protuberances uniformly distributed on the film (without excessive TiO_2 agglomeration) increase the photocatalytic surface area.

Blank films exhibited the highest height values (Z-axis) and some light sites before photocatalysis. It characterizes a continuous matrix and the presence of some protuberances, which could be attributed to the non-solubilized polymer chains. The Gel-0%TiO_2 film has protuberances more evident due to the complex protein structure that composes the gelatin

(JIANG, Y., LI, Y., CHAI, Z., & LENG, 2010). It corroborates the hypothesis that the gelatin dispersion masked TiO_2 particle size measured by DLS (section 3.3.1). The lowest height values and the highest frequency of small light sites observed in the HPMC-1%TiO_2 and Gel-1%TiO_2 topographic images confirm that 1 wt % TiO_2 has been better dispersed into the film than other TiO_2 concentrations, and it agrees with R_{RMS} values and photocatalytic activity results.

Isolated and high protuberances observed in the HPMC-0.5%TiO_2 and Gel-0.5%TiO_2 topographic images imply an insufficient TiO_2 distribution on the film surface. In contrast, the TiO_2 distribution on the films HPMC-2%TiO_2 and Gel-2%TiO_2 implies a matrix saturation, a possible TiO_2 layer stacking (columnar growth) and a matrix packing accompanied by the new protuberance rising (BASSO; DE FÁTIMA PERALTA MUNIZ MOREIRA; JOSÉ, 2018; LEPRINCE-WANG; YU-ZHANG, 2001). The columnar growth is typical behavior from TiO_2 crystal phases (LEPRINCE-WANG; YU-ZHANG, 2001).

Nanocomposite films also presented a discontinuity in their surfaces, corroborating the results discussed in Chapter 3. Probably, biphasic microstructure characterized by micro-domains rich in biopolymer or TiO_2 were formed (**Figure 21**). The surface roughness increase of biopolymer-TiO_2 films as the TiO_2 incorporation was also reported by Oleyaei et al. (2016), He et al. (2016) and Zhou; Wang; Gunasekaran (2009).

After photocatalysis, the surface of HPMC-1%TiO_2, Gel-0%TiO_2, and Gel-1%TiO_2 films visually exhibited a high light site dominance (**Figures 25 and 26**) and a significant R_{RMS} decrease (**Table 14**). On the other hand, HPMC-0%TiO_2 film did not exhibit R_{RMS} changes. It indicates that gelatin is more susceptible to photodegradation than HPMC, and TiO_2 photocatalysis accelerated the matrix erosion.

Although the supposed carbonaceous deposition has limited the photocatalysis reactions, it could be suggested that the growing exposure of TiO_2 to the UV-A light, caused by the fast gelatin matrix erosion, overcame the highest availability of water molecules generating ROS on the HPMC matrix surface. The fast gelatin erosion and its better ability to disperse TiO_2 could justify the higher k_{app} value of Gel-1%TiO_2 than HPMC-1%TiO_2 film.

4.3.5 Chemical composition of nanocomposite films

Film FTIR spectra after photocatalysis confirmed the biopolymer degradation (**Figure 28**).

Before photocatalysis, both HPMC-1%TiO_2 and Gel-1%TiO_2 spectra exhibited few alterations caused by TiO_2 incorporation. As discussed in Chapter 3 (section 3.3.2.4), HPMC-0%TiO_2 displayed a broad band centered at 3446 cm^{-1} attributed to the O-H axial stretching from the HPMC and polymer-water hydrogen bonds (DING; ZHANG; LI, 2015). This band was enlarged, and its center was displaced to 3419 cm^{-1} as the 1 wt % TiO_2 was incorporated into the HPMC. Similar behavior was observed in the Gel-0%TiO_2 and Gel-1%TiO_2 spectra. The band intensity 3396 – 2976 cm^{-1} decreased and displaced to 3500 – 2976 cm^{-1} as the 1 wt % TiO_2 were incorporated into gelatin. This band is associated with the hydrogen bonds (O-H) coupled with N-H stretching vibrations of the gelatin amide-A groups. Its intensity decrease and displacement were attributed to the electrostatic repulsion between protonated amino groups ($-NH_3^+$) and Ti^{4+} ions at pH= 3.2 (HE et al., 2016; MATOS FONSECA et al., 2019).

After photocatalysis, the intensity of bands referent to the HPMC O-H axial stretching, gelatin N-H stretching vibrations and polymer-water hydrogen bonds decreased for all films. Typical vibrations of some chemical groups such as ether C-O stretching combined with secondary alcohol hydroxyl groups (O-H) (1310 - 1027 cm^{-1}), alcohol O-H axial stretching and hydrogen bonds (3446 cm^{-1}) and C-H stretching of $-CH_3$ and $-CH_2$ groups (2914, 2851 cm^{-1}) were more slightly preserved in HPMC-1%TiO_2 than HPMC-0%TiO_2 film (JACQUOT et al., 2012; MATOS FONSECA et al., 2019). Both HPMC-1%TiO_2 and HPMC-0%TiO_2 films presented degradation of C-H bonds at 1465 cm^{-1} and polymer-glycerol interactions at wave numbers less than 1000 cm^{-1} (HAZIMAH; OOI; SALMIAH, 2003; MOHAN et al., 2012).

Figure 28 - ATR-FTIR spectra of films based on hydroxypropyl methylcellulose (HPMC) (a) and gelatin (Gel) (b) containing 0 and 1 wt% of titanium dioxide (TiO_2) HPMC-TiO_2 (a) and gelatin-TiO_2 (b) nanocomposite films before (BP) and after (AP) photocatalysis.

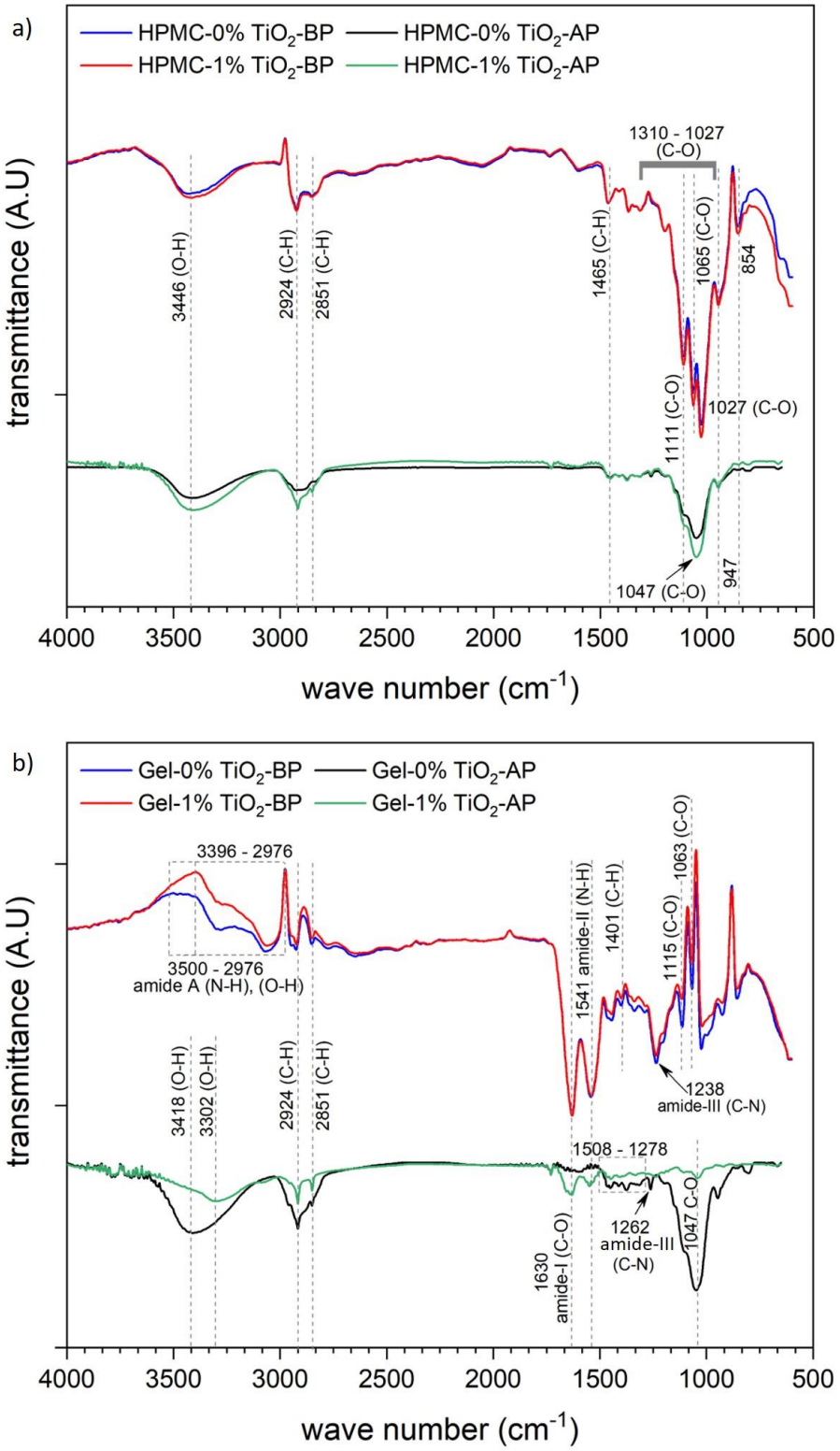

Source: Fonseca et al. (2021), with permission.

On the other hand, Gel-1%TiO_2 film was more degraded than Gel-0%TiO_2 film. The blank film exhibited higher intensity for O-H hydrogen bonds and N-H stretching (3418 cm^{-1}), C-O (1047 cm^{-1}), amide-I C-O (1630 cm^{-1}), amide-II or triple helix N-H (1541 cm^{-1}), amide-III C-N (1238 cm^{-1}) and C-H in-plane bending (1401 cm^{-1}) vibrations than Gel-1%TiO_2 film (3302, 1047, 1630, 1541, 1262, 1508 - 1278 cm^{-1}) (ARFAT et al., 2014). As well as HPMC-TiO_2 films, gelatin-TiO_2 films also showed polymer-glycerol interaction degradation (< 1000 cm^{-1}) (HAZIMAH; OOI; SALMIAH, 2003).

The film FTIR spectra changes after photocatalysis confirm the biopolymer photodegradation. Gelatin was more susceptible to UV-A light degradation than HPMC, and its decomposition was accelerated by the TiO_2 photocatalysis, as previously suggested by analyzing AFM images. The formation of different chemical groups in all spectra was not identified, corroborating the carbonaceous formation hypothesis.

4.3.6 Considerations about nanocomposite coating for the EPE foams

The choice of the most appropriate nanocomposite formulation for coating the EPE foam nets was based on the structural and photocatalytic properties of films.

TiO_2 nanoparticles embedded into Gel-1%TiO_2 films were more homogeneously dispersed and degraded faster 40 % of the batched ethylene (5 ppmv) than HPMC-1%TiO_2 films. Fast ethylene scavenging materials are interesting for climacteric fruit applications at the beginning of ripening due to the maximum ethylene production during this stage. Thus, ethylene removal should be carried out over the first days after fruit harvest. Another exciting Gel-1%TiO_2 film characteristic is its lower water solubility than HPMC-1%TiO_2 film. It hinders the nanocomposite coating or film dissolution during fruit transpiration.

Considering all these possible advantages that the Gel-1%TiO_2 nanocomposite film can offer to the fruit postharvest, its formulation was chosen as a coating material for the EPE foam nets.

4.3.7 Nanocomposite loading on EPE foam net surface and morphology

The contents of gelatin-TiO_2 dispersion (Gel-1%TiO_2) loaded on EPE foam surface are presented in **Table 15**. The Gel-1%TiO_2 monolayer content loaded on the EPE foam surface (EPE-1x-Gel-1%TiO_2) was less than the Gel-1%TiO_2 content cast in an acrylic Petri-dishes (9 cm, internal diameter) to form one film unit (10 g). On the other hand, EPE foams coated by

bilayer and tetra-layer of Gel-1%TiO_2 (EPE-2x-Gel-1%TiO_2 and EPE-4x-Gel-1%TiO_2) showed loaded dispersion contents roughly equivalent to the 2 and 5 times the Gel-1%TiO_2 dispersion weight cast to form one film unit (10 g).

As expected, these data indicate that EPE does not offer good adhesiveness to Gel-1%TiO_2 monolayer, probably due to its low surface energy compared to other materials used in engineering (SANCHIS et al., 2007). Thus, the content of TiO_2 loaded on the EPE-1x-Gel-1%TiO_2 foam surface is insufficient for photocatalysis applications.

Table 15 - Content of coating based on gelatin containing 1 wt % of titanium dioxide (Gel-1%TiO_2) loaded on the expanded polyethylene (EPE) foam net surface.

Number of Gel-1%TiO_2 layers on EPE foam nets	$\frac{W_{wc}}{EPE\ foam}$ [1] [g]	LWC[2] [g m^{-2}]	$TiO_{2\ (loaded)}$ 10^{-2} [g m^{-2}]	LDC[2] [g m^{-2}]
1	7.88 ± 0.76^{c}	59.72 ± 5.76^{c}	2.00 ± 0.21^{c}	(1.13 ± 0.09) x 10^{-2c}
2	21.71 ± 0.89^{b}	164.54 ± 6.74^{b}	6.21 ± 0.25^{b}	1.74 ± 0.11^{b}
4	53.18 ± 1.05^{a}	403.03 ± 7.96^{a}	15.22 ± 0.30^{a}	9.78 ± 0.13^{a}

[1] W_{WC}: Weight of wet nanocomposite coating loaded on the surface of one EPE foam net. [1] LWC, LDC: Loadings of wet and dry nanocomposite coating [g] on the EPE foam net surface [m^2], respectively. Means within the same column and the same group with different superscripts (minuscule letters) are different at the level of α = 0.05.

Source: Fonseca et al. (2021), with permission.

Morphological modifications on the EPE foam net surface caused by Gel-1%TiO_2 coating were evidenced in the SEM micrographs (**Figure 29**). The non-coated EPE foam net showed some roughness on its surface characterized by protuberances. It was also possible to observe the boundary of internal air bubbles formed by the industrial polyethylene expansion process. Images of these structures, obtained by optical and scanning electronic microscopy, are available in **Appendix C**. The EPE-1x-Gel-1%TiO_2 foam net showed almost imperceptible changes on its surface, corroborating the low amount of loaded Gel-1%TiO_2 dispersion (**Table 15**).

In contrast, EPE-2x-Gel-1%TiO_2 and EPE-4x-Gel-1%TiO_2 foam nets showed perceptible alterations on their surface. It was almost impossible to observe the boundary of internal air bubbles. The presence of small cracks confirms the deposition and adherence of Gel-1%TiO_2 coating on the EPE surface.

Figure 29 - SEM micrographs of expanded polyethylene (EPE) foam net surface coated with 0, 1, 2 and 4 layers of coating based on gelatin (Gel) containing 1 wt % of titanium dioxide (TiO_2).

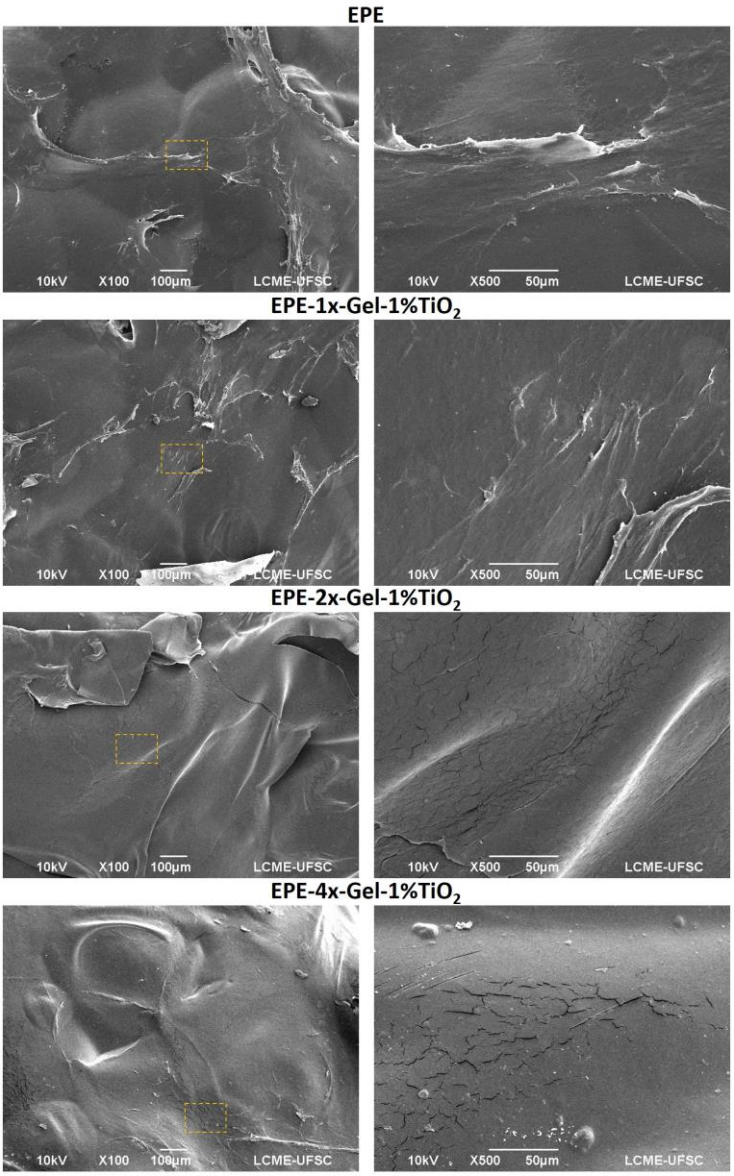

[1]EPE, EPE-1x-Gel-1% TiO_2, EPE-2x-Gel-1% TiO_2 and EPE-4x-Gel-1% TiO_2: Expanded polyethylene foams coated by 0, 1, 2 and 4 layers of gelatin-based nanocomposite solution containing 1 wt% TiO_2 (titanium dioxide), related to the polymer.

Source: Fonseca et al. (2021), with permission.

4.3.8 Chemical composition and photodegradation of EPE foam nets

UV-A light irradiation did not alter the non-coated EPE foam FTIR spectra (**Figure 30**). C-H asymmetric (2917 cm^{-1}) and symmetric (2845 cm^{-1}) stretching of $-CH_2$ groups, bending deformation (1463 cm^{-1}), C-H symmetric deformation of $-CH_3$ groups, wagging and twisting deformations (1376 - 1014 cm^{-1}) and rocking deformations (717 cm^{-1}) were preserved, which proves that EPE foams were not photodegraded by UV-A light (GULMINE et al., 2002). The

bands 3511 -3097 cm^{-1} and 1730 cm^{-1} can be attributed to the N-H vibrations of amine groups originated by UV stabilizers incorporated into the industrial EPE process (GULMINE et al., 2002).

Figure 30 - ATR-FTIR spectra of expanded polyethylene (EPE) foam nets before (BP) and after (AP) UV-A light exposure.

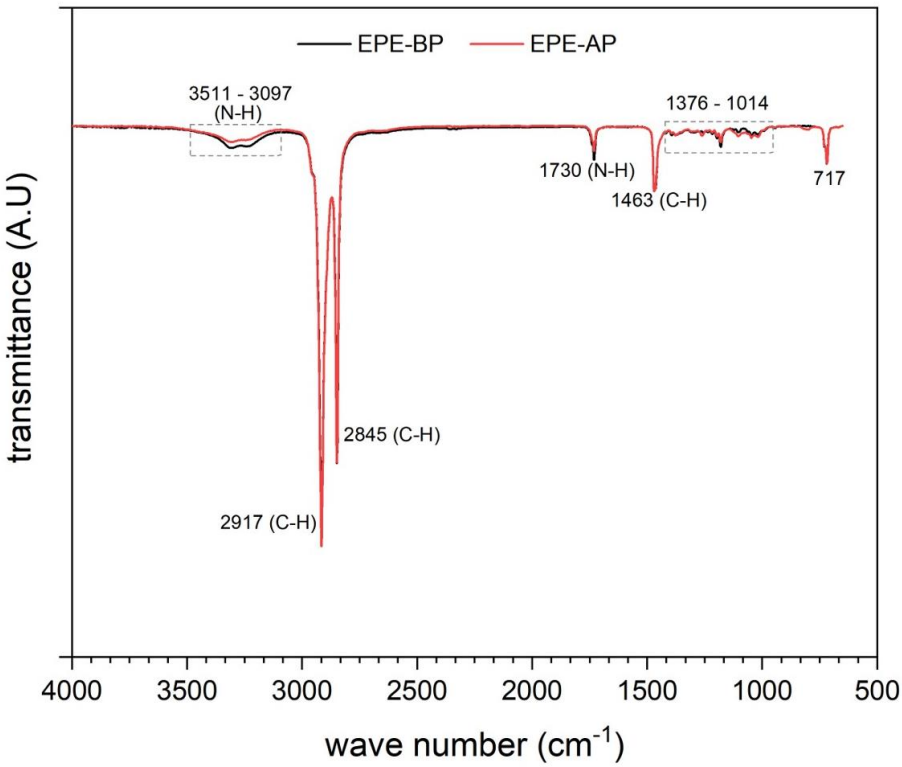

Source: Fonseca et al. (2021), with permission.

4.3.9 Ethylene degradation by gelatin-TiO_2-coated EPE foam nets

EPE, EPE-2x-Gel-1%TiO_2 and EPE-4x-Gel-1%TiO_2 foam nets were used to degrade ethylene. As expected, the non-coated EPE foam net did not exhibit photocatalytic activity. The EPE-1x-Gel-1%TiO_2 foam net was not tested due to its insufficient TiO_2 content to start photocatalytic reactions. Degradation kinetics of ethylene (C_2H_4) (**Figure 31.a**) revealed that both EPE-2x-Gel-1%TiO_2 and EPE-4x-Gel-1%TiO_2 were able to degrade ethylene, and EPE-4x-Gel-1%TiO_2 showed a slight acceleration of photocatalysis reaction when compared to EPE-2x-Gel-1%TiO_2. Both foam nets showed subsequent delaying and acceleration of ethylene degradation after 45 min and 60 min of reaction. However, EPE-2x-Gel-1%TiO_2 foam net showed faster ethylene degradation than EPE-4x-Gel-1%TiO_2 foam net after 60 min.

There was no difference between their maximum ethylene conversions ($X_{C_2H_4,\max}$), reaching approximately 23 % after 150 min.

Analyzing the determination coefficient values (R^2) (**Table 16**), the kinetic data of EPE-2x-Gel-1%TiO_2 and EPE-4x-Gel-1%TiO_2 foam nets were well-fitted to the Langmuir-Hinshelwood model as well as HPMC-1%TiO_2 and Gel-1%TiO_2 films. The highest k_{app} value estimated for the EPE-4x-Gel-1%TiO_2 foam net confirms its fastest reaction, observed over the first 60 min of photocatalysis.

In order to compare the photocatalytic efficiencies of EPE-2x-Gel-1%TiO_2 and EPE-4x-Gel-1%TiO_2 foams and HPMC-1%TiO_2 and Gel-1%TiO_2 films, the ethylene conversion data were normalized as degraded ethylene concentration per TiO_2 weight [g] loaded on the irradiated surface area [m^2] ($C_{C_2H_4,(N)}$) (**Figure 31.b**). The maximum normalized concentration of degraded ethylene ($C_{C_2H_4,max\ (N)}$) was presented in **Table 16**.

Figure 31 – Photocatalytic degradation kinetics of ethylene (C_2H_4) for the expanded polyethylene (EPE) foam nets coated with 2 and 4 layers of nanocomposite based on gelatin (Gel) containing 1 wt % of titanium dioxide (TiO_2) (a), the ethylene concentration degraded per TiO_2 weight [g] loaded on the irradiated surface area [m^2] ($C_{C_2H_4,(N)}$) for the EPE foam nets coated with gelatin-TiO_2 and films based on hydroxypropyl methylcellulose (HPMC) and gelatin containing 1 wt % TiO_2 and their fittings to the Langmuir-Hinshelwood model (b).

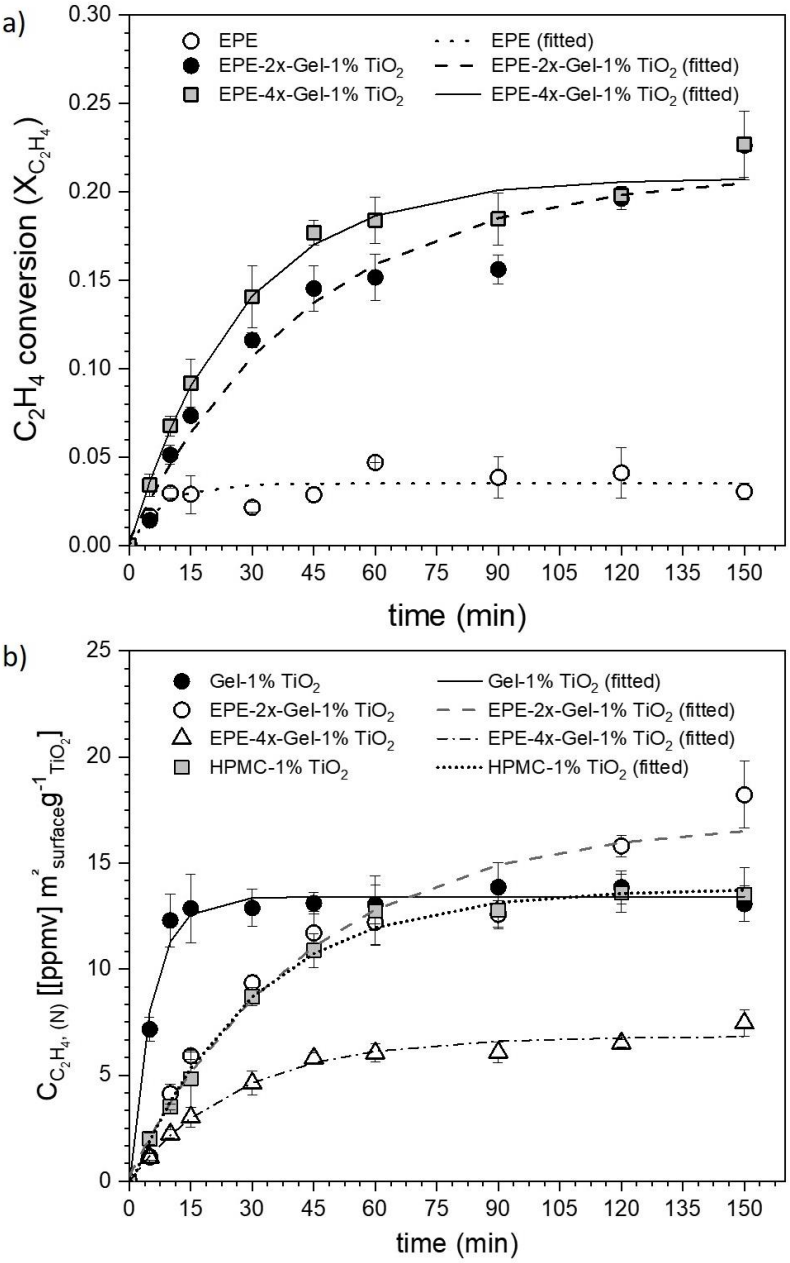

Source: Fonseca et al. (2021), with permission.

Table 16 – Summary of Langmuir-Hinshelwood model parameters and ethylene (C_2H_4) degradation efficiency for the expanded polyethylene (EPE) foam nets coated with 2 and 4 layers of nanocomposite based on gelatin (Gel) containing 1 wt % of titanium dioxide (TiO_2), the ethylene concentration degraded per TiO_2 weight loaded [g] on the irradiated surface area [m^2] ($C_{C_2H_4,(N)}$) for the EPE foam nets coated with gelatin-TiO_2 and films based on hydroxypropyl methylcellulose (HPMC) and gelatin containing 1 wt % TiO_2.

Films and foam nets[1]	k_{app} [min^{-1}]	A	B	R^2	$X_{C_2H_4,max}$ [%]	$C_{C_2H_4,max(N)}$ [[ppmv] $m^2\, g_{TiO_2}{}^{-1}$]
EPE	0.127 ± 0.065[a]	0.034 ± 0.008	0.035 ± 0.003	0.655	3.325 ± 0.439	-
EPE-2x- Gel-1%TiO_2	0.023 ± 0.005[c]	0.208 ± 0.016	0.212 ± 0.015	0.956	22.169 ± 2.956[a]	18.212 ± 1.575[a]
EPE-4x- Gel-1%TiO_2	0.038 ± 0.005[b]	0.207 ± 0.009	0.208 ± 0.007	0.981	22.688 ± 3.867[a]	7.453 ± 0.613[c]
Gel-1%TiO_2	0.186 ± 0.021[a]	0.403 ± 0.020	0.398 ± 0.008	0.979	39.447 ± 0.530	13.297 ± 0.178[b]
HPMC-1%TiO_2	0.034 ± 0.003[b]	0.418 ± 0.011	0.409 ± 0.009	0.994	39.001 ± 0.678	13.149 ± 0.229[b]

[1] k_{app}: apparent rate constant of reactions, A and B: coefficients of the model equation, R^2: coefficient of determination, $X_{C_2H_4,max}$: maximum conversion of ethylene ($0 \leq X_{C_2H_4,max} \leq 1$), $X_{C_2H_4,max}$[%]: efficiency of ethylene degradation. $C_{C_2H_4,\ \max(N)}$: maximum normalized concentration of degraded ethylene. All values were expressed as mean ± standard error (n = 3). Means within the same column with different superscripts are different at the level of α = 0.05.

Source: Fonseca et al. (2021), with permission.

Normalized curves referent to ethylene degradation by films and foam nets (**Figure 31.b**) evidenced the best photocatalytic efficiency of EPE-2x-Gel-1%TiO_2 foam net and its lowest k_{app} value ($p \leq 0.05$) (**Table 16**). The k_{app} values for EPE-4x-Gel-1%TiO_2 foam net and HPMC-1%TiO_2 film did not differ between them, and they were lower than k_{app} value calculated for the Gel-1%TiO_2 film.

When the Gel-1%TiO_2 nanocomposite was used as a coating on the foam net surface instead of film, the ethylene degradation kinetics was delayed, confirmed by the k_{app} value reduction. The difference between the k_{app} values of EPE-2x-Gel-1%TiO_2 foam net and Gel-1%TiO_2 film is related to the Gel-1%TiO_2 nanocomposite geometry and thickness depending on its application form (film or coating).

Although ethylene degradation by EPE-2x-Gel-1%TiO_2 foam net has been slower than Gel-1%TiO_2 film, this foam net did not achieve a plateau after 150 min. It means that there was neither complete photocatalyst saturation on the EPE-2x-Gel-1%TiO_2 surface nor its complete deactivation. As discussed, this deactivation was supposedly caused by the fast carbonaceous fragment deposition on the photocatalytic surface. Besides, the highest maximum normalized concentration of ethylene degraded ($C_{C_2H_4,max(N)}$) by the EPE-2x-Gel-1%TiO_2 foam net also indicates that it has a more significant number of active photocatalytic sites than Gel-1%TiO_2 films (**Table 16**). This result suggests that the high foam net surface area reduced the TiO_2 aggregation into the gelatin-based coating during its drying.

So, it is supposed that the nanocomposite coating on the EPE-2x-Gel-1%TiO_2 foam net is thinner than the coating on the EPE-4x-Gel-1%TiO_2 foam net and HPMC-1%TiO_2 and Gel-1%TiO_2 films. The reduction of nanocomposite layer thickness increased the TiO_2 light harvest and decreased the carbonaceous fragment deposition, prolonging the TiO_2 activity. The lower EPE-4x-Gel-1%TiO_2 foam efficiency probably results from the matrix saturation with TiO_2. It overlapped the photocatalytic efficiency enhancement promoted by the active surface area increase.

Zhu et al. (2019) also observed similar results in their research. The authors immobilized TiO_2 nanoparticles into nonwoven fabrics by a layer-by-layer self-assembly method, aiming for an antimicrobial action against *Escherichia coli* in packed pork meat. Before antimicrobial tests, they investigated the influence of TiO_2 loading (layers) on nanocomposite efficiency to degrade blue methylene dye (adsorbate model). Among the numbers of TiO_2 layers tested (0, 4, 8 and 12), nonwoven containing eight TiO_2 layers exhibited the highest degraded dye percentage, and its performance did not differ from nonwoven containing twelve TiO_2 layers. Authors attributed this phenomenon to the clogging

of the small gaps in the fabric mesh caused by the excessive TiO_2 loading, which reduced its specific surface area and photocatalytic activity.

4.3.10 Schematic model of ethylene degradation photocatalyzed by HPMC-TiO_2 and gelatin-TiO_2 films and gelatin-TiO_2-coated EPE foam nets

The schematic model illustrated in **Figure 32** rationalizes the idea proposed in this chapter. It involves the random TiO_2 distribution on the biopolymers and their photodegradation potentialized by photocatalysis. The supposed carbonaceous fragment deposition on TiO_2 nanoparticles hindered the ethylene diffusion from the catalyst pore inlet to photocatalytic sites in HPMC-1%TiO_2 and Gel-1%TiO_2 films. When TiO_2 is more homogeneous distributed in the matrix and the nanocomposite layer is thinner, more light is absorbed. Thus, TiO_2 photocatalytic activity is less affected by the carbonaceous fragment deposition.

In Chapter 3, the structural and physicochemical characterizations of HPMC-1%TiO_2 and Gel-1%TiO_2 films suggested that TiO_2 nanoparticles are more dispersed into gelatin than HPMC. The TiO_2 hydrophobic character under the dark and electrostatic repulsion between its cationic form (Ti^{4+}) and gelatin chain NH_3^+ groups (pH 3.2) enhanced its dispersion into gelatin.

Due to the EPE foam net three-dimensional network structure, some photocatalytic sites are unevenly irradiated or non-irradiated (dark sites). It contributes to the photocatalytic reaction deceleration. However, the highest foam net surface area ensures a better dispersion of TiO_2 nanoparticles into gelatin-based coating than gelatin-based films. Finally, the number of Gel-1%TiO_2 layers was an essential factor for ensuring the efficient TiO_2 photocatalytic activity. Just as a very thin layer (one layer) can provide an insufficient TiO_2 loading for degrading ethylene, an excessively thick layer (four layers) can cause a TiO_2 layer stacking, decreasing the coating efficiency. This photocatalyst layer stacking may have been intensified by hydrogen bonds between gelatin chains that increased as the Gel-1%TiO_2 dispersion was loaded. These interactions formed a physical reticulation that hindered the dispersion of TiO_2 crystals into the matrix, facilitating their columnar growth.

Figure 32 – Schematic model for the effects on ethylene photocatalytic degradation by dispersing titanium dioxide (TiO_2, 1 wt %) into hydroxypropyl methylcellulose (HPMC) and gelatin-based films and gelatin-based coatings on expanded polyethylene (EPE) foam net.

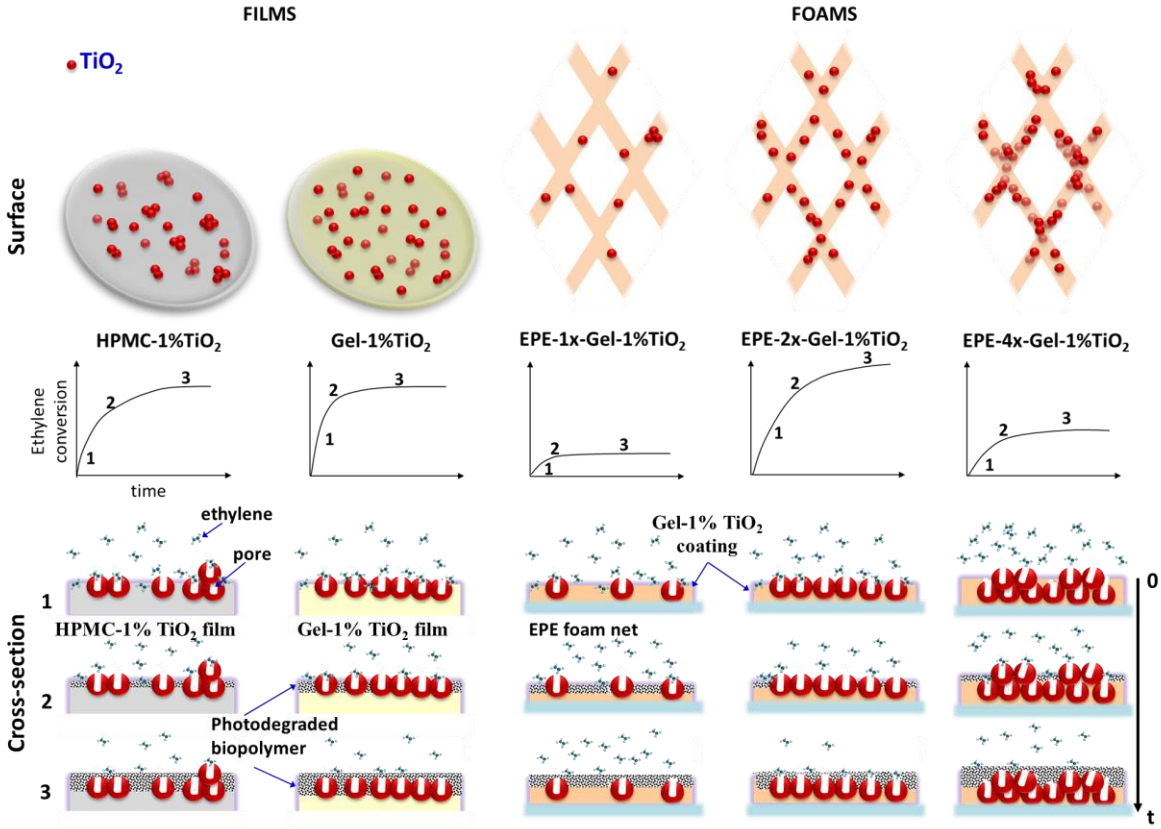

[1]EPE-1x-Gel-1% TiO_2, EPE-2x-Gel-1% TiO_2 and EPE-4x-Gel-1% TiO_2: Expanded polyethylene foams coated by 0, 1, 2 and 4 layers of Gel-1% TiO_2. [2] Gel-1% TiO_2 and HPMC-1% TiO_2: gelatin- and hydroxypropyl methylcellulose-based nanocomposite solution containing 1 wt% TiO_2 (titanium dioxide), related to the polymer)

Source: Fonseca et al. (2021), with permission.

4.4 CONCLUSIONS OF CHAPTER 4

TiO_2 exhibited photocatalytic activity when it was immobilized into both gelatin and hydroxypropyl methylcellulose (HPMC) matrices. The biopolymer photodegradation was intensified when films were exposed to UV-A light. The best TiO_2 dispersion into gelatin and its fast photodegradation accelerated the ethylene degradation over the first 15 minutes of reaction. Although a supposed carbonaceous fragment deposition on the film surface has limited the TiO_2 photocatalytic activity, the fast ethylene degradation ability is an attractive characteristic for applying ethylene scavenging materials in freshly harvested fruit.

The commercial material expanded polyethylene (EPE) foam net, which is already used to protect the fruit against mechanical injuries, was appropriate to support gelatin-based nanocomposite containing 1 wt% TiO_2 (Gel-1%TiO_2). EPE foam nets coated with Gel-

1%TiO_2 showed to be a promising material for fruit application. The nanocomposite layer thickness directly affected the TiO_2 photocatalytic activity. EPE foam net coated with a Gel-1%TiO_2 monolayer displayed an insufficient amount of TiO_2 to degrade ethylene. Also, EPE foam net coated with a Gel-1%TiO_2 tetra-layer displayed limited ethylene degradation. In contrast, this limitation was caused by the excessive amount of Gel-1%TiO_2 dispersion loaded on the foam nets. On the other hand, EPE foam net coated with a Gel-1%TiO_2 bilayer exhibited improved ethylene degradation efficiency and a delay in photocatalyst deactivation.

The optimization of other process parameters such as irradiation intensity, initial ethylene concentration, nanocomposite thickness control and reactor design can improve the gelatin-TiO_2-coated EPE nanocomposite foam net photocatalytic efficiency.

These results and perspectives encouraged the subsequent studies about the application of gelatin-TiO_2-coated EPE nanocomposite foam nets as ethylene scavengers in fruit.

Chapter 5. APPLICATION OF GELATIN-TiO_2-COATED EXPANDED POLYETHYLENE ON PAPAYA

This chapter reports the third experimental phase of this thesis, which involves the *in vivo* application of polyethylene foam nets coated with a bilayer of gelatin-TiO_2 nanocomposite (EPE-2x-Gel-1%TiO_2) as ethylene scavenger material. Papaya (*Carica papaya* L. cv. 'Golden') was used as s climacteric fruit model, and its ripening was evaluated.

From this step, it was written the third experimental article titled "*Gelatin-TiO_2-coated expanded polyethylene foam nets as ethylene scavengers for fruit postharvest application"*, published in the *Postharvest Biology and Technology* (impact factor (2020): 4.303; https://doi.org/10.1016/j.postharvbio.2021.111602). According to Elsevier subscription rules, the authors retain the right to include the article in a thesis, provided it is not published commercially.

5.1 INTRODUCTION

Developing technologies capable of extending the shelf life of perishable products such as fruit is a challenge for the agricultural and agro-industrial sectors. The main action of the postharvest technologies is to control fruit respiration and ethylene production (LELIEVRÈ et al., 1997). Although there are several technologies applied in fruit preservation, some of them require high investment cost, while others use toxic products or favor undesirable physiological disorders that compromise the fruit sensory and microbiological quality (ACOSTA LEZCANO FOSCACHES et al., 2012; AN; PAULL, 1990; MANENOI et al., 2007; OLIVEIRA-JR et al., 2006; PAULL et al., 1997).

Thus, the biopolymers-TiO_2 nanocomposites have shown to be a sustainable and efficient alternative for preserving fruit by ethylene photocatalytic degradation (KAEWKLIN et al., 2018; WANG et al., 2019; ZHANG et al., 2019). These materials can be applied as both films and coatings for other materials.

In this step, the goal was to evaluate the performance of EPE foam nets coated with gelatin-TiO_2 nanocomposite for degrading ethylene and delaying the fruit ripening (*in vivo* application). Changes in physiological, physicochemical and visual characteristics of papayas (*Carica papaya* L. cv. 'Golden') were evaluated before and after TiO_2 photocatalysis treatment.

5.2 MATERIALS AND METHODS

5.2.1 Materials

Papaya (*Carica papaya* L. cv. 'Golden') in a maturation stage 1 (90 – 100% of green peel) (CEAGESP, 2003; MARTINS; COSTA, 2003) purchased in a local supermarket were used as climacteric fruit model. Expanded polyethylene (EPE) foam nets with a surface area of 0.132 m^2 (W-paper Comércio de Embalagens Ltda-ME, São Paulo-Brazil), bovine gelatin (bloom 250, Gelnex, Brazil), glycerol (99%, Neon, Brazil), titanium dioxide (TiO_2) (average crystallite diameter < 10 nm, 100% anatase, Hombikat UV 100) and acetic acid solution were used as immobilizing support, biopolymer matrix, plasticizer, photocatalyst and solvent, respectively.

5.2.2 Methods

5.2.2.1 Preparation of EPE foam nets coated with gelatin-TiO_2

The preparation of EPE foam nets coated with gelatin-TiO_2 nanocomposite bilayer containing 1 wt% TiO_2 (EPE-2x-Gel-1%TiO_2) was carried out according to the methods previously described in section 4.2.2.1. Briefly, gelatin (40 g), once dissolved into acetic acid solution (700 g, pH 3.2) and added by glycerol (25 wt %, polymer), was heated (85°C) and kept in a water bath for 10 min. TiO_2 (1 wt%, polymer) was suspended in acetic acid solution (300 g, pH 3.2), sonicated in a bath ultrasonic (Ultrasonic Maxi Clean 1400 A Unique, 40 kHz) for 15 min, stirred (1,500 rpm) for 20 min and dripped into gelatin dispersion under vigorous stirring (55ºC, 1,500 rpm). Then, gelatin-TiO_2 dispersion was homogenized in Ultraturrax T25, IKA (16,000 rpm, 30 min) and kept at 23°C ± 1°C. EPE foam nets were immersed into gelatin-TiO_2 dispersion at a rate of 2 cm s^{-1}, kept immersed 2 min and emerged at 2 cm s^{-1}. EPE foam nets were dried in a BOD refrigerated incubator at 15°C for 30 min and immersed into gelatin-TiO_2 dispersion for the second nanocomposite layer deposition. Finally, foam nets were dried at 15°C for 30 min and then at 25°C for 48 h. All samples were stored in a chamber at a relative humidity (RH) of 58 % at least 48 h before tests.

5.2.2.2 Sanitization of papaya fruit

Papayas were purchased in the supermarket, washed in running water and sanitized by immersion in sodium hypochlorite solution (100 ppm) at room temperature (20°C) for 15 min (NETO et al., 2015). The sanitizing solution was removed by gravity and filter paper.

5.2.2.3 Photocatalytic system set-ups to degrade ethylene

Before each experiment, sanitized fruit was divided into three groups: 1- control, 2- photocatalysis and 3- visible light experiments, which were composed of six, six and three fruit samples. Three fruit specimens from the first and second groups were immediately characterized as the weight, color, firmness, pH, titratable acidity and total soluble solids content. The other three samples of each group were wrapped in blank EPE (control experiment) and EPE-2x-Gel-1%TiO_2 (photocatalysis experiment) foam nets, respectively. Each fruit group was separately stored in a cubic batch reactor (38.56 x 10^{-3} m^3, void volume) (**Figure 33**), equipped with fans, relative humidity control and UV-A light (Osram DULUX®L Blue UV-A, 24 W, λ_{peak} = 365 nm). The fruit was positioned in support fixed at 15 cm from UV-A light (1.44 mW cm^{-2}) located in the top reactor. The irradiation intensity was also measured on the top fruit (4.40 mW cm^{-2}) at 5 cm from UV-A light. The experiments were carried out at external reactor temperature of 20 ± 1°C, internal reactor temperature of 30 ± 1°C, and RH = 85 % (KCl saturated solution, a_w = 0.849, 25°C). The internal temperature of 30 ± 1°C is a UV-A light heating consequence. However, it was also considered as a severe storage condition for fruit in tropical countries at room temperature. The third fruit group (visible light experiment) was wrapped in blank EPE foam nets and stored in the reactor without UV-A illumination at 25 ± 2°C for evaluating the ethylene evolution and respiration rate of fruit under visible light.

After four days, papayas stored under UV-A light were removed from the reactor and characterized as the color, fungal growth, weight loss, firmness, pH, titratable acidity and soluble solids content. The physiology, physicochemical properties and visual aspect of fruit wrapped in both blank EPE and EPE-2x-Gel-1%TiO_2 foam nets were evaluated and compared before and after the storage period (four days).

Figure 33 - Schematic representation of the batch system used to degrade ethylene produced by papaya.

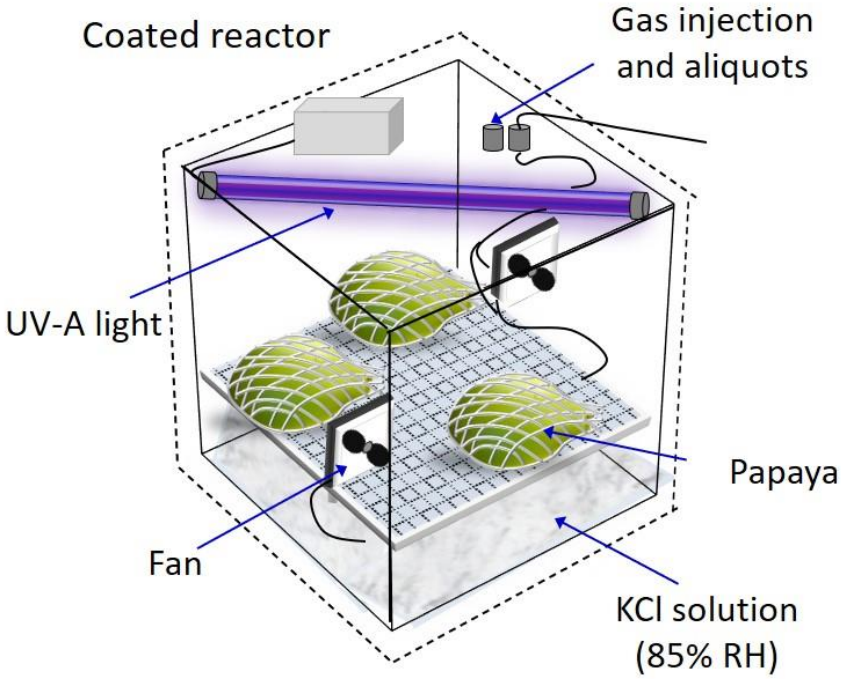

Source: Fonseca et al. (2021a), with permission.

5.2.2.4 Ethylene production and respiration rate

The ethylene concentration accumulated in the reactor was measured by gas chromatography coupled with mass spectrometry (GC-MS equipped with a triple-axis detector Agilent 5975C inert MSD®, system Agilent 7890A GC® and Supel-Q-plot, Supelco® column (32 m x 0.32 mm)). The thermal program parameters used to detect ethylene were: selected ion monitored (SIM) mode set to precisely detect the mass/charge ratio of 28 for ethylene, splitless mode and isothermal oven, injector, detector and transfer line temperatures of 28°C, 120°C, 200°C and 250°C, respectively. Helium (5.0 White Martins®) was used as carrier gas at a rate of 1.33 $ml.min^{-1}$, and a gastight syringe was used to take gas aliquots (250 µl) at first 12 h and each 24 h during four days.

The papaya respiration rate was determined from O_2 and CO_2 concentrations using a gas analyzer (CheckMate II PBI Dansensor®) (TOSATI et al., 2015) and the model proposed by Torrieri, Cavelli and Masi (TORRIERI; CAVELLA; MASI, 2009) (**equations 21** and **22**). Gas aliquots were taken and measured in the same intervals used to quantify ethylene.

$$r_{O_2}(t) = -\frac{V_v}{W}\frac{d[O_2]}{dt} \quad (21)$$

$$r_{CO_2}(t) = \frac{V_v}{W}\frac{d[CO_2]}{dt} \quad (22)$$

Where, r_{O_2} e r_{CO_2} are the O_2 consumption and CO_2 production rates [nmol kg^{-1} s^{-1}], respectively, V_v is the void reactor volume (L), W is the fruit weight [kg], and $[O_2]$ and $[CO_2]$ are O_2 and CO_2 concentrations [mol l^{-1}] over time (t, [s]), respectively.

5.2.2.5 Color and fungal growth

Fruit peel and pulp colors were evaluated using a high-resolution camera (AF-S DX NIKKOR 18–55 mm f/3.5–5.6G VR, Nikon®) coupled to an illumination diffusing chamber with a white standard plate. Four images of papaya sides were captured to evaluate peel color changes, while longitudinal cut pictures were captured to evaluate pulp color changes. The color parameters luminosity (L*) from 0 to 100%, green/red (a*) and blue/yellow (b*) chromatic coordinates were analyzed in the Color Space Converter version 4.0-Image J® software. The parameters total difference color (ΔE^*), color saturation (chroma, C^*), chroma difference (ΔC^*), hue (*h;* °) and hue difference (ΔH, °) were calculated according to **equations 23 – 26** (ALI et al., 2011; FONSECA et al., 2020; KONICA MINOLTA SENSING AMERICAS, 2019).

$$\Delta E^* = \sqrt{(\Delta L^*)^2 + (\Delta a^*)^2 + (\Delta b^*)^2} \quad (23)$$

$$C^* = \sqrt{(a^*)^2 + (b^*)^2} \quad (24)$$

$$h(°) = tan\,(\frac{b^*}{a^*}) \quad (25)$$

$$\Delta H^* = \sqrt{(\Delta L^*)^2 + (\Delta E^*)^2 + (\Delta C^*)^2} \quad (26)$$

where $\Delta L^* = L^*_{sample} - L^*_{standard}$, $\Delta a^* = a^*_{sample} - a^*_{standard}$, $\Delta b^* = b^*_{sample} - b^*_{standard}$, $\Delta C^* = C^*_{sample} - C^*_{standard}$.

The fungal growth on the papaya surface was visually evaluated on days 0 and 4 of storage in the reactor (GUERRA et al., 2015).

5.2.2.6 Weight loss and firmness

The fruit weight loss was determined by the weight percentage difference between the fruit weights before (day 0) and after (day 4) the storage period in the batch reactor (DIAS et al., 2011). The firmness was determined in a texture analyzer model TA.HDplus® equipped with a penetration probe and set at compression test mode and pre-test, test and post-test speeds of 10 mm s^{-1}, 1 mm s^{-1} and 40 mm s^{-1}, respectively. The analysis was carried out according to Souza et al., 2014, with adaptations. Three papaya regions were selected for the probe penetration (peel, pulp close to the peel and pulp close to the seeds) (**Figure 34**) due to the high variation of pulp firmness in different regions at the beginning of fruit ripening. Five equatorially equidistant points were taken on the fruit surface for measuring the peel firmness. Then, the fruit was longitudinally cut into two parts, and on the pulp, four and six points close to the peel and seeds were taken per part, respectively. Three fruit samples were used for each replicate, and the maximum penetration force was recorded in Newtons (N).

Figure 34 - Regions of papaya fruit submitted to the firmness tests.

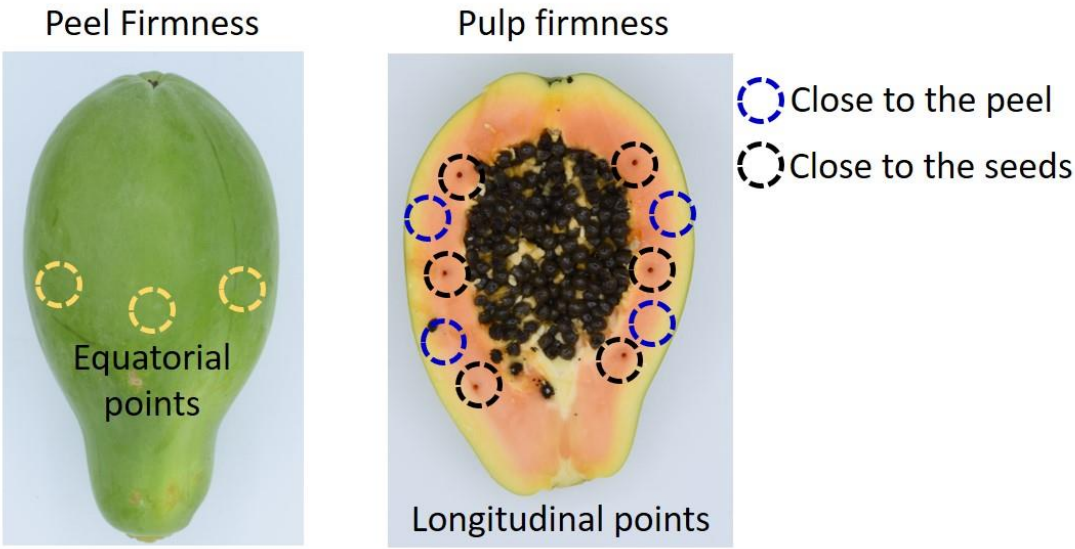

*For interpretation of the references to color in this figure legend, the reader is referred to the Web version of this article.

Source: Author.

5.2.2.7 pH, titratable acidity and total soluble solids content

Pulp and peel were separated, and pulp was ground in a blender to determine pH, titratable acidity (TTA) and total soluble solids content (TSS) of papayas. All analyses were carried out at 23 ± 2°C. The pH of each pulp sample was measured four times using a portable digital pH-meter Testo-205PH. The TTA was determined by titration using

phenolphthalein (0.1 % v/v) as an indicator in acid-base (change color at pH = 8.1) and NaOH solution (0.092 mol L^{-1}) previously standardized with potassium hydrogen phthalate as titrant solution. The pulp samples were vacuum filtered, and 0.040 kg of pulp was added into 0.120 L of distilled water for each titratable analysis (HORWITZ; LATIMER, 2005). The titrant solution volume was used to calculate the TTA [%], equivalent to [$kg_{citric\ acid}$/100 kg_{pulp}], according to **equation 27**.

$$TTA = \frac{n\, M_{acid}\ \ V_{base}\ \ M_{base}}{m_{pulp}}\ x\ 100 \qquad (27)$$

Where n = 3 is the ratio between mols of citric acid [3 mols] neutralized by 1 mol of base (NaOH), M_{acid} is the citric acid molar mass [192.124 x 10^{-2} kg mol^{-1}], M_{base} and V_{base} are standardized solution molar concentration [0.092 mol L^{-1}] and titrant solution volume [L] of NaOH and and m_{pulp} is the pulp mass [0.040 kg], respectively.

Finally, the TSS content was measured using a digital refractometer model PAL-RI ATAGO with 0 – 93 % resolution. One drop of integral pulp juice was dripped on the refractometer lens for each measurement, and distilled water was used as a liquid standard.. The measurements were taken in triplicate (SOUZA et al., 2014).

5.2.2.8 Statistical analysis

Experimental data were statistically evaluated by one-way analysis of variance (ANOVA) and Tukey test of multiple comparisons ($p \leq 0.05$) using the Statistica software (version 13.0). All experiments were carried out in triplicate.

Laboratories, in which experiments and analyses were carried out, are presented in **Table 17**.

Table 17 - Laboratories located at UFSC used to carry out the third step of this thesis.

Experiments/Characterizations	Laboratories
Determination of soluble solids, weight loss, peel and pulp color, acidity and O_2 consumption and CO_2 production rates of papaya.	Laboratório de propriedades físicas dos alimentos (PROFI/EQA).
Firmness loss analysis, quantification of ethylene from papaya and photocatalysis reactions.	Central de Análises do Departamento de Engenharia Química e de Alimentos da UFSC (CA/EQA)

Source: Author.

5.3 RESULTS AND DISCUSSIONS

5.3.1 Ethylene production and respiration rate

Papayas wrapped in the blank foam nets (control experiment) exhibited their maximum ethylene production rate [15.6 nmol kg^{-1} s^{-1}] at 12h under UV-A light (**Figure 35.a**). Respiration rate data evidenced that the climacteric peak occurred 24 h after beginning the experiments (**Figures 35.c and 35.d**). This result agrees with the typical climacteric fruit respiration pattern (**Figures 35.c and 35.d**), characterized by high O_2 consumption and CO_2 production in the initial maturation stage. It is accompanied by an increase in ethylene production rate (CHITARRA; CHITARRA, 2005; LI et al., 2013; OLIVEIRA et al., 2015; SOUZA et al., 2014). Differences between ethylene evolution and respiration patterns for the control (under UV-A light) and visible light experiments were not observed.

The ethylene production from papayas wrapped in gelatin-TiO_2-coated EPE foam nets was lower than control fruit during the photocatalysis experiment (**Figure 35.a**). After 96 h under UV-A light, photocatalysis experiment fruit showed 60 % less ethylene accumulated in the reactor than control experiment fruit (**Figure 35.b**). Besides, there was a reduction of the papaya climacteric peak, confirmed by lower O_2 consumption and CO_2 production rates at 24 h (**Figures 35.c and 35.d**). These results indicated that the gelatin-TiO_2-coated EPE foam nets were efficient to degrade ethylene, avoiding its accumulation in the reactor. They also suggest that there was a reduction of the autocatalytic ethylene production by the papayas.

The ethylene biosynthesis is managed by enzymatic conversion in the plant cell membrane (FABI; DO PRADO, 2019). First, the ethylene concentration increases in the intracellular medium, which increases the fruit respiration rate. Second, the intracellular ethylene diffuses from inside plant tissues to the environment, and the increase of its concentration stimulates its autocatalytic production. Finally, the external environment

ethylene molecules bind to the membrane protein receptors and manage the activation of specific genes responsible for coordinating the syntheses of enzymes that catalyze fruit ripening chemical reactions (LELIEVRÈ et al., 1997).

Thus, the external environment ethylene removal by the EPE-2x-Gel-1%TiO_2 foam nets, mainly at the first 24 h of the test, probably retarded the activation of the autocatalytic ethylene production, which decreased its accumulation and production rate in the reactor (**Figures 35.a and 35.b**). In contrast, the O_2 consumption and CO_2 production decrease only at 24 h (**Figures 35.c and 35.d**), suggests that the TiO_2 photocatalysis did not strongly influence the intracellular ethylene production. The evolution profiles of ethylene, O_2 and CO_2 in the reactor were preserved during photocatalysis. It indicates that the nanocomposite foam nets did not cause physiological disorder in the papayas.

Kaewklin et al. (2018) developed an active chitosan-based nanocomposite film added by 1 wt% TiO_2 to delay the ripeness of cherry tomatoes. Their results also showed that the external environment ethylene photocatalytic degradation did not alter ethylene and CO_2 production curves profiles. The ethylene removal caused a respiration rate reduction only during the tomato climacteric phase.

Figure 35 – Ethylene production rate (a), ethylene accumulated (b), O_2 consumption rate (c) and CO_2 production rate (d) of papayas wrapped with blank foam nets under visible light (at 25 ± 2°C) and UV-A light (control at 30 ± 1°C) and wrapped in gelatin-TiO_2-coated EPE foam nets (photocatalysis at 30 ± 1°C) at 85% RH

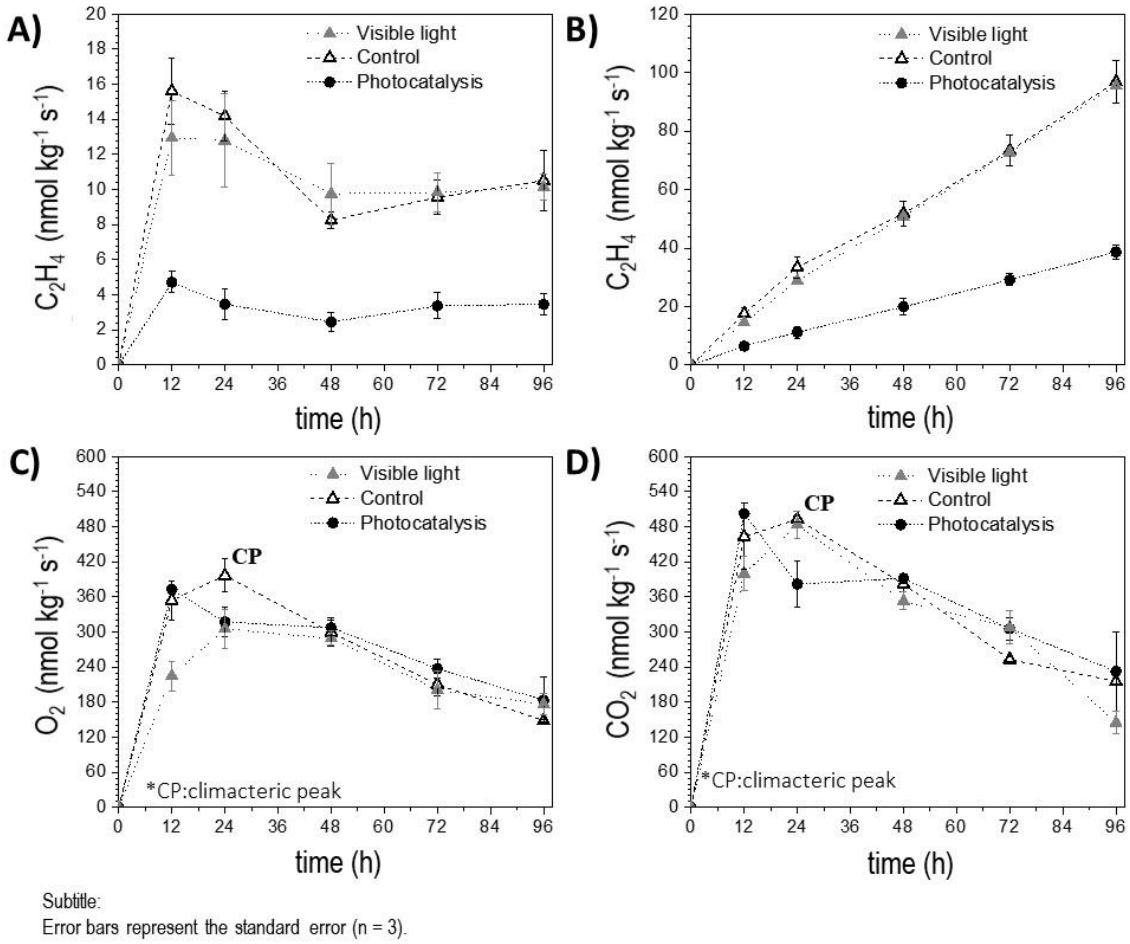

Source: Fonseca et al. (2021a), with permission.

5.3.2 Color and fungal growth

Papaya images (**Figure 36**) and color parameters (**Table 18**) before UV-A light exposure (day 0) evidence that the fruit was equally selected at the beginning of the maturation stage for carrying out the experiments: green peel and slightly orange pulp. After 96 h under UV-A light (day 4), the control fruit exhibited peel more yellowish and pulp more orange than photocatalysis experiment fruit, which was confirmed by the increase ($p \leq 0.05$) of its respective color parameters b* and a* (**Table 18**). Control fruit also exhibited higher variations of total color (ΔE*), chroma (ΔC*) and hue (ΔH*) than fruit wrapped in gelatin-TiO_2-coated EPE foam nets (**Table 18**). This result confirms that both the control fruit peel and pulp suffered a broad color change resulting in more intense and saturated colors, which

are characteristic of ripe fruit (CEAGESP, 2003). The change of pulp color from yellow to orange/red in papayas is caused by cellulose degradation and carotenoid accumulation produced by cyclases and hydrolases. The activity of these enzymes is induced by the increase of ethylene production (FABI; DO PRADO, 2019). Similar results about color parameters L*, a*, b* and *h*° for the papayas (*Carica papaya* L. cv. 'Golden') were obtained by Souza et al. (2014).

After four days, the control experiment fruit exhibited an aged aspect featured by the surface scald formation, while the photocatalysis experiment fruit was visually more preserved (**Fig. 3**). One possible hypothesis is that the gelatin-TiO_2 coating on the foam nets could have promoted a supplementary protective action against the fruit peel photo-oxidation for the group treated with photocatalysis. In this case, photogenerated reactive oxygen species (ROS) preferentially reacted with ethylene molecules, previously adsorbed on the TiO_2 surface. Thus, the attack on papaya peel compounds by ROS could have been hindered. Papaya scald formation by UV-A light has also been suggested by other authors (LOURENÇO et al., 2017b).

Lastly, the fungi growth was visualized on the control fruit surface after four days under UV-A light. The faster control fruit ripening, indicated by the broadest variation of color parameters, probably favored plant tissue degradation and, consequently, fungi development (CHITARRA; CHITARRA, 2005). Several papers have already reported the microorganism oxidation from biopolymers-TiO_2 nanocomposites (BALASUBRAMANIAN et al., 2019; HE et al., 2016; KAEWKLIN et al., 2018; MAHMOOD et al., 2020; MUKHERJEE et al., 2020; XIE; HUNG, 2018; ZHANG et al., 2017, 2019). Although the antimicrobial TiO_2 activity was not evaluated in this research, it is possible to speculate that the foam nets coated with gelatin-TiO_2 can have hindered microbial growth on the papaya surface. However, more specific antimicrobial studies need to be performed to confirm the material antimicrobial properties.

Figure 36 – Images of papayas wrapped in the blank (control) and nanocomposite (photocatalysis) foam nets before (day 0) and after (day 4) being exposed to UV-A light at 30 ± 1°C and 85% RH.

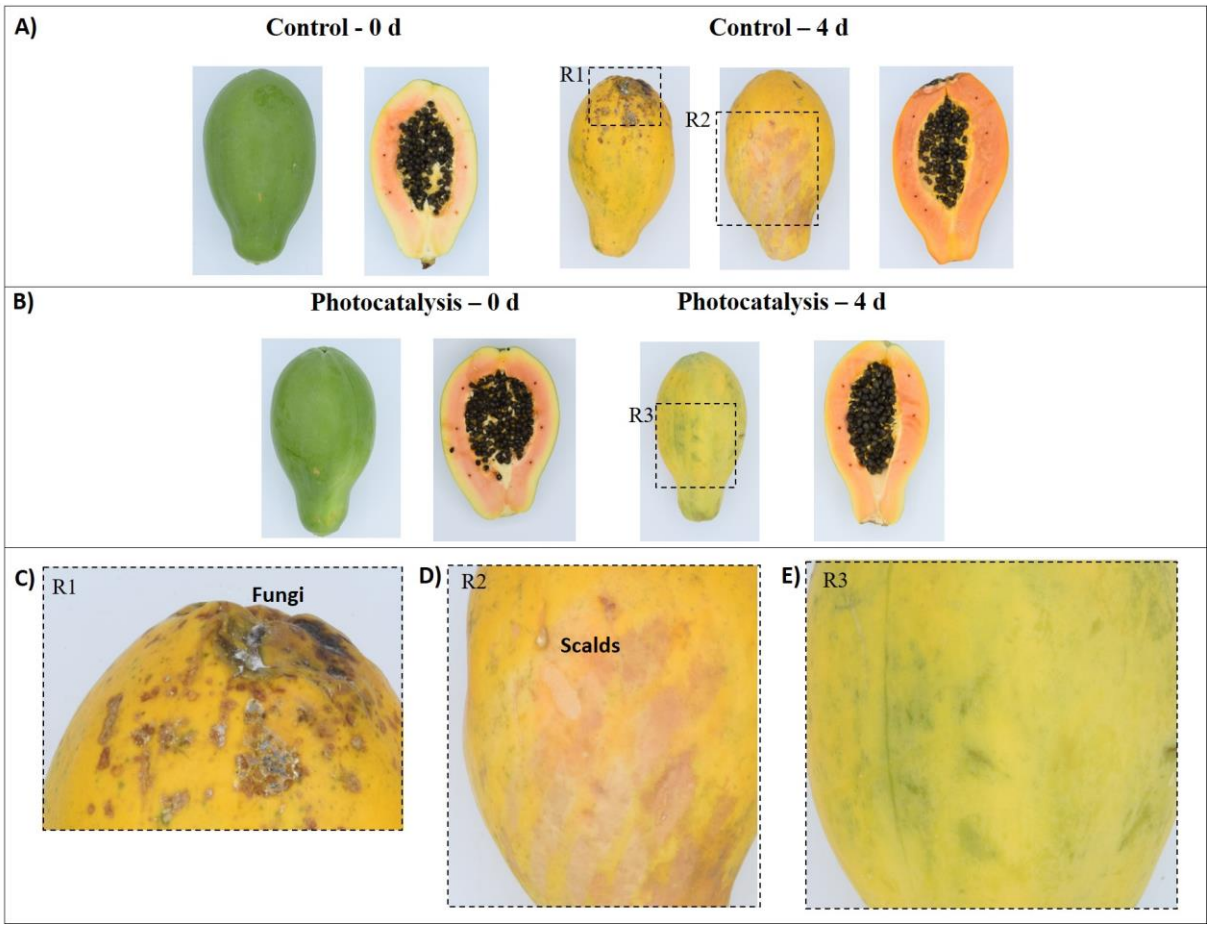

Source: Fonseca et al. (2021a), with permission.

Table 18 - Color parameters of the papayas wrapped in the blank (control) and nanocomposite (photocatalysis) foam nets before (day 0) and after (day 4) being exposed to UV-A light at 30 ± 1°C and 85% RH.

Fruit peel[1,2]				
Parameters	**Control**		**Photocatalysis**	
	Day 0	**Day 4**	**Day 0**	**Day 4**
L*	63.82 ± 0.81^{bA}	79.40 ± 1.11^{aA}	59.52 ± 3.92^{aA}	79.93 ± 4.73^{aA}
a*	-24.51 ± 0.96^{bA}	-5.92 ± 0.32^{aA}	-23.95 ± 1.19^{bA}	-8.9 ± 1.07^{aB}
b*	42.71 ± 1.60^{bA}	65.27 ± 0.50^{aA}	43.60 ± 1.63^{aA}	55.76 ± 2.21^{aB}
ΔE*	60.70 ± 0.60^{bA}	72.68 ± 0.76^{aA}	63.24 ± 2.06^{bA}	65.59 ± 0.44^{aB}
C*	49.30 ± 0.99^{bA}	65.54 ± 0.94^{aA}	49.18 ± 0.85^{bA}	56.50 ± 2.09^{aB}
ΔC*	42.39 ± 1.40^{bA}	59.49 ± 1.26^{aA}	42.34 ± 0.96^{bA}	49.78 ± 2.46^{aB}
h [°]	119.91 ± 1.84^{aA}	84.82 ± 0.25^{bB}	118.85 ± 2.13^{aA}	99.16 ± 1.31^{bA}
ΔH [°]	78.88 ± 1.05^{bA}	94.76 ± 1.29^{aA}	81.81 ± 2.60^{aA}	84.49 ± 0.79^{aB}
Fruit pulp[1,2]				
Parameters	**Control**		**Photocatalysis**	
	Day 0	**Day 4**	**Day 0**	**Day 4**
L*	83.28 ± 0.15^{aB}	70.05 ± 1.25^{bB}	78.18 ± 1.24^{aA}	80.56 ± 0.23^{aA}
a*	11.56 ± 0.57^{bA}	33.13 ± 1.10^{aA}	9.84 ± 2.11^{aA}	15.20 ± 0.52^{aB}
b*	30.98 ± 0.03^{bA}	46.06 ± 1.43^{aA}	32.33 ± 1.28^{bA}	53.37 ± 3.27^{aA}
ΔE*	41.11 ± 0.34^{bA}	62.50 ± 3.97^{aB}	37.29 ± 4.37^{bA}	63.22 ± 3.68^{aB}
C*	33.07 ± 0.23^{bA}	56.75 ± 0.65^{aA}	33.88 ± 1.83^{bA}	55.52 ± 3.09^{aA}
ΔC*	25.67 ± 0.18^{bA}	50.11 ± 0.75^{aA}	27.39 ± 1.61^{bA}	48.64 ± 2.45^{aA}
h [°]	69.55 ± 0.91^{bA}	54.29 ± 0.97^{aB}	73.38 ± 2.82^{aA}	73.98 ± 1.20^{aA}
ΔH [°]	49.12 ± 0.42^{bA}	82.87 ± 3.59^{aA}	47.37 ± 4.03^{bA}	80.44 ± 4.35^{aA}

[1]All values were expressed as mean ± standard error (n = 3). Differences at the level of α = 0.05 between days 0 and 4 for the same group (control or photocatalysis) and between groups control and photocatalysis for the same day are represented by the different minuscule and majuscule letters, respectively. [2] L*: luminosity (black-white; 0-100); a* (green/red; -a*/a*); b* (blue/yellow; -b*/b*); ΔE*: total color difference; C*: chroma (saturation); ΔC*: chroma difference; *h* [°]: hue; ΔH [°]: hue difference.

Source: Fonseca et al. (2021a), with permission.

5.3.3 Weight loss and firmness

Papayas submitted to the control and photocatalysis treatments did not show a difference ($p > 0.05$) for the weight loss, which could be expressed by an average value of 5.87 ± 0.44 %. The weight loss maintenance can be attributed to the considerably thick peel of papayas that protect them against excessive transpiration.

In contrast, comparing the fruit firmness, the control fruit exhibited higher firmness loss of the peel (60.4 %), pulp close to the peel (71.6 %) and pulp close to the seeds of (70.7 %) after being exposed to UV-A light. Fruit wrapped in gelatin-TiO_2-coated EPE foam nets exhibited firmness loss of 4.0 %, 44.0 % and 34.1 % for the peel, pulp close to the peel and pulp close to the seeds, respectively ($p \leq 0.05$) (**Figure 37**). The softening process is

associated with fast biochemical transformations that cause the reduction of turgor pressure, degradation and death of plant tissues during the senescence stage of the fruit (CHITARRA; CHITARRA, 2005). The drastic firmness loss, characteristic of the ripe papayas, is mainly caused by the increased water-soluble pectin fractions generated by the pectin enzymatic degradation (FABI; DO PRADO, 2019; MARTINS; COSTA, 2003). The softness is the most observable characteristic of the papaya ripening process (MARTINS; COSTA, 2003; SOUZA et al., 2014). The ethylene removal by the nanocomposite foam nets probably retarded the pectinase expression (FABI; DO PRADO, 2019).

Souza et al. (2014) reported an accentuated firmness loss of papayas *Carica papaya* L. cv. 'Golden' in the third day after being harvested in their maturation stage 0 (100% green peel) and Vieira et al. (2020) reported similar pulp and peel firmness values for the same fruit cultivar.

Figure 37 – Firmness of peel (a), pulp close to the peel (b) and pulp close to the seeds (c) of papayas wrapped in the blank (control) and nanocomposite (photocatalysis) foam nets before (day 0) and after (day 4) being exposed to UV-A light at 30 ± 1°C and 85% RH.

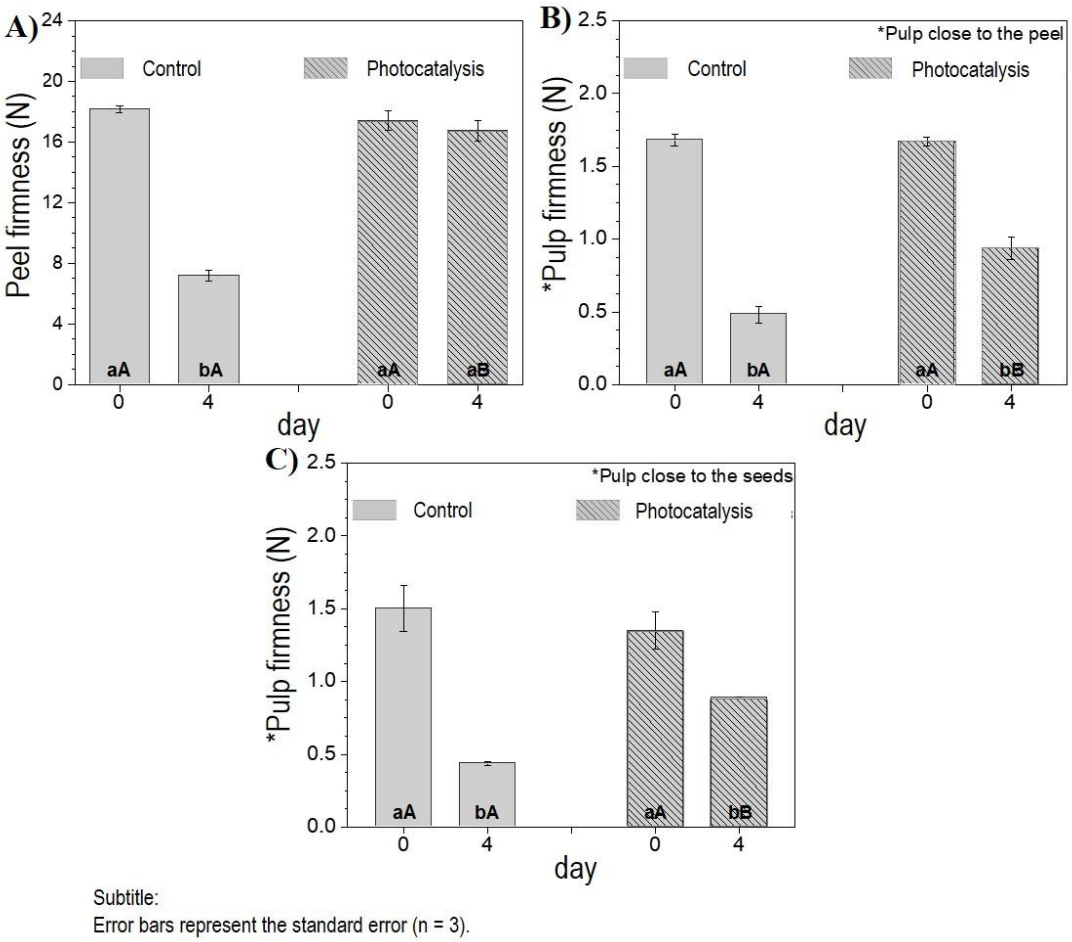

Source: Fonseca et al. (2021a), with permission.

5.3.4 pH, titratable acidity and soluble solids content

Differences in the pulp pH ($p > 0.05$) were not observed before and after being exposed to UV-A light for both control and photocatalysis treatments (pH = 5.48 ± 0.03). Compared with other fruit, papayas do not show an accentuated acidity, so the absence of pH variation and low titratable acidity (TTA) values were already expected (MARTINS; COSTA, 2003). It was also observed a TTA reduction of 36.6 % for the control samples after four days under UV-A light ($p \leq 0.05$) (**Table 19**). Malic and citric acids are the most predominant acids in the papaya pulp in equivalent percentages. The decrease of their concentrations is related to the water accumulation and dilution in the plant tissue (CALEGÁRIO et al., 1997). Martins & Costa (2003) affirm that papaya can also exhibit a slight increase in TTA, followed by a decrease during ripening. The TTA increase is attributed to galacturonic acid accumulation close to the peel caused by the pectin enzymatic degradation. The TTA value maintenance for the fruit treated with TiO_2 photocatalysis corroborates the firmness loss results and the hypothesis that pectin molecules were less degraded and turgor pressure was more preserved.

On day 0, papayas showed an average soluble solids content of 9.62 ± 0.62 %, which did not change after four days ($p > 0.05$) (**Table 19**). Papayas have insufficient starch content to be converted into glucose and to increase sweetness. The papaya sweetness raising is due to the accumulation of glucose, fructose and saccharose, whereas it is still attached to the plant (PAL; SELVARAJ, 1987; SELVARAJ et al., 1982). Although the TSS has not changed, a large discrepancy between the ratio TSS/TTA of the control samples for days 0 and 4 has been noticed. The ratio TSS/TTA is used to express the equilibrium between sweetness and acidity and its perception by the consumers (DIAS et al., 2011). Results indicate that the fruit treated with TiO_2 photocatalysis developed a minor sweetness sensation than the control fruit because it did not reach the complete maturation stage. The values of pH, TTA and TSS agree with values reported by Vieira et al. (2020), Jacomino et al. (2002) and Souza et al. (2014).

Table 19 - Titratable acidity (TTA), total soluble solids (TSS) and ratio TSS/TTA of the papayas wrapped in the blank (control) and nanocomposite (photocatalysis) foam nets before (day 0) and after (day 4) being exposed to UV-A light at 30 ± 1°C and 85% RH.

Physicochemical parameters[1]	**Control**		**Photocatalysis**	
	Day 0	**Day 4**	**Day 0**	**Day 4**
TTA [%]	$0.14 \pm (< 10^{-2})^{aA}$	$0.09 \pm (< 10^{-2})^{bB}$	$0.13 \pm (< 10^{-2})^{aA}$	$0.13 \pm (< 10^{-2})^{aA}$
TSS [%]	9.30 ± 0.64^{aA}	10.48 ± 0.40^{aA}	9.53 ± 0.71^{aA}	9.16 ± 0.72^{aA}
Ratio TSS/TTA	67.74 ± 2.52^{bA}	122.44 ± 13.64^{aB}	71.33 ± 5.21^{aA}	64.42 ± 12.04^{aA}

[1]All values were expressed as mean ± standard error (n = 3). Differences at the level of α = 0.05 between days 0 and 4 for the same group (control or photocatalysis) and between groups control and photocatalysis for the same day are represented by the different minuscule and majuscule letters, respectively.

Source: Fonseca et al. (2021a), with permission.

5.4 CONCLUSIONS OF CHAPTER 5

Polyethylene foam nets coated with gelatin-TiO_2 nanocomposite were efficient to degrade ethylene and postpone the papaya ripening under severe storage conditions studied for four days. Fruit treated with TiO_2 photocatalysis exhibited: lower ethylene production and respiration rate at the climacteric peak, higher firmness and more preservation of green peel, orange pulp, sweetness/acidity equilibrium and absence of both scalds and superficial fungal growth.

From these results, it can be inferred that the ethylene degradation by TiO_2 photocatalysis decreased the expression of enzymes that trigger the degradation of compounds present in higher concentration at the beginning of the papaya maturation stage, such as the pectin, chlorophyll, malic and citric acids. Also, nanocomposite foam nets could have played a supplementary UV-A light blocker role minimizing its absorption by the peel cells. Additional microbiological studies need to be performed to investigate and confirm the antimicrobial properties of gelatin-TiO_2-coated EPE foam nets. Finally, the postharvest technology developed in this research deserves to be tested in other fruit and storage conditions.

Chapter 6.FINAL CONCLUSIONS AND FUTURE RESEARCHES

This final chapter presents the most relevant conclusions based on results reported in the previous chapters and suggestions for future researches.

6.1 FINAL CONCLUSIONS

This thesis proposed a new fruit postharvest technology based on ethylene photocatalytic degradation. Both hydroxypropyl methylcellulose-TiO_2 and gelatin-TiO_2 nanocomposites exhibited photocatalytic activity on ethylene. However, TiO_2 nanoparticles showed to be more dispersed into gelatin- than hydroxypropyl methylcellulose-based film, which contributed to the faster ethylene degradation by the gelatin-TiO_2 film containing 1 wt % TiO_2 (Gel-1%TiO_2)

The use of expanded polyethylene (EPE) foam nets as supports for the Gel-1%TiO_2 nanocomposite coating improved its photocatalytic activity due to the increase of reactive surface area. EPE foam nets coated with a Gel-1%TiO_2 bilayer exhibited the highest ethylene concentration degraded per TiO_2 weight unit loaded on irradiated EPE surface area unit.

Papaya was an adequate climacteric fruit model to evaluate the *in vivo* application performance of gelatin-TiO_2-coated EPE foam nets. The ripening of fruit treated with photocatalysis was delayed: color and firmness were the parameters that displayed the most significant differences compared to the control. The external environment ethylene photocatalytic degradation by the gelatin-TiO_2-coated EPE foam nets at the initial maturation stage was essential to preserve the fruit peel green color and firmness. Indirectly, the fruit firmness preservation can have hindered the fungal contamination observed on the control fruit surface.

Based on the critical role played by the ethylene scavenging technology developed in this thesis on papaya ripening, the gelatin-TiO_2-coated EPE foam nets, it is expected that this innovative material induces new perspectives for the fruit postharvest sector, stimulating new researches for the scale-up and the development and upgrading of other clear technologies. It is also expected that gelatin-TiO_2-coated EPE foam nets can also extend the shelf life of other fruit and can be widely used as a fruit postharvest technology in the future.

6.2 FUTURE RESEARCHES

The photocatalytic material proposed and developed in this thesis was capable of degrading ethylene and delaying the papaya ripening. Nevertheless, some biopolymers-TiO_2 properties require further investigation and can be enhanced to potentialize their photocatalytic activity. For this, it is necessary:

- Studying the hydroxypropyl methylcellulose-TiO_2 and gelatin-TiO_2 film antimicrobial effects against fungi and Gram-positive and Gram-negative bacteria deeply.
- Improving the TiO_2 photocatalytic properties (extending light-absorption λ range) using non-toxic doping elements (*e.g.* C and N) and composite association with other semiconductors (*e.g.* ZnO and CuO).
- Accomplishing *in vivo* tests using other fruit species.

REFERENCES

ACOSTA LEZCANO FOSCACHES, C. et al. LOGÍSTICA DE FRUTAS, LEGUMES E VERDURAS (FLV): um estudo sobre embalagem, armazenamento e transporte em pequenas cidades brasileiras. **Informações Econômicas**, v. 42, n. 2, p. 37–46, 2012.

ADAMI, A. C. DE O. et al. OFERTA DE EXPORTAÇÃO DE FRUTAS DO BRASIL: O CASO DA MANGA E DO MELÃO, NO PERÍODO DE 2004 A 2015 Brasilian fruit exports: mangos and melons cases in the period 2004 to 2015. **Rev. Econ. NE, Fortaleza**, v. 47, n. 4, p. 63–78, 2017.

AHMED, M. A. Journal of Photochemistry & Photobiology, B : Biology Synthesis of mesoporous TiO 2 – curcumin nanoparticles for photocatalytic degradation of methylene blue dye. **JPB**, v. 160, p. 134–141, 2016.

ALI, A. et al. Effect of chitosan coatings on the physicochemical characteristics of Eksotika II papaya (Carica papaya L .) fruit during cold storage. **Food Chemistry**, v. 124, n. 2, p. 620–626, 2011.

ALMEIDA, R. F. DE et al. Injúria pelo frio em frutos de mamoeiro (Carica papaya L.) cv "Golden". **Revista Brasileira de Fruticultura**, v. 27, n. 1, p. 17–20, 2006.

ALTAN, M.; YILDIRIM, H. Mechanical and Antibacterial Properties of Injection Molded Propypropylene/TiO2 Nano-Composites. **Journal of Material Science Technology**, v. 28, n. 8, p. 686–692, 2012.

AMIR, S. et al. International Journal of Biological Macromolecules Physicochemical and rheo-mechanical properties of titanium dioxide reinforced sage seed gum nanohybrid hydrogel. **International Journal of Biological Macromolecules**, v. 118, p. 661–670, 2018.

AN, J.-F.; PAULL, R. E. Storage Temperature and Ethylene Influence on Ripening of Papaya Fruit. **Journal of the American Society for Horticultural Science**, v. 115, n. 6, p. 949–953, 1990.

ANI, I. J. et al. **Photocatalytic degradation of pollutants in petroleum refinery wastewater by TiO2- and ZnO-based photocatalysts: Recent developmentJournal of Cleaner Production**Elsevier Ltd, , 20 dez. 2018.

ARFAT, Y. A. et al. Development and characterisation of blend films based on fish protein isolate and fish skin gelatin. **Food Hydrocolloids**, v. 39, p. 58–67, 2014.

ARFAT, Y. A. Plasticizers for Biopolymer Films. In: **Glass Transition and Phase Transitions in Food and Biological Materials**. Chichester, UK: John Wiley & Sons, Ltd, 2017. p. 159–182.

ARZATE-VÁZQUEZ, I. et al. Image Processing Applied to Classification of Avocado Variety Hass (Persea americana Mill.) During the Ripening Process. **Food and Bioprocess Technology**, v. 4, n. 7, p. 1307–1313, 2011.

ASADI, S.; PIRSA, S. Production of Biodegradable Film Based on Polylactic Acid, Modified with Lycopene Pigment and TiO2 and Studying Its Physicochemical Properties. **Journal of Polymers and the Environment**, v. 28, n. 2, p. 433–444, fev. 2020.

ASTM. **Annual book of ASTM standards**. Pensylvania, USA: [s.n.]. v. 00.01

AZEREDO, H. M. C.; ROSA, M. F.; MATTOSO, L. H. C. Nanocellulose in bio-based food packaging applications. **Industrial Crops and Products**, v. 97, p. 664–671, 1 mar. 2017.

BACHLER, G.; VON GOETZ, N.; HUNGERBUHLER, K. Using physiologically based pharmacokinetic (PBPK) modeling for dietary risk assessment of titanium dioxide (TiO<inf>2</inf>) nanoparticles. **Nanotoxicology**, v. 9, n. 3, p. 373–380, 2015.

BALASUBRAMANIAN, R. et al. Effect of TiO 2 on highly elastic, stretchable UV protective nanocomposite films formed by using a combination of k-Carrageenan, xanthan gum and gellan gum. **International Journal of Biological Macromolecules**, v. 123, p. 1020–1027, 2019.

BASSO, A.; DE FÁTIMA PERALTA MUNIZ MOREIRA, R.; JOSÉ, H. J. Effect of operational conditions on photocatalytic ethylene degradation applied to control tomato ripening. **Journal of Photochemistry and Photobiology A: Chemistry**, v. 367, n. August, p. 294–301, 2018.

BASULTO, F. S. et al. Maduración postcosecha e índices de madurez de papaya maradol. **Interciencia**, v. 34, n. 8, p. 583 –588, 2009.

BERGER, S. et al. Microgel/clay nanohybrids as responsive scavenger systems. **Polymer**, v. 51, n. 17, p. 3829–3835, 2010.

BERGO, P.; SOBRAL, P. J. A. Effects of plasticizer on physical properties of pigskin gelatin films. **Food Hydrocolloids**, v. 21, n. 8, p. 1285–1289, 2007.

BIALE, J. B. Growth, Maturation, and Senescence in Fruits: Recent knowledge on growth regulation and on biological oxidations has been applied to studies with fruits. **Science (New York, N.Y.)**, v. 146, n. 3646, p. 880–8, 13 nov. 1964.

BIALOPIOTROWICZ, T.; JAŃCZUK, B. Surface properties of gelatin films. **Langmuir**, v. 18, n. 24, p. 9462–9468, 2002.

BILBAO-SAINZ, C. et al. HPMC reinforced with different cellulose nano-particles. **Carbohydrate Polymers**, v. 86, n. 4, p. 1549–1557, 2011.

BISWAS, A.; CHAKRABORTY, A.; JANA, N. R. Nitrogen and Fluorine Codoped, Colloidal TiO2 Nanoparticle: Tunable Doping, Large Red-Shifted Band Edge, Visible Light Induced Photocatalysis, and Cell Death. **ACS Applied Materials and Interfaces**, v. 10, n. 2, p. 1976–1986, 2018.

BRACKMANN, A. et al. Atmosfera controlada , absorção de etileno e aplicação de 1-MCP durante o armazenamento de pêssegos " Eragil " Controlled atmosphere , ethylene absorption and 1-MCP application during. **Científica, Jaboticabal**, v. 41, n. 2, p. 156–163, 2013.

CAIVANO, J. , DEL PILAR BUERA, M. **Color in Food: Technological and Psychophysical Aspects**. 1st. ed. [s.l.] CRC Press, Taylor & Francis Group, Boca Raton, 2012.

CALBO, A. G.; MORETTI, C. L.; HENZ, G. P. Respiraçao de Frutas e Hortaliças. **Comunicado Técnico**, v. 46, p. 1–10, 2007.

CALEGÁRIO, F. F. et al. Relationship Between Peel Color and Fruit Quality of Papaya (Carica Papaya L.) Harvested At Different Maturity Stages. **Proceedings of the Florida State Horticultural Society**, v. 110, p. 228–231, 1997.

CALLISTER, W. D. J.; RETHWISCH, D. G. **Materials Science and Engineering an Introduction**. 8th. ed. [s.l.] John Wiley & Sons, Inc., 2011.

CANEVAROLO JUNIOR, S. V. **Técnicas de caracterização de polímeros.** São Paulo, Brasil: Artliber, 2004.

CEAGESP-COMPANHIA DE ENTREPOSTOS E ARMAZÉNS GERAIS DE SÃO PAULO. **Programa Brasileiro de Modernização da Horticultura – Normas de Classificação do Mamão**. Disponível em: <https://www.hortibrasil.org.br/2016-06-02-10-49-06.html>. Acesso em: 14 abr. 2019.

CHANG, K. L. et al. Removal of ethylene and secondary organic aerosols using UV-C254 + 185 nm with TiO2 catalyst. **Aerosol and Air Quality Research**, v. 13, n. 2, p. 618–626, 2013.

CHATERJI, S.; KWON, I. K.; PARK, K. Smart polymeric gels: Redefining the limits of biomedical devices. **Progress in Polymer Science (Oxford)**, v. 32, n. 8-9, p. 1083–1122, 2007.

CHAWENGKIJWANICH, C.; HAYATA, Y. Development of TiO2 powder-coated food packaging film and its ability to inactivate Escherichia coli in vitro and in actual tests. **International Journal of Food Microbiology**, v. 123, n. 3, p. 288–292, abr. 2008.

CHEN, C. et al. Photocatalytic degradation of C.I. Acid Orange 52 in the presence of Zn-doped TiO2 prepared by a stearic acid gel method. **Dyes and Pigments**, v. 77, n. 1, p. 204–209, 2008.

CHITARRA, M. I. F.; CHITARRA, A. B. **Pós-colheita de frutas e hortaliças : fisiologia e manuseio**. [s.l.] UFLA, 2005.

CHOI, H. C.; JUNG, Y. M.; KIM, S. BIN. Size effects in the Raman spectra of TiO2 nanoparticles. **Vibrational Spectroscopy**, v. 37, n. 1, p. 33–38, 2005.

DA COSTA FILHO, B. M. et al. Effect of catalyst coated surface, illumination mechanism and light source in heterogeneous TiO2 photocatalysis using a mili-photoreactor for n-decane oxidation at gas phase. **Chemical Engineering Journal**, v. 366, n. November 2018, p. 560–568, 2019.

DALRYMPLE, O. K. et al. A review of the mechanisms and modeling of photocatalytic disinfection. **Applied Catalysis B: Environmental**, v. 98, n. 1-2, p. 27–38, 2010a.

DALRYMPLE, O. K. et al. Applied Catalysis B : Environmental A review of the mechanisms and modeling of photocatalytic disinfection. **"Applied Catalysis B, Environmental",** v. 98, n. 1-2, p. 27–38, 2010b.

DEHGHANI, S.; HOSSEINI, S. V.; REGENSTEIN, J. M. Edible films and coatings in seafood preservation: A review. **Food Chemistry**, v. 240, p. 505–513, 2018.

DIAS, T. C. et al. Post-harvest conservation of formosa papaya with pvc film and refrigeration. **Revista Brasileira de Fruticultura**, v. 33, n. 2, p. 666–670, 2011.

DING, C.; ZHANG, M.; LI, G. Preparation and characterization of collagen/hydroxypropyl methylcellulose (HPMC) blend film. **Carbohydrate Polymers**, v. 119, p. 194–201, 2015.

DOW. **METHOCEL Cellulose Ethers: Technical Handbook. Dow Chemical Company**. [s.l: s.n.].

DUDEFOI, W. et al. Impact of food grade and nano-TiO 2 particles on a human intestinal community. **Food and Chemical Toxicology**, v. 106, p. 242–249, 2017.

DUTU, E. et al. Principal component analysis of Raman spectra for TiO 2 nanoparticle characterization. **Applied Surface Science**, v. 417, p. 93–103, 2017.

EINAGA, H. et al. Kinetic analysis of TiO2-catalyzed heterogeneous photocatalytic oxidation of ethylene using computational fluid dynamics. **Chemical Engineering Journal**, v. 263, p. 325–335, 2015.

ETACHERI, V. et al. Visible-light activation of TiO 2 photocatalysts : Advances in theory and experiments. **Journal of Photochemistry and Photobiology C: Photochemistry Reviews**, v. 25, p. 1–29, 2015.

EVONIK INDUSTRIES. Technical Information 1243: AEROXIDE®, AERODISP® and AEROPERL® - Titanium dioxide as photocatalyst. 2015.

FABI, J. P.; DO PRADO, S. B. R. Fast and furious: Ethylene-triggered changes in the metabolism of papaya fruit during ripening. **Frontiers in Plant Science**, v. 10, n. April, 2019.

FAHS, A. et al. Hydroxypropyl methylcellulose (HPMC) formulated films: Relevance to adhesion and friction surface properties. **Carbohydrate Polymers**, v. 80, n. 1, p. 105–114, 2010.

FAO. **Food wastage footprint: Impacts on natural resources - Summary report**. [s.l: s.n.].

FAOSTAT. **Food and Agriculture Organization of the United Nations (FAOSTAT)-Crops download data**. Disponível em: <http://www.fao.org/faostat/en/#data/QC>. Acesso em: 8 jan. 2021.

FARIA, A. R. N. et al. **PLANTAR: A cultura do mamão**. [s.l: s.n.].

FARRIS, S. et al. Wetting of biopolymer coatings: Contact angle kinetics and image analysis investigation. **Langmuir**, v. 27, n. 12, p. 7563–7574, 2011.

FATHI ACHACHLOUEI, B.; ZAHEDI, Y. Fabrication and characterization of CMC-based nanocomposites reinforced with sodium montmorillonite and TiO2 nanomaterials. **Carbohydrate Polymers**, v. 199, n. February, p. 415–425, 2018.

FEI, P. et al. Effects of nano-TiO2 on the properties and structures of starch/poly(ε-caprolactone) composites. **Journal of Applied Polymer Science**, v. 130, n. 6, p. 4129–4136, 2013.

FOGLER, H. S. Catálise e Reatores Catalíticos. In: **Elementos de engenharia das reações químicas**. 4ª. ed. Rio de Janeiro: LTC, 2009. p. 853.

FONSECA, J. DE M. et al. Hydroxypropyl methylcellulose-TiO2 and gelatin-TiO2 nanocomposite films: Physicochemical and structural properties. **International Journal of Biological Macromolecules**, v. 151, p. 944 – 956, 2020.

FONSECA, J. DE M. et al. Gelatin-TiO 2 -coated expanded polyethylene foam nets as ethylene scavengers for fruit postharvest application. **Postharvest Biology and Technology**, v. 180, n. May, 2021a.

FONSECA, J. DE M. et al. Ethylene scavenging properties from hydroxypropyl methylcellulose-TiO2 and gelatin-TiO2 nanocomposites on polyethylene supports for fruit application. **International Journal of Biological Macromolecules**, 24 fev. 2021b.

FONSECA, J. DE M. et al. A review on TiO2-based photocatalytic systems applied in fruit postharvest: Set-ups and perspectives. **Food Research International**, v. 144, p. 110378, 1 jun. 2021c.

FOOD AND AGRICULTURE ORGANIZATION OF THE UNITED STATES-FAO; WORLD HEALTH ORGANIZATION. International Numbering System for Food Additives. In: **CODEX ALIMENTARUIS International Food Standarts**. [s.l: s.n.]. v. 15p. 1–94.

FRIEHS, E. et al. Toxicity, phototoxicity and biocidal activity of nanoparticles employed in photocatalysis. **Journal of Photochemistry and Photobiology C: Photochemistry Reviews**, v. 29, p. 1–28, 2016.

FRUSHOUR, B. G.; KOENIG, J. L. Raman scattering of collagen, gelatin, and elastin. **Biopolymers**, v. 14, n. 2, p. 379–391, 1975.

FU, X. et al. Effects of reaction temperature and water vapor content on the heterogeneous photocatalytic oxidation of ethylene. **Journal of Photochemistry and Photobiology A: Chemistry**, v. 97, n. 3, p. 181–186, jul. 1996.

FUJISHIMA, A.; ZHANG, X.; TRYK, D. A. TiO2 photacatalysis and related surface phenomena. **Surface Science Reports**, v. 63, p. 515–582, 2008.

GARCIA-BENITEZ, C.; MELGAREJO, P.; DE CAL, A. Fruit maturity and post-harvest environmental conditions influence the pre-penetration stages of Monilinia infections in peaches. **International Journal of Food Microbiology**, v. 241, p. 117–122, 2017.

GOMEZ-GUILLEN, M. C. et al. Functional and bioactive properties of collagen and gelatin from alternative sources: A review. **Food Hydrocolloids**, v. 25, n. 8, p. 1813–1827, 2011.

GONTARD, N.; GUILBERT, S.; CUQ, J. Edible Wheat Gluten Films : Influence of the Main Process Variables on Film Properties using Response Surface Methodology. v. 57, n. 1, 1992.

GOSWAMI, M. et al. Shelf life enhancement of muscle foods with biodegradable film packaging. n. August, 2018.

GOUDARZI, V.; SHAHABI-GHAHFARROKHI, I.; BABAEI-GHAZVINI, A. Preparation of ecofriendly UV-protective food packaging material by starch/TiO2 bio-nanocomposite: Characterization. **International Journal of Biological Macromolecules**, v. 95, p. 306–313, 2017a.

GOUDARZI, V.; SHAHABI-GHAHFARROKHI, I.; BABAEI-GHAZVINI, A. Preparation of ecofriendly UV-protective food packaging material by starch/TiO2 bio-nanocomposite: Characterization. **International Journal of Biological Macromolecules**, v. 95, n. February, p. 306–313, 2017b.

GUERRA, I. C. D. et al. Coatings comprising chitosan and Mentha piperita L. or Mentha×villosa Huds essential oils to prevent common postharvest mold infections and maintain the quality of cherry tomato fruit. **International Journal of Food Microbiology**, v. 214, p. 168–178, 2015.

GULMINE, J. V. et al. Polyethylene characterization by FTIR. **Polymer Testing**, v. 21, n. 5, p. 557–563, 2002.

HAGENMAIER, R. D.; SHAW, P. E. Gas Permeability of Fruit Coating Waxes. **Journal of the American Society for Horticultural Science**, v. 117, n. 1, p. 105–109, 1992.

HAIDER, A. et al. Synthesis and photocatalytic activity for TiO 2 nanoparticles as air purification . **MATEC Web of Conferences**, v. 162, n. October, p. 05006, 2018.

HAUCHECORNE, B. et al. Photocatalytic degradation of ethylene: An FTIR in situ study under atmospheric conditions. **Applied Catalysis B: Environmental**, v. 105, n. 1-2, p. 111–116, 2011.

HAZIMAH, A H.; OOI, T. L.; SALMIAH, A. Recovery of Glycerol and Diglycerol From Glycerol Pitch Recovery of Glycerol and Diglycerol From Glycerol Pitch. **Journal of Oil Palm Research**, v. 15, n. 1, p. 1–5, 2003.

HE, Q. et al. Fabrication of gelatin-TiO2nanocomposite film and its structural, antibacterial and physical properties. **International Journal of Biological Macromolecules**, v. 84, p. 153–160, 2016.

HOANG, V. VAN. The glass transition and thermodynamics of liquid and amorphous TiO 2 nanoparticles. **Nanotechnology**, v. 19, n. 10, 2008.

HORWITZ, W.; LATIMER, G. W. **Official Methods of Analysis**. 18th. ed. Gaithersburg, USA: AOAC International, 2005. v. 1

HUSSAIN, M. et al. Photocatalytic Degradation of Ethylene Emitted by Fruits with TiO 2 Nanoparticles. p. 2536–2543, 2011.

HUSSAIN, M.; RUSSO, N.; SARACCO, G. Photocatalytic abatement of VOCs by novel optimized TiO2 nanoparticles. **Chemical Engineering Journal**, 2011.

ICSD CODE 9161 - INORGANIC CRYSTAL STRUCTURE DATABASE. **rutile TiO2 powder X-ray pattern**. Disponível em: <https://icsd-fiz-karlsruhe-de.proxy01.dotlib.com.br/display/list.xhtml>. Acesso em: 4 mar. 2019.

ICSD CODE 9852- INORGANIC CRYSTAL STRUCTURE DATABASE. **TiO2 X-ray Powder Pattern**. Disponível em: <https://icsd-fiz-karlsruhe-de.proxy01.dotlib.com.br/display/list.xhtml>. Acesso em: 4 mar. 2019.

ISO 27448:2009. **Fine ceramics (advanced ceramics, advanced technical ceramics) -- Test method for self-cleaning performance of semiconducting photocatalytic materials -- Measurement of water contact angle**. 1. ed. [s.l: s.n.].

JACOMINO, A. P. et al. Amadurecimento e senescência de mamão com 1-metilciclopropeno. **Scientia Agricola**, v. 59, n. 2, p. 303–308, 2002.

JACQUOT, M. et al. Antioxidant capacity and light-aging study of HPMC films functionalized with natural plant extract. **Carbohydrate Polymers**, v. 89, n. 4, p. 1150–1158, 2012.

JARDIM DE MINAS, L. **SEMENTES DE MAMÃO GOLDEN PAPAYA - SEMENTES DE MAMÃO**. Disponível em: <http://jardimdeminas.com/sementes-de-mamao/sementes-de-mam-o-golden-papaya.html#>. Acesso em: 11 abr. 2019.

JIANG, Y., LI, Y., CHAI, Z., & LENG, X. Study of the Physical Properties of Whey Protein Isolate and Gelatin Composite Films. **Journal of Agricultural and Food Chemistry,** v. 58, n. 8, p. 5100–5108, 2010.

JOHLIN, J. M. Isoelectric Point of Gelatin. **Journal of biological chemistry**, v. 86, p. 231–234, 1930.

JOSÉ, H. J. et al. Photocatalytic reduction of nitrate ions in water over metal-modified TiO2. **Journal of Photochemistry and Photobiology A: Chemistry**, v. 246, p. 36–44, 2012.

KADER, A. A. **A SUMMARY OF CA REQUIREMENTS AND RECOMMENDATIONS FOR FRUITS OTHER THAN APPLES AND PEARS**. 7th. ed. Davis: [s.n.]. v. 17

KAEWKLIN, P. et al. Active packaging from chitosan-titanium dioxide nanocomposite film for prolonging storage life of tomato fruit. **International Journal of Biological Macromolecules**, v. 112, p. 523–529, 2018.

KAMRANNEJAD, M. M. et al. Photocatalytic Degradation of Polypropylene / TiO2 Nano-composites. v. 17, n. 4, p. 1039–1046, 2014.

KARTHIKEYAN, K. T.; NITHYA, A.; JOTHIVENKATACHALAM, K. Photocatalytic and antimicrobial activities of chitosan-TiO2 nanocomposite. **International Journal of Biological Macromolecules**, v. 104, p. 1762–1773, 2017.

KELLER, N. et al. Ethylene Removal and Fresh Product Storage: A Challenge at the Frontiers of Chemistry. Toward an Approach by Photocatalytic Oxidation. **Chemical Reviews**, v. 113, n. 7, p. 5029–5070, 2013.

KHALID, N. R. et al. **Carbonaceous-TiO2 nanomaterials for photocatalytic degradation of pollutants: A reviewCeramics International**Elsevier Ltd, , 1 dez. 2017.

KONICA MINOLTA SENSING AMERICAS. Espaço de cor L * C * h Medindo várias cores com um colorímetro . In: **Colorimetria: como medir diferenças de cor**. [s.l: s.n.]. p. 20–24.

LEE, D. J. et al. Photo-catalytic destruction of ethylene using microwave discharge electrodeless lamp. **Korean Journal of Chemical Engineering**, v. 32, n. 6, p. 1188–1193, 2015.

LELIEVRÈ, J. M. et al. Ethylene and Fruit Ripening. **Physiologia Plantarum**, v. 101, p. 727–739, 1997.

LEPRINCE-WANG, Y.; YU-ZHANG, K. Study of the growth morphology of TiO2thin films by AFM and TEM. **Surface and Coatings Technology**, v. 140, n. 2, p. 155–160, 2001.

LI, Q. et al. Preparation of sol – gel modi fi ed electrospun TiO 2 nano fi bers for improved photocatalytic decomposition of ethylene. v. 76, p. 169–172, 2012.

LI, X. et al. Isolation and characterization of ethylene response factor family genes during development, ethylene regulation and stress treatments in papaya fruit. **Plant Physiology and Biochemistry**, v. 70, p. 81–92, 2013.

LI, X. et al. Postharvest application of wax controls pineapple fruit ripening and improves fruit quality. **Postharvest Biology and Technology**, v. 136, p. 99–110, 1 fev. 2018.

LI, Y. et al. Fabrication and characterization of TiO2/whey protein isolate nanocomposite film. **Food Hydrocolloids**, v. 25, n. 5, p. 1098–1104, 2011.

LIAN, Z.; ZHANG, Y.; ZHAO, Y. Nano-TiO 2 particles and high hydrostatic pressure treatment for improving functionality of polyvinyl alcohol and chitosan composite fi lms and nano-TiO 2 migration from fi lm matrix in food simulants. **Innovative Food Science and Emerging Technologies**, v. 33, p. 145–153, 2016.

LIN, Y. T. et al. Effect of oxygen, moisture, and temperature on the photo oxidation of ethylene on N-doped TiO2 catalyst. **Separation and Purification Technology**, v. 134, p. 117–125, 2014.

LIN, Y. T.; WENG, C. H.; CHEN, F. Y. Key operating parameters affecting photocatalytic activity of visible-light-induced C-doped TiO2 catalyst for ethylene oxidation. **Chemical Engineering Journal**, v. 248, p. 175–183, 2014.

LIU, C. et al. Effects of nano-tio<inf>2</inf> on the performance of high-amylose starch based antibacterial films. **Journal of Applied Polymer Science**, v. 132, n. 32, p. 2–8, 2015.

LODDO, V.; RODA, G. C.; PARRINO, F. Kinetic aspects of heterogeneous catalytic versus photocatalytic reactions. In: **Heterogeneous Photocatalysis: Relationships with Heterogeneous Catalysis and Perspectives**. [s.l.] Elsevier B.V., 2019. p. 215–233.

LÓPEZ, O. V.; GARCÍA, M. A.; ZARITZKY, N. E. Film forming capacity of chemically modified corn starches. **Carbohydrate Polymers**, v. 73, n. 4, p. 573–581, 2008.

LOURENÇO, R. E. R. S. et al. Photodegradation of ethylene by use of TiO2sol-gel on polypropylene and on glass for application in the postharvest of papaya fruit. **Environmental Science and Pollution Research**, v. 24, n. 7, p. 6047–6054, 2017a.

LOURENÇO, R. E. R. S. et al. Photodegradation of ethylene by use of TiO2 sol-gel on polypropylene and on glass for application in the postharvest of papaya fruit. **Environmental Science and Pollution Research**, v. 24, n. 7, p. 6047–6054, mar. 2017b.

MAHMOOD, A.-S. et al. Preparation and characterization of functional sodium caseinate/guar gum/TiO2/cumin essetial oil composite film. **International Journal of Biological Macromolecules**, v. 145, p. 835–844, 2020.

MANDA, B. M. K.; BLOK, K.; PATEL, M. K. Science of the Total Environment Innovations in papermaking : An LCA of printing and writing paper from conventional and high yield pulp. v. 439, p. 307–320, 2012.

MANEERAT, C. et al. PHOTOCATALYTIC REACTION OF TIO2 TO DECOMPOSE ETHYLENE IN FRUIT AND VEGETABLE STORAGE. **Transactions of the ASAE**, v. 46, n. 3, p. 725, 2003.

MANEERAT, C.; HAYATA, Y. Antifungal activity of TiO2 photocatalysis against Penicillium expansum in vitro and in fruit tests. **International Journal of Food Microbiology**, v. 107, n. 2, p. 99–103, mar. 2006.

MANEERAT, C.; HAYATA, Y. Gas-Phase Photocatalytic Oxidation of Ethylene with TiO2-Coated Packaging Film for Horticultural Products. **Transactions of the ASABE**, v. 51, n. 1, p. 163–168, 2008.

MANENOI, A. et al. Utility of 1-methylcyclopropene as a papaya postharvest treatment. **Postharvest Biology and Technology**, v. 44, n. 1, p. 55–62, 2007.

MANOLE, A. et al. Combining degradation and contact angle data in assessing the photocatalytic TiO2:N surface. **Surface and Interface Analysis**, v. 42, n. 6-7, p. 947–954, 2010.

MARINESCU, C. et al. DSC investigation of nanocrystalline TiO2 powder. **Journal of Thermal Analysis and Calorimetry**, v. 103, n. 1, p. 49–57, 2011.

MARTINS, D. R.; DE RESENDE, E. D. Quality of Golden papaya stored under controlled atmosphere conditions. **Food Science and Technology International**, v. 19, n. 5, p. 473–481, 16 out. 2013.

MARTINS, D. S.; COSTA, A F. S. **A cultura do mamoeiro: tecnologias de produção**. [s.l: s.n.].

MATOS FONSECA, J. D. et al. Chitosan microparticles embedded with multi-responsive poly(N-vinylcaprolactam-co-itaconic acid-co-ethylene-glycol dimethacrylate)-based hydrogel nanoparticles as a new carrier for delivery of hydrophobic drugs. **Colloids and Surfaces B: Biointerfaces**, v. 175, p. 73–83, 1 mar. 2019.

MATSUI, K. . et al. Cassava bagasse-Kraft paper composites: analysis of influence of impregnation with starch acetate on tensile strength and water absorption properties. **Carbohydrate Polymers**, v. 55, n. 3, p. 237–243, 1 fev. 2004.

MIAO, L. et al. Preparation and characterization of polycrystalline anatase and rutile TiO2 thin films by rf magnetron sputtering. **Applied Surface Science**, v. 212-213, n. SPEC., p. 255–263, 2003.

MIDTDAL, K.; JELLE, B. P. Self-cleaning glazing products: A state-of-the-art review and future research pathways. **Solar Energy Materials and Solar Cells**, v. 109, n. 7465, p. 126–141, 2013.

MIHALY COZMUTA, A. et al. Preparation and characterization of improved gelatin films incorporating hemp and sage oils. **Food Hydrocolloids**, v. 49, p. 144–155, 2015.

MILLS, A.; CROW, M. In situ, continuous monitoring of the photoinduced superhydrophilic effect: Influence of UV-type and ambient atmospheric and droplet composition. **Journal of Physical Chemistry C**, v. 111, n. 16, p. 6009–6016, 2007.

MILLS, A.; HILL, C.; ROBERTSON, P. K. J. Overview of the current ISO tests for photocatalytic materials. **Journal of Photochemistry and Photobiology A: Chemistry**, v. 237, p. 7–23, 2012.

MILLS, A.; LE HUNTE, S. An overview of semiconductor photocatalysis. **Journal of Photochemistry and Photobiology A: Chemistry**, v. 108, n. 1, p. 1–35, 31 jul. 1997.

MOHAN, P. R. K. et al. Vibrational Spectroscopy Water soluble complexes of curcumin with cyclodextrins : Characterization by FT-Raman spectroscopy. **Vibrational Spectroscopy**, v. 62, p. 77–84, 2012.

MUKHERJEE, K. et al. TiO2 Nanoparticles Co-doped with Nitrogen and Fluorine as Visible-Light-Activated Antifungal Agents. **ACS Applied Nano Materials**, v. 3, n. 2, p. 2016–2025, 2020.

MULLAH, M. F. et al. Thermal Properties of Gelatin and Chitosan. In: **Glass Transition and Phase Transitions in Food and Biological Materials**. Chichester, UK: John Wiley & Sons, Ltd, 2017. p. 281–304.

NAN, M. et al. Recent developments in photocatalytic water treatment technology : A review. **Water Research**, v. 44, n. 10, p. 2997–3027, 2010.

NASCIMENTO, M. et al. Food Hydrocolloids Physical and morphological properties of hydroxypropyl methylcellulose fi lms with curcumin polymorphs. **Food Hydrocolloids**, v. 97, n. July, p. 105217, 2019.

NAWI, M. A. et al. Immobilized bilayer TiO 2 / chitosan system for the removal of phenol under irradiation by a 45 watt compact fl uorescent lamp. **DES**, v. 280, n. 1-3, p. 288–296, 2011.

NAZEEB, M.; BROUGHTON, W. J. STORAGE CONDITIONS AND RIPENING OF PAPAYA ' BENTONG ' AND ' TAIPING ' One of the main problems associated with the fruit industry in Malaysia is to delay fruit ripening so that release to the market can be controlled . With fruit for export there are prob. **Scientia Horticulturae**, v. 9, p. 265–277, 1978.

NELSON, D. L.; COX, M. M. **Princípios de Bioquímica de Lehninger**. 6ª. ed. Porto Alegre, RS: [s.n.].

NEPA - UNICAMP. **Tabela brasileira de composição de alimentos**. 4ª. ed. Campinas-SP: [s.n.].

NETO, E. et al. **Tecnologia e processamento de frutas e hortaliças**. Natal: IFRN, 2015.

NIELSEN, M. G. et al. Removal of low concentration contaminant species using photocatalysis: Elimination of ethene to sub-ppm levels with and without water vapor present. **Chemical Engineering Journal**, v. 262, p. 648–657, 2015.

NOORBAKHSH-SOLTANI, S. M.; ZERAFAT, M. M.; SABBAGHI, S. A comparative study of gelatin and starch-based nano-composite films modified by nano-cellulose and chitosan for food packaging applications. **Carbohydrate Polymers**, v. 189, n. February, p. 48–55, 2018.

NUR HAZIRAHA, M. A. S. P.; ISAB, M. I. N.; SARBONA, N. M. Effect of xanthan gum on the physical and mechanical properties of gelatin-carboxymethyl cellulose film blends. **Food Packaging and Shelf Life**, v. 9, p. 55–63, 2016.

OBEE, T. N.; HAY, S. O. Effects of moisture and temperature on the photooxidation of ethylene on titania. **Environmental Science and Technology**, v. 31, n. 7, p. 2034–2038, 1997.

OHNO, T. et al. Morphology of a TiO2 photocatalyst (Degussa, P-25) consisting of anatase and rutile crystalline phases. **Journal of Catalysis**, v. 203, n. 1, p. 82–86, 2001.

OHSAKA, T. Ohsaka1980.Pdf. **Journal of the Physical Society of Japan**, v. 48, n. 5, p. 1661–1668, 1980.

OLEYAEI, S. A. et al. Modification of physicochemical and thermal properties of starch films by incorporation of TiO2nanoparticles. **International Journal of Biological Macromolecules**, v. 89, p. 256–264, 2016.

OLIVEIRA, M. G. et al. Involvement of AOX and UCP pathways in the post-harvest ripening of papaya fruits. **Journal of Plant Physiology**, v. 189, p. 42–50, 2015.

OLIVEIRA-JR, L. F. G. et al. Efeito de absorvedor de etileno no armazenamento de mamão (Carica papaya L .) em diferentes temperaturas. **Ceres**, v. 53, n. 308, p. 487–494, 2006.

OLLIS, D. Connecting contact angle evolution to photocatalytic kinetics of self cleaning surfaces. **Catalysis Today**, v. 310, n. October 2017, p. 49–58, 2018.

OTHMAN, S. H. et al. Antimicrobial Activity of TiO 2 Nanoparticle-Coated Film for Potential Food Packaging Applications. v. 2014, 2014.

PACIA, M.; WARSZYŃSKI, P.; MACYK, W. UV and visible light active aqueous titanium dioxide colloids stabilized by surfactants. **Dalton Transactions**, v. 43, n. 33, p. 12480–12485, 2014.

PAL, D. K.; SELVARAJ, Y. Biochemistry of papaya (Carica papaya L.) fruit ripening: changes in RNA, DNA, protein and enzymes of mitochondrial, carbohydrate, respiratory and phosphate metabolism. **Journal of Horticultural Science**, v. 62, n. 1, p. 117–124, 1987.

PARK, D. R. et al. Photocatalytic Oxidation of Ethylene to CO2 and H2O on Ultrafine Powdered TiO2 Photocatalysts: Effect of the Presence of O2 and H2O and the Addition of Pt. **Korean Journal of Chemical Engineering**, v. 18, n. 6, p. 930–934, 2001.

PATHAK, N. et al. Photocatalytic and Photochemical Oxidation of Ethylene: Potential for Storage of Fresh Produce—a Review. **Food and Bioprocess Technology**, v. 10, n. 6, p. 982–1001, 2017.

PATHAK, N. et al. Efficacy of photocatalysis and photolysis systems for the removal of ethylene under different storage conditions. **Postharvest Biology and Technology**, v. 147, p. 68–77, jan. 2019.

PAULINO-LIMA, I. G. et al. Extremely high UV-C radiation resistant microorganisms from desert environments with different manganese concentrations. **Journal of Photochemistry and Photobiology B: Biology**, v. 163, p. 327–336, 2016.

PAULL, R. E. et al. Postharvest handling and losses during marketing of papaya (Carica papaya L.). **Postharvest Biology and Technology**, v. 11, n. 3, p. 165–179, 1997.

PELAEZ, M. et al. A review on the visible light active titanium dioxide photocatalysts for environmental applications. **Applied Catalysis B: Environmental**, v. 125, p. 331–349, 2012.

PROQUIN, H. et al. Titanium dioxide food additive (E171) induces ROS formation and genotoxicity: contribution of micro and nano-sized fractions. **Mutagenesis**, v. 32, n. 1, p. 139–149, 2017.

RAMESH, T. et al. Application of ultraviolet light assisted titanium dioxide photocatalysis for food safety : A review. **Innovative Food Science and Emerging Technologies**, v. 38, p. 105–115, 2016a.

RAMESH, T. et al. Application of ultraviolet light assisted titanium dioxide photocatalysis for food safety : A review. **Innovative Food Science and Emerging Technologies**, v. 38, p. 105–115, 2016b.

RATHOUSKÝ, J. et al. A study into the self-cleaning surface properties - The photocatalytic decomposition of oleic acid. **Catalysis Today**, v. 161, n. 1, p. 202–208, 17 mar. 2011.

REDDY, E. P.; DAVYDOV, L.; SMIRNIOTIS, P. TiO2-loaded zeolites and mesoporus materials in the sonophotocatalytic decomposition of acqueous organic pollutants: the role of the support. **Applied Catalysis B: Environmental**, v. 42, p. 1–11, 2003.

REMON, J. P. et al. Reference database of Raman spectra of pharmaceutical excipients. **Journal of Raman Spectroscopy**, v. 40, n. 3, p. 297–307, 2008.

REN, J. et al. TiO2-containing PVA/xylan composite films with enhanced mechanical properties, high hydrophobicity and UV shielding performance. **Cellulose**, v. 22, n. 1, p. 593–602, 2015.

RHODES, M. J. . The climacteric and ripening of fruits. In: HULME, A. . (Ed.). . **The Biochemistry of Fruits and their Products**. 1ª. ed. London and New York: Academic Press, 1970. p. 521–533.

RIVERO, S.; GARCÍA, M. A.; PINOTTI, A. Correlations between structural, barrier, thermal and mechanical properties of plasticized gelatin films. **Innovative Food Science and Emerging Technologies**, v. 11, n. 2, p. 369–375, 2010.

ROPERS, M.-H. et al. titanium Dioxide as Food Additive. In: JANUS, M. (Ed.). . **Application of Titanium Dioxide**. 1. ed. [s.l.] IntechOpen, 2017. p. 3–21.

ROTTA, J.; MINATTI, E.; BARRETO, P. L. M. Determination of structural and mechanical properties, diffractometry, and thermal analysis of chitosan and hydroxypropylmethylcellulose (HPMC) films plasticized with sorbitol. **Ciência e Tecnologia de Alimentos**, v. 31, n. 2, p. 450–455, 2011.

RYALL, A. L. (ALBERT L.; LIPTON, W. J.; PENTZER, W. T. (WILBUR T. **Handling, transportation, and storage of fruits and vegetables,**. [s.l.] AVI Pub. Co, 1979.

SACHTLEBEN CHEMIE GMBH. Technical Information Hombikat UV 100. p. 47184–47184, [s.d.].

SADEGHI, F. et al. Antisolvent precipitation technique: A very promising approach to crystallize curcumin in presence of polyvinyl pyrrolidon for solubility and dissolution enhancement. **Colloids and Surfaces B: Biointerfaces**, v. 147, p. 258–264, 2016.

SAHOO, N. et al. Recent advancement of gelatin nanoparticles in drug and vaccine delivery. **International Journal of Biological Macromolecules**, v. 81, p. 317–331, 1 nov. 2015.

SAKAI, N. et al. Quantitative evaluation of the photoinduced hydrophilic conversion properties of TiO2 thin film surfaces by the reciprocal of contact angle. **Journal of Physical Chemistry B**, v. 107, n. 4, p. 1028–1035, 2003.

SAKATA, Y.; SHIRAISHI, S.; OTSUKA, M. A novel white film for pharmaceutical coating formed by interaction of calcium lactate pentahydrate with hydroxypropyl methylcellulose. **International Journal of Pharmaceutics**, v. 317, n. 2, p. 120–126, 2006.

SANCHIS, R. M. et al. Enhancement of wettability in low density polyethylene films using low pressure glow discharge N2 plasma. **Journal of Polymer Science Part B: Polymer Physics**, v. 45, n. 17, p. 2390–2399, 1 set. 2007.

SANGAPPA et al. Physical and thermal properties of 8 MeV electron beam irradiated HPMC polymer films. **Nuclear Instruments and Methods in Physics Research, Section B: Beam Interactions with Materials and Atoms**, v. 266, n. 18, p. 3975–3980, 2008.

SANTOS, S. F. DOS et al. Post-harvest losses of fruits and vegetables in supply centers in Salvador, Brazil: Analysis of determinants, volumes and reduction strategies. **Waste Management**, v. 101, p. 161–170, 2020.

SELVARAJ, Y. et al. Changes in the Chemical Composition of Four Cultivars of Papaya (Carica Papaya L.) During Growth and Development. **Journal of Horticultural Science**, v. 57, n. 1, p. 135–143, 1982.

SHAYEGAN, Z.; LEE, C. S.; HAGHIGHAT, F. TiO2 photocatalyst for removal of volatile organic compounds in gas phase – A review. **Chemical Engineering Journal**, v. 334, n. August 2017, p. 2408–2439, 2018.

SHIT, S. C.; SHAH, P. M. Edible Polymers: Challenges and Opportunities. **Journal of Polymers**, v. 2014, p. 1–13, 2014.

SINGH, U. et al. Journal of Molecular Catalysis A : Chemical Photo-degradation of curcumin in the presence of TiO 2 nanoparticles : Fundamentals and application. v. 318, p. 106–111, 2010.

SIRIPATRAWAN, U.; KAEWKLIN, P. Fabrication and characterization of chitosan-titanium dioxide nanocomposite film as ethylene scavenging and antimicrobial active food packaging. **Food Hydrocolloids**, v. 84, p. 125–134, 2018.

SOUZA, A. F. et al. Fisiologia do amadurecimento de mamões de variedades comercializadas no Brasil. **Revista Brasileira de Fruticultura**, v. 36, n. 2, p. 318–328, 2014.

SOUZA, M. S. DE et al. Resposta da aplicação do 1-MCP em frutos de mamoeiro “Golden” em diferentes estádios de maturação. **Revista Brasileira de Fruticultura**, v. 31, n. 3, p. 693–700, 2009.

STEFANIAK, A.; HOOVER, M.; NANOTECHNOLOGY, N. **Occupational Exposure to Titanium Dioxide**. Washington: National Institute for Occupational Safety and Health , 2011.

TANAKA, K. et al. Improved photocatalytic activity of zeolite- and silica-incorporated TiO 2 film. **Journal of Hazardous Materials**, v. 137, n. 2, p. 947–951, 2006.

TEYMOURPOUR, S.; ABDORREZA, M. N.; NAHIDI, F. Functional, thermal, and antimicrobial properties of soluble soybean polysaccharide biocomposites reinforced by nano TiO<inf>2</inf>. **Carbohydrate Polymers**, v. 134, p. 726–731, 2015.

TORRIERI, E.; CAVELLA, S.; MASI, P. Modelling the respiration rate of fresh-cut Annurca apples to develop modified atmosphere packaging. **International Journal of Food Science and Technology**, v. 44, n. 5, p. 890–899, 2009.

TOSATI, J. V. et al. Respiration Rate of Cherry Tomatoes and Gas Permeability of Hydroxypropylmethyl Cellulose-Based Coating. **International Journal of Emerging Technology and Advanced Engineering**, v. 5, n. 3, p. 281–287, 2015.

TRINDADE, A. V. et al. **Mamão: Produção (Aspectos técnicos)**. 1ª. ed. [s.l.] Embrapa, 2000.

URBANO, I.; PEDRO, A. Classificação de frutos por “ climatério ” é conceito em extinção ? **Visão Agrícola**, v. 7, p. 8–10, 2007.

VALENCIA, G. A. et al. Physical and morphological properties of nanocomposite films based on gelatin and Laponite. **Applied Clay Science**, v. 124-125, p. 260–266, 2016.

VAN DER MOLEN, R. G. et al. Efficacy of micronized titanium dioxide-containing compounds in protection against UVB-induced immunosuppression in humans in vivo. **Journal of Photochemistry and Photobiology B: Biology**, v. 44, n. 2, p. 143–150, 1998.

VIEIRA, A. C. F. et al. Active coatings based on hydroxypropyl methylcellulose and silver nanoparticles to extend the papaya (Carica papaya L.) shelf life. **International Journal of Biological Macromolecules**, v. 164, p. 489–498, 2020.

WANG, H. et al. Construction of Bi2WO6–TiO2/starch nanocomposite films for visible-light catalytic degradation of ethylene. **Food Hydrocolloids**, v. 88, n. September 2018, p. 92–100, 2019.

WANG, S. et al. A high-sensitivity HPLC-ELSD method for HPMC-AS quantification and its application in elucidating the release mechanism of HPMC-AS based amorphous solid dispersions. **European Journal of Pharmaceutical Sciences**, v. 122, p. 303–310, 15 set. 2018.

WATKINS, C. B. The use of 1-methylcyclopropene (1-MCP) on fruits and vegetables. **Biotechnology Advances**, v. 24, n. 4, p. 389–409, 2006.

WEIR, A. et al. Titanium dioxide nanoparticles in food and personal care products. **Environmental Science and Technology**, v. 46, n. 4, p. 2242–2250, 2012.

WENG, W.; ZHENG, H. Effect of transglutaminase on properties of tilapia scale gelatin films incorporated with soy protein isolate. **Food Chemistry**, v. 169, p. 255–260, 2015.

WESTRICH, T. A. et al. High-temperature photocatalytic ethylene oxidation over TiO2. **Journal of Physical Chemistry C**, v. 115, n. 33, p. 16537–16543, 2011.

WILSON, M. D. et al. **Innovative processes and technologies for modified atmosphere packaging of fresh and fresh-cut fruits and vegetablesCritical Reviews in Food Science and Nutrition**Taylor and Francis Inc., , 4 fev. 2019.

XIE, J.; HUNG, Y. C. UV-A activated TiO2 embedded biodegradable polymer film for antimicrobial food packaging application. **Lwt**, v. 96, n. May, p. 307–314, 2018.

XING, Y. et al. Effect of chitosan/Nano-TiO2 composite coatings on the postharvest quality and physicochemical characteristics of mango fruits. **Scientia Horticulturae**, v. 263, n. December 2019, p. 109135, 2020.

YADAV, D.; KUMAR, N. Nanonization of curcumin by antisolvent precipitation: Process development, characterization, freeze drying and stability performance. **International Journal of Pharmaceutics**, v. 477, n. 1-2, p. 564–577, 30 dez. 2014.

YAMAZAKI, S.; TANAKA, S.; TSUKAMOTO, H. Kinetic studies of oxidation of ethylene over a TiO2photocatalyst. **Journal of Photochemistry and Photobiology A: Chemistry**, v. 121, n. 1, p. 55–61, 1999.

YANES, D. et al. Applied Catalysis A : General Photocatalytic inhibition of bacteria by TiO 2 nanotubes-doped polyethylene composites. v. 489, p. 255–261, 2015.

YASUDA, T.; OKUNO, T.; YASUDA, H. Contact Angle of Water on Polymer Surfaces. **Langmuir**, v. 10, n. 7, p. 2435–2439, 1994.

YOUSSEF, A. M.; EL-SAYED, S. M. Bionanocomposites materials for food packaging applications : Concepts and future outlook. **Carbohydrate Polymers**, v. 193, n. February, p. 19–27, 2018.

YUN, Y. H. et al. Physical properties and photocatalytic activity of chitosan-based nanocomposites added titanium oxide nanoparticles. **Macromolecular Research**, v. 24, n. 1, p. 51–59, 2016.

ZALESKA, A. Doped-TiO_2 : A Review. **Recent Patents on Engineering 2008, 2, 157-164**, n. 1, p. 157–164, 2008.

ZANON BARÃO, M. **Embalagens para produtos alimentíciosDossiê Técnico**. [s.l.] Serviço Brasileiro de Respostas Técnicas, 2011. Disponível em: <http://www.respostatecnica.org.br/dossie-tecnico/downloadsDT/NTY0MQ==>. Acesso em: 29 abr. 2019.

ZENG, J. et al. TiO 2 Immobilized in Cellulose Matrix for Photocatalytic Degradation of Phenol under Weak UV Light Irradiation. p. 7806–7811, 2010.

ZHANG, L. et al. Photo-induced hydrophilicity and self-cleaning: Models and reality. **Energy and Environmental Science**, v. 5, n. 6, p. 7491–7507, 2012.

ZHANG, W.; XIAO, H.; QIAN, L. Enhanced water vapour barrier and grease resistance of paper bilayer-coated with chitosan and beeswax. **Carbohydrate Polymers**, v. 101, n. 1, p. 401–406, 2014.

ZHANG, X. et al. Preparation of chitosan-TiO 2 composite film with efficient antimicrobial activities under visible light for food packaging applications. **Carbohydrate Polymers**, v. 169, p. 101–107, 2017.

ZHANG, X. et al. Development of multifunctional food packaging films based on chitosan, TiO2 nanoparticles and anthocyanin-rich black plum peel extract. **Food Hydrocolloids**, v. 94, p. 80–92, 2019.

ZHOU, J. J.; WANG, S. Y.; GUNASEKARAN, S. Preparation and characterization of whey protein film incorporated with TiO2 nanoparticles. **Journal of Food Science**, v. 74, n. 7, 2009.

ZHOU, Y. et al. Ethylene Biosynthesis, Signaling, and Crosstalk with Other Hormones in Rice. **Small Methods**, v. 4, n. 8, p. 1–20, 2020.

ZHU, Z. et al. Electrospun Nanofibers Containing TiO2 for the Photocatalytic Degradation of Ethylene and Delaying Postharvest Ripening of Bananas. **Food and Bioprocess Technology**, v. 12, n. 2, p. 281–287, 2019a.

ZHU, Z. et al. Photocatalytic effects on the quality of pork packed in the package combined with TiO {\textless}sub{\textgreater}2{\textless}/sub{\textgreater} coated nonwoven fabrics. **Journal of Food Process Engineering**, v. 42, n. 3, p. e12993, 2019b.

ZHU, Z.; CAI, H.; SUN, D. Titanium dioxide (TiO 2) photocatalysis technology for nonthermal inactivation of microorganisms in foods. **Trends in Food Science & Technology**, v. 75, n. November 2017, p. 23–35, 2018a.

ZHU, Z.; CAI, H.; SUN, D. Trends in Food Science {&} Technology Titanium dioxide (TiO 2) photocatalysis technology for nonthermal inactivation of microorganisms in foods. **Trends in Food Science {&} Technology**, v. 75, n. November 2017, p. 23–35, 2018b.

APPENDIX A – Ethylene degradation mechanism equations proposed by Hauchecorne et al. (2011)

Equations proposed by Hauchecorne et al. (2011) for the ethylene photocatalytic degradation:

Generation of electron/hole pairs and reactive oxidative species (ROS):

$TiO_2 + hv \rightarrow e^- + h^+$ (I)

$H_2O + h^+ \rightarrow OH^\bullet + H^+$ (II)

$OH^- + h^+ \rightarrow OH^\bullet$ (III)

$O_2 + e^- \rightarrow O_2^{\bullet -}$ (IV)

$O_2 + H^+ \rightarrow HO_2^\bullet$ (V)

$2 \cdot HO_2^\bullet \rightarrow O_2 + H_2O_2$ (VI)

$H_2O_2 + O_2^- \rightarrow OH^\bullet + OH^- + O_2$ (VII)

Chemical attack of ethylene molecule by hydroxyl radical ($OH^\bullet$):

$TiO_2 + hv \rightarrow e^- + h^+$ (VIII)

$H_2O + h^+ \rightarrow OH^\bullet + H^+$ (IX)

$C_2H_4 + Ti_5O_4H_4 + 2OH^\bullet \rightarrow 2CH_2 + Ti_5O_4H_2 + 2H_2O$ (X)

$2CH_2 + Ti_5O_4H_2 + 2OH^\bullet \rightarrow 2CH_2 + Ti_5O_4 + 2H_2O$ (XI)

$2CH_2 + Ti_5O_4 + 2OH^\bullet \rightarrow 2CH_2O + Ti_5O_4H_2$ (XII)

$2CH_2O + Ti5O_4H_2 + 2OH^\bullet \rightarrow 2HCO + Ti_5O_4H_2 + 2H_2O$ (XIII)

$2HCO + Ti_5O_4H_2 + 4OH^\bullet \rightarrow 2HCO_2 + Ti_5O_4H_2 + 2H_2O$ (XIV)

$2HCO_2 + Ti_5O_4H_2 \rightarrow 2CO_2 + Ti_5O_4H_4$ (XV)

$C_2H_4 + 12OH^\bullet \rightarrow 2CO_2 + 8H_2O$ (XVI)

***Eq**. (X) and (XI): intermediate formation.

Reference:

HAUCHECORNE, B. et al. Photocatalytic degradation of ethylene: An FTIR in situ study under atmospheric conditions. **Applied Catalysis B: Environmental**, v. 105, n. 1-2, p. 111–116, 2011.

APPENDIX B – Experimental data fitting of Siripatrawan and Kaewklin (2018) to the Langmuir-Hinshelwood model

Figure B.1- Ethylene photocatalytic degradation by chitosan-based films containing 0, 0.25, 0.5, 1 and 2 wt % TiO_2 (CS, CT0.25, CT0.5, CT1, CT2).

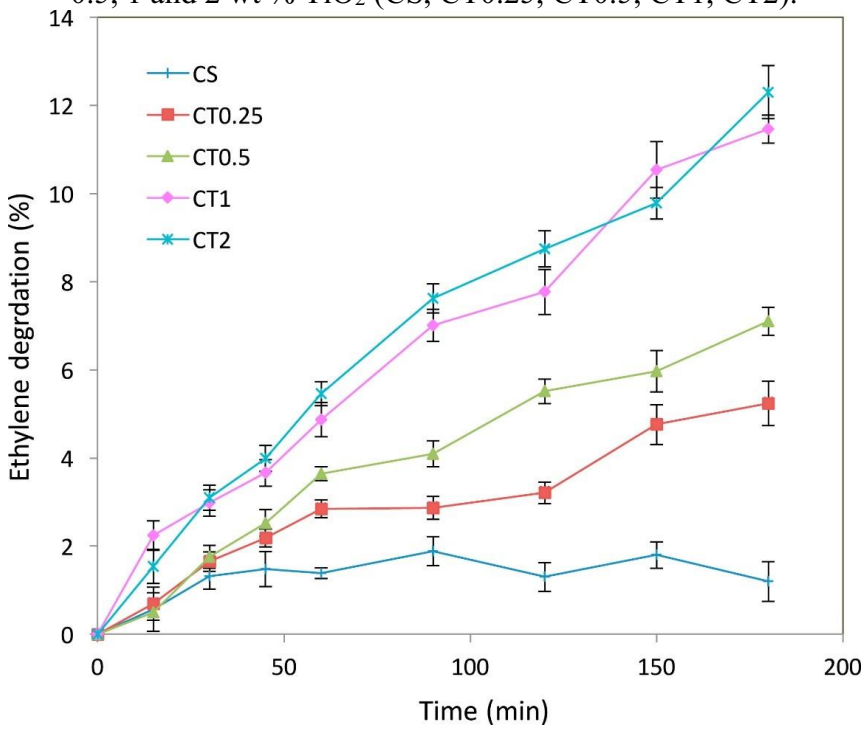

Source: Siripatrawan and Kaewklin (2018), with permission.

Ethylene conversion data were measured by a geometric scale (**Table A.1**) and used to estimate the apparent rate constant (k_{app}) (**Table A.2**) by fitting to the Langmuir-Hinshelwood model (**equation 14**). Data provide by authors as the initial ethylene concentration (5 ppmv), photocatalytic surface area (36 x 10^{-1} m^2) and the cast nanocomposite dispersion volume for its formation (190 mL) were used to calculate the maximum normalized concentration of degraded ethylene ($C_{C_2H_4,\max(N)}$).

Table B.1- Experimental data of ethylene conversion ($X_{C_2H_4}$) versus time for the chitosan-based films containing 1 wt% TiO_2 prepared by Siripatrawan and Kaewklin (2018).

Time (min)	$X_{C_2H_4}{}^{*}$
0	0
15	2.34
30	2.99
45	3.73
60	4.88
90	7.03
120	7.8
150	10.58
180	11.50

Data were obtained from scale measuring.

Table B.2- Kinetics parameters for photocatalysis performed by chitosan-based films containing 1 wt% TiO_2 prepared by Siripatrawan and Kaewklin (2018).

k_{app} [min^{-1}]	A	B	R^2	$X_{C_2H_4,max}$ [%]
0.186 ± 0.021[a]	-0.253 ± 0.116	0.258 ± 0.118	0.983	11.500 ± 0.400

$^{*}k_{app}$: apparent rate constant of reactions, A and B: coefficients of the model equation, R^2: coefficient of determination, $X_{C_2H_4,max}$: maximum conversion of ethylene [%].

Reference:

SIRIPATRAWAN, U.; KAEWKLIN, P. Fabrication and characterization of chitosan-titanium dioxide nanocomposite film as ethylene scavenging and antimicrobial active food packaging. **Food Hydrocolloids**, v. 84, p. 125–134, 2018.

Source: Fonseca et al. (2021), with permission.

APPENDIX C – Additional characterizations of EPE foam nets by optical and scanning electronic microscopy

Figure C.1- Images of EPE foam nets obtained by optical and scanning electronic microscopy.

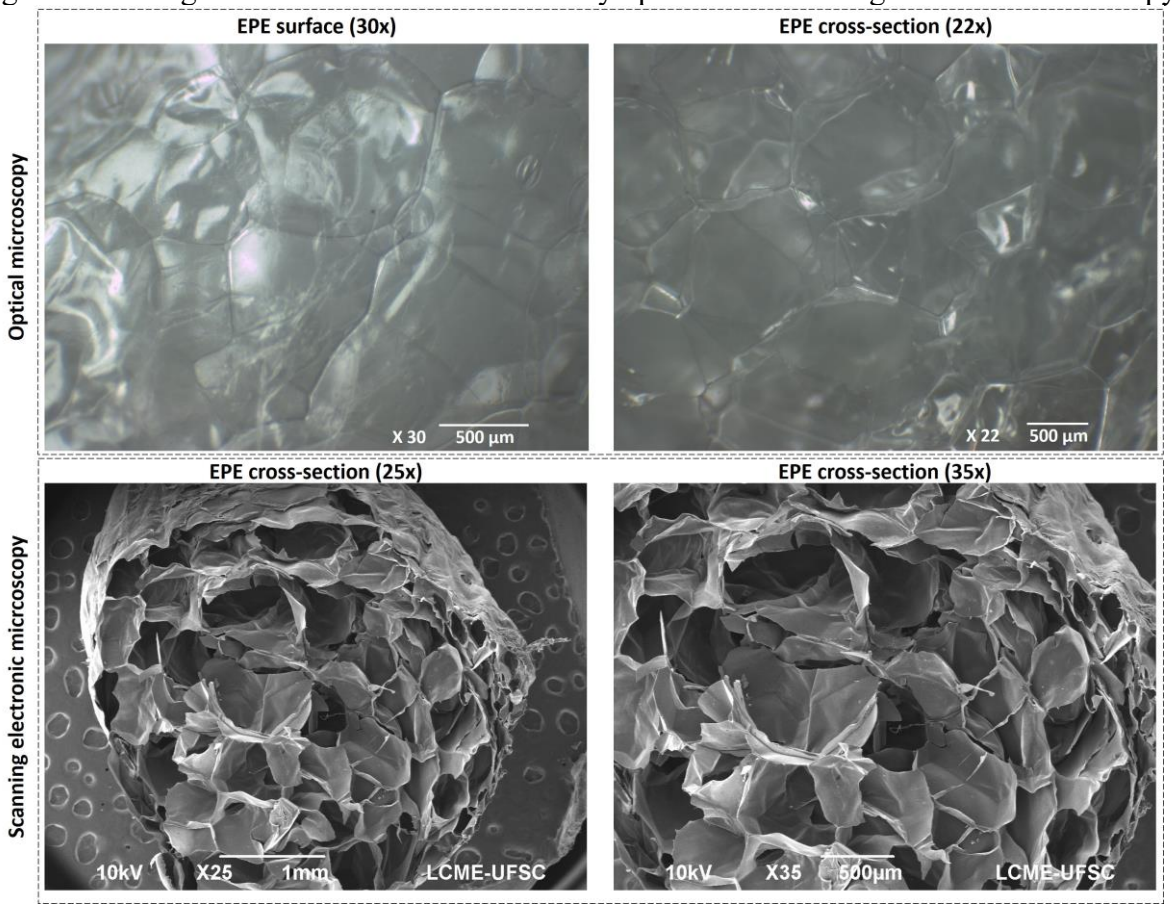

Source: Fonseca et al. (2021), with permission.

APPENDIX D – Licenses provided by Elsevier for the use of figures

Figure 5

ELSEVIER LICENSE TERMS AND CONDITIONS

Jun 05, 2021

This Agreement between Mrs. Jéssica de Matos Fonseca ("You") and Elsevier ("Elsevier") consists of your license details and the terms and conditions provided by Elsevier and Copyright Clearance Center.

License Number	5082570361752
License date	Jun 05, 2021
Licensed Content Publisher	Elsevier
Licensed Content Publication	Journal of Photochemistry and Photobiology C: Photochemistry Reviews
Licensed Content Title	Visible-light activation of TiO2 photocatalysts: Advances in theory and experiments
Licensed Content Author	Vinod kumar Etacheri, Cristiana Di Valentin, Jenny Schneider, Detlef Bahnemann, Suresh C. Pillai
Licensed Content Date	Dec 1, 2015
Licensed Content Volume	25
Licensed Content Issue	n/a
Licensed Content Pages	29
Start Page	1
End Page	29
Type of Use	reuse in a thesis/dissertation

Figure 12

ELSEVIER LICENSE TERMS AND CONDITIONS

Jun 05, 2021

This Agreement between Mrs. Jéssica de Matos Fonseca ("You") and Elsevier ("Elsevier") consists of your license details and the terms and conditions provided by Elsevier and Copyright Clearance Center.

License Number	5082570234789
License date	Jun 05, 2021
Licensed Content Publisher	Elsevier
Licensed Content Publication	Food Hydrocolloids
Licensed Content Title	Fabrication and characterization of TiO2/whey protein isolate nanocomposite film

Licensed Content Author	Yanxia Li, Yanfeng Jiang, Fei Liu, Fazheng Ren,Guanghua Zhao, Xiaojing Leng
Licensed Content Date	Jul 1, 2011
Licensed Content Volume	25
Licensed Content Issue	5
Licensed Content Pages	7
Start Page	1098
End Page	1104
Type of Use	reuse in a thesis/dissertation

Figure B.1

ELSEVIER LICENSE TERMS AND CONDITIONS

Jun 05, 2021

This Agreement between Mrs. Jéssica de Matos Fonseca ("You") and Elsevier ("Elsevier") consists of your license details and the terms and conditions provided by Elsevier and Copyright Clearance Center.

License Number	5082570085790
License date	Jun 05, 2021
Licensed Content Publisher	Elsevier
Licensed Content Publication	Food Hydrocolloids
Licensed Content Title	Fabrication and characterization of chitosan-titanium dioxide nanocomposite film as ethylene scavenging and antimicrobial active food packaging
Licensed Content Author	Ubonrat Siripatrawan, Patinya Kaewklin
Licensed Content Date	Nov 1, 2018
Licensed Content Volume	84
Licensed Content Issue	n/a
Licensed Content Pages	10
Start Page	125
End Page	134
Type of Use	reuse in a thesis/dissertation